AD-A193 311 THERMO-MECHANICAL CRACKING IN COATED MEDIA WITH A CAVITY BY A MOVING ASPE (U) NEW MEXICO UNIV ALBUQUERQUE DEPT OF MECHANICAL ENGINEERING F D JU ET AL MAR 88 NE-144(88)ONR-233-3 F/G 20/11 NL

1/3

UNCLASSIFIED

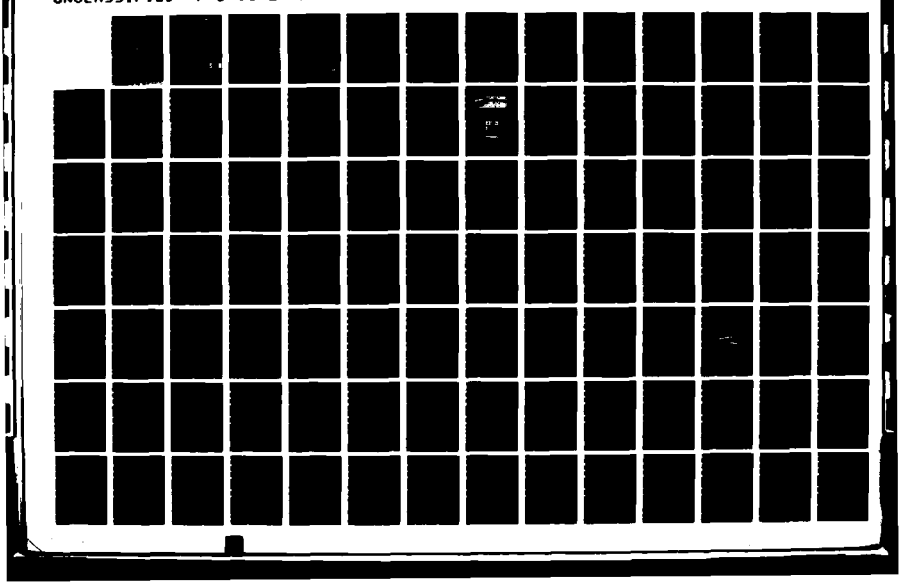

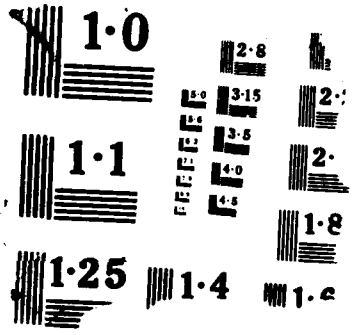
1·0
1·1
1·25
1·4
2·8
3·15
3·5
4·0
4·5
2·
1·8

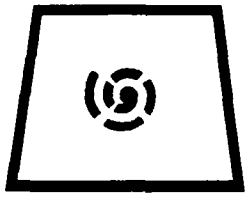

THE UNIVERSITY OF NEW MEXICO
COLLEGE OF ENGINEERING

BUREAU OF ENGINEERING RESEARCH

THERMO-MECHANICAL CRACKING IN COATED MEDIA WITH A CAVITY BY A MOVING ASPERITY FRICTION

by Frederick D. Ju and Tsu-Yen Chen
Mechanical Engineering Department
University of New Mexico

Technical Report No. ME-144(88)ONR-233-3

Work performed under ONR Grant No. 00014-84-K-0252

March 1988

Thermo-Mechanical Cracking In Coated Media With A Cavity By A Moving Asperity Friction

by

Frederick D. Ju
and
Tsu-Yen Chen

Mechanical Engineering Department
University of New Mexico
Albuquerque, New Mexico 87131

Technical Report
ME-144(88)ONR-233-3

March 1988

Work performed under ONR Grant No. 00014-84-K-0252

ACKNOWLEDGEMENT

The present research is performed under a grant from the Office of Naval Research, Grant No. N00014-84-K-0252. Dr. A. William Ruff was the program manager. Dr. Marshall Peterson is the program manager.

ABSTRACT

The research deals with the problem of asperity-excited thermomechanical field in a medium with a surface layer and a near surface void defect. The thermomechanical field governs the mode of cracking, which leads to failure in the wear surface. The presence and location of the void defect is most critical. This investigation obtained the solutions for the temperature distribution and the stress state in a layered medium with a rectangular cavity. This temperarture distribution and stress state result when the solid medium is subjected to Coulomb frictional loading from an asperity moving at a moderately high speed (of approximately 10–15 m/s). In the analysis, the coated medium was represented by a solid half space, with a thin top surface–layer of solid wear material. The cavity defect required a mathematical model in terms of the material coordinates. The corresponding governing differential equations were time–explicit and transient. A general finite difference formulation was developed to calculate both the temperature and the stress fields. The energy balance method was applied at the corners of the rectangular cavity to resolve the problem of singularities in the temperature field. The stress singularity at each corner was represented by a special element that was introduced representing the behavior of the known stress singularity at the corner and its vicinity. The general equation of the stress field, including the dynamic term, is of the regular perturbation type. The small order dynamic term is demonstrated to be a higher order effect by perturbation method, thus negligible. Numerical solutions were carried out for the zeroth order approximation and the case of uniform asperity pressure distribution.

It was shown that, at moderately high asperity speed, the thermal stress effect dominates the combined thermo–mechanical stress field, which eventually leads to failure in the no–cavity case. When a defect, such as a cavity, exists, the stress state that determines the failure phenomenon is much more severe and can be quantified depending on the location of the cavity. These results are determined through a numerical computation based on the

material properties of Stellite III. However, the parametric effects of material variations in the coating and the substrate, including changes in both thermal and mechanical properties, were also considered. The study of the cavity location also established the existence of a critical cavity location for cracking by cohesive failure. This location is defined by the critical ligament thickness (thickness between the wear surface and the top edge of the cavity), at which the cavity–influenced thermal tensile stress reaches a maximum. This thickness is important to designers when cavities at coating/substrate interfaces are either unavoidable or too expensive to control in fabrication.

TABLE OF CONTENTS

TABLE OF CONTENTS (continued)

LIST OF FIGURES

LIST OF FIGURES (continued)

LIST OF FIGURES (continued)

LIST OF FIGURES (continued)

LIST OF FIGURES (continued)

LIST OF FIGURES (continued)

NOMENCLATURE

a	asperity width
b	substrate thickness
c_1	The dilatational wave speed of the substrate
c_2	The shear wave speed of the substrate
c_I, c_{II}	specific heat of the coating layer and the substrate, respectively
$C(t)$	distance from x_1 origin to leading edge of the asperity
D	dimensionless coating thickness (=H/a)
d	half width of the cavity
e	depth of the cavity
E_I, E_{II}	Young's modulus of the coating layer and the substrate, respectively
H	coating thickness
k_I, k_{II}	thermal conductivity of the coating layer and the substrate, respectively
L'	ligament thickness
L	dimensionless ligament thickness
M	Mach number
$P(i,j)$	center point of the finite difference cell
N,R,S,W	surrounding points of $P(i,j)$
$P'(x_1,t)$	pressure over the contact area
P_0	average pressure over the contact area
$q(x_1,t)$	heat flux through the contact area
q_0	average heat flux through the contact area
Q^*	dimensionless heat flux through the contact area ($=q/q_0$)

$Q_{S\to P}$	heat flux from point S to point P
R_I, R_{II}	Péclet number of the coating layer and the substrate, respectively
T	temperature
u_1, u_2	displacement in x_1 and x_2 direction, respectively
u,v	dimensionless displacement in ξ and η direction $=(u_1/a,\ u_2/a)$, respectively
U_P	internal energy of the point P(i,j)
V	traverse speed of the asperity
x_1, x_2	material coordinates fixed to the cavity
Z	width of the plate
Z'	half width of the plate
α_I, α_{II}	coefficient of the thermal expansion of the coating and the substrate, respectively
β	the material region: I for the coating layer; II for the substrate
δ	mass density ratio $=(\rho_\beta/\rho_I)$
δ_{ij}	Kronecker delta
ξ, η	dimensionless coordinates $=(x_1/a,\ x_2/a)$
$\bar{\xi}, \bar{\eta}$	coordinates in transformed plane
κ_I, κ_{II}	thermal diffusivity of the coating layer and the substrate, respectively
λ, μ	Lamé constants
μ_f	Coulomb coefficient of friction
π_k	thermal conductivity ratio $(=k_{II}/k_I)$
Ω	thermal diffusivity ratio $(\Omega^2=\kappa_{II}/\kappa_I)$
$\sigma_{11}, \sigma_{12}, \sigma_{22}$	stress field

$\sigma_{\xi\xi}, \sigma_{\xi\eta}, \sigma_{\eta\eta}$	dimensionless stress field ($=\sigma_{11}/P_0$, σ_{12}/P_0, σ_{22}/P_0)
σ^T	dimensionless thermal principal stress
σ^M	dimensionless mechanical principal stress
σ^C	dimensionless combined principal stress
Φ	dimensionless temperature ($=Tk_I/q_0a$)
ρ	mass density
τ	dimensionless time ($=Vt/a$)

CHAPTER 1

INTRODUCTION

1.1 Statement of Problem

This investigation studies the thermomechanical cracking in a coated medium with a near surface cavity. Such cavity generally occurs in the neighborhood of the coating/substrate interface, as a result of either inclusion or poor bonding during the coating process. A typical geometry of the cavity can be shown as in Figure 1.1. To facilitate the analysis, this research will first study the effect of a rectangular cavity. The general failure mechanism is caused by the frictional excitation of a moderately high speed asperity traversing over a coated surface. The understanding of this failure process will improve the design of the modified wear surface by alleviating the problem of friction cracking or delamination.

When two flat solids, which are placed in contact under heavy loads, slide relative to each other, the nominal design pressure between the mating surfaces is based upon the nominal design contact area. When the contact pressure is evenly distributed according to design, the service life of the solids is not a serious problem, even at a high rubbing speed. However, at high operating speed, the real contact area can be reduced by several orders of magnitude. As a result, a low design pressure may result in a very high interfacial pressure, thus a very high dry frictional force in the real contact area. Kennedy [1] showed that the size of the real contact area depends on operating speed and material parameters such as thermal

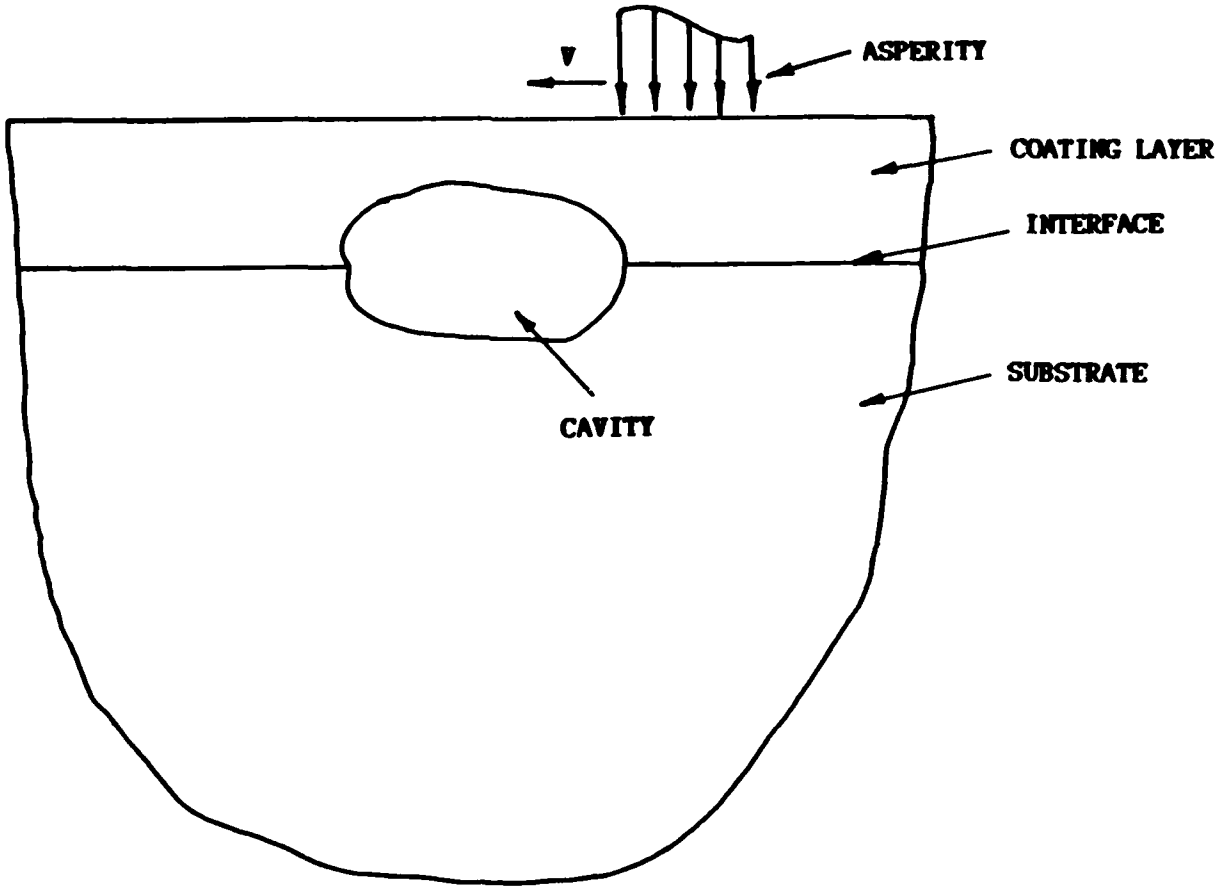

Figure 1.1 A layered medium with a cavity.

conductivity and wear resistance. He concluded that decreasing thermal conductivity, increasing wear resistance and increasing operating speed will reduce the real contact area. It was shown that, for a conservative areal ratio (contact area/nominal area) of 10^{-3} (Burton [2] considered 10^{-4} as a possible areal ratio), a low design pressure of 240 kPa (35 psi) could result in a 240 MPa (35,000 psi) local pressure in the contact zone. The high friction would generate locally an extremely high temperature, which was called "flash temperature" by Archard [3]. The local contact area is called "red banding" or "hot spot" [4], which has been experimentally demonstrated. In severe cases the temperature can be extremely high, leading to cracking of the surface [5]. This phenomenon is called "heat checking" or "thermocracking" [6]. It is frequently seen in seal rings, brakes, and rail-wheels [7,8,9,10,11,12] as shown in Figures 1.2 and 1.3. In general, it was observed that numerous radial cracks developed perpendicular to the sliding direction and almost periodically along the circumference. In order to understand these failures, in recent years, there has been increased emphasis in finding a solution of failure control, both experimentally and analytically.

1.2 Related Investigation in Progress

The phenomenon of high temperature "hot spot" was observed in the experiments by Archard [3]. A general survey of the problem of cracking through the development of a frictional hot spot was discussed by Burton [4]. Proof of the existence of hot patches of solid-to-solid contact was obtained experimentally by Bannerjee and Burton [13] in the case of metallic rings rotating against a non-metallic disk and, more recently, in actual operating face seals by Kennedy [14]. The latter

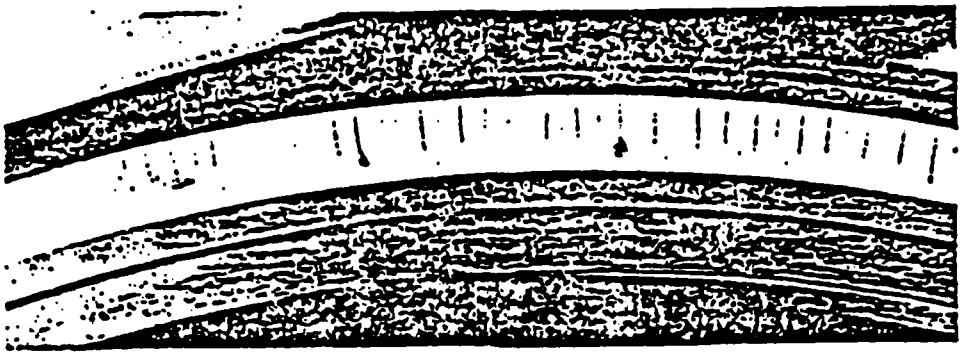

Figure 1.2 Radial hairline cracks on the metallic ring after running against a carbon ring at a high peripheral speed.

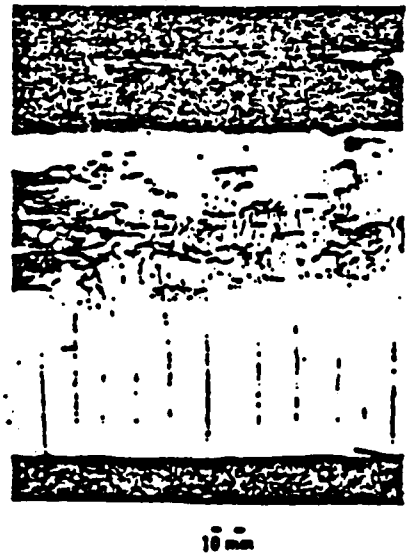

Figure 1.3 Thermal cracks on the brake shoe.

study made use of a new contact probe which enables the monitoring of contact patch sizes and locations in ring-on-ring or ring-on-disk configurations. It was proven to be quite effective in determining the geometry and movement of contact patches in dry operation of mechanical face seals. In his earlier experiment [15], Kennedy used a carbon ring against a metallic mating ring made from 440 C stainless steel, beryllium copper or 52100 bearing steel under both dry and liquid lubricated conditions. In these experiments, the existence of distinct spot asperities on the metallic ring was also observed. It was found that the spots tend to remain stationary with respect to the metallic mating ring of the seal, whether that ring is stationary or rotating. However, other investigations have shown hot patches moving relative to the mating ring and stationary on the primary ring [13,16]. Burton [17] also reported that, for an aluminum ring sliding on a glass disc, the hot spot precessed at a much lower speed than the rubbing speed. The uncertainty of this observed discrepancy on the speed of the moving asperities remains, but there is no doubt about the existence of the moving asperities due to thermoelastic instability on mechanical face seals. Several analytical studies of the failure due to the existence of the moving asperities have been developed. Surface displacements, temperature field and stress state of a convective elastic half space under an arbitrarily distributed fast-moving line heat source were obtained, using integral transform techniques, by Ling et al [18,19,20] and Mow and Cheng [21]. Kilaparti and Burton [22] have developed an exact Fourier series solution for a periodic strip heat input. Their series is rather unwieldly, but, at large Peclet number ($R=Va/\kappa$), it reduces to a form [23] that is simpler than that of Ling and Mow [18].

Recently, Barber [24] employed the Green's function for the problem of Kilaparti and Burton, and obtained the thermoelastic displacements and stresses due to a heat source moving over the surface of a half plane. A finite element analysis was developed by Kennedy [25] to study the surface temperatures resulting from frictional heating in sliding systems. He also applied finite element techniques to study the stresses in the mechanical face seals [6] and showed that the dominant stresses in the seal components are thermal stresses. The surface stress component (parallel to the surface) resulting from a periodic row of moving hot patches, with width 2a each, and a spacing of 2m was investigated by Tseng and Burton [26]. They concluded that the tensile stress would appear instantaneously with each passage of the heat source. Two- dimensional models of heat checking in the contact zone of a face seal were presented by Ju and Huang [27]. Because of the three-dimensional aspect of those observed "hot spots", Ju and Huang reformulated the problem in three-dimensional theory of thermoelasticity [28,29,30]. The investigation concluded that the highest tensile stress occurs, for an asperity speed of 10-15 m/s (400-600 in/s), at a depth of the order of one-tenth the asperity size. This depth defines the critical depth of the material. The physical depth is therefore 50-100 μm. At such a asperity speed, the stresses from the thermal effect of the asperity friction are an order of magnitude larger than those from its mechanical traction effect. Ju and Huang [31] also demonstrated that, when asperities excite the surface periodically in close intervals (a numerical example used a spacing of twelve asperity size), the thermomechanical effects accumulate, yet tending to a limiting magnitude, even though the

mechanical stress dissipates with no residue effect. The cumulative effect definitely depends on the interval of periodic excitations. At a relatively large interval of approximately 1000 asperity size, no cumulative effect is evident.

For improvement of the wear property of the surface, recent effort has been directed toward surface modifications. Research to understand the behavior of coated surfaces under asperity excitation, hence, has gained importance. Ju and Chen [32,33] first solved for the case of a moderately thick coating (thickness of the order of the asperity size). Later Ju and Liu [34] extended the general formulation of [32,33] to study the thickness effect of the coating layer for various mechanical and thermal impedance matchings between the surface coating layer and the substrate. It is concluded by Ju et al that: (i) a stiff surface layer would result in higher thermal stress; (ii) the stress state in layered media is influenced by the layer thickness, reaching a worst state when the coating layer thickness is in the neighborhood of the critical depth; (iii) a substrate of lower thermal expansion coefficient, higher Young's modulus, higher thermal conductivity and capacity will result in lower stresses in the coating layer; (iv) for the thin coating layer, the shearing stress at the coating/substrate interface is by no means trivial, depending again on the surface coating thickness. The interface shear reaches a maximum when the coating thickness is in the neighborhood of the thermal layer. These results are important for designing the bonding of the surface coating.

In the previous work on the moving asperity problem, the analyses dealt with basically uniform solid media; that is, the material and asperity properties are invariant in the direction of the asperity

motion. In such cases, since the time effect can be rendered implicit in the Fourier and the Navier equations by using a coordinate system fixed to the traversing asperity (called the convective coordinate system), the resulting solutions are steady-state. However, when the material has a cavity, uniformity in the direction of the asperity motion no longer exists. Consequently, a coordinate system fixed either to the cavity or to the material (referred to as the material coordinates) must be employed. The governing equations and their solutions, therefore, are transient. The present investigation not only obtains the temperature field solutions but also analyzes the stress field caused by the input of a moving heat source. In this study, since the Fourier and the thermoelastic Navier's equations in the material coordinates are time explicit, the finite difference method is considered more appropriate. Although a specific numerical solution does not show the effects of parameters, a general trend of the parameters effects can be obtained with adequate numerical solutions for a series of given parametric values.

1.3 General Theory

The phenomenon of thermomechanical cracking, as observed from experiments and operational damages, is connected with relatively hard materials; such as cast iron and Stellite III. Blau [35] and Ruff and Blau [36] demonstrated experimentally that the plastic wear and surface shear for hard wear material are restricted to a very thin surface layer (about 4-8μ). Ju et al [27,28,29,30,33,34] also proved that the critical depth is at a depth of an order of magnitude larger than plastic depth. Therefore, the linear thermoelastic theory holds. The basic mathematical formulation of uncoupled thermoelasticity consists

of the following equations:

$$\mu \nabla^2 \mathbf{u} + (\lambda+\mu)\ \text{grad div}\ \mathbf{u} - (3\lambda+2\mu)\ \alpha\ \text{grad}\ T = \rho \ddot{\mathbf{u}} \qquad (1.1)$$

and $$k \nabla^2 T = \rho c \dot{T} \qquad (1.2)$$

where T and **u** are temperature and displacement fields, respectivity, k is the thermal conductivity, ρ is the mass density, c is the specific heat, λ,μ are the Lamé constants, and α is the coefficient of thermal expansion. The coupling term is negligible except for conditions in which the temperature distributions have sharp variations in their time histories, which often occurs during the propagation of thermoelastic waves in the aftermath of thermal shocks [37,38,39,40,41,42]. For the current problem, since the asperity speed under consideration is much slower than the elastic wave speed, the uncoupled thermoelastic theory is applied.

The dynamic effect may result from either a dynamic loading state or a non-steady thermal state in which the time rate of temperature change could keep up with the stress waves in the material. Duhamel [43] stated that the inertia term can be disregarded if the time rate of change of temperature is slow enough. Parkus [44] showed that the significant effect from the inertia term can arise only when there is an instantaneous change in the surface temperature or in the temperature of the surrounding medium. In fact, the dynamic effect is greatly reduced if the temperature change occurs in a very short, but finite, interval of time. This was confirmed by Danilovskaya [45,46], who studied the dynamic effect due to a thermal shock on the surface of

a half-space and demonstrated that the maximum dynamic stress is reduced to 86% even for the extremely short duration heating of 10^{-12} seconds. In general, under usual conditions of heat exchange, the rate of temperature change is small in comparison with the speed of sound in the material. Thus, at any instant, the thermal stress state can be determined by the instantaneous values of the temperature field.

For the cavity problem, the effect of the dynamic term in Equation (1.1) will be studied quantitatively with a perturbation method. That is, the solution to Equation (1.1) can be expressed in an asymptotic series. Substituting this series into Equation (1.1) leads to a set of linear equations for **u**. Each set of linear equations represents a different order of solution of the asymptotic series. The details of the perturbation procedure will be addressed in Chapter 4.

CHAPTER 2

ANALYTICAL MODEL AND BASIC EQUATIONS

The experiments performed by Kennedy [47] have shown that contact between two flat conforming rings is concentrated in several (1 to 5) patches, with a few small solid-solid contact spots occurring within each patch. Each contact spot is identical and the contacts are equally spaced around the ring circumference. A ring could therefore be divided into as many sections as the number of contact spots and only one such section would have to be analyzed. Kennedy [15] also proved that the width of the contact spot (asperity) is about 0.1 to 1 mm (0.004 to 0.04 in.); however, the size of a typical mating ring is several orders of magnitude larger than the asperity size. Because of this size difference between the contact area and the mating rings, the analytical model is represented by a semi-infinite body with a thin coating layer and a rectangular cavity in the neighborhood of the coating layer/substrate interface. The half space surface is subjected to the frictional heating of a moving asperity over the wear surface (Figure 2.1), and the material coordinate system (fixed to the cavity) is used. As presented in Chapter 1, the linear thermoelastic theory applies for the current problem. The advantage of the linear theory is the application of the superposition principle, which allows a separation of the stress field to a contribution of the mechanical load of the pressure and friction from the moving asperity and another contribution of the heat input from the rate of the frictional energy dissipation. The combined effects will then determine the possibility

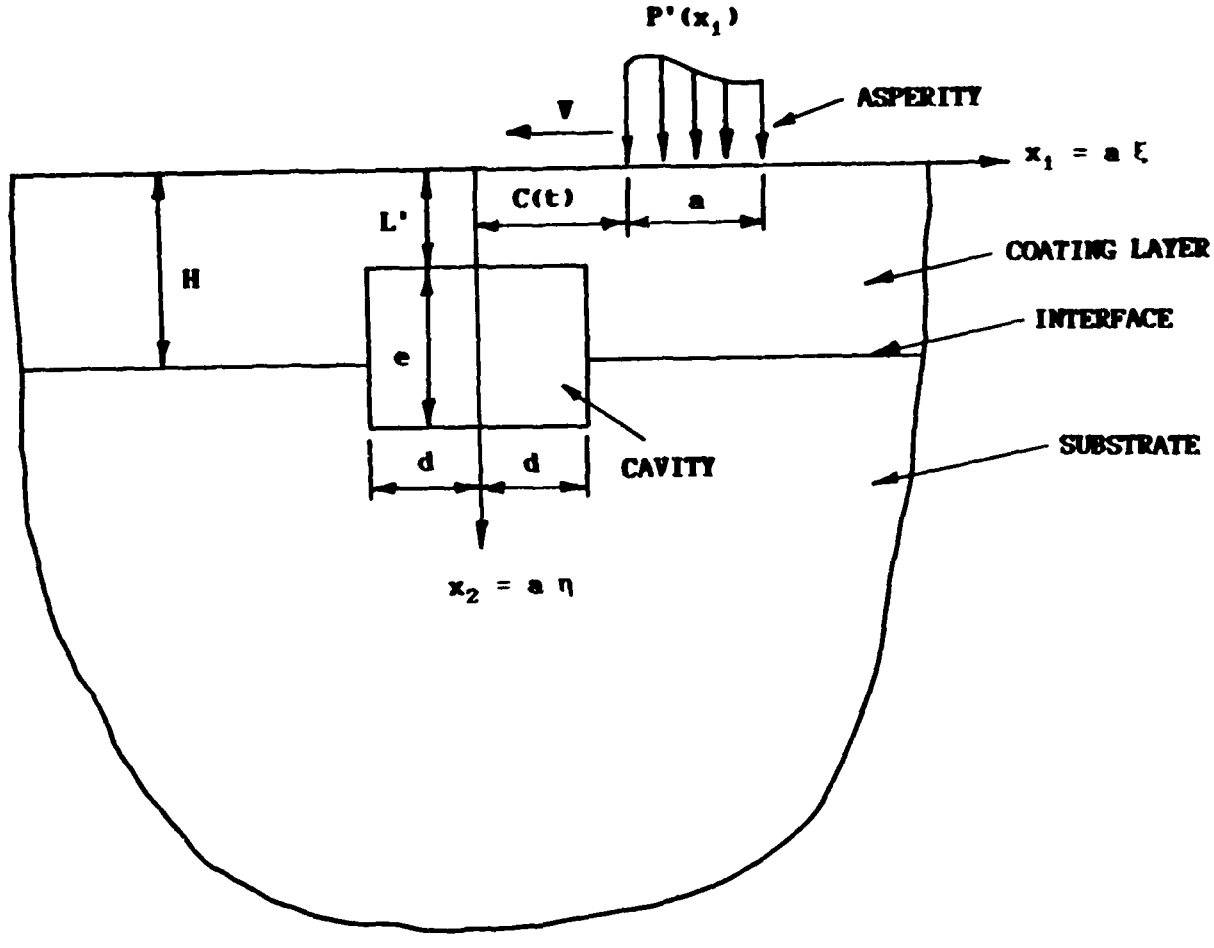

Figure 2.1 Two-dimensional model of a coated wear surface with a cavity.

of fracture initiation. The governing differential equations for the temperature and the stress fields are the Fourier equation and the thermoelastic Navier's equation, respectively.

2.1 Temperature Field

The governing equation for the temperature field is

$$\frac{\partial}{\partial x_1}\left(k_\beta \frac{\partial T^\beta}{\partial x_1}\right) + \frac{\partial}{\partial x_2}\left(k_\beta \frac{\partial T^\beta}{\partial x_2}\right) = \rho_\beta c_\beta \frac{\partial T^\beta}{\partial t} \qquad (2.1)$$

where T is the temperature; k is the thermal conductivity; ρ is the mass density; c is the specific heat; and β denotes the layered region: I for the coating surface, II for the substrate.

The temperature field T must satisfy the initial condition,

$$T^\beta(x_1, x_2, 0) = 0, \qquad (2.2)$$

and the boundary conditions:

(i) The regularity condition holds at infinity ($x_1^2+x_2^2\to\infty$),

$$T^\beta = 0. \qquad (2.3)$$

(ii) In the asperity contact surface ($c(t)\le x_1 \le c(t)+a$, $x_2=0$), the maximum heat input through the boundary is the rate of the frictional energy

$$-k_I \frac{\partial T^I}{\partial x_2} = q = \mu_f V p'(x_1), \qquad (2.4)$$

where μ_f is the Coulomb coefficient of friction; V is the asperity

velocity; $p'(x_1)$ is the pressure over the contact area; q is the heat flux through the contact area; and c(t) is the distance from x_1 origin to the leading edge of the asperity.

(iii) Outside the contact surface, $x_1 < c(t)$ or $x_1 > c(t)+a$, $x_2 = 0$, the convective heat loss, being of small order, is neglected without loss of generality,

$$- \frac{\partial T^I}{\partial x_2} = 0. \tag{2.5}$$

(iv) At the coating layer/substrate interface, $x_2 = H$, the continuity conditions hold

$$T^I = T^{II} , \tag{2.6}$$

$$k_I \frac{\partial T^I}{\partial x_2} = k_{II} \frac{\partial T^{II}}{\partial x_2} , \tag{2.7}$$

where H is the layer thickness.

(v) Adiabatic conditions at cavity boundaries,

$$\frac{\partial T^\beta}{\partial x_2} = 0, \text{ at } -d \leq x_1 \leq d, \; x_2 = L' \tag{2.8}$$

$$\frac{\partial T^\beta}{\partial x_2} = 0, \text{ at } -d \leq x_1 \leq d, \; x_2 = L'+e \tag{2.9}$$

$$\frac{\partial T^\beta}{\partial x_1} = 0, \text{ at } x_1 = d, \; L' \leq x_2 \leq L'+e \tag{2.10}$$

$$\frac{\partial T^\beta}{\partial x_1} = 0, \text{ at } x_1 = -d, \; L' \leq x_2 \leq L'+e \tag{2.11}$$

where d is the half width of the cavity and e is the depth of the cavity. The region between the cavity and the wear surface, which is important in determining the magnitude of the temperature field and the stress state, shall be designated descriptively as the ligament region. The distance between the surface and the cavity top edge is therefore the ligament thickness L' (see Figure 2.1).

2.2 Mechanical stress field

The elastic Navier's equation and the Hooke's law equation are

$$\frac{\partial}{\partial x_i}\left(\lambda_\beta \frac{\partial u_k^\beta}{\partial x_k}\right) + \frac{\partial}{\partial x_j}\left(\mu_\beta \frac{\partial u_i^\beta}{\partial x_j}\right) + \frac{\partial}{\partial x_j}\left(\mu_\beta \frac{\partial u_j^\beta}{\partial x_i}\right) =$$

$$= \rho_\beta \frac{\partial^2 u_i^\beta}{\partial t^2}, \qquad i,j,k = 1,2 \tag{2.12}$$

and $$\sigma_{ij}^\beta = \lambda_\beta \delta_{ij}\left(\frac{\partial u_k^\beta}{\partial x_k}\right) + \mu_\beta\left(\frac{\partial u_i^\beta}{\partial x_j} + \frac{\partial u_j^\beta}{\partial x_i}\right), \quad i,j,k = 1,2 \tag{2.13}$$

where u_1 and u_2 are the displacements in x_1 and x_2 direction, respectively; $\sigma_{11}, \sigma_{12}, \sigma_{22}$ are stress components; λ and μ are the Lamé constants; and δ_{ij} is the Kronecker delta. The summation convention is used for all repeated indices of Roman minuscules.

The mechanical stress field is initially homogeneous.

The boundary conditions are:

(i) On the contact surface ($c(t) \leq x_1 \leq c(t)+a$, $x_2 = 0$), tractions are prescribed by

$$\sigma_{12}^I = \mu_f p'(x_1), \tag{2.14}$$

$$\sigma_{22}^I = -p'(x_1). \tag{2.15}$$

(ii) Outside the contact area, the region given by $x_1 < c(t)$ or $x_1 > c(t)+a$, $x_2 = 0$, the surface tractions are identically zero:

$$\sigma_{i2}^{I} = 0, \tag{2.16}$$

$$\sigma_{22}^{I} = 0. \tag{2.17}$$

(iii) The regularity conditions hold at infinity ($x_1^2+x_2^2 \to \infty$),

$$u_i^{\beta} = 0, \tag{2.18}$$

$$\sigma_{ij}^{\beta} = 0. \tag{2.19}$$

(iv) At the coating layer/substrate interface, $x_2 = H$, the continuity conditions are

$$u_i^{I} = u_i^{II} , \tag{2.20}$$

$$\sigma_{i2}^{I} = \sigma_{i2}^{II} . \tag{2.21}$$

(v) The cavity boundary is traction free; that is,

$$\sigma_{i2}^{\beta} = \sigma_{22}^{\beta} = 0, \text{ at } -d \leq x_1 \leq d , \; x_2 = L' \tag{2.22}$$

$$\sigma_{i2}^{\beta} = \sigma_{22}^{\beta} = 0, \text{ at } -d \leq x_1 \leq d , \; x_2 = L'+e \tag{2.23}$$

$$\sigma_{i1}^{\beta} = \sigma_{i2}^{\beta} = 0, \text{ at } x_1 = d , \; L' \leq x_2 \leq L'+e \tag{2.24}$$

$$\sigma^{\beta}_{i1} = \sigma^{\beta}_{i2} = 0, \text{ at } x_1 = -d \ , \ L' \leq x_2 \leq L'+e \qquad (2.25)$$

2.3 Thermal Stress Field

The thermoelastic Navier's equation is

$$\frac{\partial}{\partial x_i} \left(\lambda_\beta \frac{\partial u^{\beta}_k}{\partial x_k} \right) + \frac{\partial}{\partial x_j} \left(\mu_\beta \frac{\partial u^{\beta}_i}{\partial x_j} \right) + \frac{\partial}{\partial x_j} \left(\mu_\beta \frac{\partial u^{\beta}_j}{\partial x_i} \right) -$$

$$- \frac{\partial}{\partial x_i} \left[(3\lambda_\beta + 2\mu_\beta) \alpha_\beta (T-T_o) \right] = \rho_\beta \frac{\partial^2 u^{\beta}_i}{\partial t^2} \ , \ i,j,k = 1,2 \qquad (2.26)$$

and the Hooke's law equation is

$$\sigma^{\beta}_{ij} = \lambda_\beta \delta_{ij} \left(\frac{\partial u^{\beta}_k}{\partial x_k} \right) + \mu_\beta \left(\frac{\partial u^{\beta}_i}{\partial x_j} + \frac{\partial u^{\beta}_j}{\partial x_i} \right) -$$

$$- (3\lambda_\beta + 2\mu_\beta) \alpha_\beta \delta_{ij} (T-T_o) \ , \qquad (2.27)$$

where α is the coefficient of thermal expansion, T and its derivatives are derived from the temperature field.

The initial conditions for the thermal stress field are

$$u^{\beta}_i (x_1, x_2, 0) = 0, \qquad (2.28)$$

$$\sigma^{\beta}_{ij}(x_1, x_2, 0) = 0. \qquad (2.29)$$

The boundary conditions are:

(1) The surface, $x_2 = 0$, is traction free, i.e.

$$\sigma^{I}_{i2} = 0, \qquad (2.30)$$

$$\sigma_{22}^{I} = 0. \tag{2.31}$$

(ii) The regularity conditions hold at infinity, $x_1^2+x_2^2 \to \infty$, i.e.

$$u_i^{\beta} = 0, \tag{2.32}$$

$$\sigma_{ij}^{\beta} = 0. \tag{2.33}$$

(iii) Continuity conditions hold at the interface, $x_2 = H$, i.e.

$$u_i^{I} = u_i^{II} , \tag{2.34}$$

$$\sigma_{i2}^{I} = \sigma_{i2}^{II} . \tag{2.35}$$

(iv) The cavity boundary is traction free, i.e.

$$\sigma_{12}^{\beta} = \sigma_{22}^{\beta} = 0, \text{ at } -d \leq x_1 \leq d , \; x_2 = L' \tag{2.36}$$

$$\sigma_{12}^{\beta} = \sigma_{22}^{\beta} = 0, \text{ at } -d \leq x_1 \leq d , \; x_2 = L'+e \tag{2.37}$$

$$\sigma_{11}^{\beta} = \sigma_{12}^{\beta} = 0, \text{ at } x_1 = d , \; L' \leq x_2 \leq L'+e \tag{2.38}$$

$$\sigma_{11}^{\beta} = \sigma_{12}^{\beta} = 0, \text{ at } x_1 = -d , \; L' \leq x_2 \leq L'+e \tag{2.39}$$

The solution techniques and the numerical results of the temperature and the stress fields shall be given in Chapters 3 and 4.

CHAPTER 3

TEMPERATURE SOLUTIONS

Since a high temperature and its gradients are the source of the high thermal stresses, which can lead to the thermocracking of the wear medium. Therefore, it is of primary importance that a temperature solution is available. The governing equations in the dimensionless form are as follows:

In the coating layer, $0<\eta<D$, denoted by the superscript I,

$$\frac{\partial^2 \phi^I}{\partial \xi^2} + \frac{\partial^2 \phi^I}{\partial \eta^2} = R_I \frac{\partial \phi^I}{\partial \tau} , \tag{3.1}$$

In the substrate region, $D<\eta<\infty$, denoted by superscript II,

$$\frac{\partial^2 \phi^{II}}{\partial \xi^2} + \frac{\partial^2 \phi^{II}}{\partial \eta^2} = R_{II} \frac{\partial \phi^{II}}{\partial \tau} . \tag{3.2}$$

where $\phi^\beta (=T^\beta k_I/q_0 a)$ is the dimensionless temperature; $(\xi,\eta)=(x_1/a, x_2/a)$ are the dimensionless coordinates in the direction opposed to the asperity motion and the depth direction, respectivelv (as shown in Figure 2.1); $\tau=(Vt/a)$ is the dimensionless time; $D=H/a$ is the dimensionless coating thickness; $R_\beta=(Va/\kappa_\beta)$ are the Peclet numbers in the coating layer (β=I) and in the substrate (β=II); q_0 is the average heat flux through the contact area; and T, K, κ, a, x_1, x_2, V, t, H are the same as defined in Chapter 2.

3.1 Difference Formulation

Because of the analytical complexity of the mathematical model, the

explicit finite difference method is employed to solve the current problem [48,49,50,51,52,53,54,55,]. A brief discussion of the finite difference method is given in Appendix I. In the finite difference method, the semi-infinite body is replaced by a sufficiently large rectangular region (Figure 3.1). A central difference is used for the space derivatives, and a two-point forward difference is used for the time derivative of the first time step, then a three-point forward difference is employed for the following time steps. The reason for using the three-point forward difference after the first time step is that it is more accurate than the two-point forward difference. But, for the first time step, we have information only on one previous time line (initial condition), and, therefore, only the two-point difference formula may be used.

The governing differential equations in the difference form are: In the coating layer

$$\phi^I(i,j,n) = r_1\phi^I(i-1,j,n-1) + [1 - 2(r_1 + r_2)]\phi^I(i,j,n-1) + r_1\phi^I(i+1,j,n-1) + r_2\phi^I(i,j-1,n-1) + r_2\phi^I(i,j+1,n-1), \qquad n=1 \quad (3.3a)$$

and

$$\phi^I(i,j,n) = \frac{1}{3}[-\phi^I(i,j,n-2) + 2r_1\phi^I(i-1,j,n-1) + 4(1 - r_1 - r_2)\phi^I(i,j,n-1) + 2r_1\phi^I(i+1,j,n-1) +$$

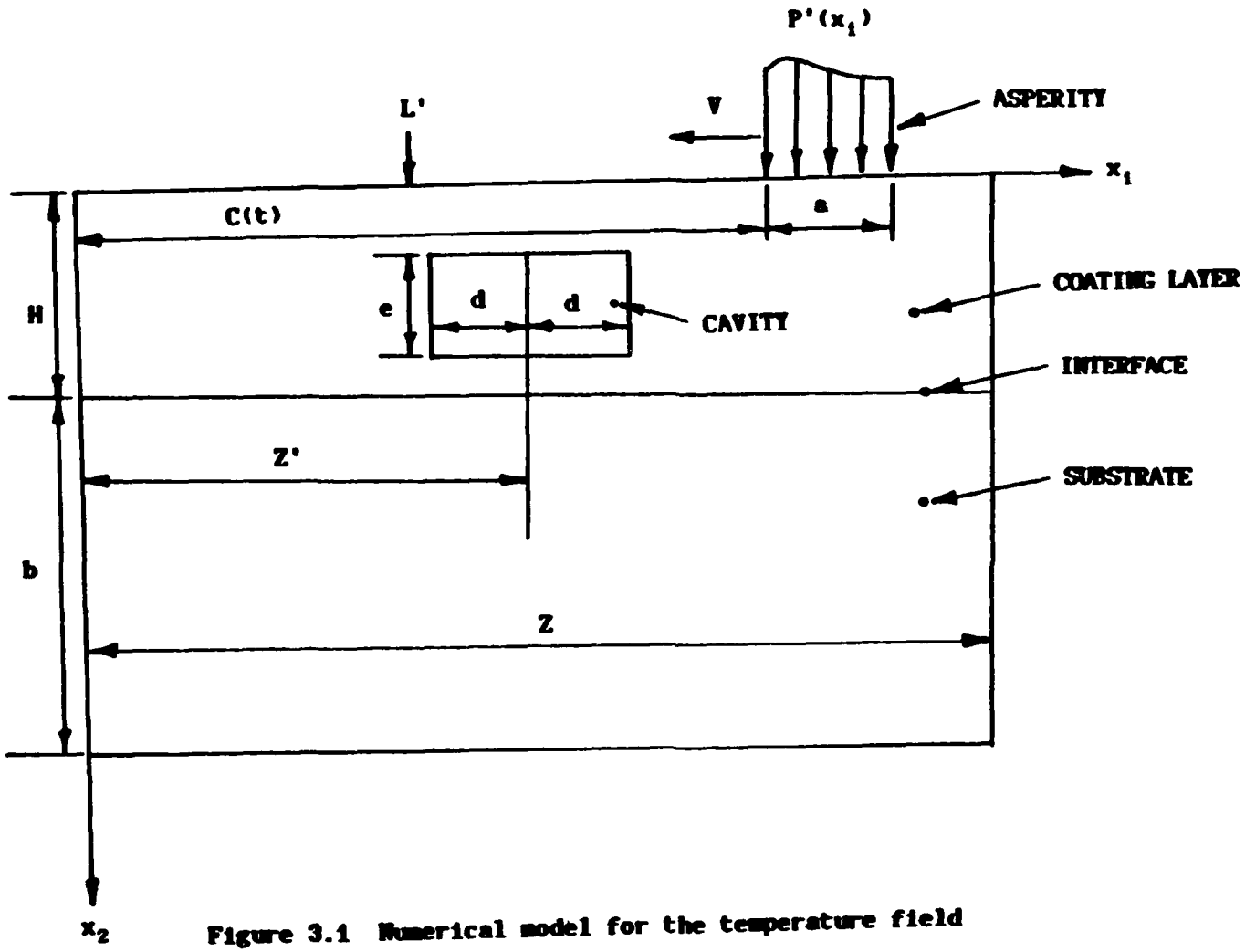

Figure 3.1 Numerical model for the temperature field

$$+ 2r_2\phi^{I}(i,j-1,n-1) + 2r_2\phi^{I}(i,j+1,n-1)] \ , \quad n>1 \quad (3.3b)$$

In the substrate

$$\phi^{II}(i,j,n) = \Omega^2 r_1\phi^{II}(i-1,j,n-1) + [1 - (2\Omega^2 r_1+2\Omega^2 r_2)]\phi^{II}(i,j,n-1)+$$

$$+ \Omega^2 r_1\phi^{II}(i+1,j,n-1) + \Omega^2 r_2\phi^{II}(i,j-1,n-1) +$$

$$+ \Omega^2 r_2\phi^{II}(i,j+1,n-1) \ , \qquad n=1 \quad (3.4a)$$

and

$$\phi^{II}(i,j,n) = \frac{1}{3}[-\phi^{II}(i,j,n-2) + 2\Omega^2 r_1\phi^{II}(i-1,j,n-1) +$$

$$+ 4(1 - \Omega^2 r_1 - \Omega^2 r_2)\phi^{II}(i,j,n-1)+2\Omega^2 r_1\phi^{II}(i+1,j,n-1) +$$

$$+ 2\Omega^2 r_2\phi^{II}(i,j-1,n-1)+2\Omega^2 r_2\phi^{II}(i,j+1,n-1)]. \ n>2 \ (3.4b)$$

where $r_1=\Delta\tau/(R_I\cdot\Delta\xi^2)$, $r_2=\Delta\tau/(R_{II}\cdot\Delta\eta^2)$, $\Omega^2=\kappa_{II}/\kappa_I$, and (i,j,n) denotes the two spatial indices and the time step, respectively. For the explicit scheme, the time step $\Delta\tau$ must satisfy a stability criterion. The most commonly used method of stability analysis is Von Neumann's method [48,50,54,55]. In this method, a finite Fourier series expansion of the solution to a model equation is made, and the decay or amplification of each mode is considered separately to determine stability or instability, as we now demonstrate.

Consider first the difference form of Equation (3.1) of the

coating layer

$$\phi^I(i,j,n) = \phi^I(i,j,n-1) + r_1[\phi^I(i-1,j,n-1) - 2\phi^I(i,j,n-1) + \phi^I(i+1,j,n)] + r_2[\phi^I(i,j-1,n-1) - 2\phi^I(i,j,n-1) + \phi^I(i,j+1,n-1)] \quad . \tag{3.5}$$

Each Fourier component of the solution is written as

$$\phi^I(i,j,n) = V^n e^{JK_\xi(i\Delta\xi)} e^{JK_\eta(i\Delta\eta)} \quad , \tag{3.6a}$$

where V^n is the amplitude function at time-level n of the particular component whose wave numbers are K_ξ and K_η in ξ and η directions and $J=\sqrt{-1}$. If $\theta=K_\xi\Delta\xi$ and $\phi=K_\eta\Delta\eta$ we obtain

$$\phi^I(i,j,n) = V^n e^{J(i\theta+j\phi)} \quad . \tag{3.6b}$$

Substituting Equation (3.6b) into Equation (3.5) gives

$$V^n e^{J(i\theta+j\phi)} = V^{n-1} e^{J(i\theta+j\phi)} + r_1\{V^{n-1} e^{J[(i-1)\theta+j\phi]} - 2V^{n-1} e^{J(i\theta+j\phi)} + V^{n-1} e^{J[(i+1)\theta+j\phi]}\} + r_2\{V^{n-1} e^{J[i\theta+(j-1)\phi]} - 2V^{n-1} e^{(i\theta+j\phi)} + V^{n-1} e^{J[i\theta+(j+1)\phi]}\} \quad . \tag{3.7}$$

Canceling the common term $e^{J(i\theta+j\phi)}$ gives

$$V^n = V^{n-1}\{1 + r_1(e^{J\theta} + e^{-J\theta} - 2) + r_2(e^{J\phi} + e^{-J\phi} - 2)\} . \quad (3.8)$$

Using the identity $e^{J\theta}+e^{-J\theta}=2\cos\theta$ and $2\sin^2(\theta/2)=1-\cos\theta$, Equation (3.8) becomes

$$V^n = GV^{n-1} = \{1 - 4r_1\sin^2(\frac{\theta}{2}) - 4r_2\sin^2(\frac{\phi}{2})\}V^{n-1} . \quad (3.9)$$

where G is the amplification factor. Equation (3.9) shows clearly that, if solutions are to remain bounded, we must have $|G|\leq 1$ for all θ and ϕ. This is the stability criterion for the heat conduction equation.

For $|G|\leq 1$, we have

$$|1 - 4r_1\sin^2(\frac{\theta}{2}) - 4r_2\sin^2(\frac{\phi}{2})| \leq 1 , \quad (3.10)$$

which is true only if

$$4r_1\sin^2(\frac{\theta}{2}) + 4r_2\sin^2(\frac{\phi}{2}) \leq 2 . \quad \text{for all } \theta, \phi \quad (3.11)$$

The stability requirement is then

$$r_1 + r_2 \leq \frac{1}{2} , \quad (3.12)$$

or

$$\frac{\Delta\tau}{R_1}\left(\frac{1}{\Delta\xi^2} + \frac{1}{\Delta\eta^2}\right) \leq \frac{1}{2} . \quad (3.13)$$

Similarly, the equation for the stability criterion for the substrate is

$$\Omega^2(r_1 + r_2) \leq \frac{1}{2} \quad , \tag{3.14}$$

or

$$\frac{\Omega^2\Delta\tau}{R_1}\left(\frac{1}{\Delta\xi^2} + \frac{1}{\Delta\eta^2}\right) \leq \frac{1}{2} \quad . \tag{3.15}$$

If Ω^2 is less than 1, Equation (3.13) is the stability criterion; otherwise Equation (3.15) is the stability criterion for the current problem.

Based on previous results in references [28,29,30,31,33,34,35], we know that high temperature and high thermal stresses occur in the region near the asperity. Therefore, in that region and in the region near the cavity, a very fine mesh must be used to calculate accurate solutions. In the regions far away from the asperity and the cavity, a relatively coarse mesh can be used to save computing time. This non-uniform mesh can be transformed to a uniform mesh by using the general coordinate transformation proposed in references [54,55,56]. The non-uniform mesh and general coordinate transformation are discussed in Appendix II.

The heat conduction equation (3.1) and (3.2) in the transformed plane $(\bar{\xi},\bar{\eta})$ can be written as

$$(A_1\phi^{\beta}_{\bar{\xi}\bar{\xi}} - 2A_2\phi^{\beta}_{\bar{\xi}\bar{\eta}} + A_3\phi^{\beta}_{\bar{\eta}\bar{\eta}} + A_4\phi^{\beta}_{\bar{\xi}} + A_5\phi^{\beta}_{\bar{\eta}})/J^2 = R_{\beta}\phi^{\beta}_{\tau} \quad , \beta=I,II \tag{3.16}$$

where $J=\xi_{\bar{\xi}}\eta_{\bar{\eta}} - \xi_{\bar{\eta}}\eta_{\bar{\xi}}$ is the Jacobian of the transformation, the subcripts $(\xi,\eta,\bar{\xi},\bar{\eta},\tau)$ denote partial derivatives in those coordinates and time, respectively, and

$$A_1 = \xi_{\bar{\eta}}^2 + \eta_{\bar{\eta}}^2, \tag{3.17}$$

$$A_2 = \xi_{\bar{\xi}}\xi_{\bar{\eta}} + \eta_{\bar{\xi}}\eta_{\bar{\eta}} , \tag{3.18}$$

$$A_3 = \xi_{\bar{\xi}}^2 + \eta_{\bar{\xi}}^2 , \tag{3.19}$$

$$A_4 = (\xi_{\bar{\eta}}A_7 - \eta_{\bar{\eta}}A_6)/J , \tag{3.20}$$

$$A_5 = (\eta_{\bar{\xi}}A_6 - \xi_{\bar{\xi}}A_7)/J , \tag{3.21}$$

$$A_6 = A_1\xi_{\bar{\xi}\bar{\xi}} - 2A_2\xi_{\bar{\xi}\bar{\eta}} + A_3\xi_{\bar{\eta}\bar{\eta}} , \tag{3.22}$$

$$A_7 = A_1\eta_{\bar{\xi}\bar{\xi}} - 2A_2\eta_{\bar{\xi}\bar{\eta}} + A_3\eta_{\bar{\eta}\bar{\eta}} . \tag{3.23}$$

In the coating layer, the transformed heat conduction equation (3.16) in the difference form is

$$\phi^I(i,j,n) = \phi^I(i,j,n-1) + \frac{\Delta\tau}{R_I} AA , \qquad n=1 \tag{3.24a}$$

$$\phi^I(i,j,n) = \frac{1}{3}\{-\phi^I(i,j,n-2) + 4\phi^I(i,j,n-1) + \frac{2\Delta\tau}{R_I} AA\} , \quad n>1 \tag{3.24b}$$

where

$$AA = \{(A_1/\Delta\bar{\xi}^2)\,[\phi^I(i-1,j,n-1) - 2\phi^I(i,j,n-1) + \phi^I(i+1,j,n-1)] -$$

$$- (A_1/2\Delta\bar{\xi}\Delta\bar{\eta})[\phi^I(i+1,j+1,n-1) - \phi^I(i+1,j-1,n-1) - \phi^I(i-1,j+1,n-1) +$$

$$+ \phi^I(i-1,j-1,n-1)] + (A_3/\Delta\bar{\eta}^2)\,[\phi^I(i,j-1,n-1) - 2\phi^I(i,j,n-1) +$$

$$+ \phi^I(i,j+1,n-1)] + (A_4/2\Delta\bar{\xi})\,[\phi^I(i+1,j,n-1) - \phi^I(i-1,j,n-1)] +$$

$$+ (A_5/2\Delta\bar{\eta})\,[\phi^I(i,j+1,n-1) - \phi^I(i,j-1,n-1)]\}/J^2 \,. \qquad (3.25)$$

In the substrate, the corresponding difference form of Equation (3.16) is given by

$$\phi^{II}(i,j,n) = \phi^{II}(i,j,n-1) + \frac{\Delta\tau}{R_{II}}\,AAA \,, \qquad n=1 \quad (3.26a)$$

$$\phi^{II}(i,j,n) = \frac{1}{3}\,[-\phi^{II}(i,j,n-2) + 4\phi^{II}(i,j,n-1) +$$

$$+ \frac{2\Delta\tau}{R_{II}}\,AAA] \,, \qquad n>1 \quad (3.26b)$$

where

$$AAA = [(A_1/\Delta\bar{\xi}^2)\,[\phi^{II}(i-1,j,n-1) - 2\phi^{II}(i,j,n-1) + \phi^{II}(i+1,j,n-1)] -$$

$$-(A_2/2\Delta\bar{\xi}\Delta\bar{\eta})[\phi^{II}(i+1,j+1,n-1) - \phi^{II}(i+1,j-1,n-1) - \phi^{II}(i-1,j+1,n-1) +$$

$$+\phi^{II}(i-1,j-1,n-1)] + (A_3/\Delta\bar{\eta}^2)\,[\phi^{II}(i,j-1,n-1) - 2\phi^{II}(i,j,n-1) +$$

$$+\phi^{II}(i,j+1,n-1)] + (A_4/2\Delta\bar{\xi})\,[\phi^{II}(i+1,j,n-1) - \phi^{II}(i-1,j,n-1)]+$$

$$+(A_5/2\Delta\bar{\eta})\,[\phi^{II}(i,j+1,n-1) - \phi^{II}(i,j-1,n-1)]]/J^2 \ . \qquad (3.27)$$

At the outer boundaries of the rectangular region (excluding the surface), $\phi^{\beta}(i,j,n)=0$ is the nominal value. The remaining conditions, on the surface, the cavity boundaries and at the interface, will be incorporated with an energy balance scheme.

3.2 Energy Balance

The cavity boundaries, the moving asperity and the interface of the medium are taken care of with the use of the energy balance method [57].

(i) Energy balance at the interface (see Figure 3.2)

For material *I (coating layer)*, the heat fluxes toward the central point P of the element at the interface from material points W, R and S in the coating layer are

$$Q_{W\to P} = k_I(\Delta y/2)\,\frac{T(i-1,j) - T(i,j)}{\Delta x_1} \ , \qquad (3.28)$$

$$Q_{R\to P} = k_I(\Delta y/2)\,\frac{T(i+1,j) - T(i,j)}{\Delta x_2} \ , \qquad (3.29)$$

$$Q_{S\to P} = k_I\left(\frac{\Delta x_1+\Delta x_2}{2}\right)\,\frac{T(i,j-1) - T(i,j)}{\Delta y} \ , \qquad (3.30)$$

where Q is the heat flux, indexed by the direction.

For material II (substrate), the heat fluxes toward the point P from material points W, R and N in the substrate region are

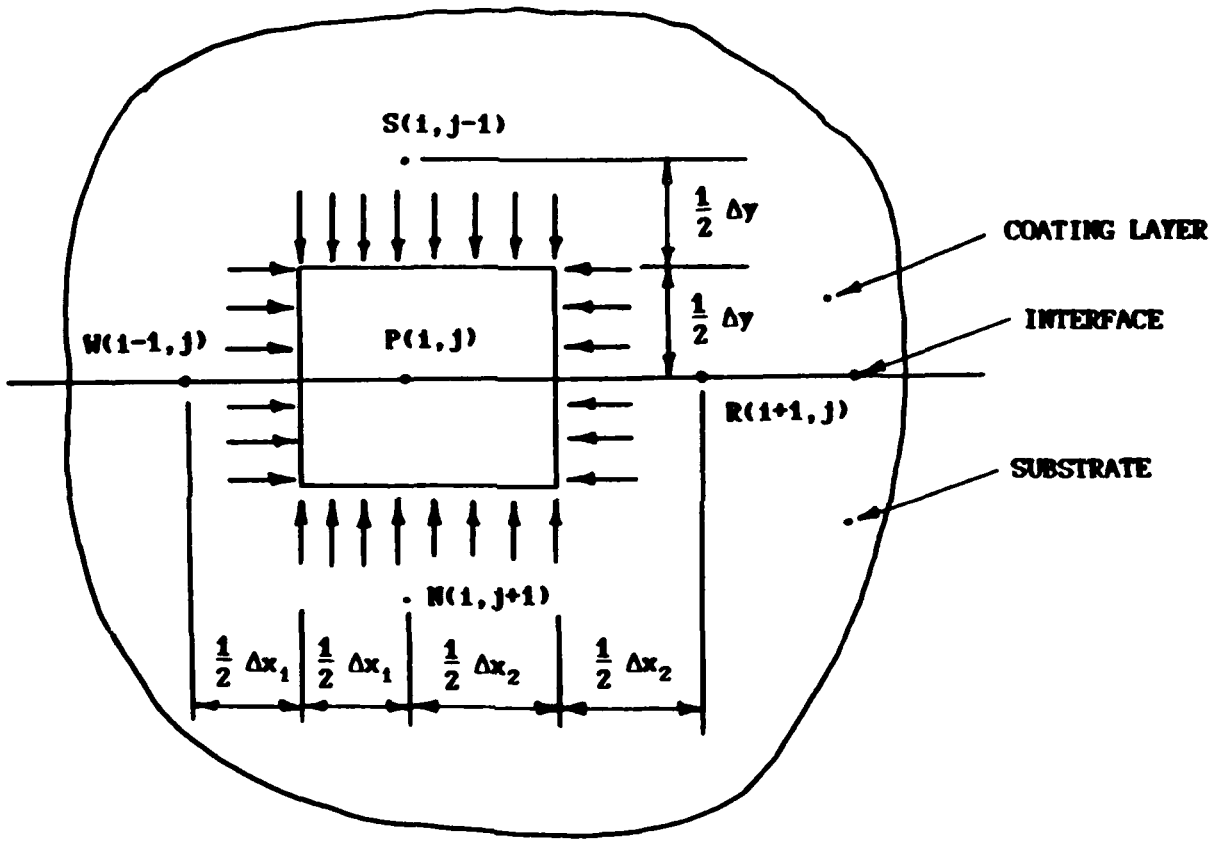

Figure 3.2 Energy balance at the interface.

$$Q_{W\to P} = k_{II}(\Delta y/2)\,\frac{T(i-1,j) - T(i,j)}{\Delta x_1}\,, \tag{3.31}$$

$$Q_{R\to P} = k_{II}(\Delta y/2)\,\frac{T(i+1,j) - T(i,j)}{\Delta x_2}\,, \tag{3.32}$$

$$Q_{S\to P} = k_{II}\left(\frac{\Delta x_1+\Delta x_2}{2}\right)\,\frac{T(i,j+1) - T(i,j)}{\Delta y}\,. \tag{3.33}$$

The total heat flux going to the interface point P(i,j) is

$$Q_{sum} = (k_I + k_{II})(\Delta y/2)\left[\frac{T(i-1,j) - T(i,j)}{\Delta x_1} + \frac{T(i+1,j) - T(i,j)}{\Delta x_2}\right] +$$

$$+ k_I\left(\frac{\Delta x_1+\Delta x_2}{2}\right)\frac{T(i,j-1)-T(i,j)}{\Delta y} + k_{II}\left(\frac{\Delta x_1+\Delta x_2}{2}\right)\frac{T(i,j+1)-T(i,j)}{\Delta y}\,. \tag{3.34}$$

The rate of change of internal energy $\dot{U}$ in the time interval Δt at the point P(i,j) is

$$\dot{U}_P = \dot{U}_{1P} + \dot{U}_{2P}$$

$$\dot{U}_P = (\rho_I c_I+\rho_{II} c_{II})\left[(\Delta x_1+\Delta x_2)\frac{\Delta y}{4}\right]\frac{T(i,j,n)-T(i,j,n-1)}{\Delta t}\,,\quad n=1 \tag{3.35a}$$

$$\dot{U}_P = (\rho_I c_I+\rho_{II} c_{II})\left[(\Delta x_1+\Delta x_2)\frac{\Delta y}{4}\right]\frac{3T(i,j,n)-4T(i,j,n-1)+T(i,j,n-2)}{2\Delta t}\,.$$

$$n>1 \tag{3.35b}$$

Conservation of energy requires that the algebraic sum of the heat flowing into the point P is equal to the rate of change of internal energy at the same point ($Q_{sum}=\dot{U}_p$). From conservation of energy, one

can obtain the equation for the continuity condition at the interface point P(i,j) at the time step n.

$$T(i,j,n) = T(i,j,n-1) + AA_1 \ , \qquad n=1 \qquad (3.36a)$$

$$T(i,j,n) = \frac{1}{3}\left[-T(i,j,n-2) + 4T(i,j,n-1) + 2AA_1\right] \ , \qquad n>1 \qquad (3.36b)$$

where

$$AA_1 = \frac{\Delta t}{\rho_I c_I + \rho_{II} c_{II}} \left\{ \frac{2(k_I+k_{II})}{\Delta x_1^2+\Delta x_1 \Delta x_2} \left[T(i-1,j,n-1) - T(i,j,n-1)\right] + \right.$$

$$+ \frac{2(K_I+K_{II})}{\Delta x_1 \Delta x_2+\Delta x_2^2} \left[T(i+1,j,n-1)-T(i,j,n-1)\right] + \frac{2k_I}{\Delta y^2} \left[T(i,j-1,n-1) - \right.$$

$$\left. \left. - T(i,j,n-1)\right] + \frac{2k_{II}}{\Delta y^2} \left[T(i,j+1,n-1) - T(i,j,n-1)\right]\right] \ . \qquad (3.37)$$

Equations (3.36a,b) in dimensionless form are given by

$$\phi(i,j,n) = \phi(i,j,n-1) + AA_2 \ , \qquad n=1 \qquad (3.38a)$$

$$\phi(i,j,n) = \frac{1}{3}\left[-\phi(i,j,n-2) + 4\phi(i,j,n-1) + 2AA_2\right] \ , \qquad n>1 \qquad (3.38b)$$

where

$$AA_2 = \frac{2\Delta\tau}{R_I+\eta_k R_{II}} \left\{ \frac{(1+\eta_k)}{\Delta\xi_1^2+\Delta\xi_1\Delta\xi_2} \left[\phi(i-1,j,n-1) - \phi(i,j,n-1)\right] + \right.$$

$$+ \frac{(1+\eta_k)}{\Delta\xi_1\Delta\xi_2+\Delta\xi_2^2} \left[\phi(i+1,j,n-1)-\phi(i,j,n-1)\right] + \frac{1}{\Delta\eta^2} \left[\phi(i,j-1,n-1)-\right.$$

$$-\phi(i,j,n-1)] + \frac{\pi_k}{\Delta\eta^2}\,[\phi(i,j+1,n-1) - \phi(i,j,n-1)] \ , \qquad (3.39)$$

where $\pi_k = k_{II}/k_I$.

Details of the energy balance method on the other boundary conditions are given in Appendix III. The dimensionless form of these boundary conditions are listed below.

(ii) Energy balance on the cavity boundaries (see Figure 3.3)

On face AB:

$$\phi^I(i,j,n) = \phi^I(i,j,n-1) + AA_3 \ , \qquad n=1 \qquad (3.40a)$$

$$\phi^I(i,j,n) = \frac{1}{3}\,[-\phi^I(i,j,n-2) + 4\phi^I(i,j,n-1) + 2AA_3] \ , \quad n>1 \qquad (3.40b)$$

where

$$AA_3 = \frac{\Delta\tau}{R_I}\,\{[\phi^I(i-1,j,n-1) - 2\phi^I(i,j,n-1) + \phi^I(i+1,j,n-1)]/\Delta\xi^2 +$$

$$+ 2[\phi^I(i,j-1,n-1) - \phi^I(i,j,n-1)]/\Delta\eta^2] \ . \qquad (3.41)$$

On face AC:

$$\phi^{II}(i,j,n) = \phi^{II}(i,j,n-1) + AA_4 \ , \qquad n=1 \qquad (3.42a)$$

$$\phi^{II}(i,j,n) = \frac{1}{3}\,[-\phi^{II}(i,j,n-2)+4\phi^{II}(i,j,n-1)+2AA_4] \ , \quad n>1 \qquad (3.42b)$$

where

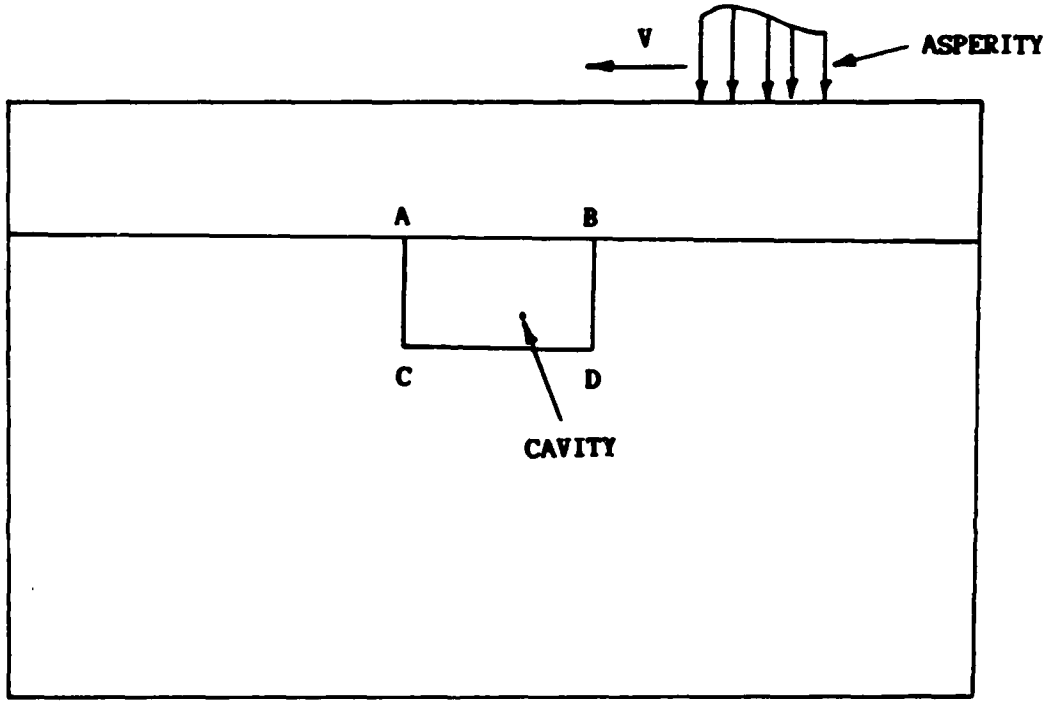

Figure 3.3 Energy balance on the cavity boundary.

$$AA_4 = \frac{2\Delta\tau}{R_{II}} \left\{ \frac{1}{\Delta\xi^2} \left[\phi^{II}(i-1,j,n-1) - \phi^{II}(i,j,n-1)\right] + \right.$$

$$+ \frac{1}{\Delta\eta_1{}^2+\Delta\eta_1\Delta\eta_2} \left[\phi^{II}(i,j-1,n-1) - \phi^{II}(i,j,n-1)\right] +$$

$$\left. + \frac{1}{\Delta\eta_2{}^2+\Delta\eta_1\Delta\eta_2} \left[\phi^{II}(i,j+1,n-1) - \phi^{II}(i,j,n-1)\right]\right\} . \qquad (3.43)$$

On face BD:

$$\phi^{II}(i,j,n) = \phi^{II}(i,j,n-1) + AA_5 , \qquad n=1 \quad (3.44a)$$

$$\phi^{II}(i,j,n) = \frac{1}{3}\left[-\phi^{II}(i,j,n-2)+4\phi^{II}(i,j,n-1)+2AA_5\right] , \quad n>1 \quad (3.44b)$$

where

$$AA_5 = \frac{2\Delta\tau}{R_{II}} \left\{ \frac{1}{\Delta\xi^2} \left[\phi^{II}(i+1,j,n-1) - \phi^{II}(i,j,n-1)\right] + \right.$$

$$+ \frac{1}{\Delta\eta_1{}^2+\Delta\eta_1\Delta\eta_2} \left[\phi^{II}(i,j-1,n-1) - \phi^{II}(i,j,n-1)\right] +$$

$$\left. + \frac{1}{\Delta\eta_2{}^2+\Delta\eta_1\Delta\eta_2} \left[\phi^{II}(i,j+1,n-1) - \phi^{II}(i,j,n-1)\right]\right\} . \qquad (3.45)$$

On face CD:

$$\phi^{II}(i,j,n) = \phi^{II}(i,j,n-1) + AA_6 , \qquad n=1 \quad (3.46a)$$

$$\phi^{II}(i,j,n) = \frac{1}{3}\left[-\phi^{II}(i,j,n-2)+4\phi^{II}(i,j,n-1)+2AA_6\right] , \quad n>1 \quad (3.46b)$$

wher

$$AA_6 = \frac{\Delta\tau}{R_{II}} \{[\phi^{II}(i-1,j,n-1) - 2\phi^{II}(i,j,n-1) + \phi^{II}(i+1,j,n-1)]/\Delta\xi^2 +$$

$$+ 2[\phi^{II}(i,j+1,n-1) - \phi^{II}(i,j,n-1)]\} \ . \qquad (3.47)$$

(iii) Energy balance at the corner of the cavity (Figure 3.3)

The points at the four corners of the cavity are singularities, because at each of those four points there are two boundary conditions, $\partial T/\partial x_1 = \partial T/\partial x_2 = 0$, with only one unknown T. However, by applying an energy balance scheme, one can resolve such problems at the corners. The dimensionless form for the corner points are:

Corner A:

$$\phi(i,j,n) = \phi(i,j,n-1) + AA_7 \ , \qquad n=1 \quad (3.48a)$$

$$\phi(i,j,n) = \frac{1}{3}[-\phi(i,j,n-2) + 4\phi(i,j,n-1) + 2AA_7] \ , \qquad n>1 \quad (3.48b)$$

where

$$AA_7 = \frac{\Delta\tau}{R_I/2 + \eta_k R_{II}/4} \{ \frac{1+\eta_k}{2} [\phi(i-1,j,n-1) - \phi(i,j,n-1)]/\Delta\xi^2 +$$

$$+ \frac{1}{2}[\phi(i+1,j,n-1) - \phi(i,j,n-1)]/\Delta\xi^2 + \frac{\eta_k}{2}[\phi(i,j+1,n-1) -$$

$$- \phi(i,j,n-1)]/\Delta\eta^2 + [\phi(i,j-1,n-1) - \phi(i,j,n-1)]/\Delta\eta^2] \ . \quad (3.49)$$

Corner B:

$$\Phi(i,j,n) = \Phi(i,j,n-1) + AA_8 \ , \qquad n=1 \qquad (3.50a)$$

$$\Phi(i,j,n) = \frac{1}{3}\,[-\Phi(i,j,n-2) + 4\Phi(i,j,n-1) + 2AA_8] \ , \qquad n>1 \qquad (3.50b)$$

where

$$AA_8 = \frac{\Delta\tau}{R_I/2 + \pi_k R_{II}/4}\,\{\frac{1}{2}\,[\Phi(i-1,j,n-1) - \Phi(i,j,n-1)]/\Delta\xi^2 +$$

$$+ \frac{1+\pi_k}{2}\,[\Phi(i+1,j,n-1) - \Phi(i,j,n-1)]/\Delta\xi^2 + \frac{\pi_k}{2}\,[\Phi(i,j+1,n-1) -$$

$$- \Phi(i,j,n-1)]/\Delta\eta^2 + [\Phi(i,j-1,n-1) - \Phi(i,j,n-1)]/\Delta\eta^2\} \ . \qquad (3.51)$$

Corner C:

$$\Phi^{II}(i,j,n) = \Phi^{II}(i,j,n-1) + AA_9 \ , \qquad n=1 \qquad (3.52a)$$

$$\Phi^{II}(i,j,n) = \frac{1}{3}\,[-\Phi^{II}(i,j,n-2)+4\Phi^{II}(i,j,n-1)+2AA_9] \ , \qquad n>1 \qquad (3.52b)$$

where

$$AA_9 = \frac{2}{3}\,\frac{\Delta\tau}{R_{II}}\,\{[2\Phi^{II}(i-1,j,n-1) - 3\Phi^{II}(i,j,n-1) + \Phi^{II}(i+1,j,n-1)]/\Delta\xi^2 +$$

$$+ [\Phi^{II}(i,j-1,n-1) - 3\Phi^{II}(i,j,n-1) + 2\Phi^{II}(i,j+1,n-1)]/\Delta\eta^2\}. \qquad (3.53)$$

Corner D:

$$\phi^{II}(i,j,n) = \phi^{II}(i,j,n-1) + AA_{10} , \qquad n=1 \quad (3.54a)$$

$$\phi^{II}(i,j,n) = \frac{1}{3}\left[-\phi^{II}(i,j,n-2)+4\phi^{II}(i,j,n-1)+2AA_{10}\right] , \quad n>1 \quad (3.54b)$$

where

$$AA_{10} = \frac{2}{3}\frac{\Delta\tau}{R_{II}}\{[\phi^{II}(i-1,j,n-1) - 3\phi^{II}(i,j,n-1) + 2\phi^{II}(i+1,j,n-1)]/\Delta\xi^2 +$$

$$+ [\phi^{II}(i,j-1,n-1)-3\phi^{II}(i,j,n-1)+2\phi^{II}(i,j+1,n-1)]/\Delta\eta^2\}. \quad (3.55)$$

(iv) Energy balance on the surface boundary (the moving asperity)

The dimensionless form for the surface boundary condition is:

$$\phi^{I}(i,1,n) = \phi^{I}(i,1,n-1) + (1+h')\frac{\Delta\tau}{R_I\Delta\eta} + AA_{11} , \qquad n=1 \quad (3.56a)$$

$$\phi^{I}(i,1,n) = \frac{1}{3}\left[-\phi^{I}(i,1,n-2) + 4\phi^{I}(i,1,n-1) + (1+h')\frac{\Delta\tau}{R_I\Delta\eta} + 2AA_{11}\right] , \quad n=2 \quad (3.56b)$$

where $h'=h/(\Delta x/2)$, h is defined in Appendix III, and

$$AA_{11} = \frac{\Delta\tau}{R_I}\{[\phi^{I}(i-1,1,n-1) - 2\phi^{I}(i,1,n-1) + \phi^{I}(i+1,1,n-1)]/\Delta\xi^2 +$$

$$+ 2[\phi^{I}(i,2,n-1) - \phi^{I}(i,1,n-1)]/\Delta\eta^2\} . \quad (3.57)$$

Equations (3.24, 3.26, 3.38, 3.40, 3.42, 3.44, 3.46, 3.48, 3.50,

3.52, 3.54, 3.56) constitute the general formulation of the problem with a complete set of difference equations for the solutions of the discrete temperature field $\{\phi(i,j,n)\}$ at some specific time. The computer programs which are used to compute the temperature field solutions are given in Appendix IV.

3.3 Numerical Results

Numerical results are obtained by using the non-uniform rectangular mesh corresponding to different cases of material properties and geometry. For the surface layer of silicon carbide, k_I=1.047 J/cm.^{0}C.s, κ_I=0.49 cm^2/s, and c_I=712 J/kg.^{0}C. For the substrate of aluminum, k_{II}=2.02 J/cm.^{0}C.s, κ_{II}=0.961 cm^2/s, and c_{II}=917 J/kg.^{0}C. The other numerical parameters on the asperity and the cavity are: v=15 m/s, w=10a, H=1.2a, b=1.9a, d=0.3a, e=0.5a, a=1mm, the smallest $\Delta\xi$ and $\Delta\eta$ are 0.02 and 0.01 respectively, and $\Delta\tau$=0.01. In the limiting case of no cavity, the maximum dimensionless temperature at the surface of the coated media was found to be 0.124 by using the Fourier transform method [33, 34]. The result at the same point by the current finite difference formulation is 0.123. The error is less than 1%. The numerical scheme is therefore confirmed by the benchmark problem.

The solutions for a single material with and without a cavity would then be compared with two limiting cases. For the first case, the cavity is located entirely in the surface layer, Figure 3.4a. In the second case, the top edge of the cavity is at the layer/substrate interface, Figure 3.4b. The solutions for the single material without and with a cavity are designated as the third and the fourth cases, respectively, included for the purpose of comparison. Different cases of the temperature field solutions are given in Table 1. In Case 1,

Table 1

case	k_I	k_{II}	$(\rho c)_I$	$(\rho c)_{II}$	κ_I	κ_{II}	L	cavity location
1A	$1k_I$	$1k_{II}$	$1(\rho c)_I$	$1(\rho c)_{II}$	$1\kappa_I$	$1\kappa_{II}$	0.04	coating layer
1B	$1k_I$	$1k_{II}$	$1(\rho c)_I$	$1(\rho c)_{II}$	$1\kappa_I$	$1\kappa_{II}$	0.06	coating layer
1C	$1k_I$	$1k_{II}$	$\frac{1}{2}(\rho c)_I$	$1(\rho c)_{II}$	$2\kappa_I$	$1\kappa_{II}$	0.04	coating layer
1D	$\frac{7}{4}k_I$	$1k_{II}$	$\frac{7}{4}(\rho c)_I$	$1(\rho c)_{II}$	$1\kappa_I$	$1\kappa_{II}$	0.04	coating layer
1E	$1k_I$	$1k_{II}$	$1(\rho c)_I$	$1(\rho c)_{II}$	$1\kappa_I$	$1\kappa_{II}$	0.1	coating layer
2A	$1k_I$	$1k_{II}$	$1(\rho c)_I$	$1(\rho c)_{II}$	$1\kappa_I$	$1\kappa_{II}$	0.04	interface
2B	$1k_I$	$2k_I$	$1(\rho c)_I$	$2(\rho c)_I$	$1\kappa_I$	$1\kappa_I$	0.04	interface
2C	$1k_I$	$\frac{1}{2}k_I$	$1(\rho c)_I$	$\frac{1}{2}(\rho c)_I$	$1\kappa_I$	$1\kappa_I$	0.04	interface
2D	$1k_I$	$1k_I$	$1(\rho c)_I$	$\frac{1}{2}(\rho c)_I$	$1\kappa_I$	$2\kappa_I$	0.04	interface
2E	$1k_I$	$2k_I$	$1(\rho c)_I$	$1(\rho c)_I$	$1\kappa_I$	$2\kappa_I$	0.04	interface
3	$1k_I$		$1(\rho c)_I$		$1\kappa_I$			no cavity
4	$1k$		$1(\rho c)$		1κ		0.04	single material

* Base materials for the coating layer and the substrate are silicon carbide and aluminum, respectively.

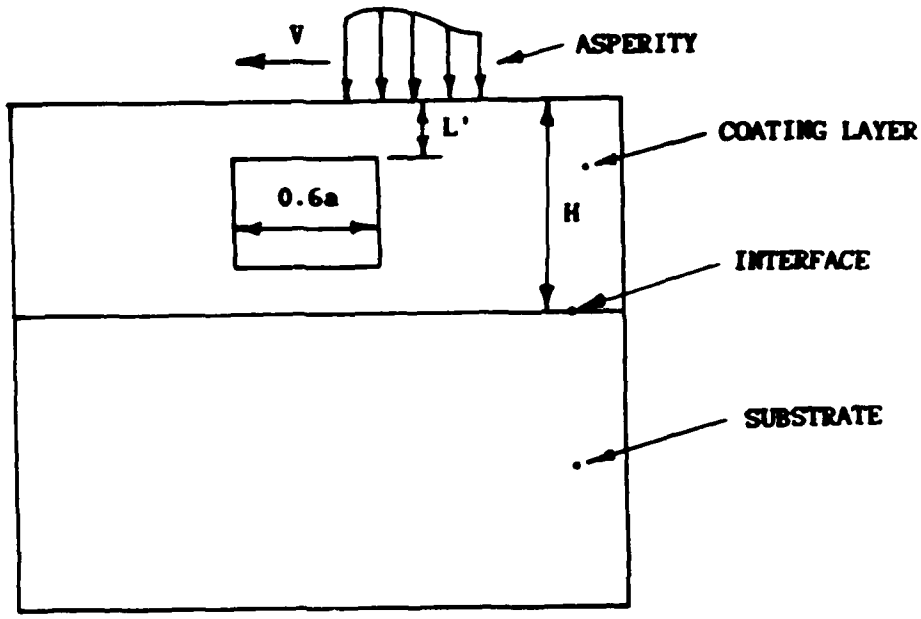

(a) cavity is in the coating layer

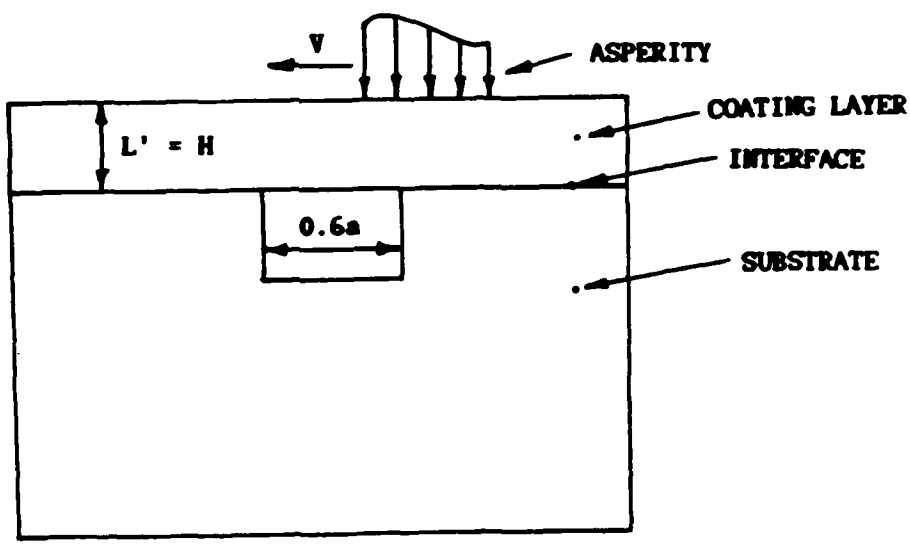

(b) top edge of the cavity is at the interface

Figure 3.4 Numerical examples with different cavity position.

three different values of the ligament thickness: 0.04 (Case 1A), 0.06 (Case 1B), and 0.1 (Case 1E), are used to illustrate the effect of the ligament volume. The temperature fields at two depths, for all three Cases 1A, 1B and 1E are shown in Figure 3.5. In the figure, the cavity width is from ξ=1.6 to 2.2. The asperity position, at the dimensionless time τ=1.04, respresenting the worst case, is from ξ=1.2 to 2.2. The relative positions of the asperity and the cavity is shown in Figure 3.6.

The Case 1A then is compared with Case 2 of the same ligament thickness for which the top edge of the cavity is at the layer/substrate interface. The effect of the relative position of the cavity to the interface is shown in Figure 3.7. It is noticed that when the top edge of the cavity is at the interface, the temperature field in the region immediately on the trailing edge of the asperity will be affected by the substrate material.

The effect of the heat capacity and thermal conductivity of the surface layer for Case 1A is shown in Figure 3.8. The figure shows the original value as Case 1A. Case 1C represents a reduction of thermal capacity of the surface layer by half. Case 1D shows the result of an increase in thermal conductivity of the surface layer by 75%. The thermal conductivity of the surface layer is shown to have little effect on the nondimensional surface temperature. But the real temperature field, $T=q_o a\phi/k_I$, is lowered with increasing thermal conductivity k_I.

Figures 3.9 and 3.10 illustrate the effect of a cavity on the direction of heat flux. The figures show the nondimensional heat flux components in ξ and η directions of a single material without a cavity

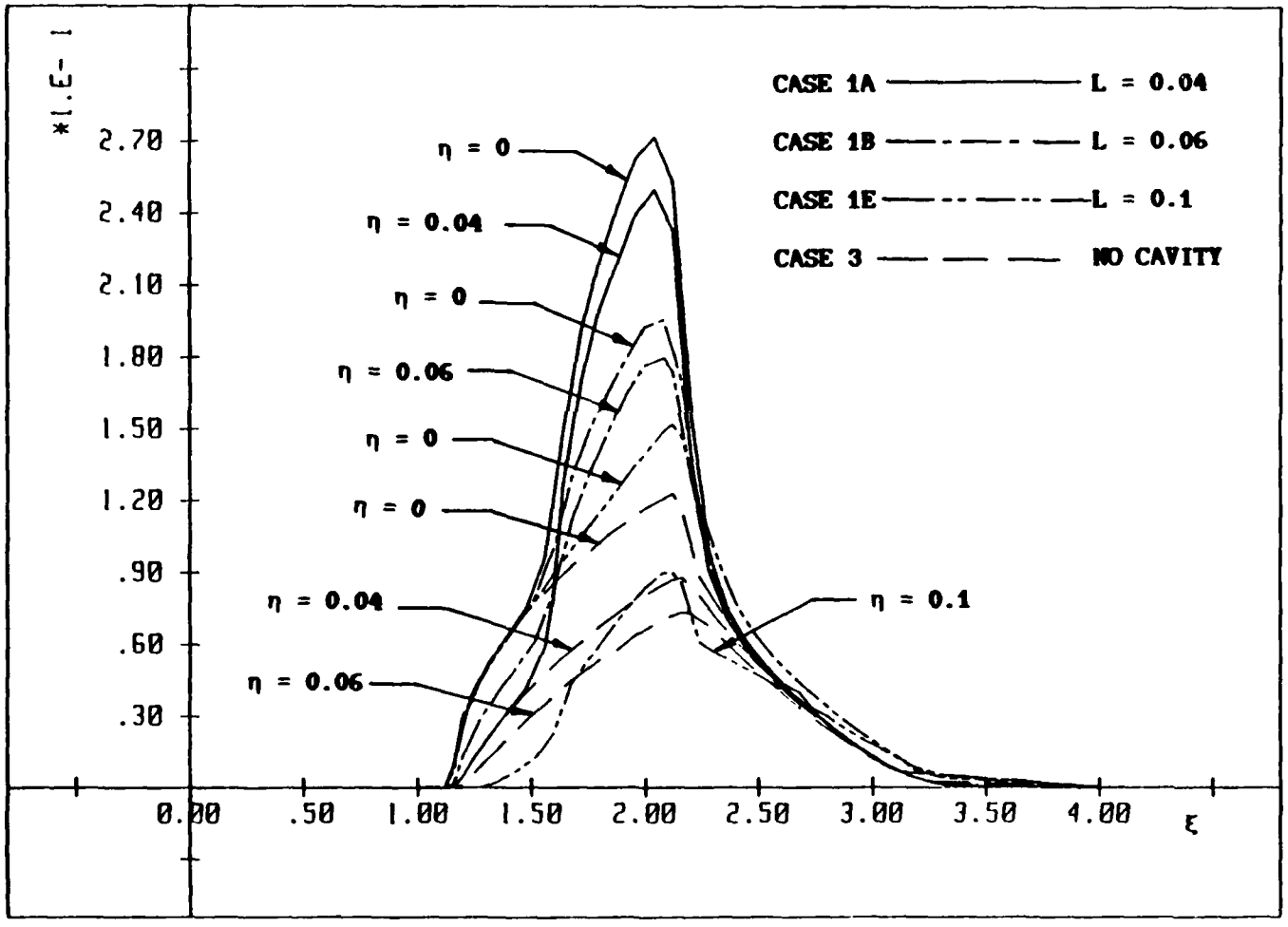

Figure 3.5 Dimensionless temperature field (cases 1A,1B,1E,3).

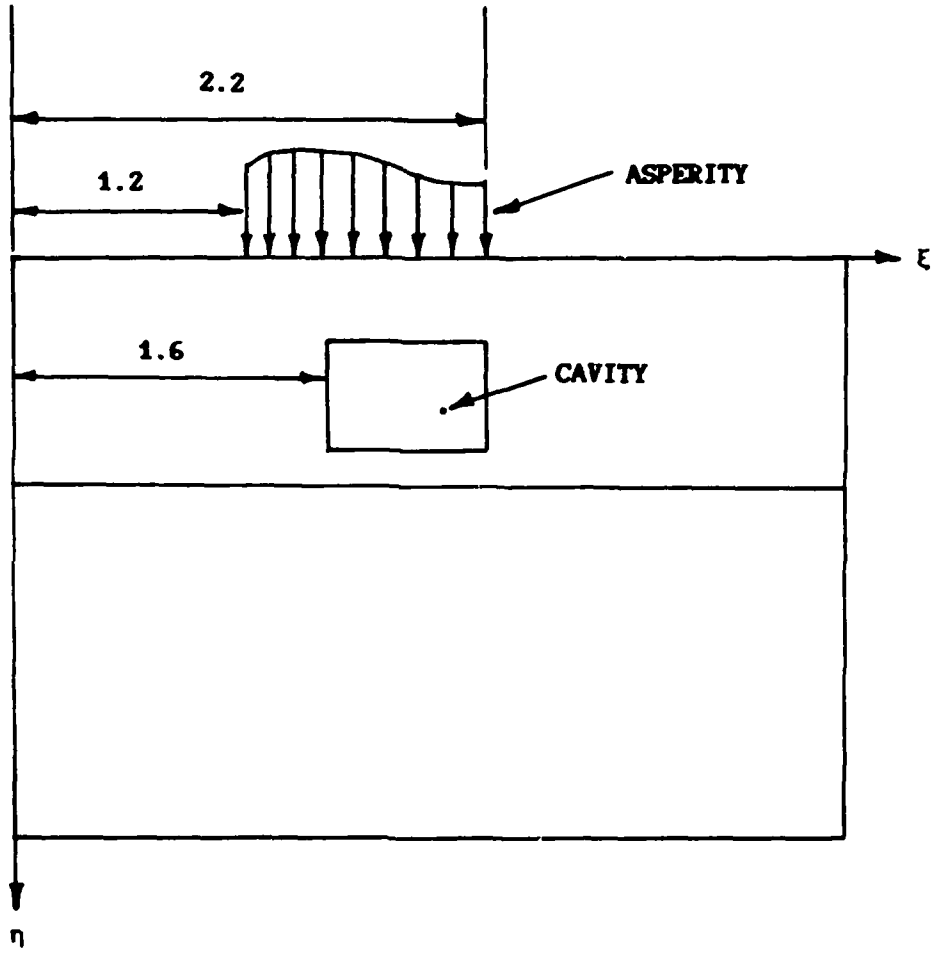

Figure 3.6 The relative positions of the cavity and the asperity at $\tau = 1.04$.

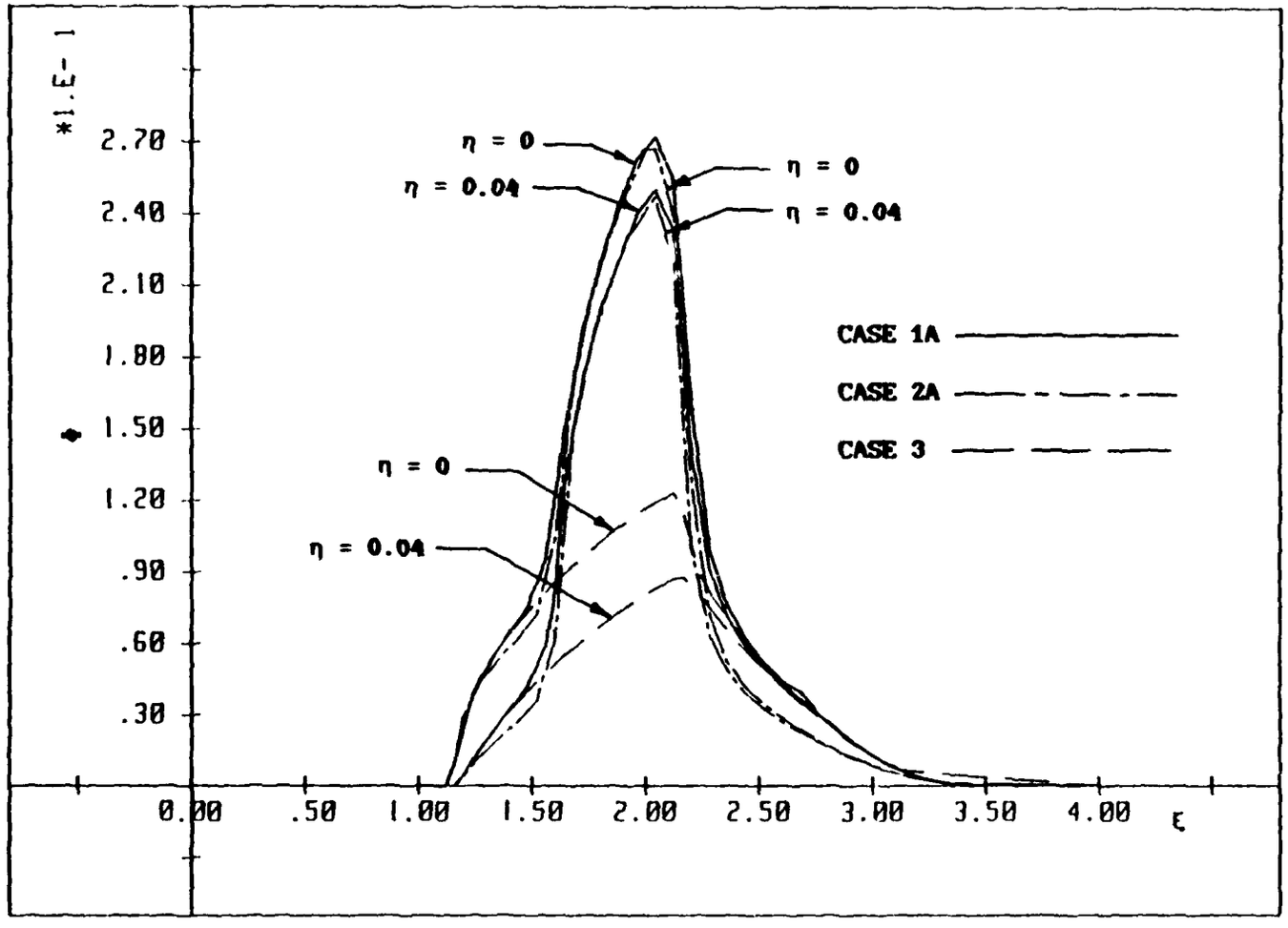

Figure 3.7 Dimensionless temperature field (cases 1A,2A,3).

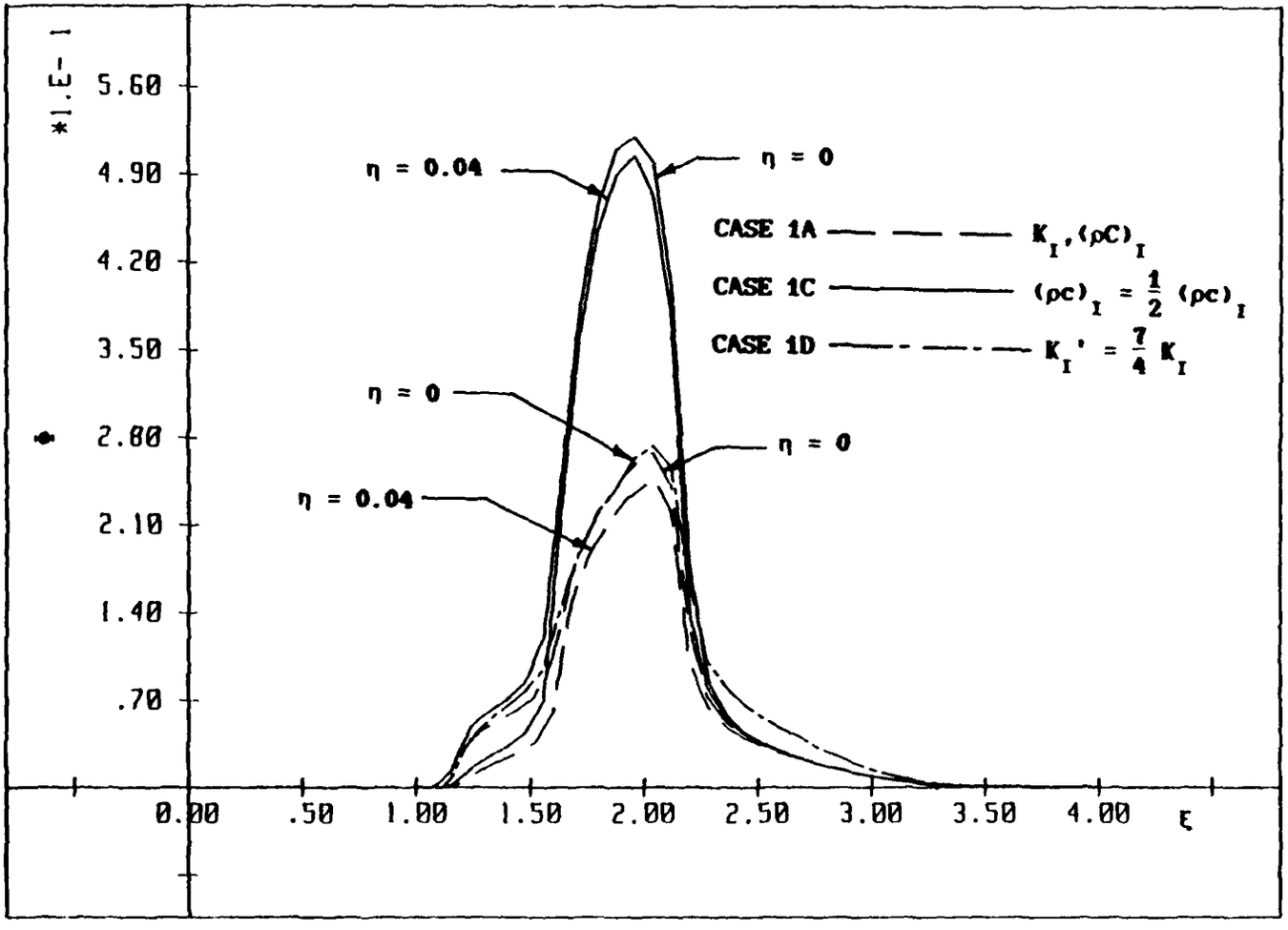

Figure 3.8 Dimensionless temperature field (cases 1A,1C,1D).

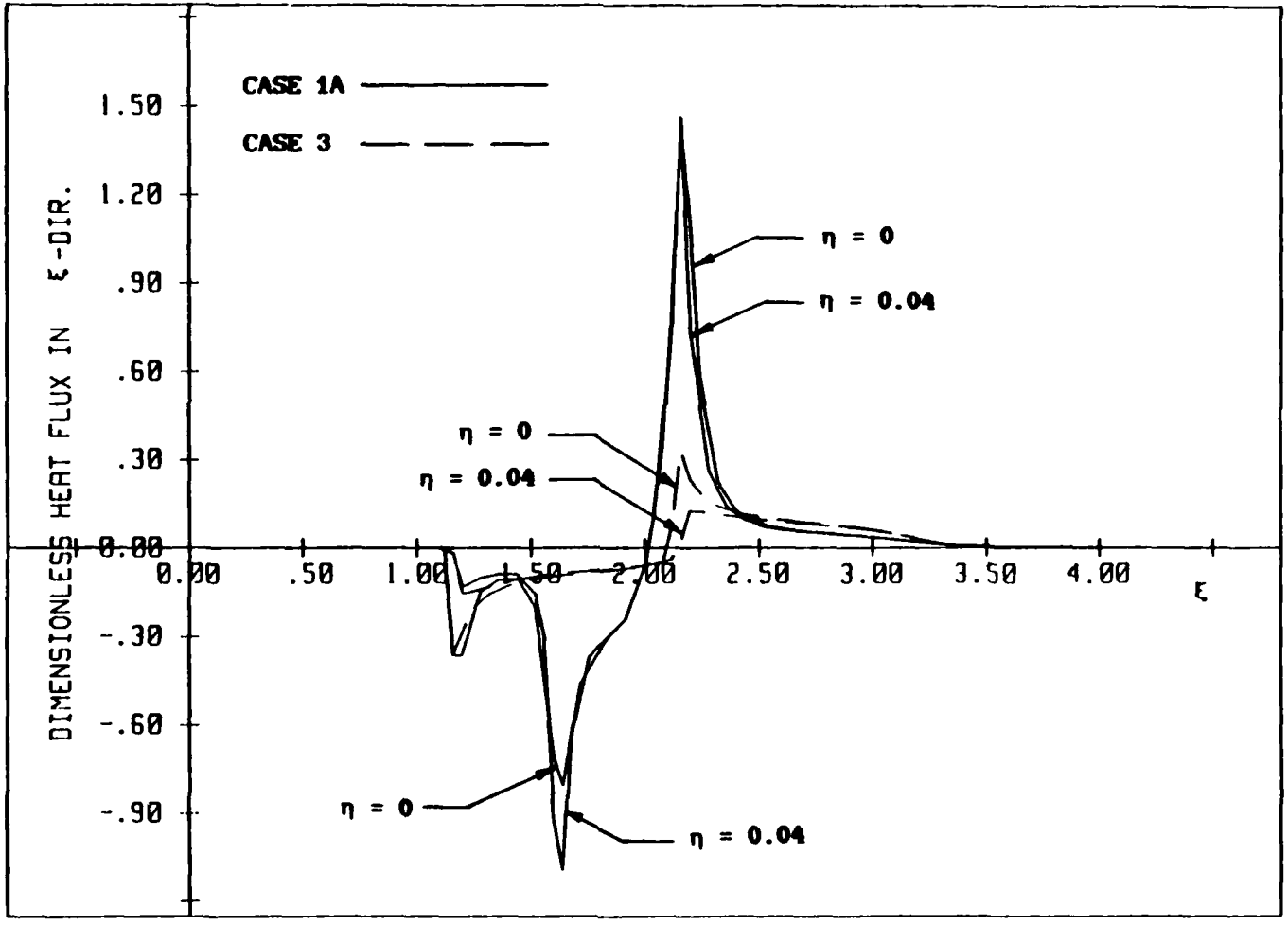

Figure 3.9 Dimensionless heat flux in ξ direction (cases 1A,3).

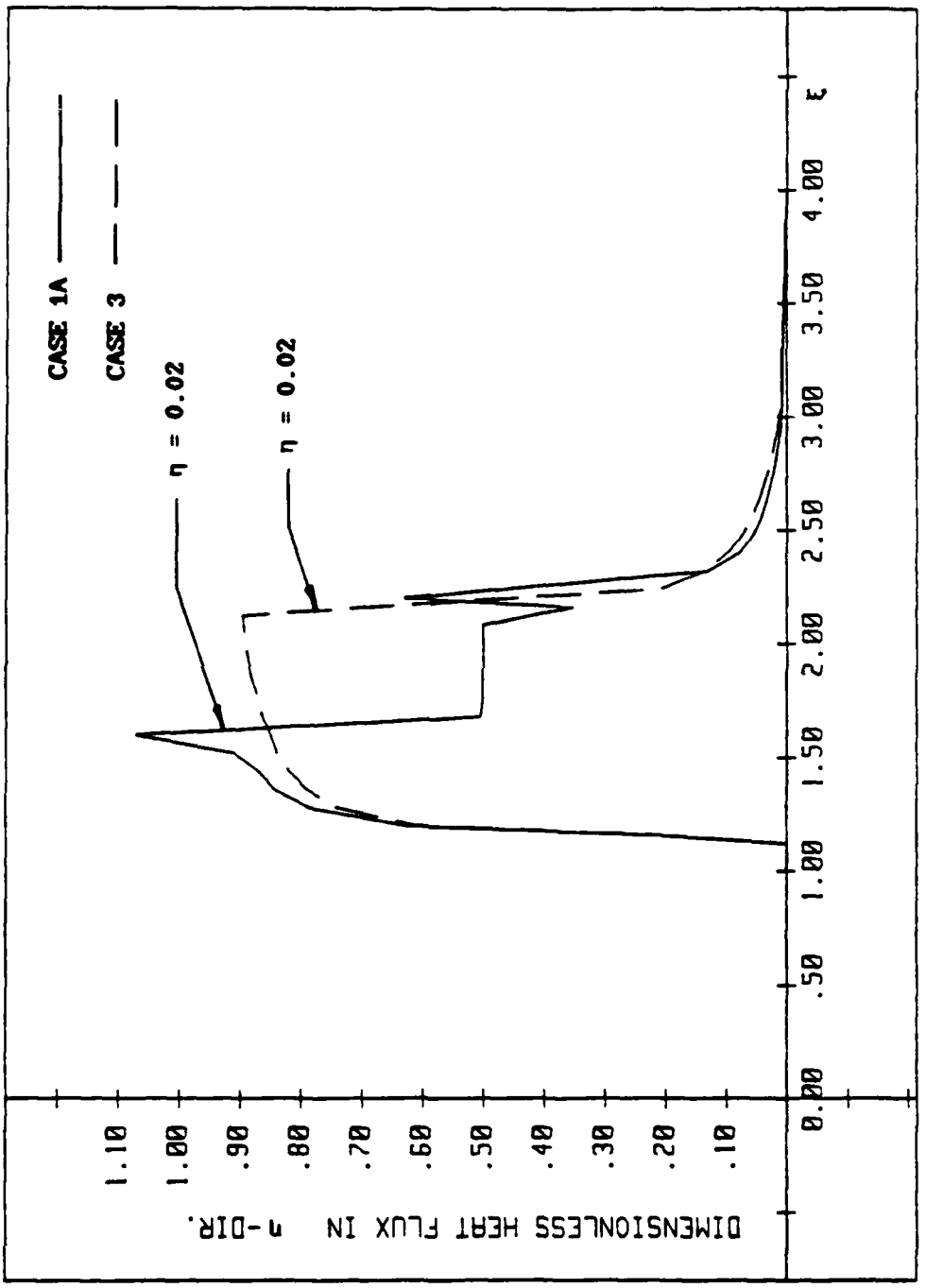

Figure 3.10 Dimensionless heat flux in η direction (cases 1A,3)

(Case 3) and a layered medium with a cavity (Case 1A). From the figures, it is observed that, with no cavity, the heat flux at ξ=2.2, and η=0.04 has a magnitude of 0.7 at an angle of 82^0 to the wear surface. With a cavity, at the same location, the magnitude is increased to 1.5 at an angle 23^0 to the wear surface. Hence, the existence of the cavity will increase the heat flux tremendously, especially in the ξ direction near the upper trailing corner of the cavity. Figures 3.9 and 3.10 demonstrate not only an increase in magnitude of the heat flux, hence the temperature gradient, but also the flux at a more oblique angle to the wear surface.

Ju [28] has studied the effect of thermal properties of a single material subjected to the high-speed asperity excitation. It was pointed out that thermal conductivity (k) and thermal capacity (ρc) are the parameters controlling the temperature field. For layered media, a similar effect was found by Ju and Liu [35]. For the case of a layered medium with a cavity, the thermal property variation in the coating layer can be accordingly extrapolated. It is the effect of the substrate in the neighborhood of the cavity that would be influential in determining the temperature field in the critical region. The effect of thermal property variation for the substrate is therefore studied numerically for the Case 2, for which the coating/substrate interface is at the top edge of the cavity. For this case, the thermal properties of the substrate will be of immediate influence to the temperature field in the vicinity of the top trailing corner of the cavity. For the purpose of demonstrating the individual effect, a benchmark case is chosen for comparison in which both the coating and the substrate are of silicon carbide, (k_I=k_{II}=1.047 J/cm.^{0}C.s,

$\kappa_I=\kappa_{II}$=0.49 cm^2/s, $\rho_I c_I=\rho_{II} c_{II}$=2.137 $J/cm^3.C$), designated as Case 4. Figure 3.11 illustrates the temperature field near the top surface and at the coating/substrate interface for cases with marked changes in thermal properties from those given in Case 4. Case 2B shows no change in the substrate diffusivity, but both the thermal conductivity and the thermal capacity are doubled. The ensuing improved conductivity and capacity in the substrate allow a significant heat flow into the substrate; thus a high temperature gradient is also found. The Case 2C, at the same diffusivity, but with both the thermal conductivity and the thermal capacity halved, shows a reduced heat flow into the substrate, with a corresponding low temperature gradient. Cases 2D and 2E, with doubled diffusivity, but with half capacity and double conductivity, respectively, showed reduced and increased heat flow into the substrate, respectively. The heat flux, being proportional to the temperature gradient, is illustrated in Figures 3.12 and 3.13 for the surface region and at the interface.

Figure 3.14 shows the transient temperature for Case 1A (cavity in the coating and ligament thickness of 0.04) in comparison to the case of a single material without cavity (Case 3). The dimensionless temperature, $\phi=Tk_I/q_0 a$, plotted against dimensionless time, $\tau=vt/a$, at the surface and at the ligament depth, $\eta=0.04$, for the position $\xi=2.2$, where the temperature is maximum in the vicinity of the cavity. It is shown that, before the asperity reaches the point, the temperature is low. Then the surface temperature increases and reaches a maximum when the asperity just passes over the trailing edge of the cavity. After the passing of the asperity, the temperature at the trailing corner of the cavity drops again.

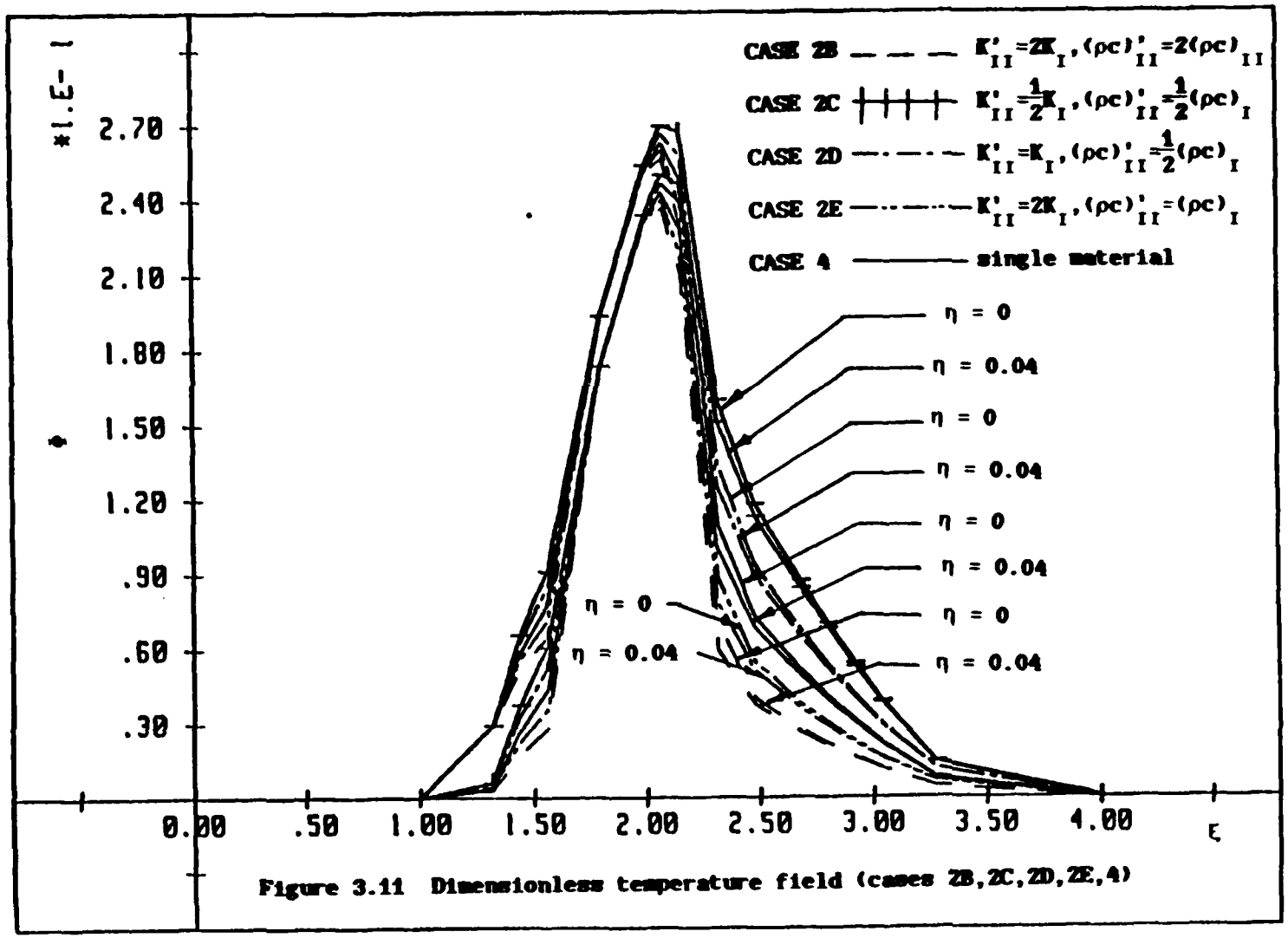

Figure 3.11 Dimensionless temperature field (cases 2B,2C,2D,2E,4)

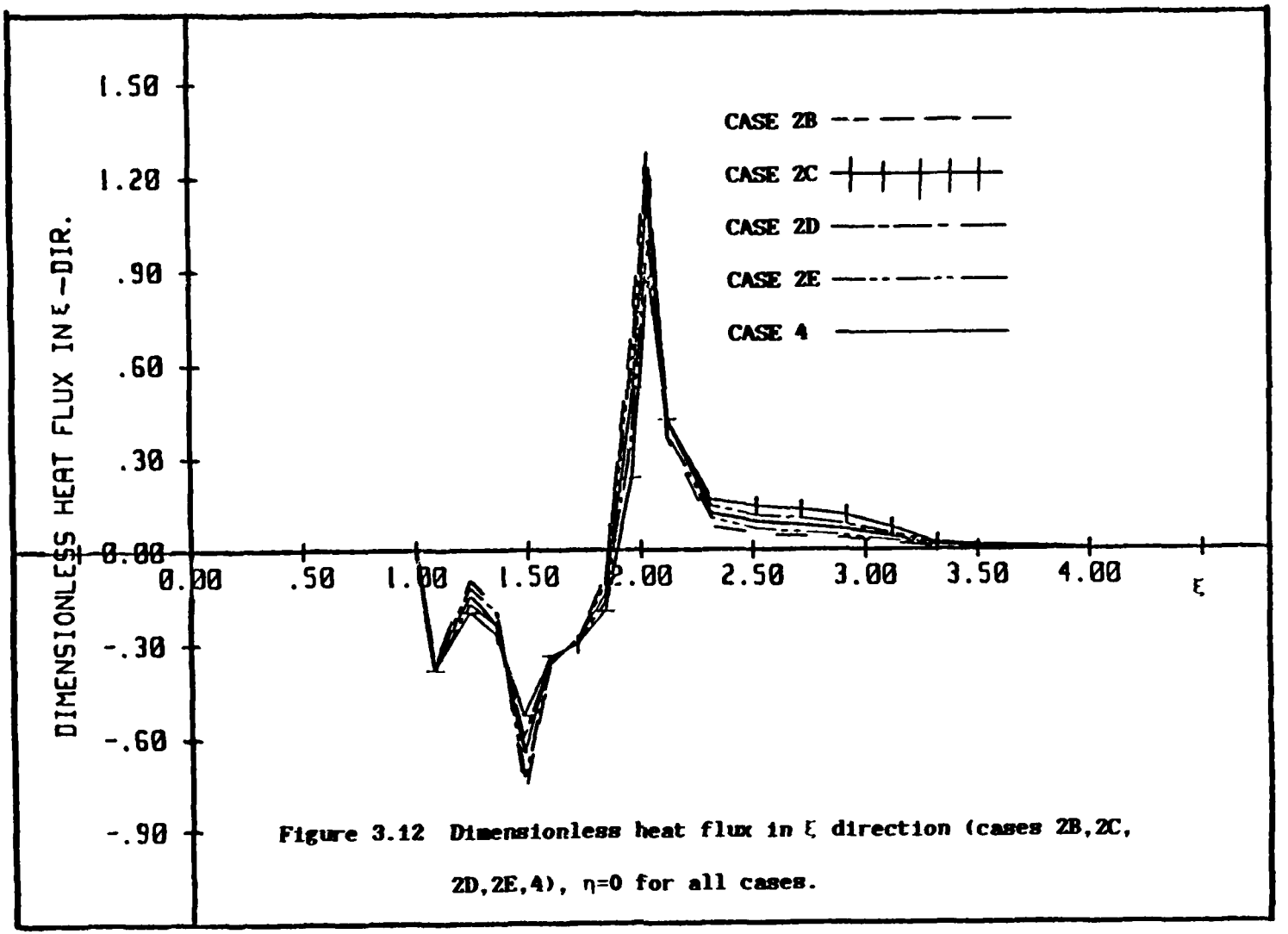

Figure 3.12 Dimensionless heat flux in ξ direction (cases 2B,2C, 2D,2E,4), η=0 for all cases.

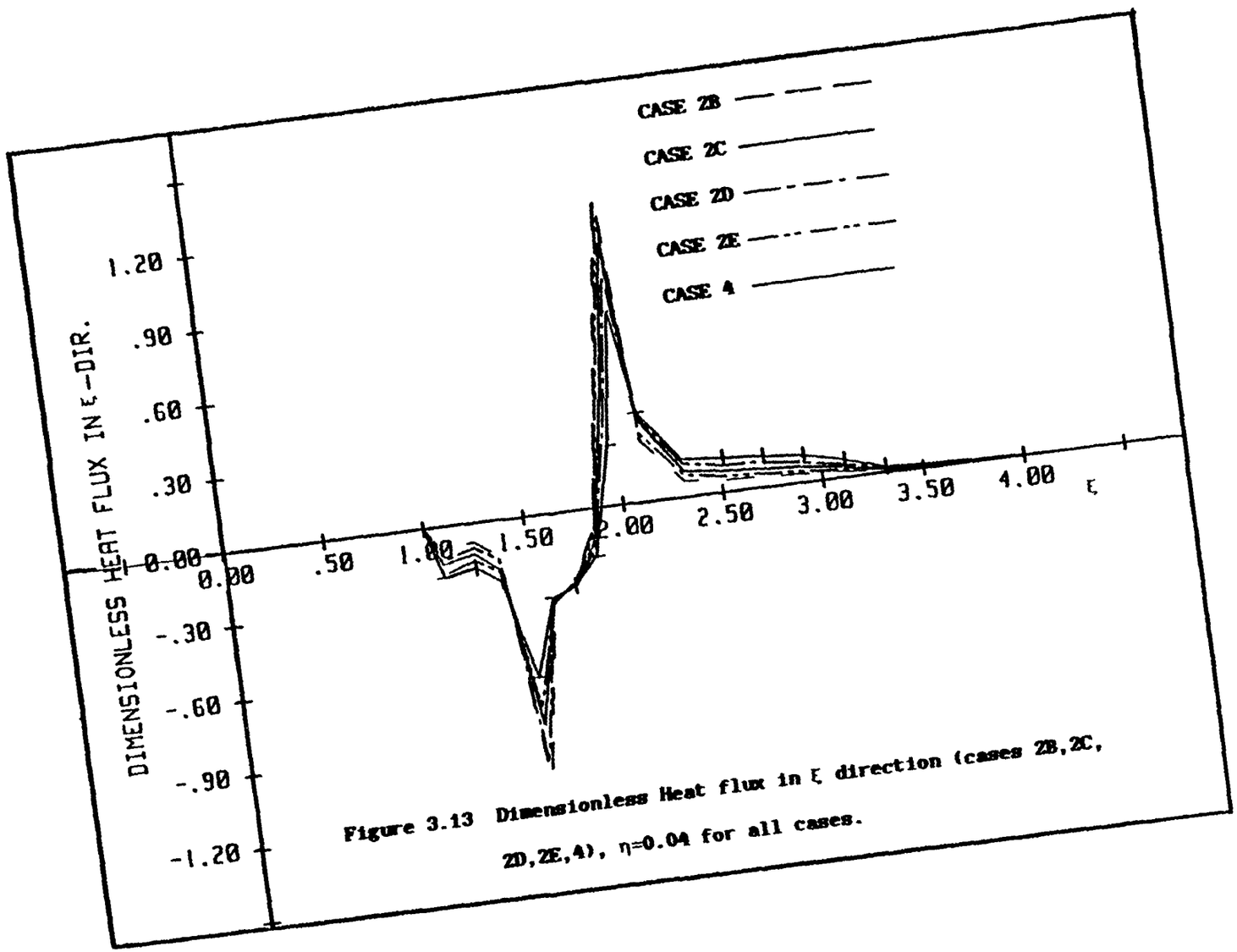

Figure 3.13 Dimensionless Heat flux in ξ direction (cases 2B,2C, 2D,2E,4), η=0.04 for all cases.

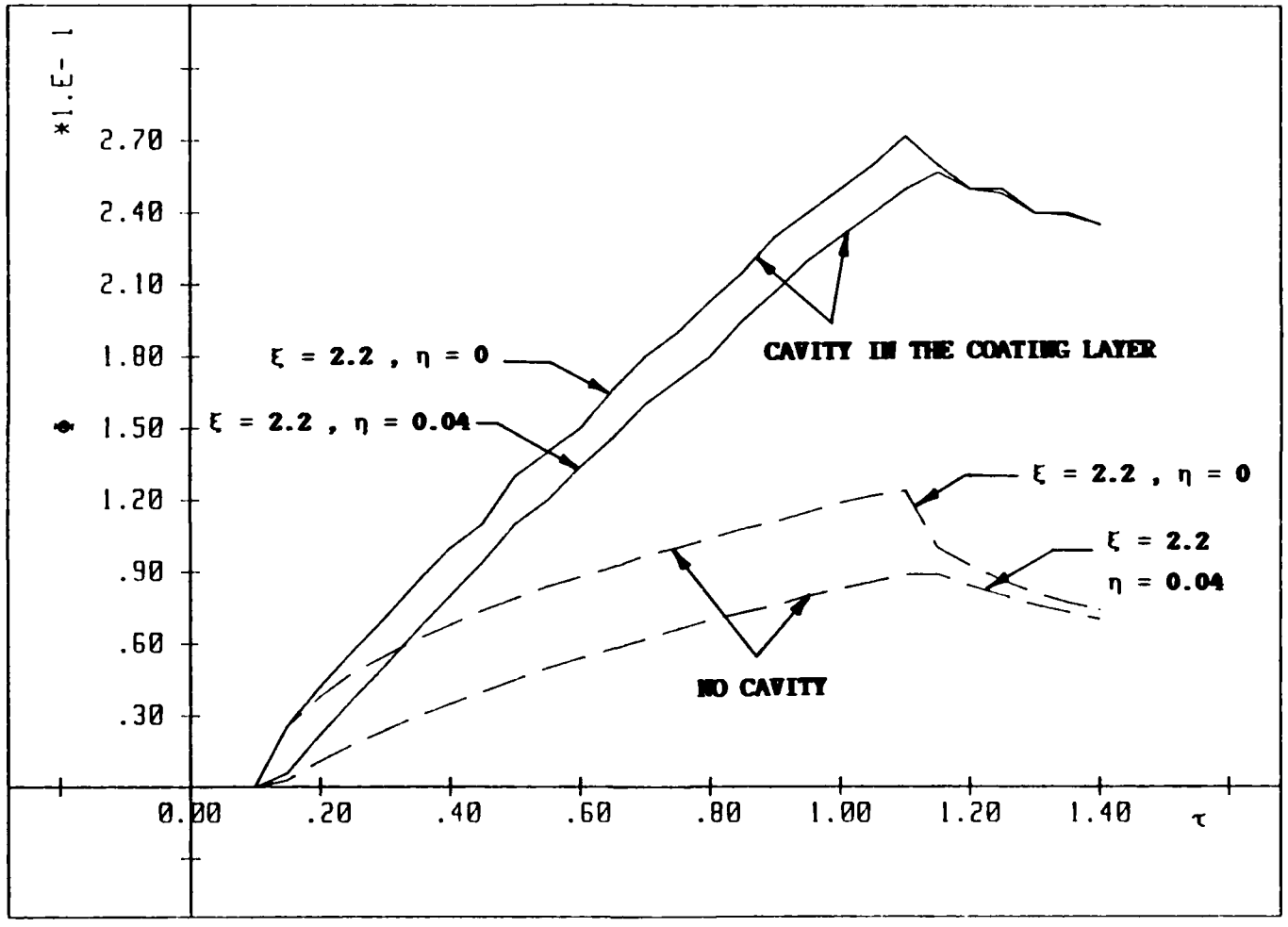

Figure 3.14 Dimensionless temperature field (cases 1A,3).

CHAPTER 4

STRESS SOLUTION

Ju et al [28,29,30,31,32,33,34] established that, for a moderately high-speed asperity excitation, the thermal stress effect dominates the stress field and eventually leads to failure in the no-cavity case. Liu [58] in his thesis also showed that, if the asperity speed is larger than 0.127 m/s (5 in/s), the thermal stress dominates the failure, and the mechanical stress becomes less important. However, the mechanical stress may not be trivial when a cavity exists. Therefore, both the mechanical and thermal stress field will be presented in this chapter.

The thermoelastic Navier's equations and the Hooke's law in dimensionless form are:

$$\frac{\partial}{\partial\xi}\left(N_1\frac{\partial u^\beta}{\partial\xi}\right)+\frac{\partial}{\partial\xi}\left(N_2\frac{\partial v^\beta}{\partial\eta}\right)+\frac{\partial}{\partial\eta}\left(N_3\frac{\partial v^\beta}{\partial\xi}\right)+\frac{\partial}{\partial\eta}\left(N_3\frac{\partial u^\beta}{\partial\eta}\right)-$$

$$-\frac{\partial}{\partial\xi}\left(\frac{b_\beta^2\gamma_\beta}{c_2^2}\phi^\beta\right)=\delta M^2\frac{\partial^2 u^\beta}{\partial\tau^2}\quad, \tag{4.1}$$

$$\frac{\partial}{\partial\xi}\left(N_3\frac{\partial v^\beta}{\partial\xi}\right)+\frac{\partial}{\partial\eta}\left(N_2\frac{\partial u^\beta}{\partial\xi}\right)+\frac{\partial}{\partial\xi}\left(N_3\frac{\partial u^\beta}{\partial\eta}\right)+\frac{\partial}{\partial\eta}\left(N_1\frac{\partial v^\beta}{\partial\eta}\right)-$$

$$-\frac{\partial}{\partial\eta}\left(\frac{b_\beta^2\gamma_\beta}{c_2^2}\phi^\beta\right)=\delta M^2\frac{\partial^2 v^\beta}{\partial\tau^2}\quad, \tag{4.2}$$

$$\sigma_{\xi\xi}^\beta=\frac{\mu_2}{P_0}\delta\left(N_1\frac{\partial u^\beta}{\partial\xi}+N_2\frac{\partial v^\beta}{\partial\eta}-\frac{b_\beta^2\gamma_\beta}{c_2^2}\phi^\beta\right), \tag{4.3}$$

$$\sigma_{\xi\eta}^\beta=\frac{\mu_2}{P_0}\delta N_3\left(\frac{\partial u^\beta}{\partial\eta}+\frac{\partial v^\beta}{\partial\xi}\right), \tag{4.4}$$

and

$$\sigma^{\beta}_{\eta\eta} = \frac{\mu_2}{P_0}\,\delta\,\left(N_2 \frac{\partial u^{\beta}}{\partial \xi} + N_1 \frac{\partial v^{\beta}}{\partial \eta} - \frac{b_{\beta}^2 \gamma_{\beta}}{c_2^2}\,\phi^{\beta} \right) . \qquad (4.5)$$

where u^{β} and v^{β} are respectively the dimensionless stress modulated by the average pressure P_0; $M=(v/c_2)$ is the Mach number; V is the asperity speed; $N_1=(\lambda_{\beta} + 2\mu_{\beta})/\rho_{II}c_2$; $N_2=\lambda_{\beta}/\rho_{II}c_2$; $N_3=\mu_{\beta}/\rho_{II}c_2$; $b_{\beta}^2=(3\lambda_{\beta}+2\mu_{\beta})/\rho_{II}$; $\gamma_{\beta}=(q_0 a\alpha_{\beta})/k_I$; $\delta=\rho_{\beta}/\rho_{II}$, $c_1 = [(\lambda_{II} + 2\mu_{II})/\rho_{II}]^{1/2}$, $c_2 = (\mu_{II}/\rho_{II})^{1/2}$ are the dilatational and shear wave speed, respectively; ξ, η, τ, λ, μ_{β}, α_{β}, ρ_{β} and ϕ^{β} were defined in Chapters 2 and 3.

Equations for the mechanical stress field are the same as the thermal stress field except that there is no temperature effect.

4.1 Perturbation Method

For hard wear materials, such as Stellite *III*, the Mach number *M* is of the order of 10^{-3}. Since M^2 is a parameter which is sufficiently small, Equations (4.1) and (4.2) can be solved by the perturbation method.

Let the solutions to (4.1) and (4.2) be expressed as a power series of $\epsilon=M^2$; that is

$$u^{\beta}(\xi,\eta,\tau,\epsilon) = u_0^{\beta}(\xi,\eta,\tau) + \epsilon u_1^{\beta}(\xi,\eta,\tau) + \epsilon^2 u_2^{\beta}(\xi,\eta,\tau) + \ldots , \qquad (4.6)$$

$$v^{\beta}(\xi,\eta,\tau,\epsilon) = v_0^{\beta}(\xi,\eta,\tau) + \epsilon v_1^{\beta}(\xi,\eta,\tau) + \epsilon^2 v_2^{\beta}(\xi,\eta,\tau) + \ldots , \qquad (4.7)$$

when equations (4.6) and (4.7) are substituted into equations (4.1) and (4.2), the terms with the same power of ϵ are grouped, leading to a set of equations for u_0^{β}, u_1^{β}, u_2^{β}, ..., and v_0^{β}, v_1^{β}, v_2^{β}, ..., as

follows:

For the terms of the zeroth order in ϵ,

$$\frac{\partial}{\partial\xi}\left(N_1\frac{\partial u_0^\beta}{\partial\xi}\right)+\frac{\partial}{\partial\xi}\left(N_2\frac{\partial v_0^\beta}{\partial\eta}\right)+\frac{\partial}{\partial\eta}\left(N_3\frac{\partial v_0^\beta}{\partial\xi}\right)+\frac{\partial}{\partial\eta}\left(N_3\frac{\partial u_0^\beta}{\partial\eta}\right)=$$

$$=\frac{\partial}{\partial\xi}\left(\frac{b_\beta^2\gamma_\beta}{c_2^2}\phi^\beta\right), \tag{4.8}$$

$$\frac{\partial}{\partial\xi}\left(N_3\frac{\partial v_0^\beta}{\partial\xi}\right)+\frac{\partial}{\partial\eta}\left(N_2\frac{\partial u_0^\beta}{\partial\xi}\right)+\frac{\partial}{\partial\xi}\left(N_3\frac{\partial u_0^\beta}{\partial\eta}\right)+\frac{\partial}{\partial\eta}\left(N_1\frac{\partial v_0^\beta}{\partial\eta}\right)=$$

$$=\frac{\partial}{\partial\eta}\left(\frac{b_\beta^2\gamma_\beta}{c_2^2}\phi^\beta\right). \tag{4.9}$$

For the terms of the first order in ϵ,

$$\frac{\partial}{\partial\xi}\left(N_1\frac{\partial u_1^\beta}{\partial\xi}\right)+\frac{\partial}{\partial\xi}\left(N_2\frac{\partial v_1^\beta}{\partial\eta}\right)+\frac{\partial}{\partial\eta}\left(N_3\frac{\partial v_1^\beta}{\partial\xi}\right)+\frac{\partial}{\partial\eta}\left(N_3\frac{\partial u_1^\beta}{\partial\eta}\right)=$$

$$=\delta\frac{\partial^2 u_0^\beta}{\partial\tau^2}, \tag{4.10}$$

$$\frac{\partial}{\partial\xi}\left(N_3\frac{\partial v_1^\beta}{\partial\xi}\right)+\frac{\partial}{\partial\eta}\left(N_2\frac{\partial u_1^\beta}{\partial\xi}\right)+\frac{\partial}{\partial\xi}\left(N_3\frac{\partial u_1^\beta}{\partial\eta}\right)+\frac{\partial}{\partial\eta}\left(N_1\frac{\partial v_1^\beta}{\partial\eta}\right)=$$

$$=\delta\frac{\partial^2 v_0^\beta}{\partial\tau^2}. \tag{4.11}$$

For the higher order solutions, it is evident that the equations are recursive. Accordingly, the recurrence formulas can be written as:

$$\frac{\partial}{\partial\xi}\left(N_1\frac{\partial u_i^\beta}{\partial\xi}\right)+\frac{\partial}{\partial\xi}\left(N_2\frac{\partial v_i^\beta}{\partial\eta}\right)+\frac{\partial}{\partial\eta}\left(N_3\frac{\partial v_i^\beta}{\partial\xi}\right)+\frac{\partial}{\partial\eta}\left(N_3\frac{\partial u_i^\beta}{\partial\eta}\right)=$$

$$=\delta_{i0}\frac{\partial}{\partial\xi}\left(\frac{b_\beta^2\gamma_\beta}{c_2^2}\phi^\beta\right)+(1-\delta_{i0})\delta\frac{\partial^2 u_{i-1}^\beta}{\partial\tau^2}, \tag{4.12}$$

$$\frac{\partial}{\partial\xi}\left(N_3\frac{\partial v_i^\beta}{\partial\xi}\right)+\frac{\partial}{\partial\eta}\left(N_2\frac{\partial u_i^\beta}{\partial\xi}\right)+\frac{\partial}{\partial\xi}\left(N_3\frac{\partial u_i^\beta}{\partial\eta}\right)+\frac{\partial}{\partial\eta}\left(N_1\frac{\partial v_i^\beta}{\partial\eta}\right)=$$

$$=\delta_{io}\frac{\partial}{\partial\eta}\left(\frac{b_\beta^2\gamma_\beta}{c_2^2}\phi^\beta\right)+(1-\delta_{io})\delta\frac{\partial^2 v_{i-1}^\beta}{\partial\tau^2}\ , \qquad (4.13)$$

where δ_{io} is Kronecker delta.

Similarly, we can obtain a set of equations for the stress field as follows:

For the terms of the zeroth order in ϵ,

$${}^o\sigma_{\xi\xi}^\beta=\frac{\mu_2}{P_o}\delta\left(N_1\frac{\partial u_0^\beta}{\partial\xi}+N_2\frac{\partial v_0^\beta}{\partial\eta}-\frac{b_\beta^2\gamma_\beta}{c_2^2}\phi^\beta\right), \qquad (4.14)$$

$${}^o\sigma_{\xi\eta}^\beta=\frac{\mu_2}{P_o}\delta N_3\left(\frac{\partial u_0^\beta}{\partial\eta}+\frac{\partial v_0^\beta}{\partial\xi}\right), \qquad (4.15)$$

$${}^o\sigma_{\eta\eta}^\beta=\frac{\mu_2}{P_o}\delta\left(N_2\frac{\partial u_0^\beta}{\partial\xi}+N_1\frac{\partial v_0^\beta}{\partial\eta}-\frac{b_\beta^2\gamma_\beta}{c_2^2}\phi^\beta\right). \qquad (4.16)$$

For the terms of the first order in ϵ,

$${}^1\sigma_{\xi\xi}^\beta=\frac{\mu_2}{P_o}\delta\left(N_1\frac{\partial u_1^\beta}{\partial\xi}+N_2\frac{\partial v_1^\beta}{\partial\eta}-\frac{b_\beta^2\gamma_\beta}{c_2^2}\phi^\beta\right), \qquad (4.17)$$

$${}^1\sigma_{\xi\eta}^\beta=\frac{\mu_2}{P_o}\delta N_3\left(\frac{\partial u_1^\beta}{\partial\eta}+\frac{\partial v_1^\beta}{\partial\xi}\right), \qquad (4.18)$$

$${}^1\sigma_{\eta\eta}^\beta=\frac{\mu_2}{P_o}\delta\left(N_2\frac{\partial u_1^\beta}{\partial\xi}+N_1\frac{\partial v_1^\beta}{\partial\eta}-\frac{b_\beta^2\gamma_\beta}{c_2^2}\phi^\beta\right). \qquad (4.19)$$

The recurrence formulas for the stress field are

$${}^i\sigma_{\xi\xi}^\beta=\frac{\mu_2}{P_o}\delta\left(N_1\frac{\partial u_i^\beta}{\partial\xi}+N_2\frac{\partial v_i^\beta}{\partial\eta}-\frac{b_\beta^2\gamma_\beta}{c_2^2}\phi^\beta\right), \qquad (4.20)$$

$$ {}^{i}\sigma^{\beta}_{\xi\eta} = \frac{\mu_2}{P_0}\,\delta N_3 \left(\frac{\partial u_1^{\beta}}{\partial \eta} + \frac{\partial v_1^{\beta}}{\partial \xi} \right) , \tag{4.21} $$

$$ {}^{i}\sigma^{\beta}_{\eta\eta} = \frac{\mu_2}{P_0}\,\delta \left(N_2 \frac{\partial u_1^{\beta}}{\partial \xi} + N_1 \frac{\partial v_1^{\beta}}{\partial \eta} - \frac{b_\beta^2 \gamma_\beta}{{c_2}^2}\,\phi^{\beta} \right) . \tag{4.22} $$

The boundary conditions are as follows:

For the zeroth order solutions,

(i) the surface $(c(t)/a \leq \xi \leq [c(t)/a + 1],\ \eta=0)$ is traction prescribed

$$ {}^{o}\sigma^{I}_{\xi\eta} = \mu_f G , \tag{4.23} $$

$$ {}^{o}\sigma^{I}_{\eta\eta} = -G , \tag{4.24} $$

where

$$ G = \begin{cases} P'(\xi) , & \text{for the mechanical stress field} \\ 0 , & \text{for the thermal stress field} \end{cases} $$

(ii) the regularity conditions at infinity, $\xi^2+\eta^2 \to \infty$, are

$$ u_0^{\beta},\ v_0^{\beta},\ {}^{o}\sigma^{\beta}_{\xi\xi},\ {}^{o}\sigma^{\beta}_{\xi\eta},\ {}^{o}\sigma^{\beta}_{\eta\eta} = 0 , \tag{4.25} $$

(iii) the continuity conditions, at $\eta=0$, are

$$ u_0^{I} = u_0^{II} , \qquad v_0^{I} = v_0^{II} , \tag{4.26} $$

$$ {}^{o}\sigma^{I}_{\xi\eta} = {}^{o}\sigma^{II}_{\xi\eta} , \qquad {}^{o}\sigma^{I}_{\eta\eta} = {}^{o}\sigma^{II}_{\eta\eta} , \tag{4.27} $$

(iv) the cavity boundary conditions are traction free.

For the nth order solutions, the surface is traction free and the remaining boundary conditions are the same as for the zeroth order solutions. The solutions of each perturbative order can be obtained by applying the finite difference method.

4.2 Difference Formulation

Because of the complexity of the geometry and the boundary conditions, the finite difference method is considered more appropriate than the transform method, which was used in the cases without a cavity. In this section, only the zeroth order solutions of the thermal stress field will be discussed in detail, the solutions of higher order and the mechanical stress field can be obtained similarly.

In the finite difference method, the semi-infinite body is replaced by a sufficiently large rectangular region (Figure 4.1), and a non-uniform mesh must be used as we stated in Chapter 3. The non-uniform mesh is transformed to the uniform mesh by applying the general coordinate transformation (Appendix II). The stress field can then be solved in the transformed plane (computational plane) $(\bar{\xi},\bar{\eta})$. The finite difference form of the thermoelastic Navier's equations (4.8) and (4.9) in the computational plane $(\bar{\xi},\bar{\eta})$ can be written as:

$$a_1 v^{\beta}(i-1,j-1,n) + a_2 u^{\beta}(i-1,j,n) + a_3 v^{\beta}(i-1,j+1,n) + a_4 u^{\beta}(i,j-1,n) +$$

$$+ a_5 u^{\beta}(i,j,n) + a_6 u^{\beta}(i,j+1,n) + a_7 v^{\beta}(i+1,j-1,n) + a_8 u^{\beta}(i+1,j,n) +$$

$$+ a_9 v^{\beta}(i+1,j+1,n) = \frac{\partial}{\partial \xi}\left[\frac{b_\beta^2 \gamma_\beta}{c_2^2}\,\phi^{\beta}(i,j,n)\right], \qquad (4.28)$$

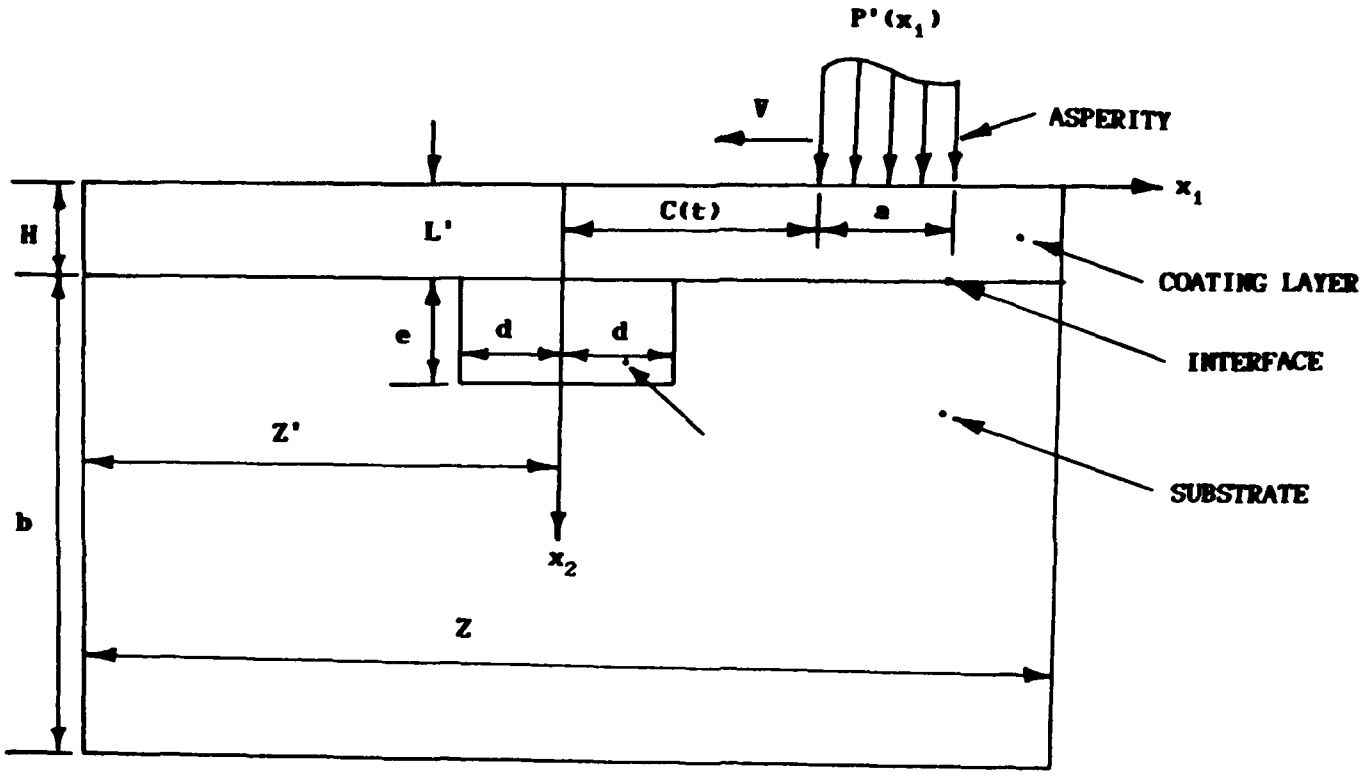

Figure 4.1 Numerical model for the stress field.

and

$$a_{10}u^{\beta}(i-1,j-1,n) + a_{11}v^{\beta}(i-1,j,n) + a_{12}u^{\beta}(i-1,j+1,n) +$$

$$+ a_{13}v^{\beta}(i,j-1,n) + a_{14}v^{\beta}(i,j,n) + a_{15}v^{\beta}(i,j+1,n)+a_{16}u^{\beta}(i+1,j-1,n) +$$

$$+ a_{17}v^{\beta}(i+1,j,n) + a_{18}u^{\beta}(i+1,j+1,n) = \frac{\partial}{\partial\eta}\left[\frac{b_{\beta}^{2}\gamma_{\beta}}{c_{2}^{2}}\,\phi^{\beta}(i,j,n)\right] , \quad (4.29)$$

where

$$a_1 = [N_2(i-1,j) + N_3(i,j-1)]/(4\xi_{\bar{\xi}}\eta_{\bar{\eta}}\Delta\bar{\xi}\Delta\bar{\eta}) , \quad (4.30)$$

$$a_2 = N_1(i-\tfrac{1}{2},j)/(\xi_{\bar{\xi}}^{2}\Delta\bar{\xi}^{2}) + N_1(i,j)\xi_{\bar{\xi}\bar{\xi}}/(2\xi_{\bar{\xi}}^{3}\Delta\bar{\xi}) , \quad (4.31)$$

$$a_3 = -[N_2(i-1,j) + N_3(i,j+1)]/(4\xi_{\bar{\xi}}\eta_{\bar{\eta}}\Delta\bar{\xi}\Delta\bar{\eta}) , \quad (4.32)$$

$$a_4 = N_3(i,j-\tfrac{1}{2})/(\eta_{\bar{\eta}}^{2}\Delta\bar{\eta}^{2}) + N_3(i,j)\eta_{\bar{\eta}\bar{\eta}}/(2\eta_{\bar{\eta}}^{3}\Delta\bar{\eta}) , \quad (4.33)$$

$$a_5 = -[N_1(i+\tfrac{1}{2},j) + N_1(i-\tfrac{1}{2},j)]/(\xi_{\bar{\xi}}^{2}\Delta\bar{\xi}^{2}) -$$

$$- [N_3(i,j+\tfrac{1}{2}) + N_3(i,j-\tfrac{1}{2})]/(\eta_{\bar{\eta}}^{2}\Delta\bar{\eta}^{2}) , \quad (4.34)$$

$$a_6 = N_3(i,j+\tfrac{1}{2})/(\eta_{\bar{\eta}}^{2}\Delta\bar{\eta}^{2}) - N_3(i,j)\eta_{\bar{\eta}\bar{\eta}}/(2\eta_{\bar{\eta}}^{3}\Delta\bar{\eta}) , \quad (4.35)$$

$$a_7 = -[N_2(i+1,j) + N_3(i,j-1)]/(4\xi_{\bar{\xi}}\eta_{\bar{\eta}}\Delta\bar{\xi}\Delta\bar{\eta}) , \quad (4.36)$$

$$a_8 = N_1(i+\tfrac{1}{2},j)/(\xi_{\bar{\xi}}^{2}\Delta\bar{\xi}^{2}) - N_1(i,j)\xi_{\bar{\xi}\bar{\xi}}/(2\xi_{\bar{\xi}}^{3}\Delta\bar{\xi}) , \quad (4.37)$$

$$a_9 = [N_2(i+1,j) + N_3(i,j+1)]/(4\xi_{,\xi}\eta_{,\eta}\Delta\bar{\xi}\Delta\bar{\eta}) \ , \tag{4.38}$$

$$a_{10} = [N_2(i,j-1) + N_3(i-1,j)]/(4\xi_{,\xi}\eta_{,\eta}\Delta\bar{\xi}\Delta\bar{\eta}) \ , \tag{4.39}$$

$$a_{11} = N_3(i-\tfrac{1}{2},j)/(\xi_{,\xi}^2\Delta\bar{\xi}^2) + N_3(i,j)\xi_{,\xi\xi}/(2\xi_{,\xi}^3\Delta\bar{\xi}) \ , \tag{4.40}$$

$$a_{12} = -[N_2(i,j+1) + N_3(i-1,j)]/(4\xi_{,\xi}\eta_{,\eta}\Delta\bar{\xi}\Delta\bar{\eta}) \ , \tag{4.41}$$

$$a_{13} = N_1(i,j-\tfrac{1}{2})/(\eta_{,\eta}^2\Delta\bar{\eta}^2) + N_1(i,j)\eta_{,\eta\eta}/(2\eta_{,\eta}^3\Delta\bar{\eta}) \ , \tag{4.42}$$

$$a_{14} = -[N_3(i-\tfrac{1}{2},j) + N_3(i+\tfrac{1}{2},j)]/(\xi_{,\xi}^2\Delta\bar{\xi}^2) -$$

$$- [N_1(i,j+\tfrac{1}{2}) + N_1(i,j-\tfrac{1}{2})]/(\eta_{,\eta}^2\Delta\bar{\eta}^2) \ , \tag{4.43}$$

$$a_{15} = N_1(i,j+\tfrac{1}{2})/(\eta_{,\eta}^2\Delta\bar{\eta}^2) - N_1(i,j)\eta_{,\eta\eta}/(2\eta_{,\eta}^3\Delta\bar{\eta}) \ , \tag{4.44}$$

$$a_{16} = -[N_2(i,j-1) + N_3(i+1,j)]/(4\xi_{,\xi}\eta_{,\eta}\Delta\bar{\xi}\Delta\bar{\eta}) \ , \tag{4.45}$$

$$a_{17} = N_3(i+\tfrac{1}{2},j)/(\xi_{,\xi}^2\Delta\bar{\xi}^2) - N_3(i,j)\xi_{,\xi\xi}/(2\xi_{,\xi}^3\Delta\bar{\xi}) \ , \tag{4.46}$$

$$a_{18} = [N_2(i,j+1) + N_3(i+1,j)]/(4\xi_{,\xi}\eta_{,\eta}\Delta\bar{\xi}\Delta\bar{\eta}) \ . \tag{4.47}$$

The traction surface boundary conditions are expressed in terms of the displacements:

$$- v^I(i-1,1,n)/(2\xi_{,\xi}\Delta\bar{\xi}) - 3u^I(i,1,n)/(2\eta_{,\eta}\Delta\bar{\eta}) + 2u^I(i,2,n)/(\eta_{,\eta}\Delta\bar{\eta}) -$$

$$- u^I(i,3,n)/(2\eta_{\eta}\Delta\bar{\eta}) + v^I(i+1,1,n)/(2\xi_{\xi}\Delta\bar{\xi}) = 0 \ , \qquad (4.48)$$

and

$$- N_2(i,1)u^I(i-1,1,n)/(2\xi_{\xi}\Delta\bar{\xi}) - 3N_1(i,1)v^I(i,1,n)/(2\eta_{\eta}\Delta\bar{\eta}) +$$

$$+ 2N_1(i,1)v^I(i,2,n)/(\eta_{\eta}\Delta\bar{\eta}) - N_1(i,1)v^I(i,3,n)/(2\eta_{\eta}\Delta\bar{\eta}) +$$

$$+ N_2(i,1)u^I(i+1,1,n)/(2\xi_{\xi}\Delta\bar{\xi}) = \frac{b_1^2\gamma_I}{c_2^2}\,\phi^I(i,1,n) \ . \qquad (4.49)$$

The traction free boundary conditions on the cavity (Figure 3.3) are:

On face AB:

$$- v^I(i-1,j,n)/(2\xi_{\xi}\Delta\bar{\xi}) + u^I(i,j-2,n)/(2\eta_{\eta}\Delta\bar{\eta}) - 2u^I(i,j-1,n)/(\eta_{\eta}\Delta\bar{\eta}) +$$

$$+ 3u^I(i,j,n)/(2\eta_{\eta}\Delta\bar{\eta}) + v^I(i+1,j,n)/(2\xi_{\xi}\Delta\bar{\xi}) = 0 \ , \qquad (4.50)$$

and

$$- N_2(i,j)u^I(i-1,j,n)/(2\xi_{\xi}\Delta\bar{\xi}) + N_1(i,j)v^I(i,j-2,n)/(2\eta_{\eta}\Delta\bar{\eta}) -$$

$$- 2N_1(i,j)v^I(i,j-1,n)/(\eta_{\eta}\Delta\bar{\eta}) + 3N_1(i,j)v^I(i,j,n)/(2\eta_{\eta}\Delta\bar{\eta}) +$$

$$+ N_2(i,j)u^I(i+1,j,n)/(2\xi_{\xi}\Delta\bar{\xi}) = \frac{b_1^2\gamma_I}{c_2^2}\,\phi^I(i,j,n) \ , \qquad (4.51)$$

On face AC:

$$- N_1(i,j)u^{II}(i-1,j,n)/(\xi\_\Delta\bar{\xi}) - N_2(i,j)v^{II}(i,j-1,n)/(2\eta\_\Delta\bar{\eta}) +$$

$$+ N_1(i,j)u^{II}(i,j,n)/(\xi\_\Delta\bar{\xi}) + N_2(i.j)v^{II}(i,j+1,n)/(2\eta\_\Delta\bar{\eta}) =$$

$$= \frac{b_{II}^2\gamma_{II}}{c_2^2}\,\phi^{II}(i,j,n) \ , \qquad (4.52)$$

and

$$- v^{II}(i-1,j,n)/(\xi\_\Delta\bar{\xi}) - u^{II}(i,j-1,n)/(2\eta\_\Delta\bar{\eta}) + v^{II}(i,j,n)/(\xi\_\Delta\bar{\xi}) +$$

$$+ u^{II}(i,j+1,n)/(2\eta\_\Delta\bar{\eta}) = 0 \ , \qquad (4.53)$$

On face BD:

$$- N_2(i,j)v^{II}(i,j-1,n)/(2\eta\_\Delta\bar{\eta}) - N_1(i,j)u^{II}(i,j,n)/(\xi\_\Delta\bar{\xi}) +$$

$$+ N_2(i,j)v^{II}(i,j+1,n)/(2\eta\_\Delta\bar{\eta}) + N_1(i,j)u^{II}(i+1,j,n)/(\xi\_\Delta\bar{\xi}) =$$

$$= \frac{b_{II}^2\gamma_{II}}{c_2^2}\,\phi^{II}(i,j,n) \ , \qquad (4.54)$$

and

$$- u^{II}(i,j-1,n)/(2\eta\_\Delta\bar{\eta}) - v^{II}(i,j,n)/(\xi\_\Delta\bar{\xi}) +$$

$$+ u^{II}(i,j+1,n)/(2\eta\_\Delta\bar{\eta}) + v^{II}(i+1,j,n)/(\xi\_\Delta\bar{\xi}) = 0 \ , \qquad (4.55)$$

On face CD:

$$- v^{II}(i-1,j,n)/(2\xi_{\xi}\Delta\bar{\xi}) - 3u^{II}(i,j,n)/(2\eta_{\eta}\Delta\bar{\eta}) +$$

$$+ 2u^{II}(i,j+1,n)/(\eta_{\eta}\Delta\bar{\eta}) - u^{II}(i,j+2,n)/(2\eta_{\eta}\Delta\bar{\eta}) +$$

$$+ v^{II}(i+1,j,n)/(2\xi_{\xi}\Delta\bar{\xi}) = 0 , \qquad (4.56)$$

and

$$- N_2(i,j)u^{II}(i-1,j,n)/(2\xi_{\xi}\Delta\bar{\xi}) - 3N_1(i,j)v^{II}(i,j,n)/(2\eta_{\eta}\Delta\bar{\eta}) +$$

$$+ 2N_1(i,j)v^{II}(i,j+1,n)/(\eta_{\eta}\Delta\bar{\eta}) - N_1(i,j)v^{II}(i,j+1,n)/(2\eta_{\eta}\Delta\bar{\eta}) +$$

$$+ N_2(i,j)u^{II}(i+1,j,n)/(2\xi_{\xi}\Delta\bar{\xi}) = \frac{b_{II}^2\gamma_{II}}{c_2^2}\,\phi^{II}(i,j,n), \qquad (4.57)$$

where $\phi^{\beta}(i,j,n)$, $\partial\phi^{\beta}(i,j,n)/\partial\xi$, and $\partial\phi^{\beta}(i,j,n)/\partial\eta$ are input data obtained from the temperature field solutions (re: Chapter 3).

4.3 Cavity Corners Singularities

When values of a solution of a boundary-value problem or its derivatives approach infinity at points, lines, or surfaces in the domain, the solution is said to possess singularities at these places. The approximation of functions with singularities presents some serious numerical difficulties. Nevertheless, calculation of solutions with singularities is extremely important; such problems arise in fracture mechanics, various flow phenomena, heat conduction problems, and in

fact, in any boundary-value problem in which strong irregularities occur in one or more of the following: (a) the geometry of the domain, (b) the coefficients in the governing differential equation, or (c) the prescribed functions, and so on.

Despite the difficulties, numerical methods can be devised that yield excellent results for singular problems. Basically, there are two general ways the problem can be approached:

Nonuniform Meshes: This means that a finer gradation of the mesh is used in the neighborhood of singular points in order to capture large changes in the gradients of the solution nearby. This is often a straight forward and effective way to handle singularities and it requires no special modification of the code or special elements, but it may be expensive owing to the necessity of a large number of grid points.

Special Singular Elements: The scheme in this case is to devise special elements in which the approximation simulates the diverging rate in elements in the vicinity of the singular point. However, this method can be used only when the behavior of the singularity is known. The procedure of this method is to assume a series which consists of both the regular terms and the singular terms. For thermomechanical problems, the series form of the asymptotic expansion can be written in the form [59,60,61,62,63]:

$$u(r,\theta) = \text{regular term} + \sum A_n r^{n\pi/\zeta} f(\theta) , \qquad (4.58)$$

where r, θ, and ζ are defined in Figure 4.2. Indeed, when π/ζ is not an integer, the derivatives of the leading term in the singular part of

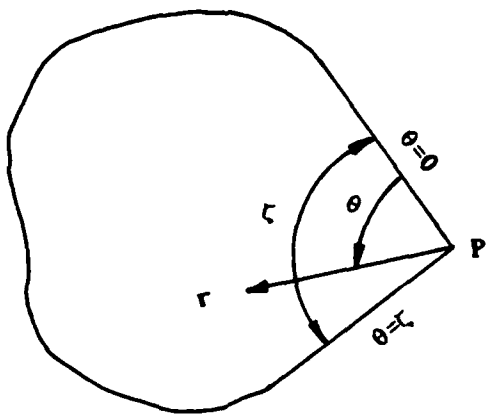

Figure 4.2 Polar coordinates for a domain with a corner at p.

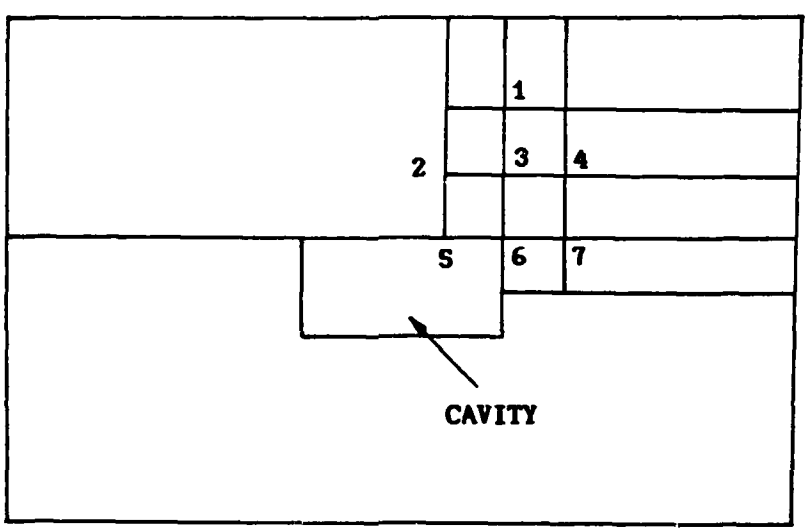

Figure 4.3 Special elements.

u may become unbounded. The order of the singularity increases as ζ increases. If $\pi/\zeta < 1$, P is referred to as a reentrant corner and the first derivatives of u are then unbounded as $r \to 0$. For the present problem, $\zeta = 3\pi/2$.

For the current problem, the stress singularity at the cavity corner can be resolved by using the results of Williams [64] and Sih [65]. The series form for the displacements in the neighborhood of the cavity corner are:

$$u(r,\theta) = a_1 r^{2/3}\cos(2\theta/3) + a_2 r^{2/3}\sin(2\theta/3) + a_3 r^{2/3}\cos(4\theta/3) + a_4 r^{2/3}\sin(4\theta/3) + a_5 r^{4/3}\cos(4\theta/3) + a_6 r^{4/3}\sin(4\theta/3) + \text{regular term} , \tag{4.59}$$

and

$$v(r,\theta) = b_1 r^{2/3}\cos(2\theta/3) + b_2 r^{2/3}\sin(2\theta/3) + b_3 r^{2/3}\cos(4\theta/3) + b_4 r^{2/3}\sin(4\theta/3) + b_5 r^{4/3}\cos(4\theta/3) + b_6 r^{4/3}\cos(4\theta/3) + \text{regular term} . \tag{4.60}$$

In the special elements, parts of the coefficients of the series can be determined by substituting equations (4.59) and (4.60) into Navier's Equations (4.8) and (4.9) and the traction free conditions on the cavity. The remaining coefficients can then be solved by using the difference form (4.28) and (4.29). As illustrated in Figure 4.3

for one specific corner, one can use Equations (4.8) and (4.9) at points 3 and 7 and the traction free condition at point 5 incorporating the singular behavior; then one can use the difference form (4.28) and (4.29) at points 1, 2, 4, 6 to determine the other coefficients of the series.

Equations (4.28, 4.29, 4.48, 4.49, 4.50, 4.51, 4.52, 4.53, 4.54, 4.55, 4.56, 4.57) and the special elements compose a complete set of difference equations for finding the stress field. For the zeroth order solutions, we have to solve a set of simultaneous algebraic equations, which can be separated into two groups, depending on whether the coefficient matrix is dense (few zero elements) or the coefficient matrix is sparse (many zero elements). The two commonly used methods of solving simultaneous algebraic equations include the direct method and the iterative method [66, 67, 68, 69, 70, 71].

Figure 4.4 shows the element pattern of the matrix for the zeroth order solutions. It is a large, banded, but unsymmetric matrix. Because of the dimension of the matrix ($\doteq$ 4400x4400), it is almost impossible (too expensive) to store all of the elements. Fortunately, the matrix is banded, therefore we can only store the elements inside the bandwidth by using the one-dimensional array as shown in Figure 4.5, and then using Gauss elimination to solve the system. The computer programs for solving the thermal stress field are given in Appendix IV.

4.4 Numerical Results

For the numerical examples, Stellite III is used as the base material. The mechanical and thermal properties of stellite III are: $E=240\times10^3$ Mpa, $\nu=0.285$, $\rho=8.3\times10^3$ kg/m^3, K=9.7 J/m·^{0}K·s, $\kappa=2.77\times10^{-6}$

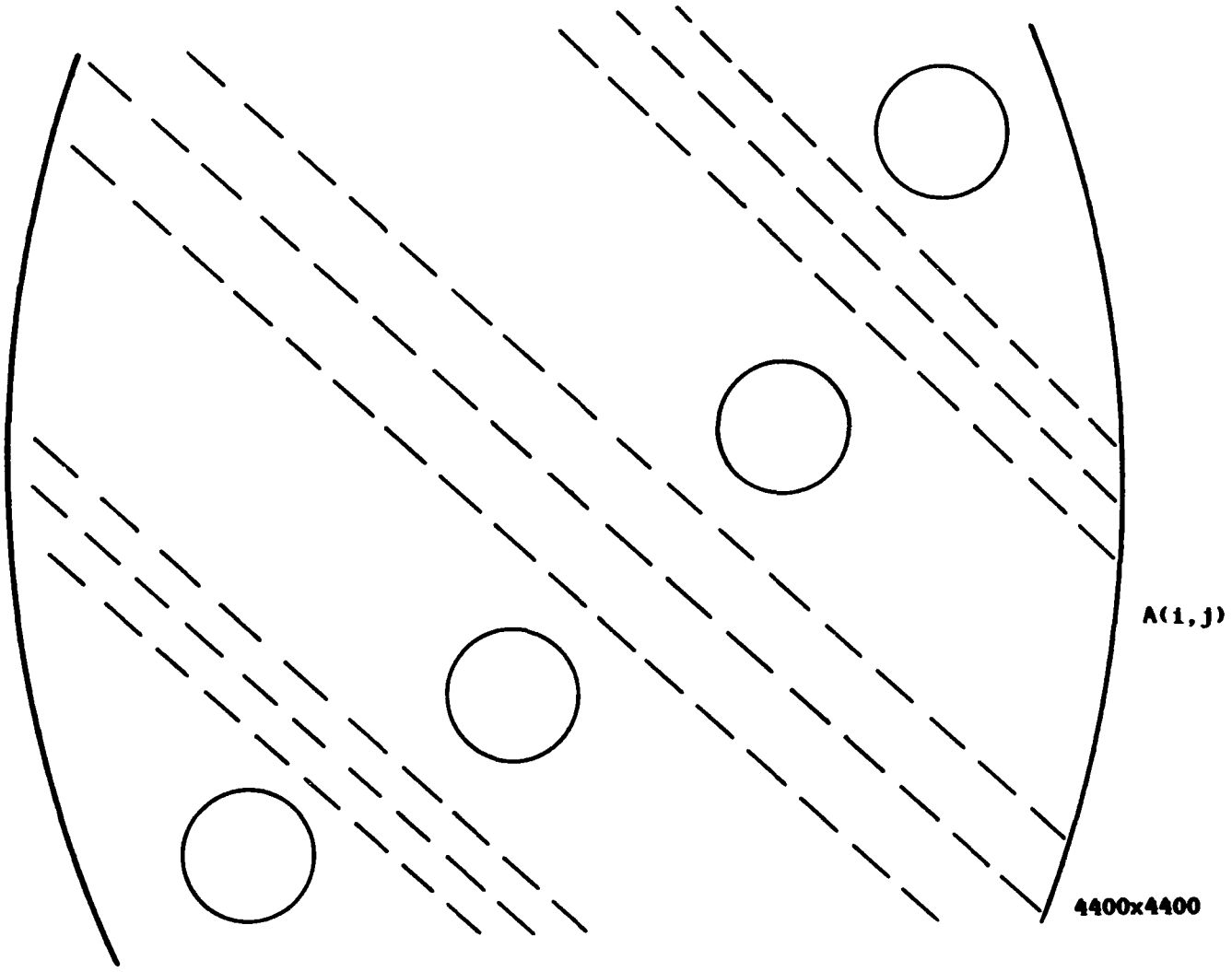

Figure 4.4 Banded matrix for the stress field.

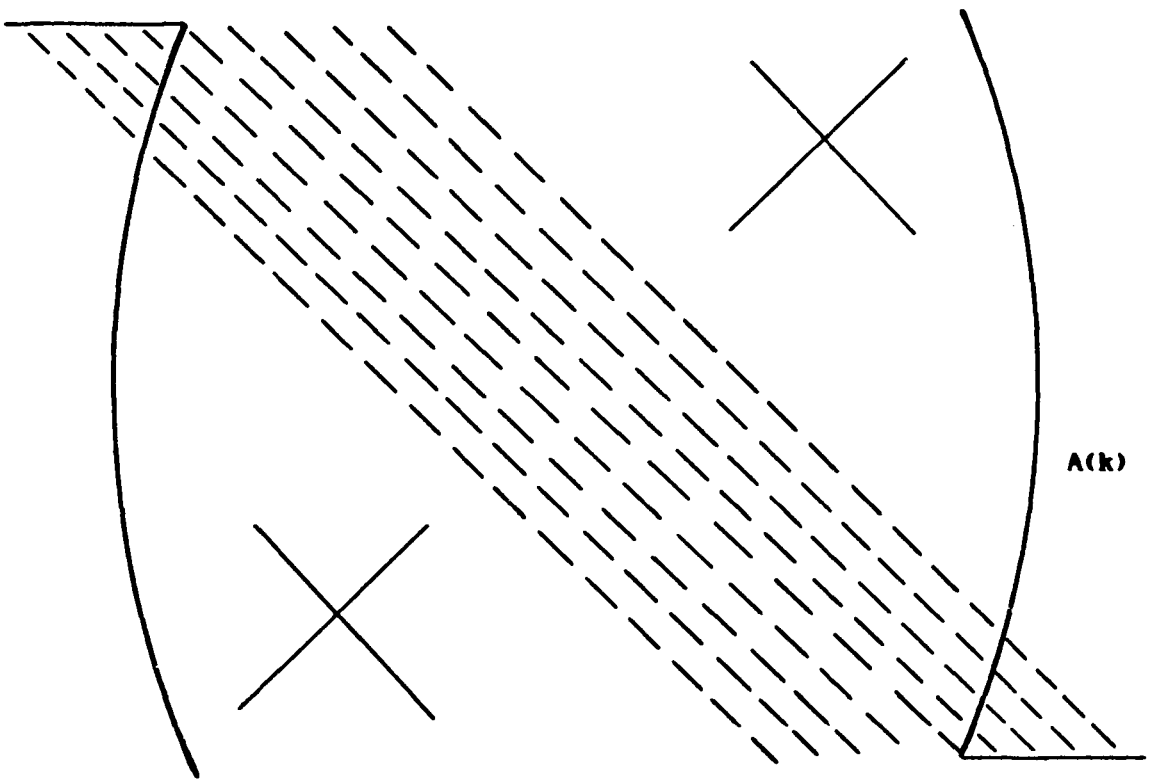

Figure 4.5 One-dimensional array to store banded matrix.

m^2/s, $\alpha=11.3\times10^{-6}$ $m/m\cdot{}^0K$, and $\mu_f=0.5$. For this problem, the smallest $\Delta\xi$ and $\Delta\eta$ in the stress field are 0.02 and 0.006, respectively. The total grid points in ξ and η directions are 67 and 35. The other important numerical parameters are: V=15 m/s, w=30a, d=0.3a, e=0.5a, and a=1 mm.

In the numerical results, the effect of the cavity location and the effects of the mechanical and thermal properties on the stress field are also studied. All figures (Figures 4.7 through 4.24) are plotted for the worst case of the asperity position, that is when the asperity is right over the cavity or when the trailing edges of the asperity and the cavity are aligned as shown in Figure 4.6 (asperity position in from $\xi=-0.7$ to $\xi=0.3$; cavity location is from $\xi=-0.3$ to $\xi=0.3$).

When the cavity is located entirely in the surface layer, because the coating layer is thick, the effect is similar to the effect of a single material [33,34,35]. Figures 4.7 to 4.12 plot the thermal principal stresses along the asperity traverse direction at the critical depth for the cases of a single material with a cavity. Different cases of a single material with a cavity are tabulated in Table 2. Figure 4.7 compares the dimensionless principal thermal stress of the single material with (case 1A) and without (case 2) a cavity. The maximum dimensionless tensile thermal stress is 0.98 for no-cavity case occurring at a depth $\eta=0.16$, while it is 5.9 at a depth of 0.088 for the medium with a cavity at a ligament thickness 0.094.

The location of the cavity from the wear surface, as indicated by the ligament thickness, influences the temperature field in the total volume available for heat content generated by frictional heating. As a consequence, the thermal stress state is strongly affected. Figure

Table 2

case	k	ρc	E	α	L	cavity	stress computed
1A	1k	1ρc	1E	1α	0.094	Yes	thermal stress
1B	1k	1ρc	1E	1α	0.06	Yes	thermal stress
1C	1k	1ρc	1E	1α	0.122	Yes	thermal stress
1D	1k	1ρc	1E	1α	0.159	Yes	thermal stress
2	1k	1ρc	1E	1α		No	thermal stress
3A	$\frac{1}{2}$k	1ρc	1E	1α	0.094	Yes	thermal stress
3B	2k	1ρc	1E	1α	0.094	Yes	thermal stress
4A	k	2ρc	1E	1α	0.094	Yes	thermal stress
4B	k	$\frac{1}{2}$ρc	1E	1α	0.094	Yes	thermal stress
5A	k	ρc	3E	1α	0.094	Yes	thermal stress
5B	k	ρc	$\frac{1}{2}$E	1α	0.094	Yes	thermal stress
5C	k	ρc	2E	1α	0.094	Yes	thermal stress
6A	k	ρc	E	2α	0.094	Yes	thermal stress
6B	k	ρc	E	$\frac{1}{2}$α	0.094	Yes	thermal stress

* Base material is Stellite III.

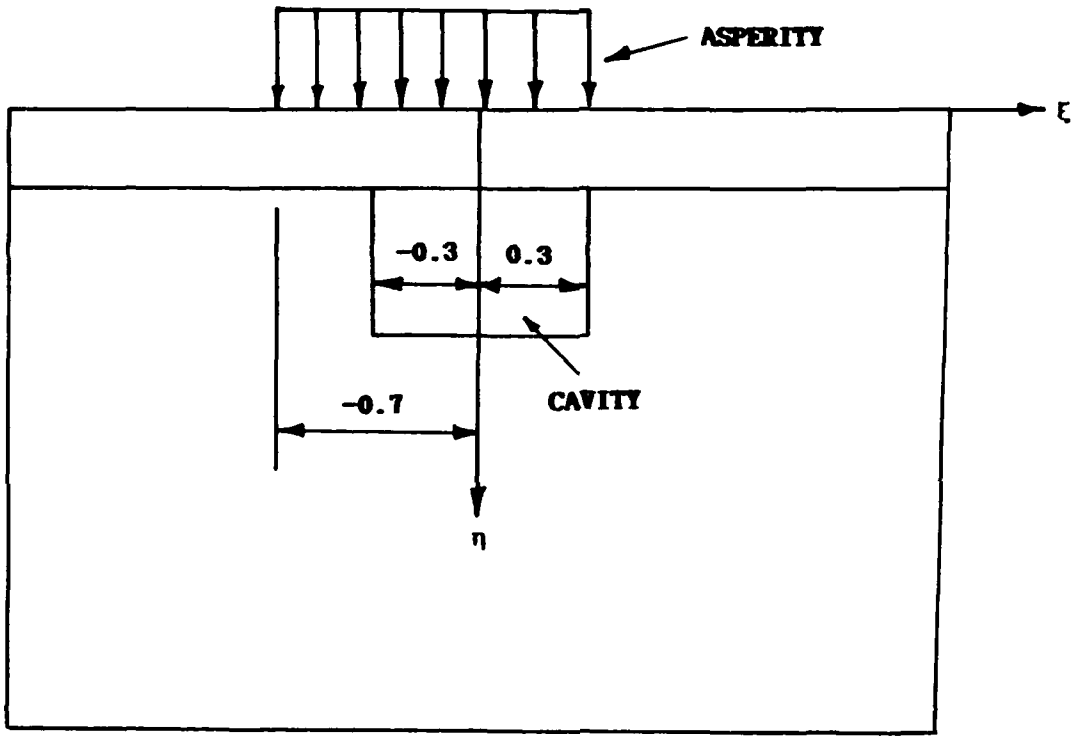

Figure 4.6 The relative positions of the cavity and the asperity.

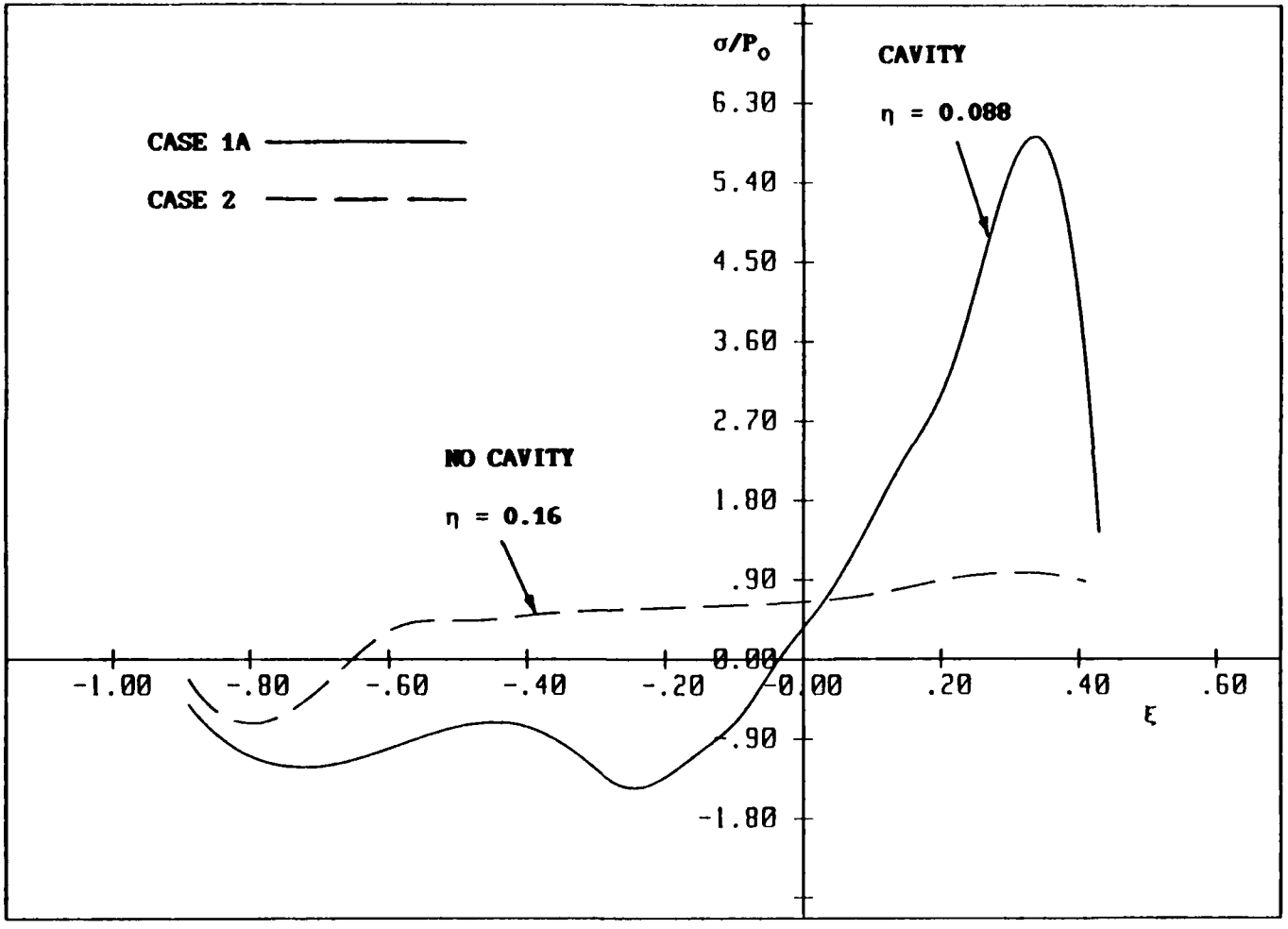

Figure 4.7 Thermal principal stress (cases 1A,2).

4.8 shows the effect of various cavity locations on the thermal stress field. Ju et al [27,32,58] showed that, without a cavity, the critical depth at which the tensile thermal stress reaches a maximum is η=0.16 for a moving line asperity excitation over Stellite III. However, with a near-surface cavity, both the temperature distribution and its gradients are different, thus changing the critical depth. The maximum tensile stress is optimized with respect to various ligament thickness. The worst case for the maximum tensile stress for Stellite III is obtained when the top edge of the cavity is at η=0.094.

Figure 4.9 presents the effect of the thermal conductivity. Case 1A is of Stellite III. Case 3A shows the effect that the thermal conductivity is reduced by half, while case 3B demonstrates the effect that the thermal conductivity is twice that of Stellite III. Figure 4.9 establishes that the principal thermal stress increases with decreasing thermal conductivity. In Figure 4.10, cases 4A and 4B show the results of doubling and halving the thermal capacity, respectively. We observe that decreasing heat capacity will increase thermal stress. Figures 4.11 and 4.12 demonstrate the effects of Young's modulus and the coefficient of thermal expansion. In Figure 4.11, Young's moduli for cases 5A and 5B are, respectively, three times and one-half that of Stellite III. In Figure 4.12, the thermal expansion coefficients for cases 6A and 6B are, respectively, twice and one-half that of Stellite III. These two figures clearly show that increasing either Young's modulus or the thermal expansion coefficient induces higher thermal stress.

When the top edge of the cavity is at the interface, both the coating layer and the substrate will influence the stress field.

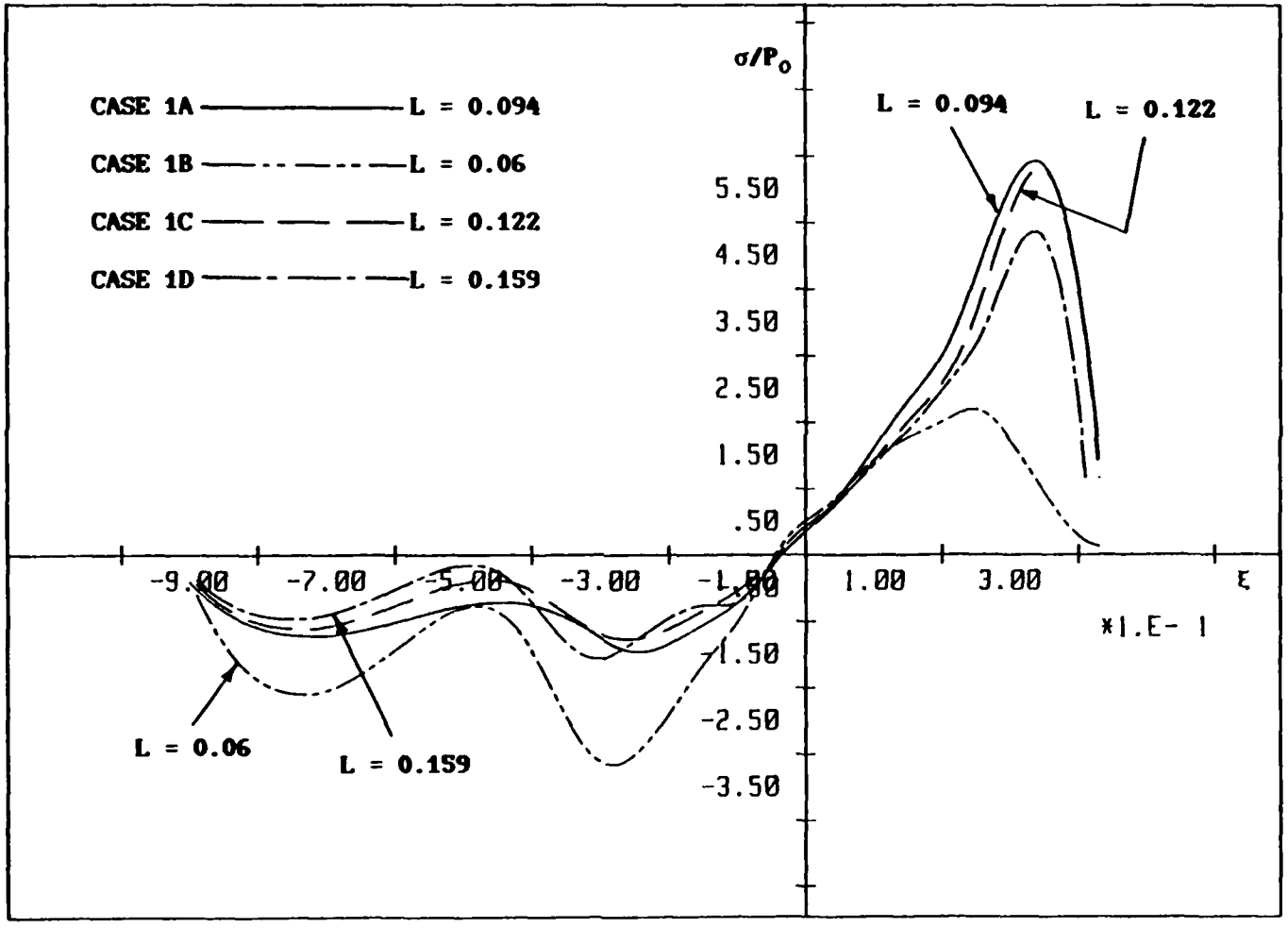

Figure 4.8 Thermal principal stress (cases 1A,1B,1C,1D). η=0.06 above the top edge of the cavity for all cases.

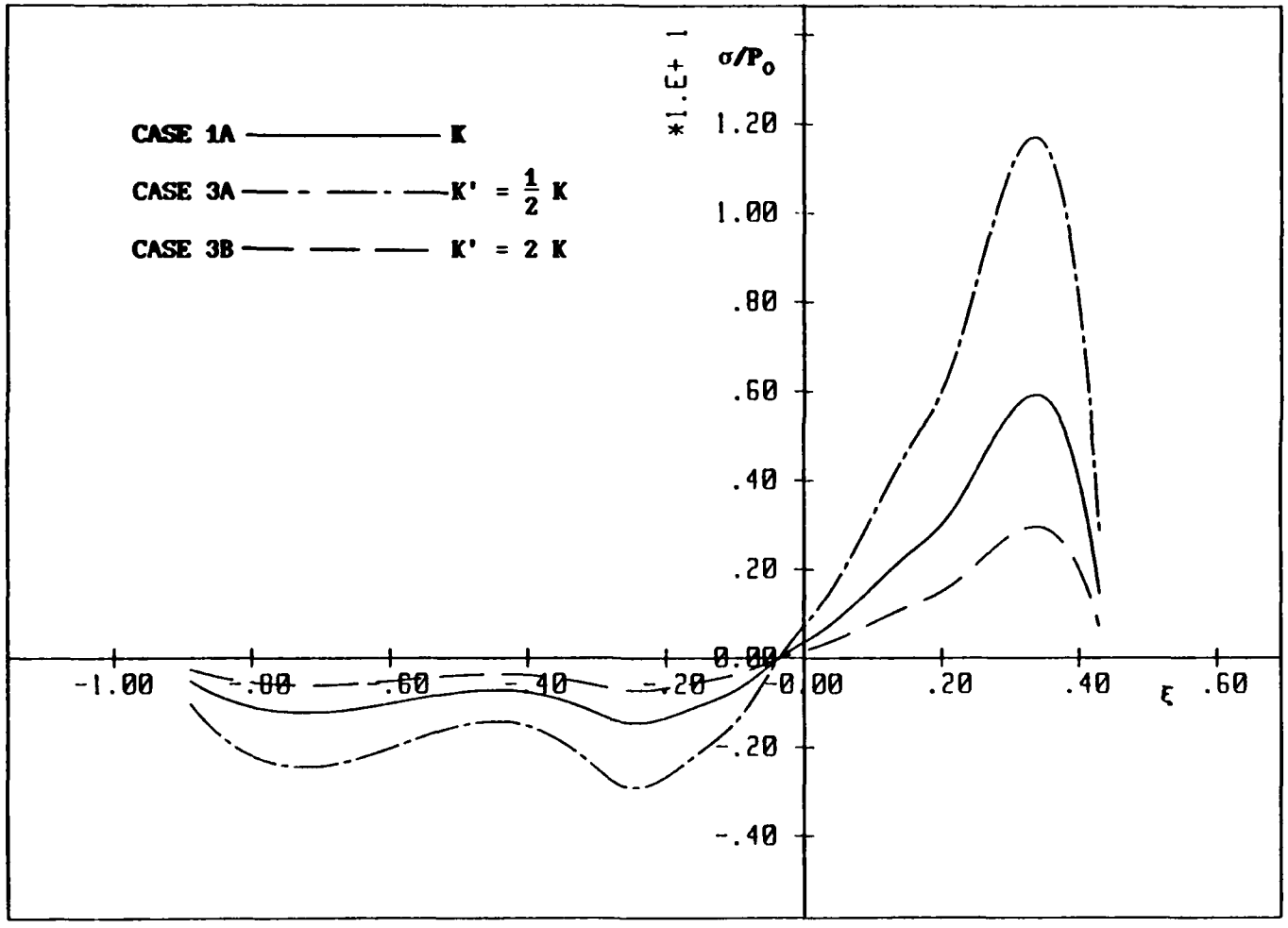

Figure 4.9 Thermal principal stress (cases 1A,3A,3B). L=0.094, and η=0.06 above the top edge of the cavity for all cases.

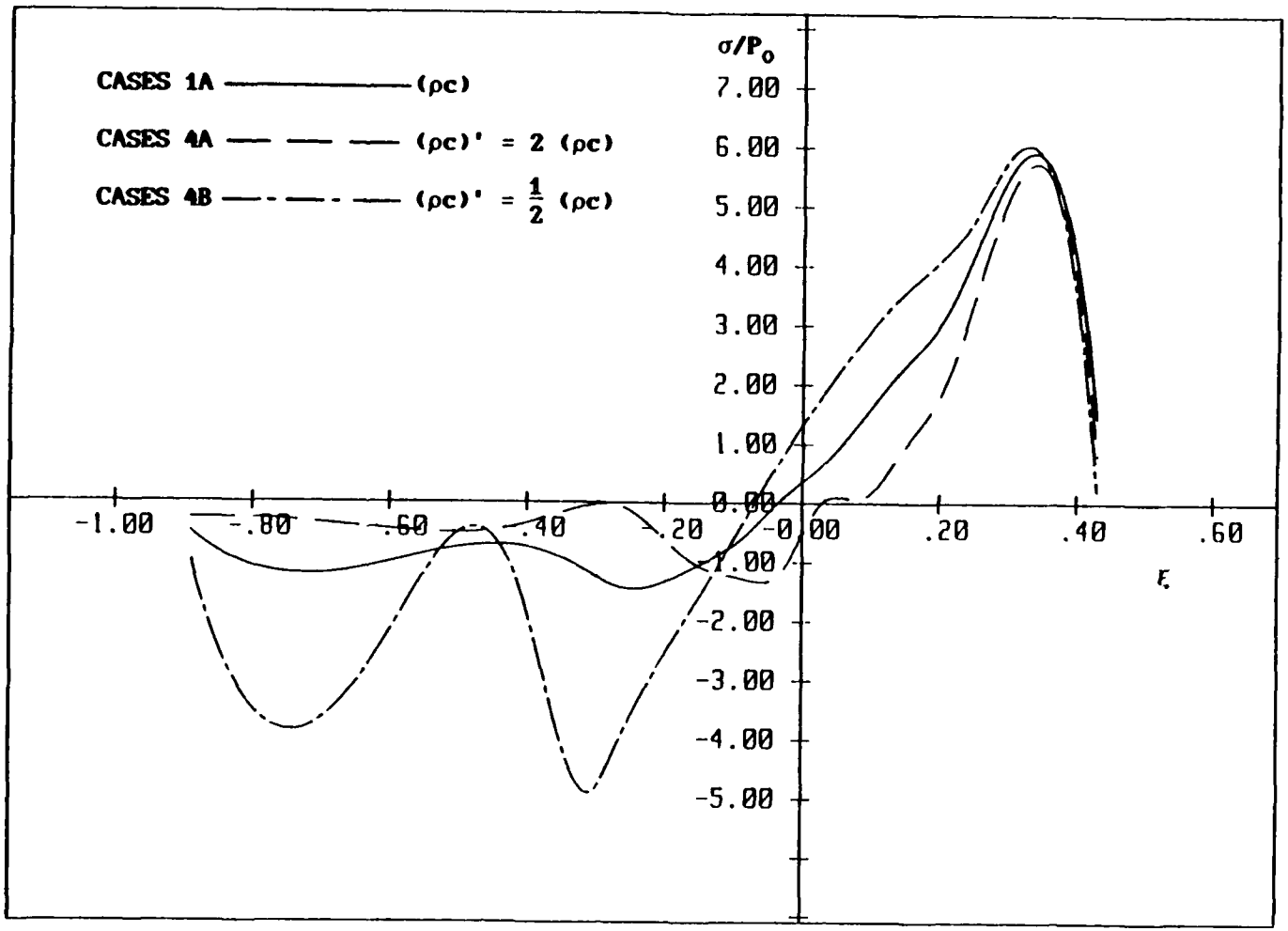

Figure 4.10 Thermal principal stress (cases 1A,4A,4B). L=0.094, and η=0.06 above the top edge of the cavity for all cases.

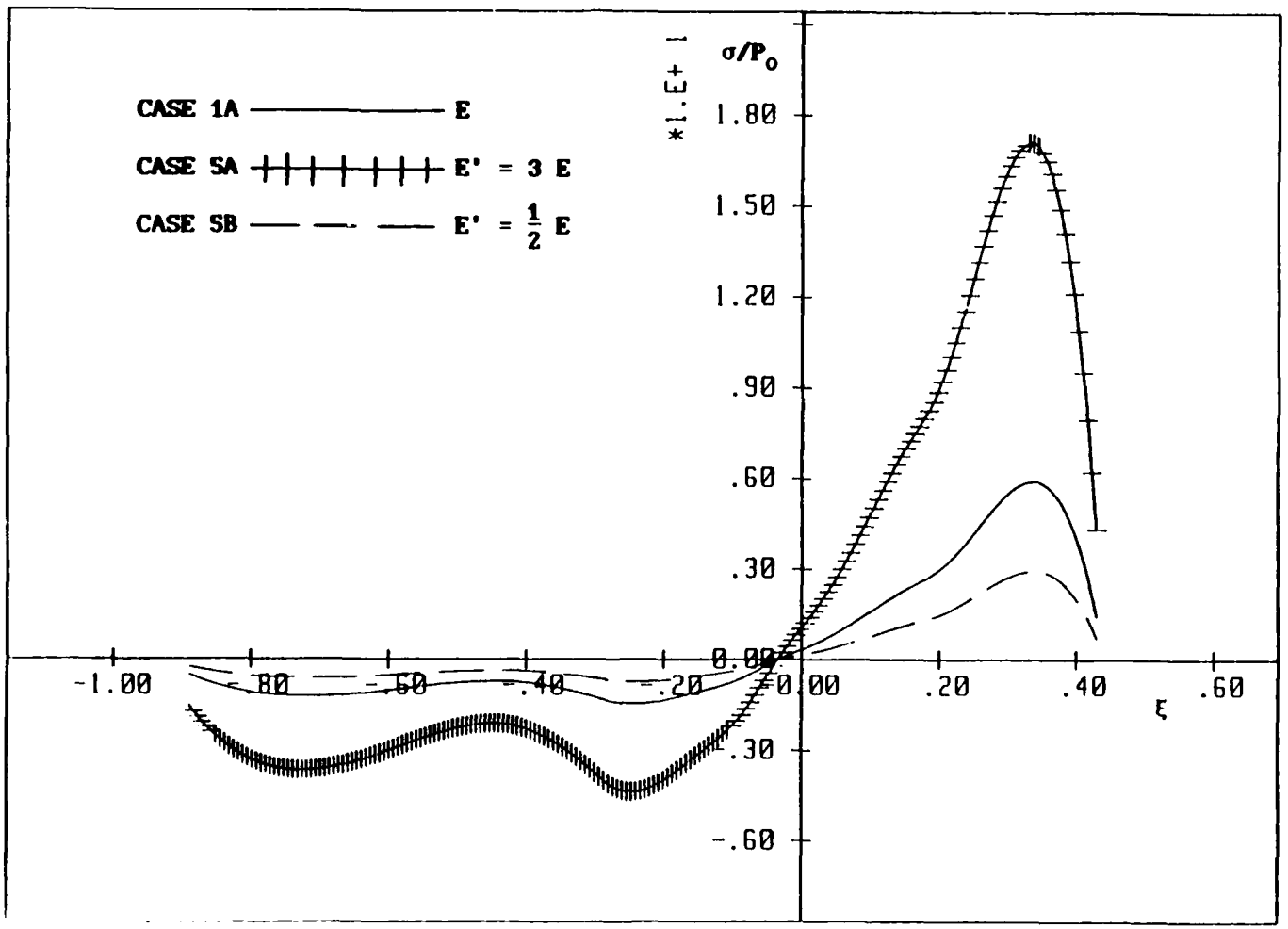

Figure 4.11 Thermal principal stress (cases 1A,SA,SB). L=0.094, and η=0.06 above the top edge of the cavity for all cases.

AD-A193 311 THERMO-MECHANICAL CRACKING IN COATED MEDIA WITH A CAVITY BY A MOVING ASPE (U) NEW MEXICO UNIV ALBUQUERQUE DEPT OF MECHANICAL ENGINEERING 2/3

UNCLASSIFIED F D JU ET AL MAR 88 ME-144(88)ONR-233-3 F/G 20/11 NL

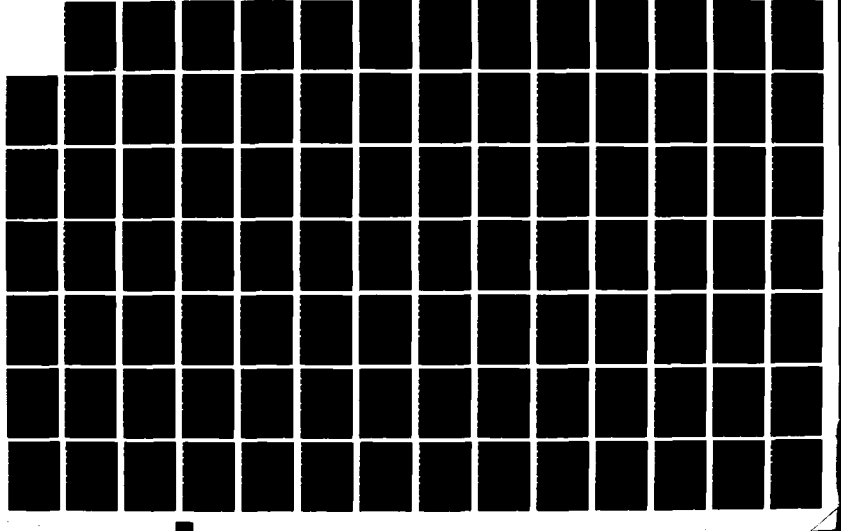

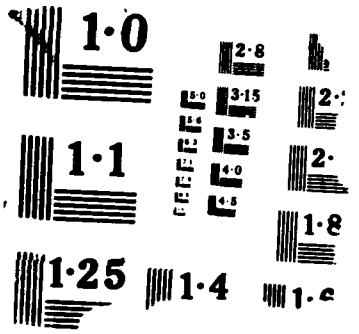
1·0
1·1
1·25
1·4
2·8
3·15
3·5
4·0
2·
1·8

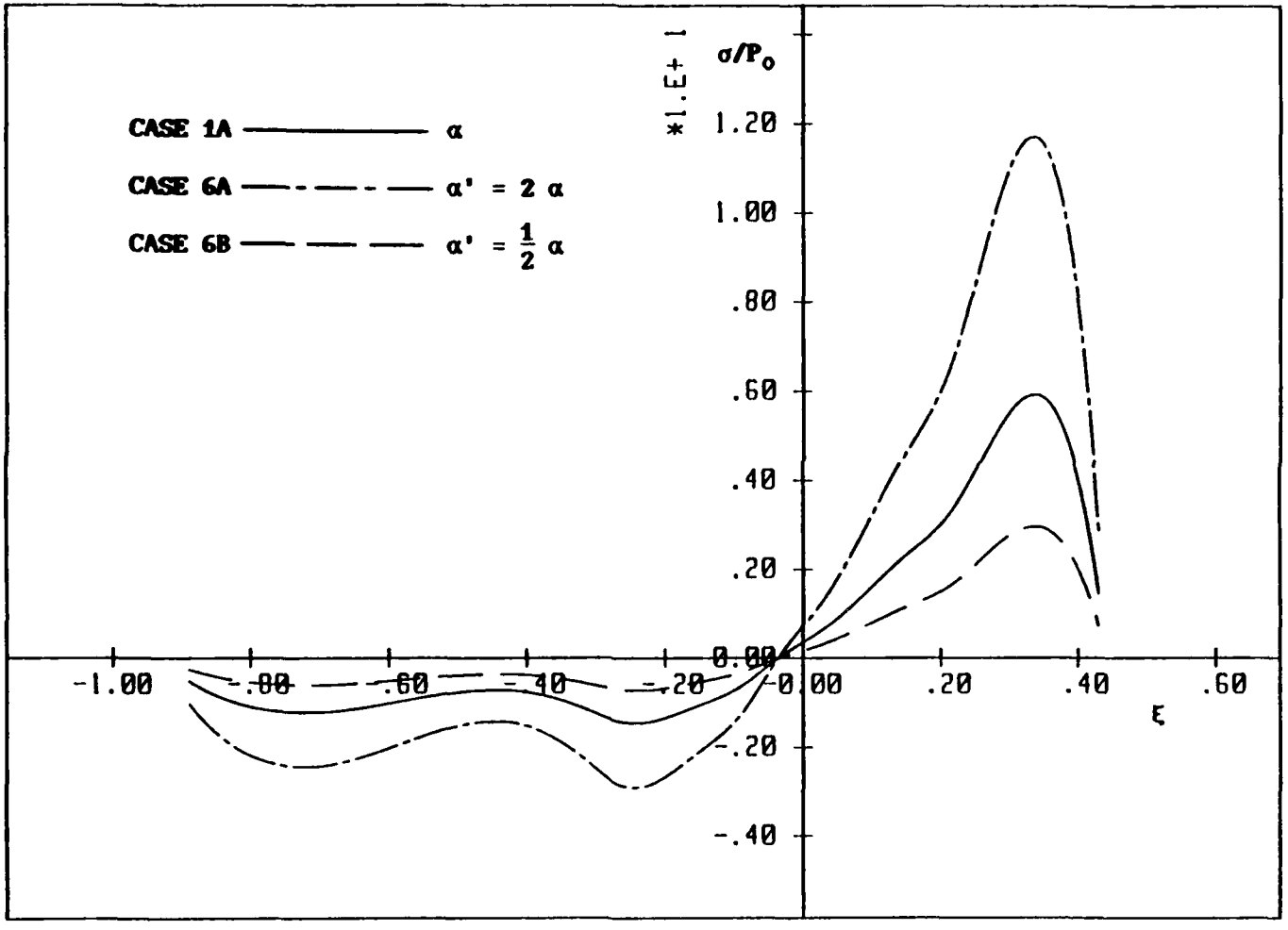

Figure 4.12 Thermal principal stress (cases 1A,6A,6B). L=0.094, and η=0.06 above the top edge of the cavity for all cases.

Figures 4.13 to 4.24 show the results of the cases in which the top edge of the cavity is at the interface. Different cases of a layered medium with a cavity are listed in Table 3.

In the case of a medium with no-cavity, the effect of the mechanical stress field is small enough to be neglected. When a cavity exists, the effect of the mechanical stress field is no longer negligible. Figure 4.13 plots the principal thermal stress field (case 7A), mechanical stress field (case 7B), and combined stress field (case 7C). In this figure, the material of the substrate is Stellite III, and the material properties of the coating layer are the same as Stellite III except that Young's modulus is twice that of Stellite III. This figure establishes that the tensile thermal stress is larger than the tensile mechanical stress. However, the mechanical stress field is not so small that we can neglect it as indicated in the no-cavity case.

The effect of the cavity location on the thermal stress field for a layered medium is presented in Figure 4.14. From this figure, one can see that the maximum tensile stress occurs when the ligament thickness L=0.094, which is the same value as in the case of a single material with a cavity. Figures 4.15 and 4.16 present the effects of Young's modulus of the coating layer and the substrate, respectively. In Figure 4.15, the material of the substrate is Stellite III for all cases. Young's modulus of the surface layer for different cases is: case 1A is the same as Stellite III; case 7A is twice that of Sellite III, case 9A and case 9B are, respectively, three times and one-half that of Stellite III. From this figure, one can see that the principal thermal stress field is strongly influenced by the Young's modulus of the coating layer; increasing Young's modulus of the coating layer will

Table 3

case	k_I	k_{II}	E_I	E_{II}	α_I	α_{II}	L	cavity	stress computed
7A	$1k_I$	$1k_{II}$	$2E_I$	$1E_{II}$	$1\alpha_I$	$1\alpha_{II}$	0.094	Yes	thermal stress
7B	$1k_I$	$1k_{II}$	$2E_I$	$1E_{II}$	$1\alpha_I$	$1\alpha_{II}$	0.094	Yes	mech. stress
7C	$1k_I$	$1k_{II}$	$2E_I$	$1E_{II}$	$1\alpha_I$	$1\alpha_{II}$	0.094	Yes	combined stress
8A	$1k_I$	$1k_{II}$	$2E_I$	$1E_{II}$	$1\alpha_I$	$1\alpha_{II}$	0.06	Yes	thermal stress
8B	$1k_I$	$1k_{II}$	$2E_I$	$1E_{II}$	$1\alpha_I$	$1\alpha_{II}$	0.07	Yes	thermal stress
8C	$1k_I$	$1k_{II}$	$2E_I$	$1E_{II}$	$1\alpha_I$	$1\alpha_{II}$	0.12	Yes	thermal stress
8D	$1k_I$	$1k_{II}$	$2E_I$	$1E_{II}$	$1\alpha_I$	$1\alpha_{II}$	0.159	Yes	thermal stress
9A	$1k_I$	$1k_{II}$	$\frac{1}{2}E_I$	$1E_{II}$	$1\alpha_I$	$1\alpha_{II}$	0.094	Yes	thermal stress
9B	$1k_I$	$1k_{II}$	$3E_I$	$1E_{II}$	$1\alpha_I$	$1\alpha_{II}$	0.094	Yes	thermal stress
10A	$1k_I$	$1k_{II}$	$1E_I$	$\frac{1}{5}E_{II}$	$1\alpha_I$	$1\alpha_{II}$	0.094	Yes	thermal stress
10B	$1k_I$	$1k_{II}$	$1E_I$	$\frac{1}{2}E_{II}$	$1\alpha_I$	$1\alpha_{II}$	0.094	Yes	thermal stress
10C	$1k_I$	$1k_{II}$	$1E_I$	$5E_{II}$	$1\alpha_I$	$1\alpha_{II}$	0.094	Yes	thermal stress
11A	$\frac{1}{2}k_I$	$1k_{II}$	$1E_I$	$1E_{II}$	$1\alpha_I$	$1\alpha_{II}$	0.094	Yes	thermal stress
11B	$2k_I$	$1k_{II}$	$1E_I$	$1E_{II}$	$1\alpha_I$	$1\alpha_{II}$	0.094	Yes	thermal stress
12A	$1k_I$	$1k_{II}$	$1E_I$	$1E_{II}$	$2\alpha_I$	$1\alpha_{II}$	0.094	Yes	thermal strcss
12B	$1k_I$	$1k_{II}$	$1E_I$	$1E_{II}$	$\frac{1}{2}\alpha_I$	$1\alpha_{II}$	0.094	Yes	thermal stress

* Base materials for both the coating layer and the substrate are Stellite III.

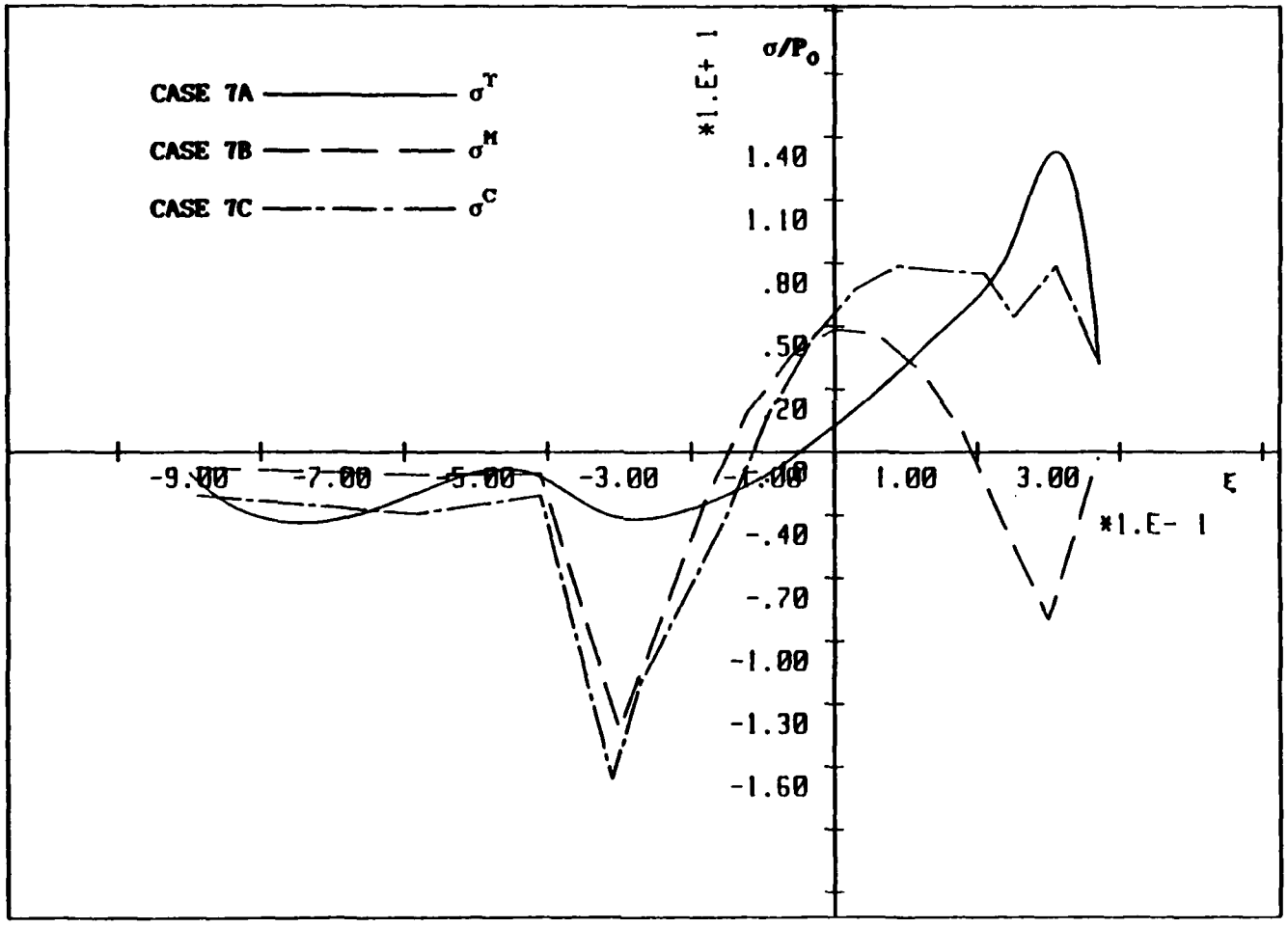

Figure 4.13 Thermal, mechanical, and combined principal stress (cases 7A,7B,7C). L=0.094, and η=0.06 above the top edge of the cavity for all cases.

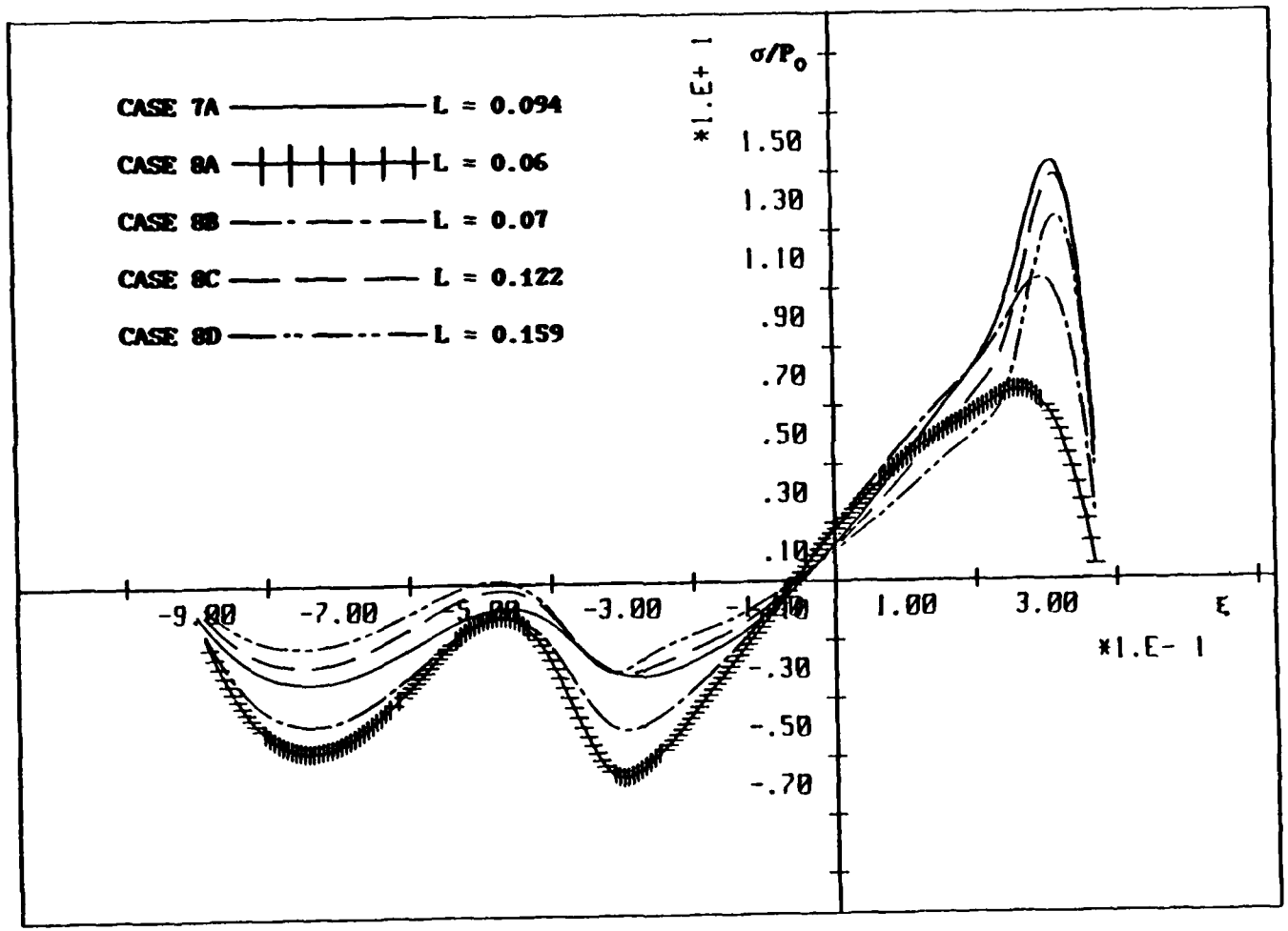

Figure 4.14 Thermal principal stress (cases 7A,8A,8B,8C,8D). η=0.06 above the top edge of the cavity for all cases.

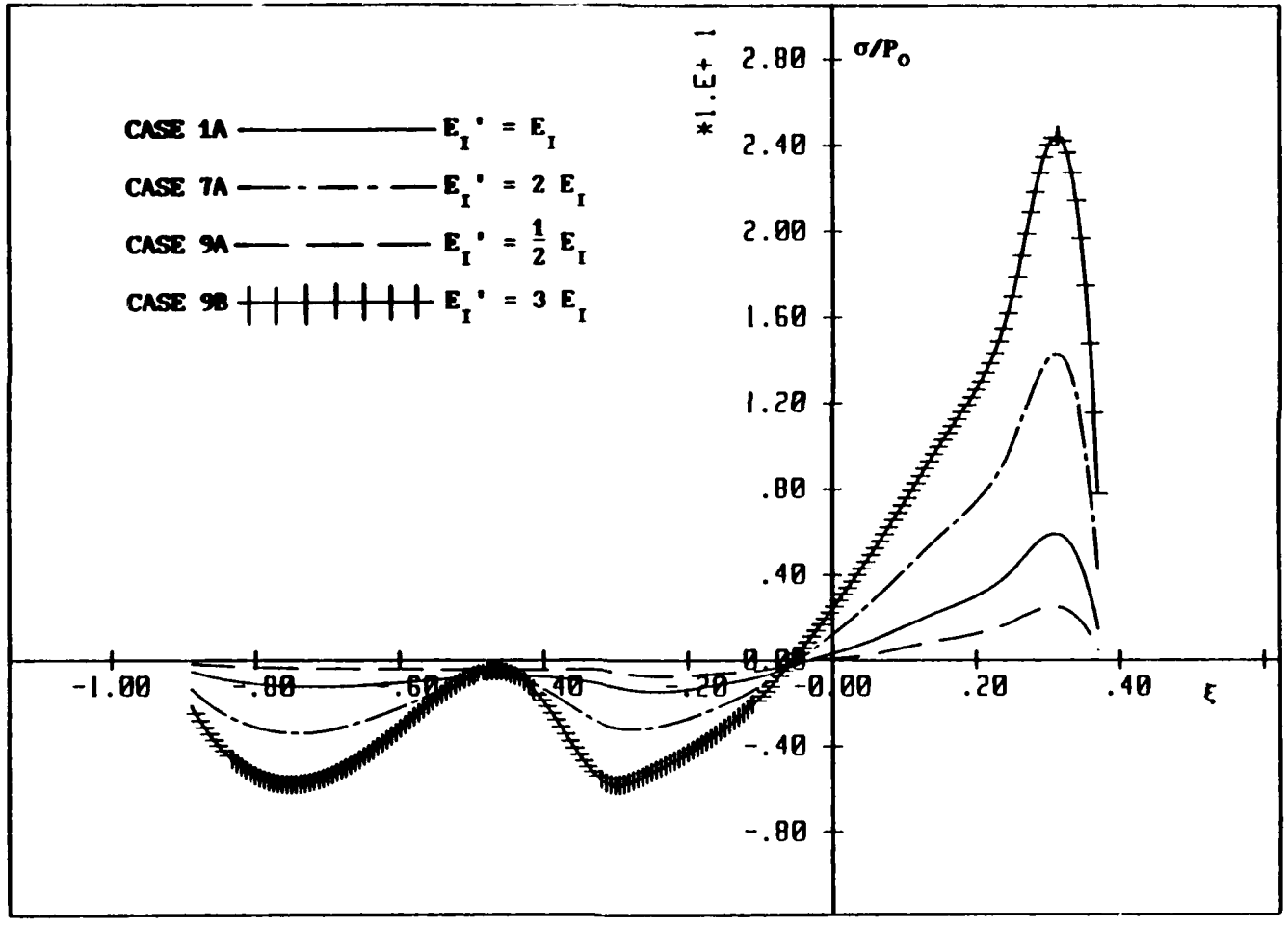

Figure 4.15 Thermal principal stress (cases 1A,7A,9A,9B). L=0.094, and η=0.06 above the top edge of the cavity for all cases.

increase the principal thermal stress. In Figure 4.16, the material of the coating layer is Stellite III for all cases. Young's modulus of the substrate is one-fifth (case 10A), one-half (case 10B), and five times (case 10C) that of Stellite III. This figure shows that decreasing Young's modulus in the substrate will result in increasing the thermal stress field, but the influence from the substrate is weaker than from the coating layer. Figure 4.17 compares the effect of Young's modulus on the thermal stress field from a single material and from a layered medium. In the figure, dashed lines represent the case of a single material with a cavity, while solid lines represent the case of a layered medium with a cavity. From this figure, we observe that thermal stress increases linearly in proportion to Young's modulus for the single material case. For the layered medium case, however, increasing by the same amount Young's modulus in the coating layer will result in higher thermal stress than in the case of a single material. This is because we will have a relative softer substrate by increasing Young's modulus in the coating layer. The effects from thermal conductivity and the coefficient of thermal expansion are presented in Figures 4.18 and 4.19. These effects are similar to those found in the case of a single material with a cavity.

From the failure specimen for the case of a single material with no-cavity (Figures 1.1 and 1.2), we observe that the thermomechanical cracking is perpendicular to the wear surface. However, Ju and Liu [34] showed that, in the case of a layered medium with no-cavity, shear delamination (cracking is parallel to the wear surface) may occur caused by the changing of principal directions (larger angle of principal direction), therefore, it is important to understand what

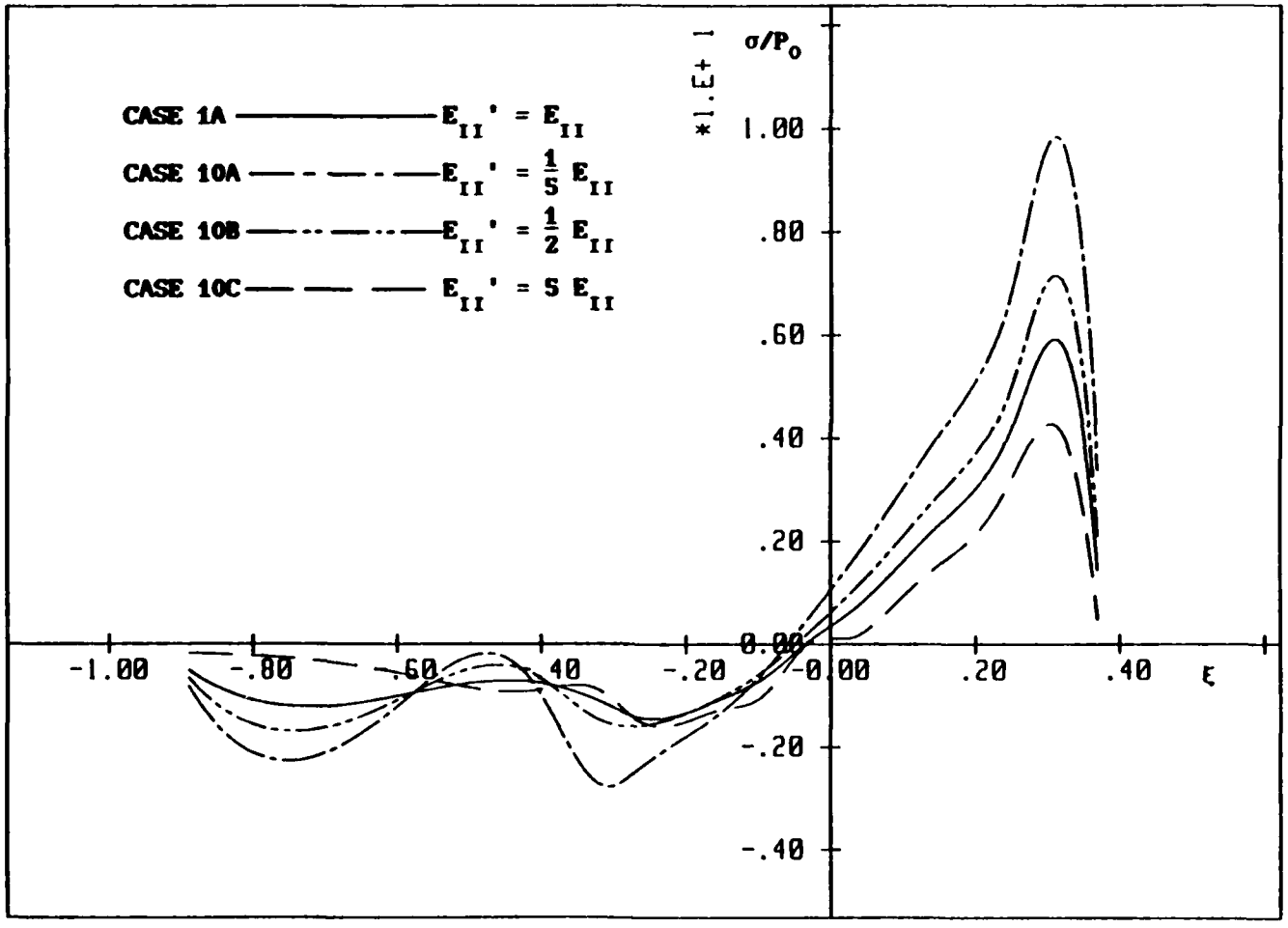

Figure 4.16 Thermal principal stress (cases 1A,10A,10B,10C). L=0.094, and η=0.06 above the top edge of the cavity for all cases.

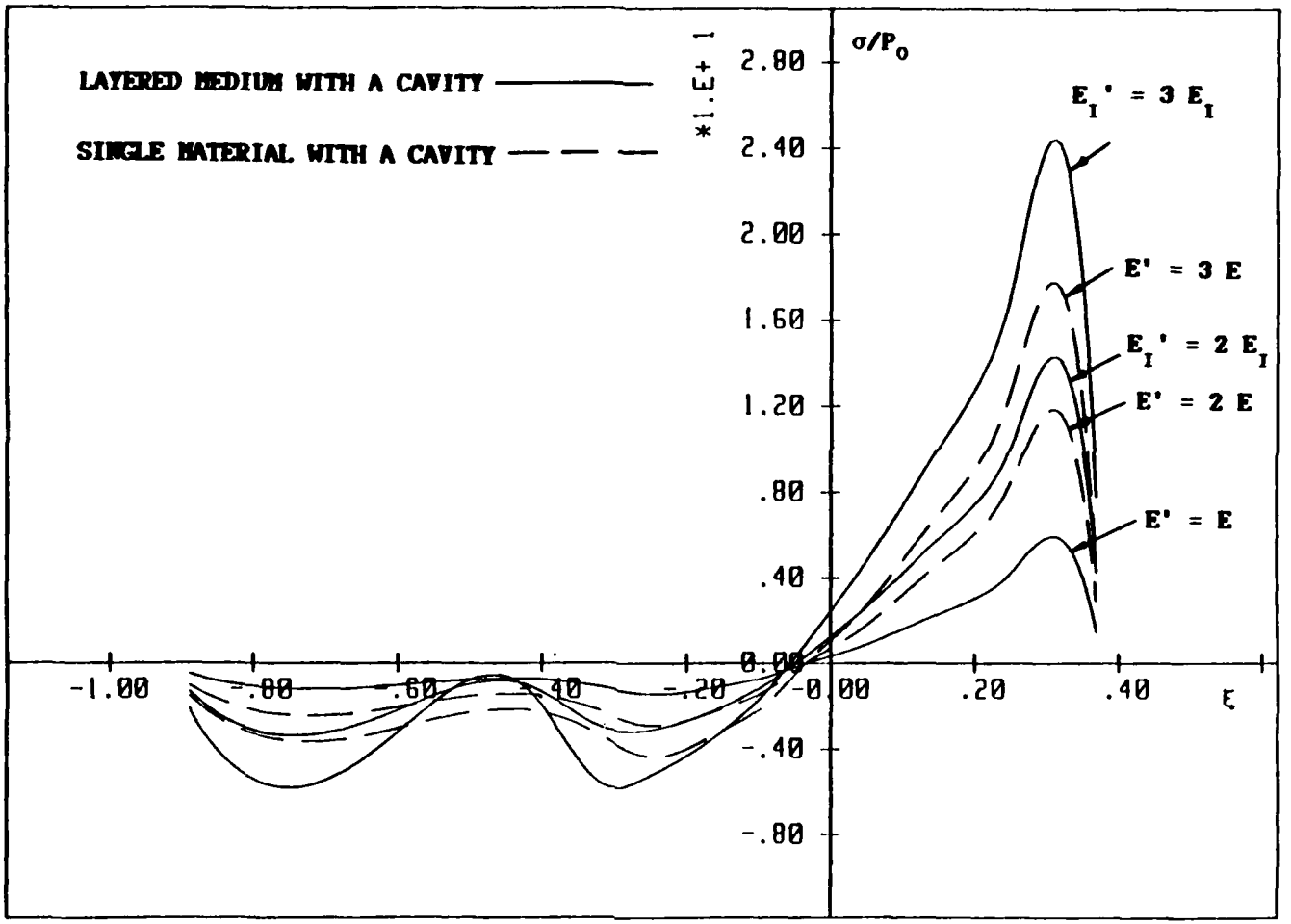

Figure 4.17 Thermal principal stress (cases 1A,5A,5C,7A,9B). L=0.094, and η=0.06 above the top edge of the cavity for all cases.

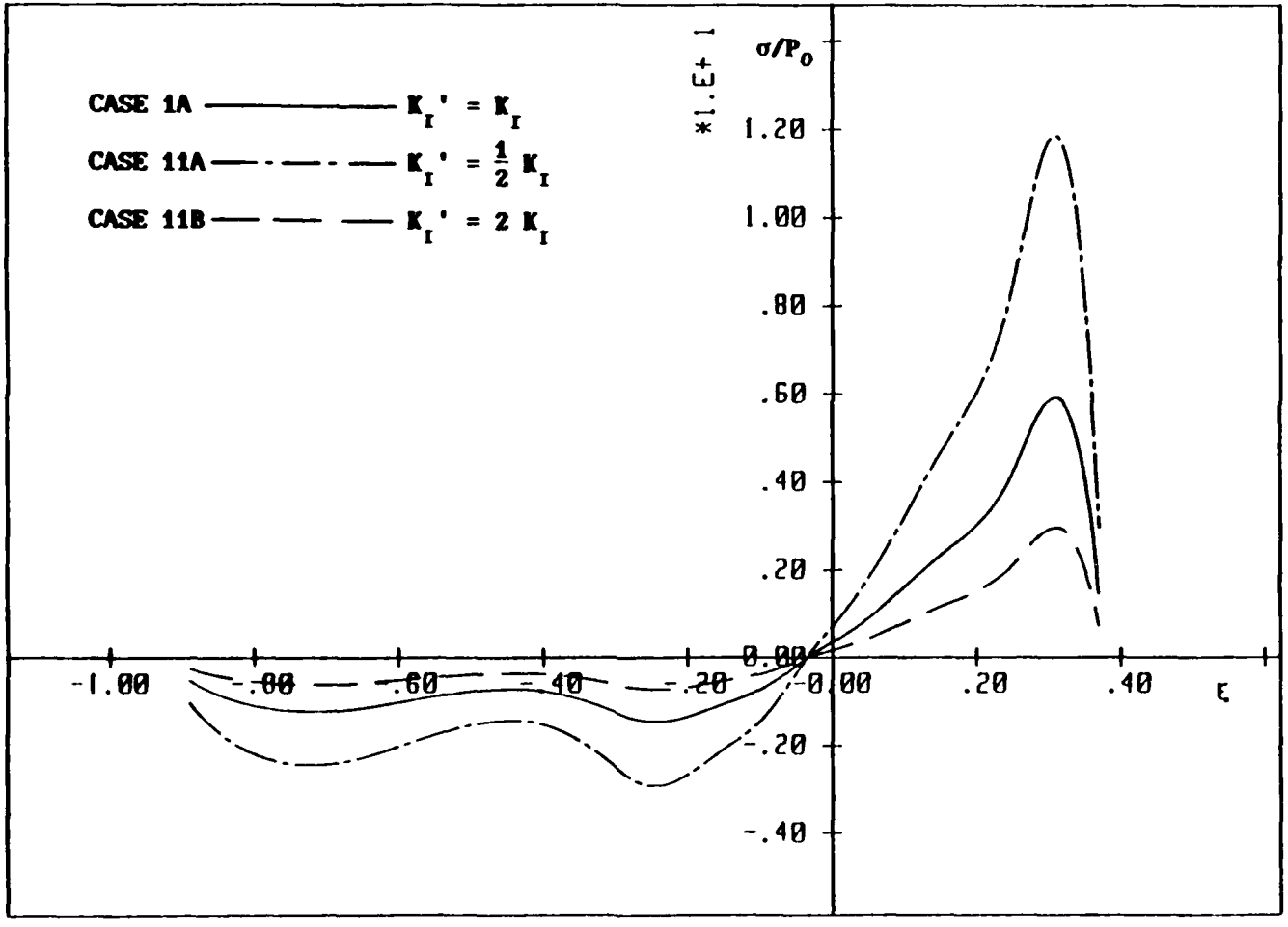

Figure 4.18 Thermal principal stress (1A,11A,11B). L=0.094, and η=0.06 above the top edge of the cavity for all cases.

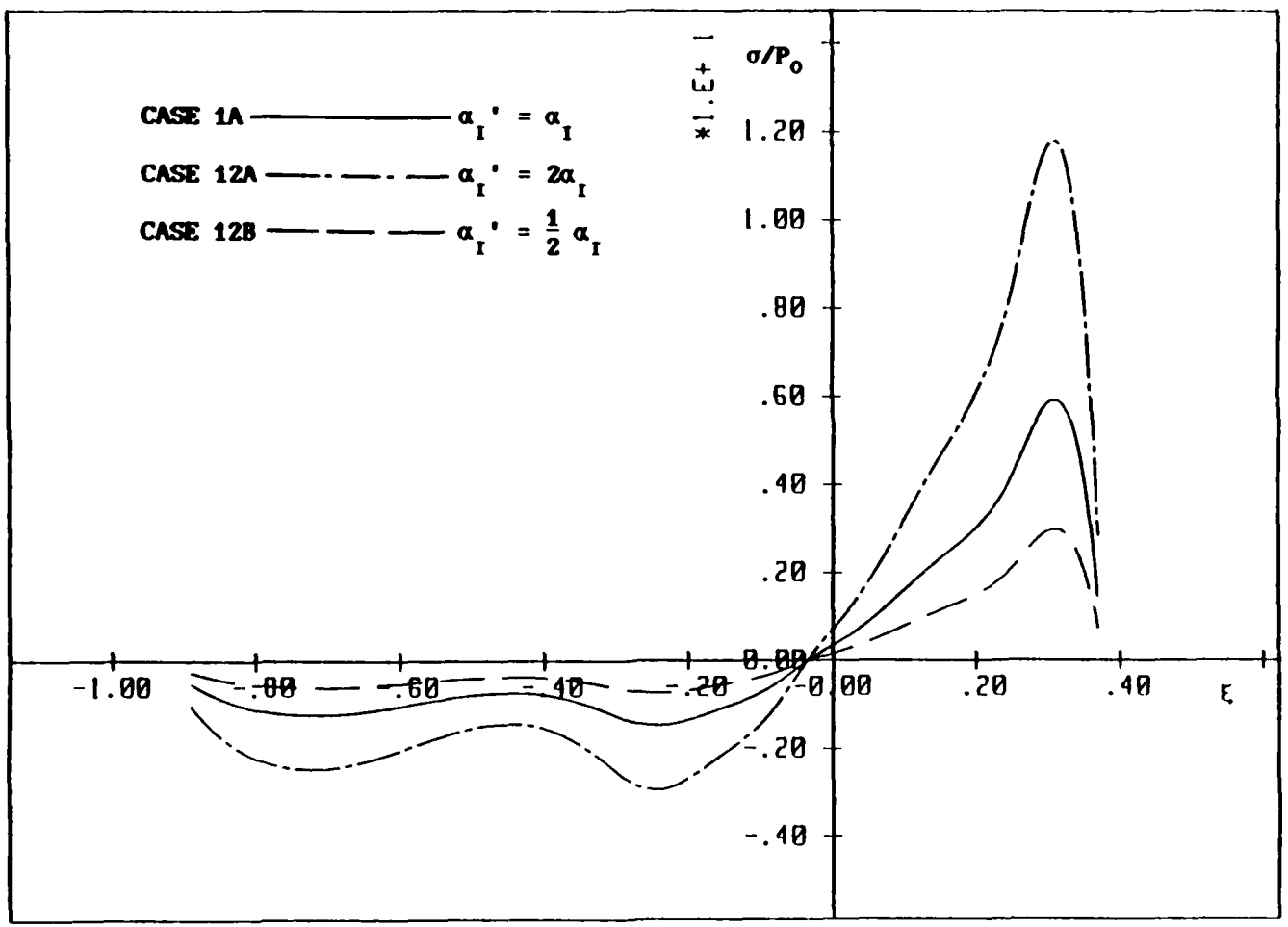

Figure 4.19 Thermal principal stress (cases 1A,12A,12B). L=0.094, and η=0.06 above the top edge of the cavity for all cases.

will affect principal directions. Figure 4.20 shows the effect of the ligament thickness (cavity location) on principal directions at the point ξ=0.3 and η=0.006 above the cavity top edge. From this figure, we observe that increasing the ligament thickness will result in larger angle of principal direction, and the angle of principal direction changes drastically when L=0.094, the value which gives the maximun tensile stress. Figures 4.21 and 4.22 compare the effect of Young's modulus on principal directions for the case of a single material with a cavity (dashed line) and for the case of a layered medium with a cavity (solid line). These two figures establish that decreasing Young's modulus in the coating layer (E_I) or increasing Young's modulus in the substrate (E_{II}) will increase the angle of principal direction. Nevertheless, changing Young's modulus in the case of a single material with a cavity will not affect the principal directions. Figures 4.23 and 4.24 illustrate the effects of the thermal conductivity and the coefficient of thermal expansion on principal directions for the case of a single material with a cavity (dashed line) and the case of a layered medium with a cavity (solid line). From these two figures, one can see that thermal conductivity and the coefficient of thermal expansion will not influence principal directions significantly.

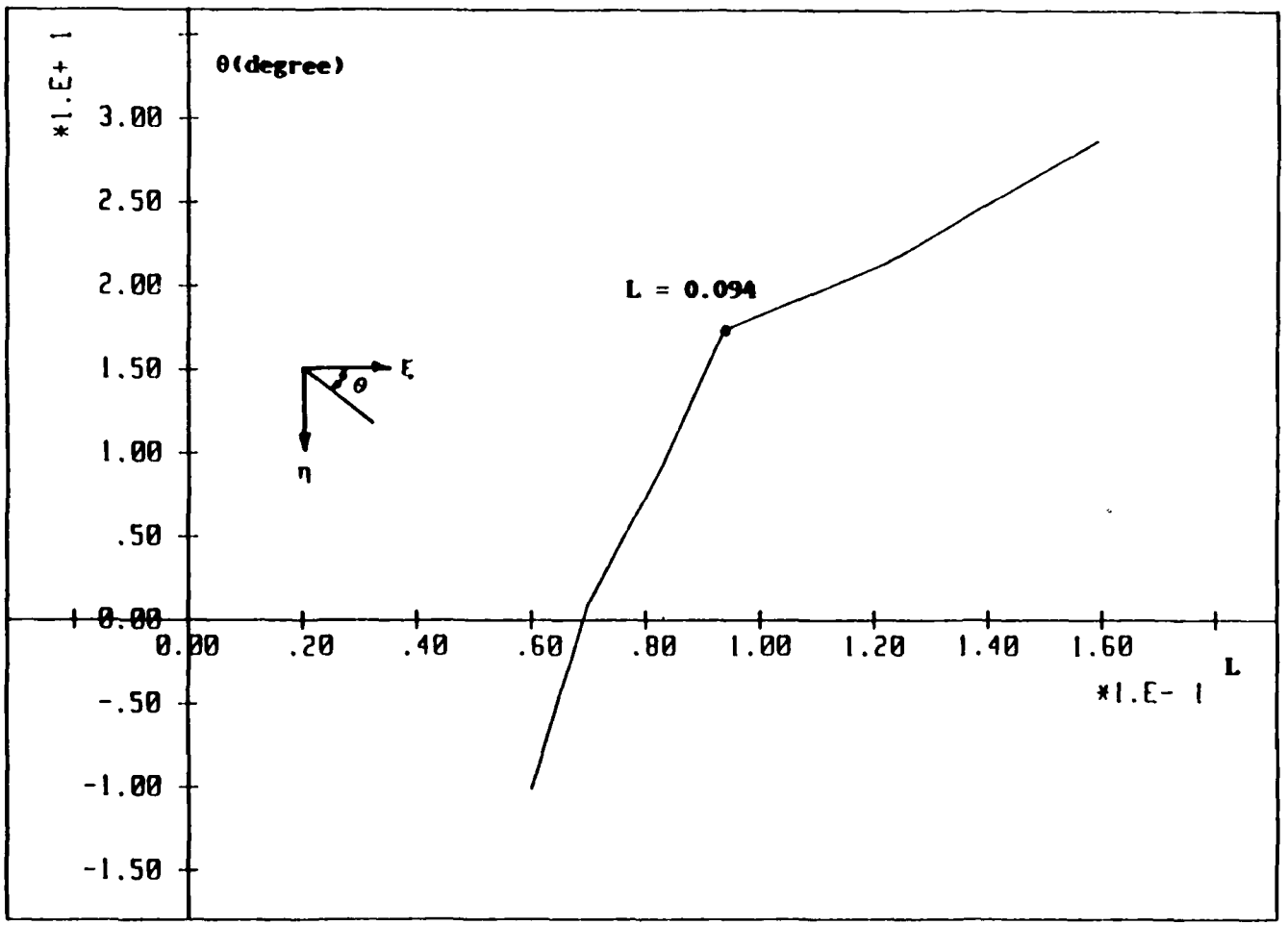

Figure 4.20 The effect of the ligament thickness on the angle of principal direction of the thermal stress field.

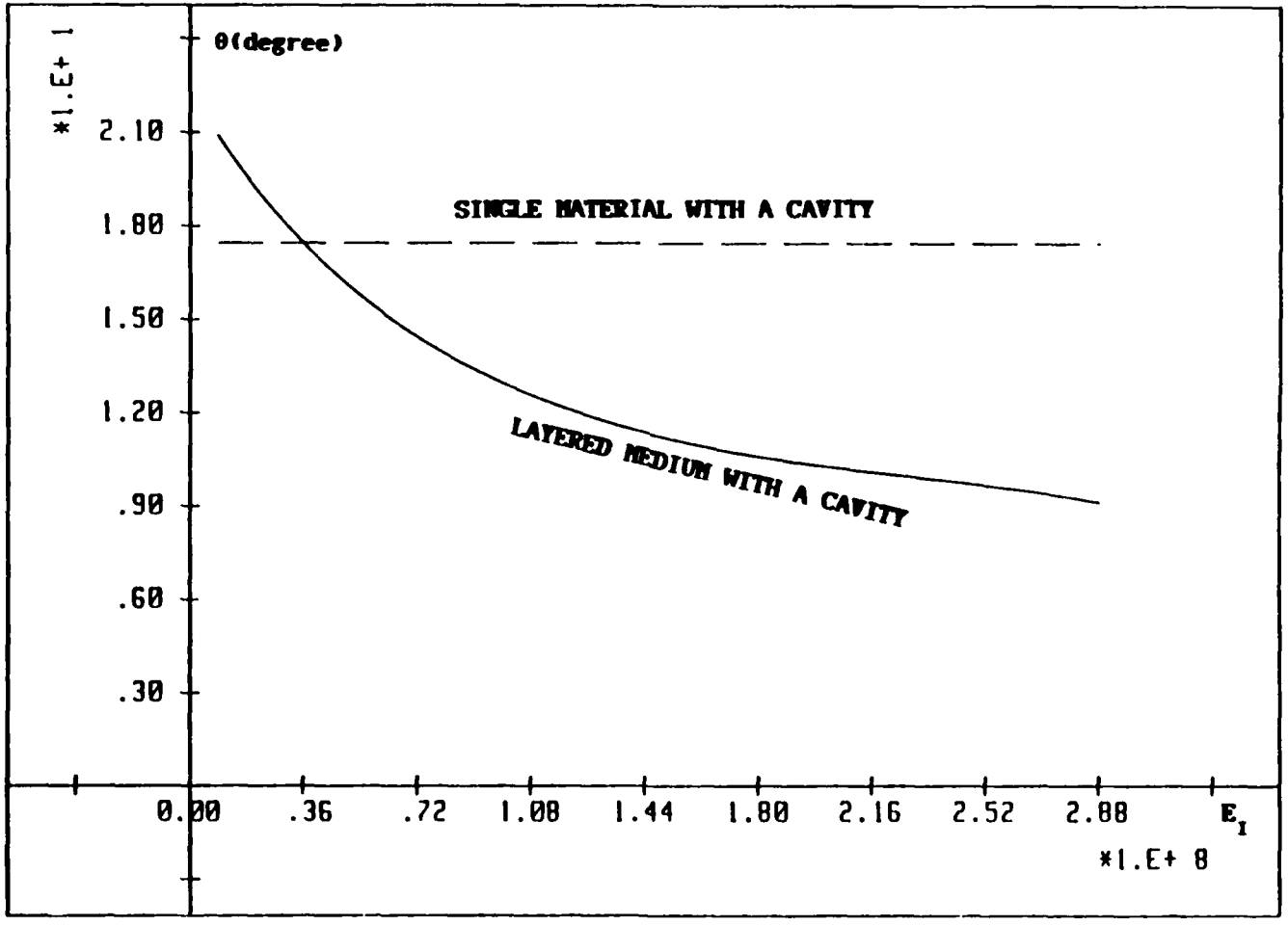

Figure 4.21 The effect of Young's modulus of the coating layer on the angle of principal direction of the thermal stress field. L=0.094, and η=0.06 above the top edge of the cavity for all cases.

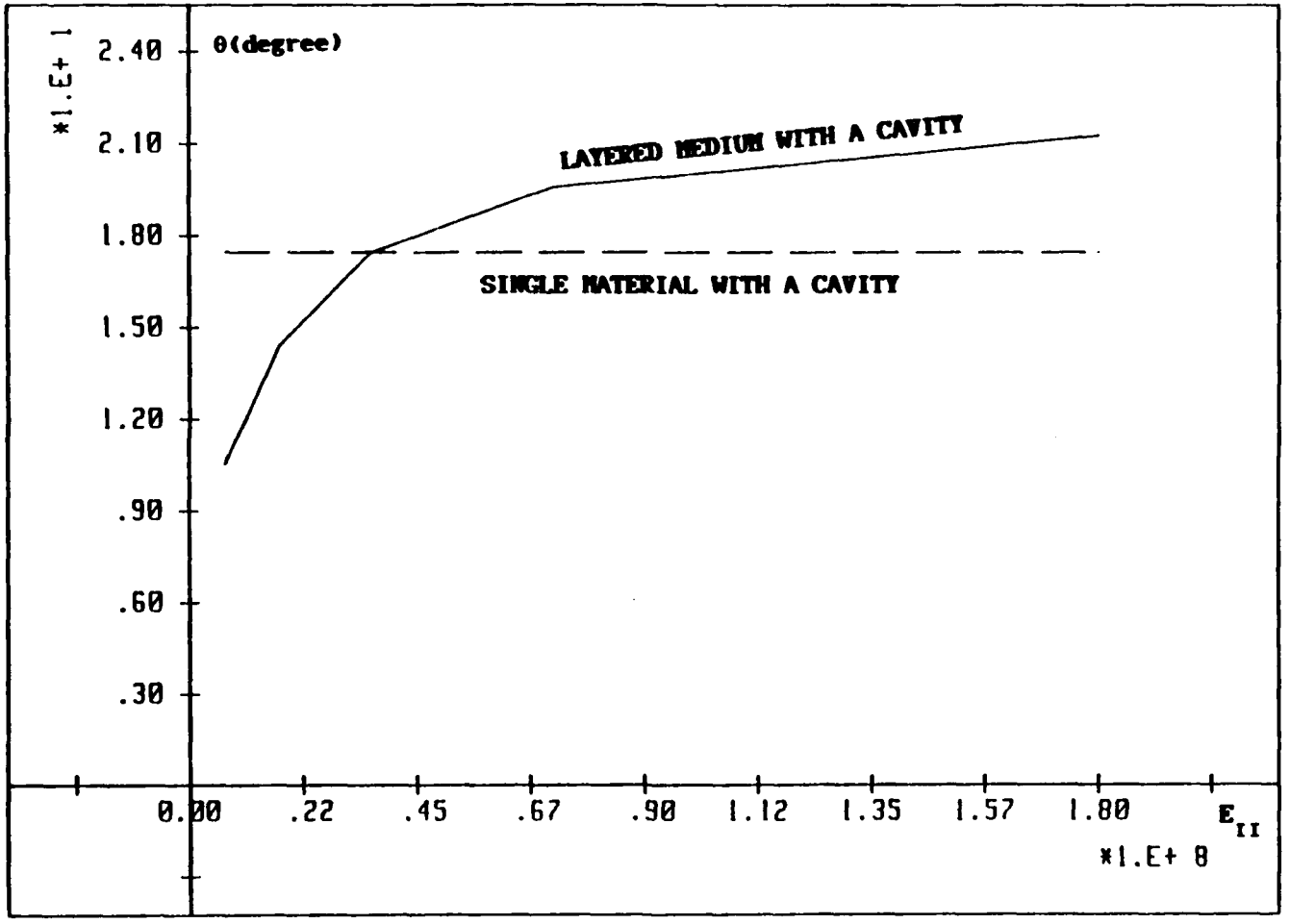

Figure 4.22 The effect of Young's modulus of the substrate on the angle of principal direction of the thermal stress field. L=0.094, and η=0.06 above the top edge of the cavity for all cases.

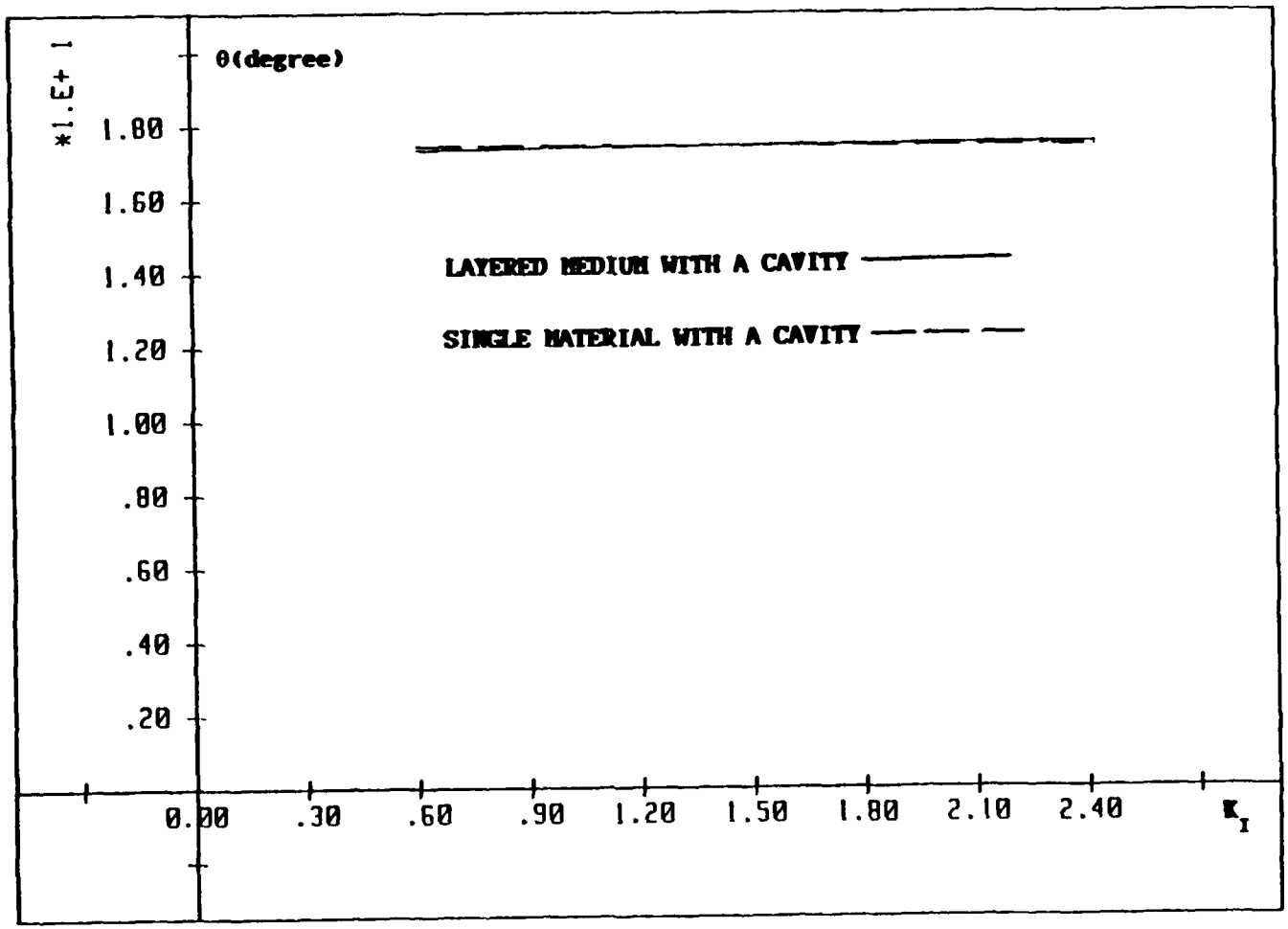

Figure 4.23 The effect of thermal conductivity of the coating layer on the angle of principal direction of the thermal stress field. L=0.094, and η=0.06 above the top edge of the cavity for all cases.

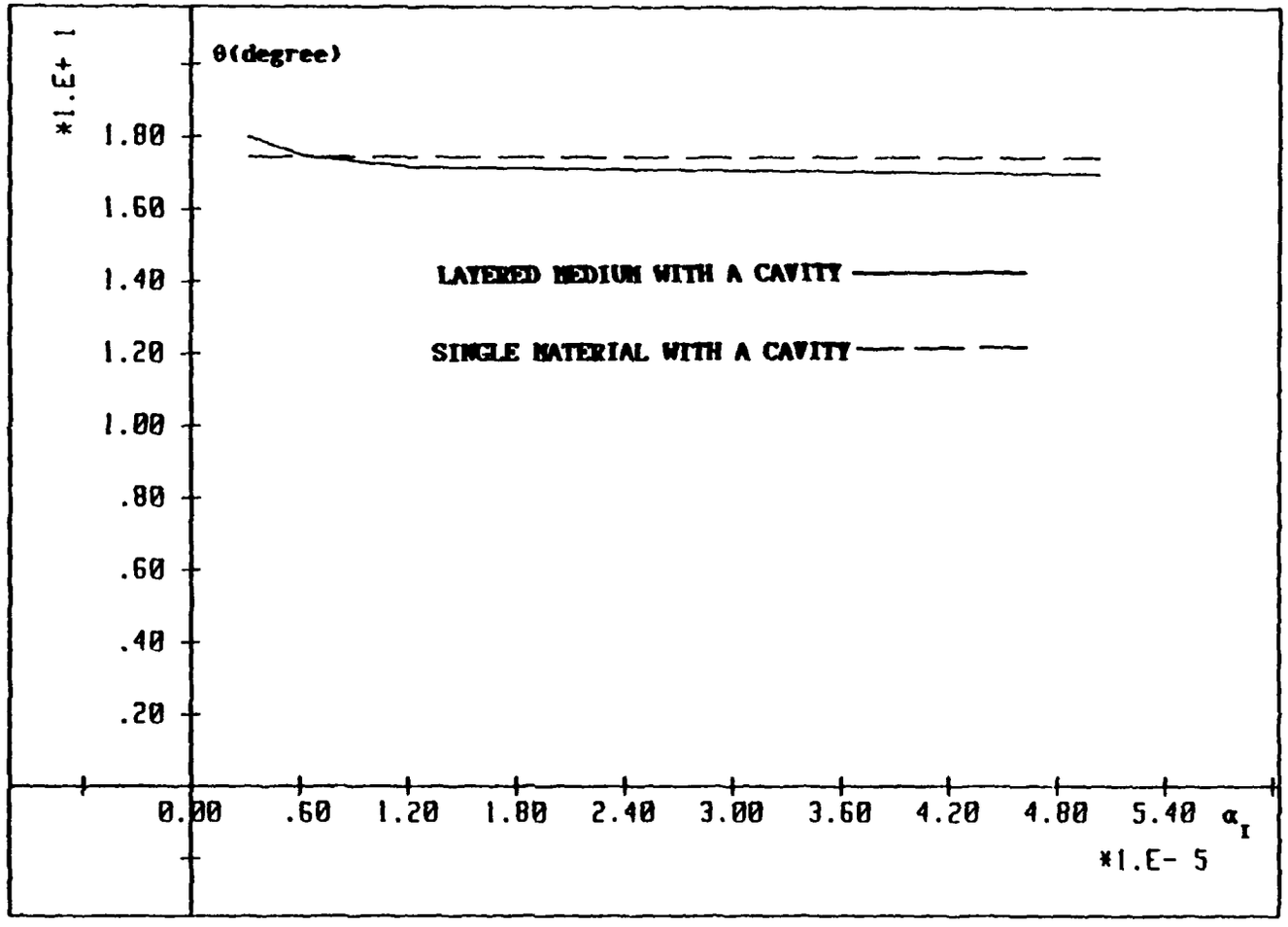

Figure 4.24 The effect of the coefficient of thermal expansion of the coating layer on the angle of principal direction of the thermal stress field. L=0.094, and η=0.06 above the top edge of the cavity for all cases.

CHAPTER 5

DISCUSSION AND CONCLUSIONS

The present investigation demonstrates the effect of a near-surface rectangular cavity on the temperature and stress fields caused by the frictional excitation of a moving asperity. The effects of a coating layer are demonstrated by the material parameter variations in the coating layer and the substrate, including changes on both thermal and mechanical properties. The mathematical model, because of the geometry, is time explicit. Since the transient solution to a multiple-boundary problem is always complex, numerical solutions become necessary for analyses in specific cases. In the present problem, it has been demonstrated that: (i) the transient governing differential equations (2.1, 2.12, and 2.26), can be formulated in difference forms; (ii) the nonuniform mesh (ξ,η), which must be employed due to strong local effects, can be transformed into a uniform mesh $(\bar{\xi},\bar{\eta})$; (iii) boundary conditions in temperature and/or heat flux can be expressed through the energy balance method, thus avoiding the singularity problem at the cavity corner; (iv) the stress singularity at each corner of the cavity can be taken care of by embedding a known stress singularity in the vicinity of the corner; (v) the numerical solution can be tested by comparing with a known analytical solution, showing a satisfactory accuracy; and (vi) the numerical scheme can be extended to compute the solution for other geometries, such as those including cracks and circular cavities, using proper coordinate transformations.

Like most numerical solutions, functional relationships can not be

obtained without voluminous computations. However, significant conclusions can be reached through a careful selection of pertinent cases for the numerical results. The conclusions for the present problem are:

Temperature field

1. Because of the discontinuity in heat transfer across the cavity, temperature will rise higher in the ligament region than the no-cavity case.

2. The temperature rise is inverse to the ligament volume, represented by the ligament thickness.

3. Increasing the thermal conductivity and heat capacity of the coating layer, will decrease the surface temperature.

4. When the coating/substrate interface is at the ligament depth, the thermal property of the substrate will influence the temperature field in the region on the trailing edge of the asperity.

5. Because of the necessary heat transfer in the lateral direction, the heat flux will be at a large oblique angle to the wear surface. In the case of a layered medium without a cavity, the near surface heat flux at the critical position is in a direction approximately 90^{o} to the wear surface. With the presence of a cavity, not only the magnitude of the temperature gradient increases, but also the direction of the temperature gradient is rotated to a more oblique angle to the wear surface. This will affect principal directions in the thermal stress field.

Stress field

1. In the governing differential equation, the small order coefficients of the dynamic terms would have required an extremely

small time step for the consideration of stability and truncation error. This difficulty was circumvented by using the perturbation method. The solutions of the differential equations (4.12) and (4.13) of the various perturbation orders are well-behaved. The magnification, (u_{i+1}/u_i), is of order 10^2. Since $\epsilon(=M^2)$ is of the order 10^{-6}, each perturbation term in equations (4.12) and (4.13) is of order 10^{-4} of its preceding term. Because the series converges rapidly, all computations are deemed adequate by using only one term.

2. When a cavity exists, the stress state that determines the failure phenomenon is much more severe than in the no-cavity case. This will lead to earlier failure of the mechanism.

3. The mechanical effect, which can be neglected in the no-cavity case, is not negligible when cavities exist.

4. The effects of the mechanical and thermal properties on the stress field are consistent with those obtained in the no-cavity case in reference [32]. These effects may be summarized as follows: thermal stress can be reduced by decreasing Young's modulus in the coating layer, increasing Young's modulus in the substrate, increasing thermal conductivity and thermal capacity of the coating layer, and decreasing the coefficient of thermal expansion of the coating layer.

5. For a thin coated medium, the cavity location and the material properties matching (especially Young's modulus) will influence the principal directions of the thermal stress field. When the angle of principal direction becomes larger, shear stress at the coating/substrate interface becomes dominant, leading toward delamination of the coating.

6. The location of the cavity influences the critical depth at

which the thermal tensile stress reaches a maximum. When the cavity occurs closer to the wear surface, not only the critical depth is reduced but also a higher stress results, which reaches its maximum at a critical ligament thickness. Further reduction of the ligament thickness would increase the ligament temperature, resulting in an extension of the thermal compressive region therein. Correspondingly, the thermal tensile stress decreases near the ligament region. The illustration for Stellite III shows that the critical thickness is at L_{cr}=0.094 for both cases of a single material and a layered medium with a thickness of approximately 40% of the critical depth of the no-cavity case. For the normal design of coating thickness, the critical depth of the specific coating material can function as a guide. However, if cavities are either unavoidable or too expensive to control, the design thickness should avoid the critical ligament thickness.

APPENDIX I

INTRODUCTION TO THE FINITE DIFFERENCE METHOD

The use of numerical methods for solving problems is a result of the complexity of the analytical solutions associated with practical engineering problems. Often times, analytical solutions are impossible. In engineering problems, factors that bring about the use of numerical methods are complex geometry, nonlinearity, nonuniform boundary conditions, time-dependent boundary conditions, temperature-dependent properties, and so on. In some cases, analytical solutions are possible, in principle, but the mechanics of obtaining the exact solution may be much more difficult than the task of solving the problem numerically. For example, in the problem of finding the stress solution of a composite multilayered body with nonhomogeneous boundary conditions, it is relatively easy to set up the differential equations. The solution, however, is extremely complex, because it is necessary to deal with simultaneous partial differential equations. In all such cases and many others, if one is equipped with the knowledge of numerical methods and computer programming, the required solution can be successfully obtained.

Finite difference approximations for derivatives were already in use by Euler in 1768. The simplest finite difference procedure for dealing with the problem $dx/dt=f(x)$, $x(0)=a$ is obtained by replacing $(dx/dt)_{n-1}$ with the crude approximation $(x_n - x_{n-1})/\Delta t$. This leads to the recurrence relation $x_0=a$, $x_n= x_{n-1}+ \Delta t\ f(x_{n-1},t_{n-1})$ for $n > 0$. This procedure is known as Euler's method. Thus we see

that, for one-dimensional systems, the finite difference approach has been deeply ingrained in computational algorithms for quite some time.

I.1 Finite Difference Approximation of Derivatives Through Taylor's Series

The derivative of a function at a given point can be represented by a finite difference approximation using a Taylor series expansion of the function about that point. Let f(x) be a function that can be expanded in a Taylor series. Then a Taylor series expansion of the functions f(x+h) and f(x-h) about x, as illustrated in Figure I.1, is given by

$$f(x+h) = f(x) + h\,f'(x) + \frac{h^2}{2!}\,f''(x) + \frac{h^3}{3!}\,f'''(x) + \ldots, \qquad (I.1)$$

$$f(x-h) = f(x) - h\,f'(x) + \frac{h^2}{2!}\,f''(x) - \frac{h^3}{3!}\,f'''(x) + \ldots, \qquad (I.2)$$

where primes denote derivatives with respect to x. The first- and second-order derivatives f'(x) and f''(x) can be represented in the finite difference form in many different ways by utilizing Taylor series expansions given by equations (I.1) and (I.2) as now described.

First Derivatives

To obtain expressions for the finite difference form of the first-order derivative f'(x), equations (I.1) and (I.2) are solved for f'(x). We, respectively, obtain

$$f'(x) = \frac{f(x+h) - f(x)}{h} - \frac{h}{2}\,f''(x) - \frac{h^2}{6}\,f'''(x) + \ldots, \qquad (I.3)$$

$$f'(x) = \frac{f(x) - f(x-h)}{h} + \frac{h}{2}\,f''(x) - \frac{h^2}{6}\,f'''(x) + \ldots, \qquad (I.4)$$

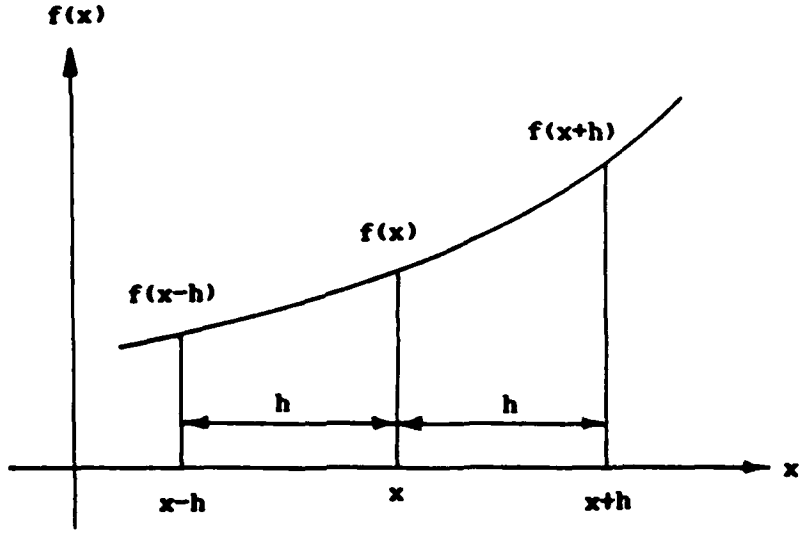

Figure I.1 Nomenclature for a Taylor series representation.

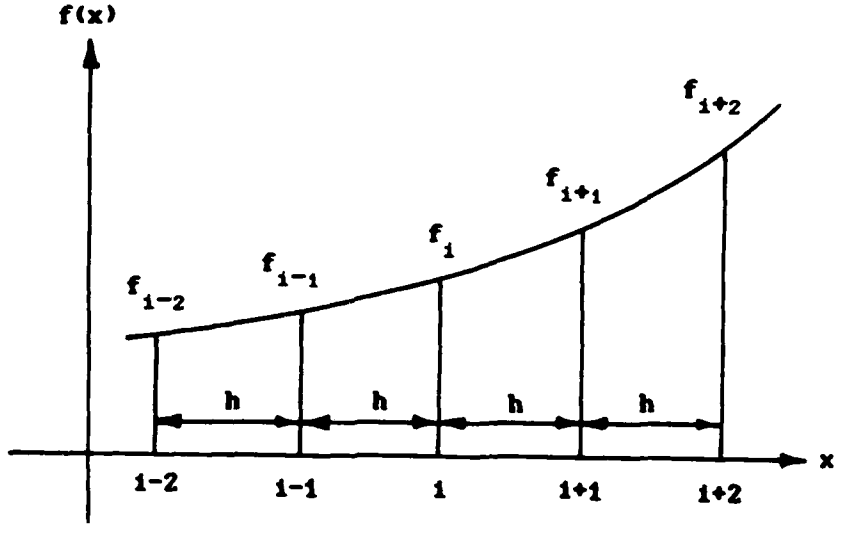

Figure I.2 Nomenclature for finite difference representation of f(x).

Subtracting equations (I.1) and (I.2) and solving for $f'(x)$ we obtain

$$f'(x) = \frac{f(x+h) - f(x-h)}{2h} - \frac{h^2}{6} f'''(x) + \ldots, \qquad (I.5)$$

From equations (I.3) to (I.5), the following approximations can be written respectively for the first derivative of a function $f(x)$ about the point x.

$$f'_i = \frac{f_{i+1} - f_i}{h} + O(h), \text{ forward difference} \qquad (I.6)$$

$$f'_i = \frac{f_i - f_{i-1}}{h} + O(h), \text{ backward difference} \qquad (I.7)$$

$$f'_i = \frac{f_{i+1} - f_{i-1}}{2h} + O(h^2), \text{ central difference} \qquad (I.8)$$

here the notation $O(h)$ is used to show that the truncation error involved is of the order of h; similarly $O(h^2)$ is for the truncation error of the order of h^2, and

$$x = ih, \quad x+h = (i+1)h, \quad x-h = (i-1)h, \quad \text{etc}, \qquad (I.9)$$

$$f(x) = f_i, \quad f(x+h) = f_{i+1}, \quad f(x-h) = f_{i-1}, \quad \text{etc}, \qquad (I.10)$$

as illustrated in Figure I.2. We note that forward and backward differences are accurate to the order h whereas the central difference expression is accurate to the order h^2. More accurate expressions can be obtained for the forward and backward difference representation of the first-order derivative as will be dicussed later.

Second Derivatives

We now proceed to the finite difference representation of the second derivative $f''(x)$ of a function $f(x)$ about the point x. To obtain such results we consider a Taylor series expansion of functions $f(x+2h)$ and $f(x-2h)$ about x as

$$f(x+2h) = f(x) + 2h\, f'(x) + 2h^2\, f''(x) + \frac{4}{3} h^3\, f'''(x) + \ldots, \quad (I.11)$$

$$f(x-2h) = f(x) - 2h\, f'(x) + 2h^2\, f''(x) - \frac{4}{3} h^3\, f'''(x) + \ldots, \quad (I.12)$$

Eliminating $f'(x)$ between equations (I.1) and (I.11) we obtain

$$f''(x) = \frac{f(x) + f(x+2h) - 2f(x+h)}{h^2} - h\, f'''(x) + \ldots, \quad (I.13)$$

Similarly, eliminating $f'(x)$ between equations (I.2) and (I.12), we find

$$f''(x) = \frac{f(x-2h) + f(x) - 2f(x-h)}{h^2} + h\, f'''(x) + \ldots, \quad (I.14)$$

Eliminating $f'(x)$ between equations (I.1) and (I.2) we obtain

$$f''(x) = \frac{f(x-h) + f(x+h) - 2f(x)}{h^2} - \frac{1}{12} h^2\, f''''(x) + \ldots, \quad (I.15)$$

Using the subscript notation defined by equations (I.9) and (I.10), various forms of the finite difference representation of the second-order derivative $f''(x)$ about the point x given by equations (I.13) to

(I.15) are written, respectively, as

$$f_i'' = \frac{f_i - 2f_{i+1} + f_{i+2}}{h^2} + O(h), \quad \text{forward difference} \qquad (I.16)$$

$$f_i'' = \frac{f_{i-2} - 2f_{i-1} + f_i}{h^2} + O(h), \quad \text{backward difference} \qquad (I.17)$$

$$f_i'' = \frac{f_{i-1} - 2f_i + f_{i+1}}{h^2} + O(h^2). \quad \text{central difference} \qquad (I.18)$$

We note that the central difference representation is accurate to $O(h^2)$ whereas the forward and backward differences to $O(h)$.

More Accurate Finite Difference Representations

The forward and backward finite difference representations given above are accurate to $O(h)$. More accurate expressions can be obtained as now described. Suppose $f'(x)$ is to be represented in forward difference to $O(h^2)$. Equation (I.13) is introduced into equation (I.3) and $f''(x)$ is eliminated. We obtain

$$f'(x) = \frac{-3f(x) + 4f(x+h) - f(x+2h)}{2h} + \frac{1}{3} h^2 f'''(x) + \ldots, \qquad (I.19)$$

which is written more compactly in the form

$$f_i' = \frac{-3f_i + 4f_{i+1} - f_{i+2}}{2h} + O(h^2), \quad \text{forward difference} \qquad (I.20)$$

Similarly, introducing equation (I.14) into equation (I.4) to eliminate $f''(x)$, we find

$$f_i' = \frac{f_{i-2} - 4f_{i-1} + 3f_i}{2h} + O(h^2), \quad \text{backward difference} \qquad (I.21)$$

The above procedure can be extended to obtain more accurate expressions for the first and second derivatives. Such expressions are presented in reference [47] for various order derivatives.

The derivative of a function in non-uniform spacing (Figure I.3) can also be approximated by finite difference using a Taylor series expansion. A summary of the finite difference representation of the first- and second-order derivatives of a function f(x) in non-uniform spacing is given below

$$f'_i = -\frac{2h_1 + h_2}{h_1\,(h_1+h_2)}\,f_i + \frac{h_1 + h_2}{h_1 h_2}\,f_{i+1} - \frac{h_1}{h_2\,(h_1+h_2)}\,f_{i+2}\,,$$

forward difference (I.22)

$$f'_i = \frac{h_2}{h_1\,(h_1+h_2)}\,f_{i-2} - \frac{h_1 + h_2}{h_1 h_2}\,f_{i-1} + \frac{h_1 + 2h_2}{h_2\,(h_1+h_2)}\,f_i\,,$$

backward difference (I.23)

$$f'_i = -\frac{h_2}{h_1\,(h_1+h_2)}\,f_{i-1} + \frac{h_2 - h_1}{h_1 h_2}\,f_i + \frac{h_1}{h_2\,(h_1+h_2)}\,f_{i+1}\,,$$

central difference (I.24)

$$f''_i = \frac{2}{h_1\,(h_1+h_2)}\,f_{i-1} - \frac{2}{h_1 h_2}\,f_i + \frac{2}{h_2\,(h_1+h_2)}\,f_{i+1}\,.$$

central difference (I.25)

Using equations (I.22) to (I.25) is very cumbersome, and it may lead to loss of accuracy. A more elegant method, general coordinates transformation, can be employed in the non-uniform mesh to avoid these problems. This transformation will be discussed in detail later.

I.2 Errors Involved in Numerical Solutions

In numerical solutions using the method of finite differences, the partial differential equation is approximated with finite difference

expressions at each nodal point, and as a result the solution of the differential equation is transformed to the solution of a set of algebraic equations. We have seen that, whenever a derivative is approximated by finite difference using a Taylor series expansion, an error is involved. Such an error is called the truncation error or the discretization error. These errors appear because a continuous operator such as the first, or the second-order derivative, is replaced by a finite difference approximation. In addition, numerical calculations are carried out only to a finite number of decimal places or significant figures; as a result, at each step in the calculation, some error is introduced due to this rounding-off, called the round-off error.

Clearly, if the finite difference approximation is made by using formulas having truncation errors of high order, the truncation error at each step is minimum. Also, by decreasing the step size, the truncation error is reduced for each step; however, a limit also is reached at which further reduction in step size increases the total number of calculations and as a result the round-off error may become dominant.

Ideally, if it were possible to carry out the finite difference calculations with extremely small steps and to perform the calculations to an infinite number of decimal places, the resulting solution would be exact. However, due to the cumulative effects of the rounding off error and the discretization errors, the solutions obtained by the finite difference method is expected to deviate from the exact result; therefore, the solution computed is the numerical solution but not the exact result. It is very difficult to determine the cumulative

departure of the numerical solution from the exact result due to the cumulative effects of such errors. Comparison of numerical solutions with exact analytic solutions reveals that, for most cases, the results are very close indeed. After some experience with different methods and different step sizes, a suitable combination can be chosen for the numerical solution of a given problem.

I.3 Time Dependent Problem

The stability consideration plays an important role in the finite difference solution of time dependent problems. There are several schemes available to express the time dependent problems in finite difference form. Each of these differencing schemes has its advantages and limitations. We now discuss some of them by using the one-dimensional time-dependent heat conduction equation as examples.

Explicit Method

The one-dimensional, time-dependent heat conduction equation for a finite region $0 \leq x \leq L$ is

$$\frac{\partial T}{\partial t} = k \frac{\partial^2 T}{\partial x^2} , \tag{I.26}$$

If $\frac{\partial^2 T}{\partial x^2}$ and $\frac{\partial T}{\partial t}$ are replaced by the central and forward differences, respectively, and using a uniform mesh size Δx in the x domain and Δt for the time step, equation (I.26) can be rewritten in the finite-difference form as

$$\frac{T(i,n+1) - T(i,n)}{\Delta t} = k \frac{T(i-1,n) - 2T(i,n) + T(i+1,n)}{\Delta x^2} , \tag{I.27}$$

with a truncation error of $O(\Delta t)+O(\Delta x^2)$. Where $T(x,t)$ is

represented by $T(x,t) = T(i\Delta x, n\Delta t) = T(i,n)$. Solving equation (I.27) for $T(i,n+1)$ one obtains

$$T(i,n+1) = rT(i-1,n) + (1-2r)T(i,n) + rT(i+1,n), \qquad (I.28)$$

where $r = \frac{k\Delta t}{\Delta x^2}$.

The equation is called the explicit form because the unknown temperature $T(i,n+1)$ at the time step $(n+1)$ can be directly determined from the temperatures $T(i-1,n)$, $T(i,n)$, and $T(i+1,n)$ at the previous time step. The explicit scheme provides a relatively straightforward expression for the determination of the unknown $T(i,n+1)$. The only disadvantage of this method is that once k and Δx are fixed, there is a maximum permissible step size Δt, which, by instability considerations should not be exceeded. For example, when the boundary conditions at $x=0$ and $x=L$ are both of the first kind (i.e., specified temperature), the restriction imposed on the parameter r is

$$0 \leq r \leq \frac{1}{2} . \qquad (I.29)$$

That is, for given values of k and Δx, if the time step Δt exceeds the limit imposed by the above criteria, the numerical calculations become unstable, as a result of the amplification of errors. Figure I.4 illustrates what happens to the numerical calculations when the above stability criteria is violated. In this figure, the numerical calculations performed with a time step satisfying the condition $r = \frac{5}{11} < \frac{1}{2}$ is in good agreement with the exact solution; whereas the numerical solution of the same problem with slightly larger time step,

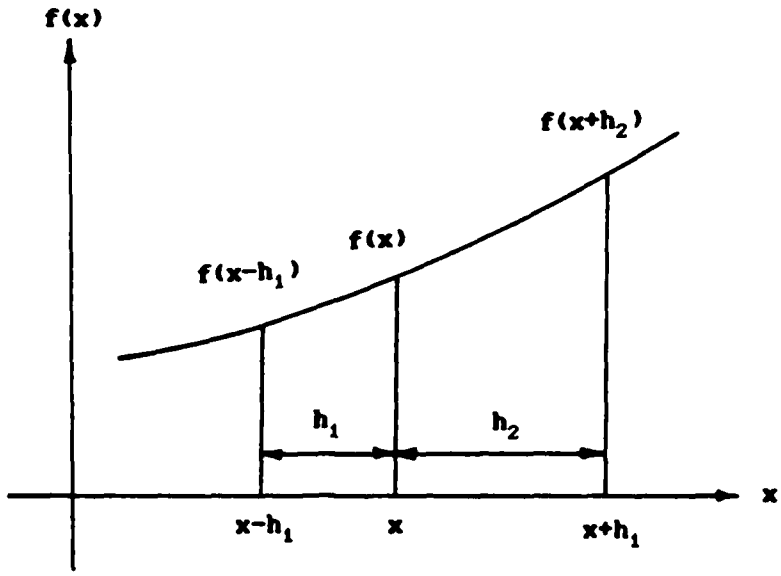

Figure I.3 Nonuniform mesh.

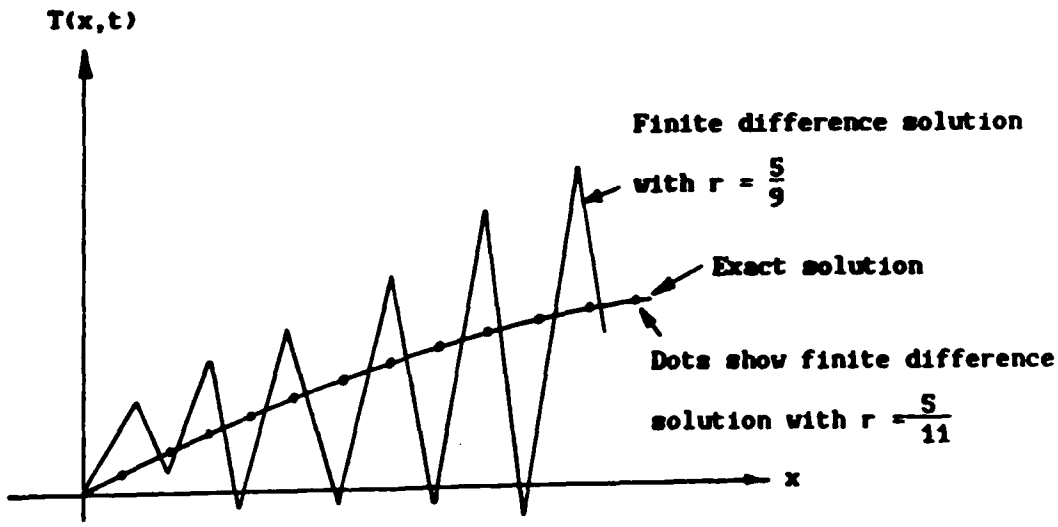

Figure I.4 Effects of parameter $r=\kappa\Delta t/(\Delta x)^2$ on the stability of finite difference solution.

which violates the above stability criteria, i.e., $r=\frac{5}{9}>\frac{1}{2}$, results in an unstable solution.

Implicit Method

The explicit method discussed above is simple computationally, but very small time step should be used because of stability considerations. Therefore, a prohibitively large number of time steps may be required if solutions are to be computed over a large period of time. It is for this reason that other finite difference forms, found to be less restrictive to the size of time step Δt, have been developed. One such scheme is the fully implicit method. We illustrate this method by considering the finite difference representation of the heat conduction equation (I.26). The partial derivative $\frac{\partial^2 T}{\partial x^2}$ is represented in finite difference form using the central difference formula, whereas the time derivative $\frac{\partial T}{\partial t}$ is represented in the finite difference form using the backward difference expression.

Then, the finite difference form of equation (I.26) becomes

$$\frac{T(i,n+1) - T(i,n)}{\Delta t} = k \frac{T(i-1,n+1) - 2T(i,n+1) + T(i+1,n+1)}{\Delta x^2} , \quad (I.30)$$

This is called an implicit form of the finite difference representation, because to determine the unknowns T(i,n+1), a set of simultaneous algebraic equations are to be solved. The advantage of the implicit method is that it is stable for all sizes of time step Δt. Thus, there is no size restriction on Δt. The only size restriction on Δt is due to the consideration of the truncation error.

The truncation errors for both explicit and implicit forms of the

finite difference representations of the heat conduction equation is of the order $(\Delta x^2)+(\Delta t)$. But the actual accumulated error in both methods need not be the same. Depending on the nature of the problem, one of the methods may be preferred to the other.

Crank-Nicolson Method

Crank and Nicolson [47] suggested a modified implicit method. In this method, the heat conduction equation (I.26) is represented in finite difference form by taking the arithmetic average of the right-hand sides of the explicit form (I.26) and the implicit form (I.30). Then, equation (I.26) becomes

$$\frac{T(i,n+1) - T(i,n)}{\Delta t} = \frac{k}{2}\left[\frac{T(i-1,n+1) - 2T(i,n+1) + T(i,n+1)}{\Delta x^2} + \right.$$

$$\left. + \frac{T(i-1,n) - 2T(i,n) + T(i+1,n)}{\Delta x^2}\right]. \qquad (I.31)$$

The advantage of this mehtod is that, for given values of the space and time steps Δx and Δt, the resulting solution involves less truncation error due to Δt than the explicit and the implicit forms discussed above. On the other hand the Crank-Nicolson form involves additional computation.

To provide a better insight to the physical significance of the Crank-Nicolson representation, equation (I.31) can be written in a more general form by taking a weighted average of the two terms in the brackets

$$\frac{T(i,n+1) - T(i,n)}{\Delta t} = k\left[\eta\frac{T(i-1,n+1) - 2T(i,n+1) + T(i+1,n+1)}{\Delta x^2} + \right.$$

$$+ (1-\eta) \frac{T(i-1,n) - 2T(i,n) + T(i+1,n)}{\Delta x^2} \Big], \quad (I.32)$$

where $0 \leq \eta \leq 1$ is called the degree of implicitness. Clearly, equation (I.32) reduces to the explicit form given by equation (I.27) for $\eta=0$, to the implicit form given by equation (I.30) for $\eta=1$ and the Crank-Nicolson form (I.31) for $\eta=\frac{1}{2}$.

Alternating-Direction Implicit Method

The implicit methods discussed above are advantageous to us because of the superior stability properties. On the other hand, becuase a large number of simultaneous equations need to be solved at each time step, the computational problems become enormous when they are applied to the solution of time dependent problems involving two or three space dimensions. For example, for a three-dimensional problem with N interior nodal points in each direction, there are a total of N^3 nodes, hence $N^3 \times N^3$ matrix equations must be solved for each time increment.

The alternating-direction implicit (A.D.I.) method introduced by Peaceman and Rachford [48], provides an efficient method for solving problems involving large number of nodes. To illustrate the procedure, a two-dimensional, time dependent heat conduction equation is considered

$$\frac{\partial^2 T}{\partial x^2} + \frac{\partial^2 T}{\partial y^2} = \frac{1}{\kappa} \frac{\partial T}{\partial t}, \quad \text{in the region } R \quad (I.33)$$

To represent the space derivatives in finite difference form, the central difference formula is used with an implicit and explicit difference approximation alternatively for $\frac{\partial^2 T}{\partial x^2}$ and $\frac{\partial^2 T}{\partial y^2}$. For example, if $\frac{\partial^2 T}{\partial x^2}$

is represented in the implicit form, the derivative $\frac{\partial^2 T}{\partial y^2}$ is represented by an explicit approximation. Then, the finite difference form of equation (I.33), to proceed the solution from the (n)th step to (n+1)th step, becomes

$$\frac{1}{\kappa}\frac{T(i,j,n+1) - T(i,j,n)}{\Delta t} = \frac{T(i-1,j,n+1) - 2T(i,j,n+1) + T(i+1,j,n+1)}{\Delta x^2} +$$

$$+ \frac{T(i,j-1,n) - 2T(i,j,n) + T(i,j+1,n)}{\Delta y^2} . \qquad (I.34)$$

The finite difference form of equation (I.33), to proceed the solution from the (n+1)th step to the (n+2)th step, is written using an explicit form for $\frac{\partial^2 T}{\partial x^2}$ and implicit form for $\frac{\partial^2 T}{\partial y^2}$ as

$$\frac{1}{\kappa}\frac{T(i,j,n+2)-T(i,j,n+1)}{\Delta t} = \frac{T(i-1,j,n+1) - 2T(i,j,n+1) + T(i+1,j,n+1)}{\Delta x^2} +$$

$$+ \frac{T(i,j-1,n+2) - 2T(i,j,n+2) + T(i,j+1,n+2)}{\Delta y^2} . \qquad (I.35)$$

The procedure is repeated alternately in the subsequent time steps.

The advantage of the A.D.I. method over the implicit method results from the fact that it reduces the number of equations to be solved simultaneously for each time step. Consider for example a two-dimensional, time dependent problem with N internal nodes along the x-axis and N nodes along the y-axis. The A.D.I. method requires the solution of N simultaneous equation N times for each time step, whereas the implicit method requires the solution of N^2 equation at each time step. There are other methods, for example, the alternating direction

explicit (A.D.E) method [49], the Douglas-Rachford implicit scheme [48],..., etc. The reader should consult these references for further discussion of these methods.

APPENDIX II

NON-UNIFORM MESH AND GENERAL COORDINATES TRANSFORMATION

The solution of a system of partial differential equations can be greatly simplified by a well-constructed grid. On the other hand, a grid which is not well suited to the problem can lead to an unsatisfactory result. In some applications, improper choice of grid point locations can lead to an apparent instability or lack of convergence. For many applications, a non-uniform mesh must be used in order to obtain an accurate solution and to save computing time. One can solve the problem in the physical plane (original plane) by applying the difference formulas on the non-uniform mesh directly, or transform the non-uniform mesh to a uniform mesh and solve the problem in the computational plane. Generally, the coordinate transformation gives a more accurate solution than mesh changes.

II.1 Non-Uniform Mesh

The simplest variation of the rectangular mesh system is obtained by simply changing the mesh spacing in one direction at some point. This would be done for the purpose of obtaining higher resolution (and hopefully higher accuracy) in some region where the gradients were expected to change rapidly. To illustrate this technique, we consider the obvious method of changing from Δx_1 to Δx_2 between node points at some node i=m, as shown in Figure II.1.

Expanding a function in a Taylor series forward and backward from i=m gives

$$f_{m+1} = f_m + \left.\frac{\partial f}{\partial x}\right|_m \Delta x_2 + \frac{1}{2}\left.\frac{\partial^2 f}{\partial x^2}\right|_m \Delta x_2^2 + \frac{1}{6}\left.\frac{\partial^3 f}{\partial x^3}\right|_m \Delta x_2^3 + O(\Delta x_2^4), \quad \text{(II.1)}$$

$$f_{m-1} = f_m - \left.\frac{\partial f}{\partial x}\right|_m \Delta x_1 + \frac{1}{2}\left.\frac{\partial^2 f}{\partial x^2}\right|_m \Delta x_1^2 - \frac{1}{6}\left.\frac{\partial^3 f}{\partial x^3}\right|_m \Delta x_1^3 + O(\Delta x_1^4), \quad \text{(II.2)}$$

The expression for $\left.\frac{\partial f}{\partial x}\right|_m$ is obtained by subtracting equation (II.2) from (II.1)

$$f_{m+1} - f_{m-1} = \left.\frac{\partial f}{\partial x}\right|_m (\Delta x_1 + \Delta x_2) + \frac{1}{2}\left.\frac{\partial^2 f}{\partial x^2}\right|_m (\Delta x_2^2 - \Delta x_1^2) + O(\Delta x^3), \quad \text{(II.3)}$$

where by $O(\Delta x^3)$ we mean the largest of $O(\Delta x_1^3)$ or $O(\Delta x_2^3)$. Solving for $\left.\frac{\partial f}{\partial x}\right|_m$ gives

$$\left.\frac{\partial f}{\partial x}\right|_m = \frac{f_{m+1} - f_{m-1}}{\Delta x_1 + \Delta x_2} - \frac{1}{2}\left.\frac{\partial^2 f}{\partial x^2}\right|_m \frac{\Delta x_2^2 - \Delta x_1^2}{\Delta x_1 + \Delta x_2} + O(\Delta x^2), \quad \text{(II.4)}$$

This means that the form

$$\left.\frac{\partial f}{\partial x}\right|_m = \frac{f_{m+1} - f_{m-1}}{\Delta x_1 + \Delta x_2}, \quad \text{(II.5)}$$

is second-order accurate only if

$$O\left[\frac{\Delta x_2^2 - \Delta x_1^2}{\Delta x_1 + \Delta x_2}\right] \leq O(\Delta x_1^2). \quad \text{(II.6)}$$

Note that, for Δx_2 very small, the accuracy at m deteriorates to first order in Δx_1.

The expression for the second derivative is obtained by multiplying equation (II.2) by $s^2=(\Delta x_2/\Delta x_1)^2$ and adding the result to (II.1).

$$f_{m+1} + (1+s^2)f_m + s^2 f_{m-1} = \left.\frac{\partial f}{\partial x}\right|_m \Delta x_2(1-s) + \left.\frac{\partial^2 f}{\partial x^2}\right|_m \Delta x_2{}^2 +$$

$$+ \frac{1}{6}\left.\frac{\partial^3 f}{\partial x^3}\right|_m \Delta x_2{}^2\,(\Delta x_2 - \Delta x_1) + O(\Delta x^4), \qquad \text{(II.7)}$$

$$\left.\frac{\partial^2 f}{\partial x^2}\right|_m = \frac{f_{m+1} + (1+s^2)f_m + s^2 f_{m-1}}{\Delta x_2{}^2} - \left.\frac{\partial f}{\partial x}\right|_m \left(\frac{1-s}{\Delta x_2}\right) +$$

$$+ O[(\Delta x_2 - \Delta x_1), \Delta x^2]\ . \qquad \text{(II.8)}$$

The resulting expression now requires $s=O(1-\Delta x_1{}^2)$ just to be first-order accurate at i=m.

It is clear from the above equations that, unless the mesh spacing is changed slowly, the formal truncation error is actually degraded, *rather than improved.*

II.2 Coordinates Transformations

Early work using finite difference methods was restricted to problems where suitable coordinate systems could be selected in order to solve the governing equations in that base system. As experience in computing complex problem was gained, general mappings were employed to transform the physical plane into a computational domain. Numerous advantages accrue when this procedure is followed. For example, when the untransformed equations are differenced in the expanding mesh, the result is a deterioration of formal accuracy, as we have seen; but the transformed equations may be differenced in a regular mesh (such as constant $\Delta\bar{x}$, $\Delta\bar{y}$) with no deterioration in the formal order of truncation error, except that it will now be $O(\Delta\bar{y}^2)$ rather than $O(\Delta y^2)$, also, the body surface can be selected as a

boundary in the computational plane permitting easy application of surface boundary conditions. In general, transformations are used which lead to a uniform space grid in the computational plane while points in physical space may be unequally spaced. This situation is shown in Figure II.2. When this procedure is used, it is necessary to include the derivatives of the mapping in the differential equation.

II.2.1 Simple Transformations

In this section, simple independent variable transformations are used to illustrate how the governing equations are transformed. As a first example, the problem of clustering grids near a wall is considered. Figure II.3a shows a mesh above a flat plate in which grid points are clustered near the plate in the normal direction (y). While the spacing is not uniform in the y direction, it is convenient to apply a transformation to the y coordinate so that the governing equations can be solved on a uniformly spaced grid in the computational plane $(\bar{x},\bar{y})$ as seen in Figure II.3b. A suitable transformation for a two-dimensional problem is given by

Transformation 1:

$$\bar{x} = x \ , \tag{II.9}$$

$$\bar{y} = 1 - \frac{\ln[[\beta + 1 - (y/h)]/[\beta - 1 + (y/h)]}{\ln[(\beta + 1)/(\beta - 1)]} \ , \quad 1 < \beta < \infty \tag{II.10}$$

This stretching transformation clusters more points near y=0 as the stretching parameter β approaches 1.

In order to apply this transformation to the governing equations, the following partial derivatives are formed

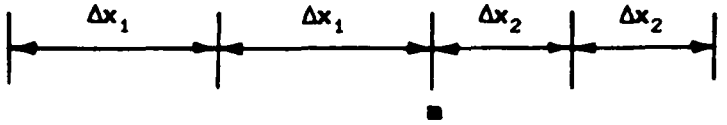

Figure II.1 Nonuniform spacing.

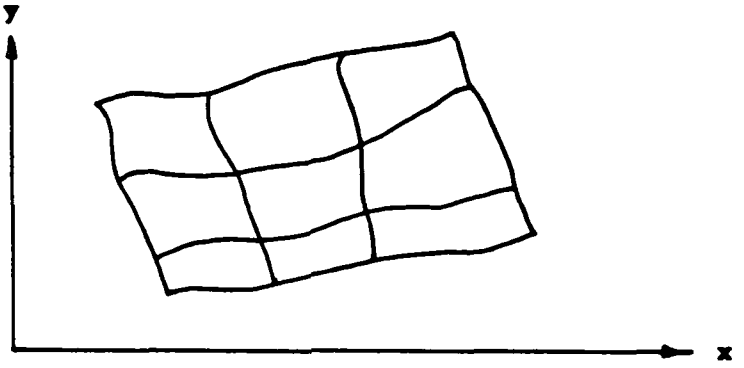

(a) physical plane

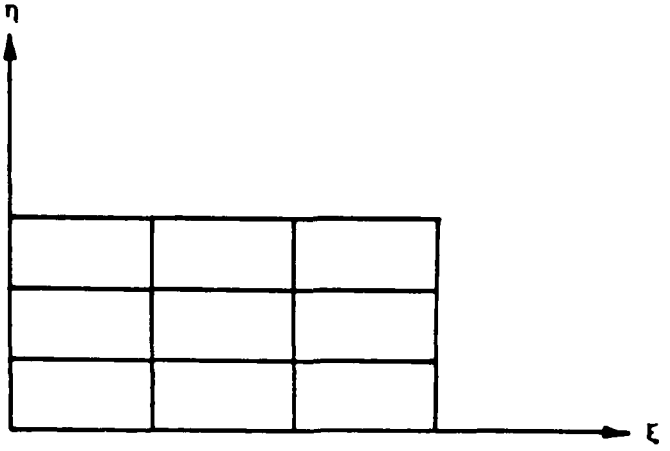

(b) computational plane

Figure II.2 Mapping to comput

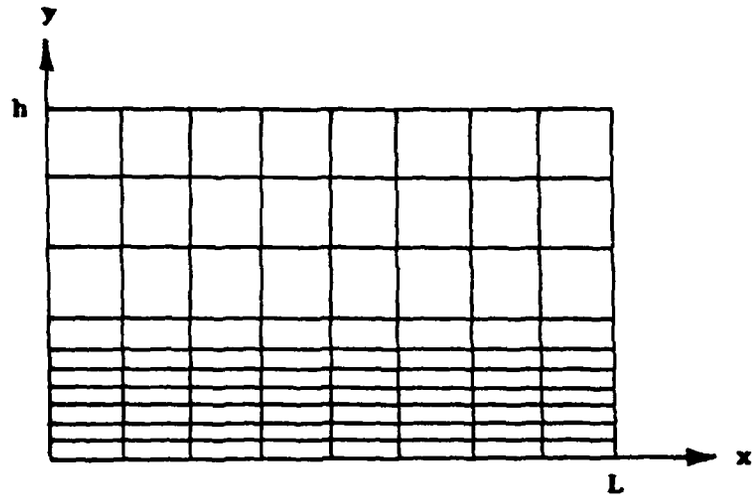

(a) physical plane

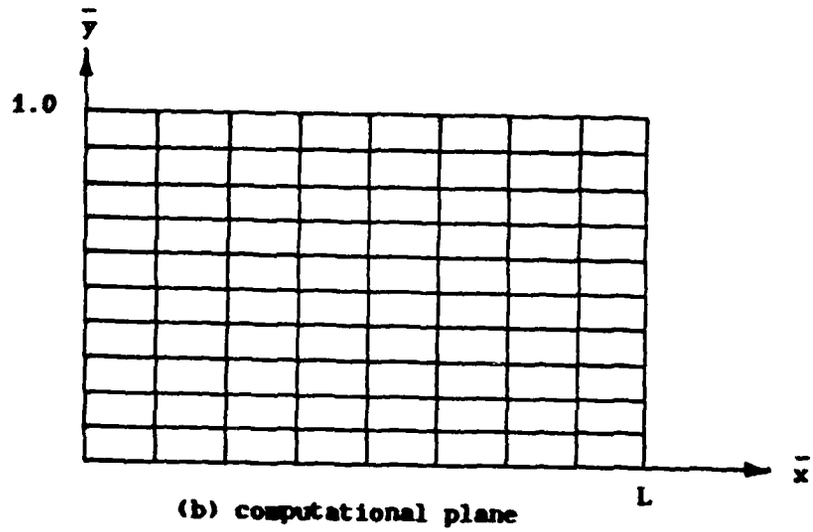

(b) computational plane

Figure II.3 Grid clustering near a wall.

$$\frac{\partial}{\partial x} = \frac{\partial \bar{x}}{\partial x}\frac{\partial}{\partial \bar{x}} + \frac{\partial \bar{y}}{\partial x}\frac{\partial}{\partial \bar{y}} , \tag{II.11}$$

$$\frac{\partial}{\partial y} = \frac{\partial \bar{x}}{\partial y}\frac{\partial}{\partial \bar{x}} + \frac{\partial \bar{y}}{\partial y}\frac{\partial}{\partial \bar{y}} , \tag{II.12}$$

where

$$\frac{\partial \bar{x}}{\partial x} = 1 , \quad \frac{\partial \bar{y}}{\partial x} = 0 , \quad \frac{\partial \bar{x}}{\partial y} = 0 ,$$

and $$\frac{\partial \bar{y}}{\partial y} = \frac{2\beta}{h\{\beta^2 - [1 - (y/h)]^2\}\ln[(\beta + 1)/(\beta - 1)]} .$$

As a result, the partial derivatives simplify to

$$\frac{\partial}{\partial x} = \frac{\partial}{\partial \bar{x}} , \tag{II.13}$$

$$\frac{\partial}{\partial y} = \left(\frac{\partial \bar{y}}{\partial y}\right)\frac{\partial}{\partial \bar{y}} , \tag{II.14}$$

If we now apply this transformation to the following equation

$$\frac{\partial u}{\partial x} + \frac{\partial u}{\partial y} = 0, \tag{II.15}$$

the following transformed equation is obtained

$$\frac{\partial u}{\partial \bar{x}} + \left(\frac{\partial \bar{y}}{\partial y}\right)\frac{\partial u}{\partial \bar{y}} = 0. \tag{II.16}$$

This transformed equation can now be differenced on the uniformly spaced grid in the computational plane. We note that the expression

for the derivative $\frac{\partial \bar{y}}{\partial y}$ contains y so that we must be able to express y as a function of $\bar{y}$. This is refered to as the inverse of the transformation. For the present transformation, given by equations (II.9) and (II.10), the inverse can be readily found as

$$x = \bar{x} \ ,$$

$$y = \frac{(\beta + 1) - (\beta - 1)\{[(\beta + 1)/(\beta - 1)]^{1-\bar{y}}\}}{[(\beta + 1)/(\beta - 1)]^{1-\bar{y}} + 1} \ . \qquad \text{(II.18)}$$

Transformation 2:

$$\bar{x} = x \ , \qquad \text{(II.19)}$$

$$\bar{y} = \alpha + (1 - \alpha)\frac{\ln\left(\{\beta+[y(2\alpha+1)/h]-2\alpha\}/\{\beta-[y(2\alpha+1)/h]+2\alpha\}\right)}{\ln[(\beta+1)/(\beta-1)]} \ . \qquad \text{(II.20)}$$

For this transformation, if $\alpha=0$ the mesh will be refined near y=h only, whereas, if $\alpha=\frac{1}{2}$ the mesh will be refined equally near y=0 (Figure II.4). It has been shown that the stretching parameter β is related (approximately) to the nondimensional thickness (δ/h) by

$$\beta = \frac{1}{(1 - \delta/h)^{1/2}} \ , \qquad 0 < \delta/h < 1 \qquad \text{(II.21)}$$

where h is the height of the mesh. For the transformation given by equations (II.19) and (II.20), the derivative $\frac{\partial \bar{y}}{\partial y}$ is

$$\frac{\partial \bar{y}}{\partial y} = \frac{2\beta(1 - \alpha)(2\alpha + 1)}{h[\beta^2 - [y(2\alpha + 1)/h - 2\alpha]^2]\ln[(\beta + 1)/(\beta - 1)]} \ , \qquad \text{(II.22)}$$

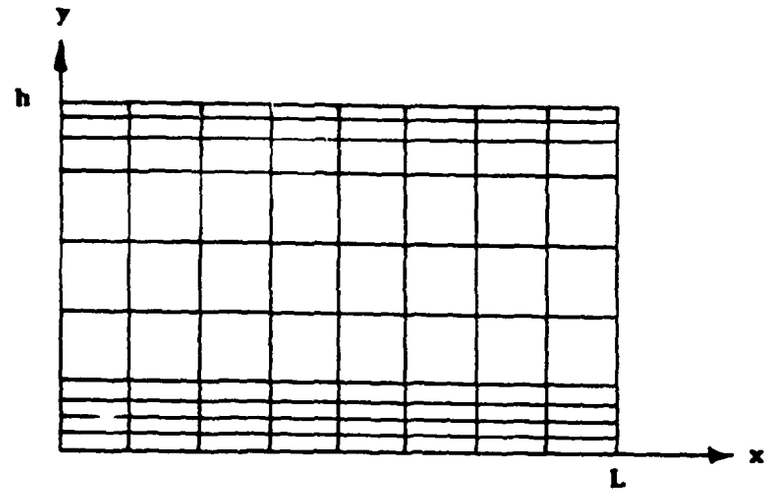

(a) physical plane

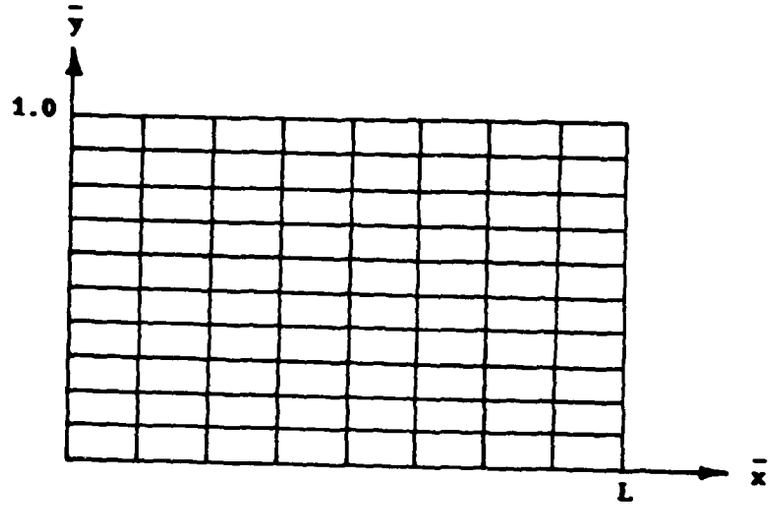

(b) computational plane

Figure II.4 Grid clustering in a duct.

and the inverse transformation becomes

$$x = \bar{x} \ , \tag{II.23}$$

$$y = h \frac{(\beta + 2\alpha)[(\beta + 1)/(\beta - 1)]^{(\bar{y}-\alpha)/(1-\alpha)} - \beta + 2\alpha}{(2\alpha + 1)\{1 + [(\beta + 1)/(\beta - 1)]^{(\bar{y}-\alpha)/(1-\alpha)}\}} \ . \tag{II.24}$$

A useful transformation for refining the mesh above some interior point y_c (see Figure II.5) is given by

Transformation 3:

$$\bar{x} = x \ , \tag{II.25}$$

$$\bar{y} = B + \frac{1}{\tau} \sinh^{-1} \left[\left(\frac{y}{y_c} - 1 \right) \sinh(\tau B) \right] \ , \tag{II.26}$$

where

$$B = \frac{1}{2\tau} \ln \left(\frac{1 + (e^{\tau} - 1)(y_c/h)}{1 + (e^{-\tau} - 1)(y_c/h)} \right) \ . \quad 0 < \tau < \infty \tag{II.27}$$

In this transformation, τ is the stretching parameter which varies from zero (no stretching) to large values which produce the most refinement near $y=y_c$. The metric $\frac{\partial \bar{y}}{\partial y}$ and y become

$$\frac{\partial \bar{y}}{\partial y} = \frac{\sinh(\tau B)}{\tau y_c \{1 + [(y/y_c) - 1]^2 \sinh^2(\tau B)\}^{1/2}} \ , \tag{II.28}$$

$$y = y_c \left\{ 1 + \frac{\sinh[\tau(\bar{y} - B)]}{\sinh(\tau B)} \right\} \ . \tag{II.29}$$

For our final transformation, a simple transformation which can be

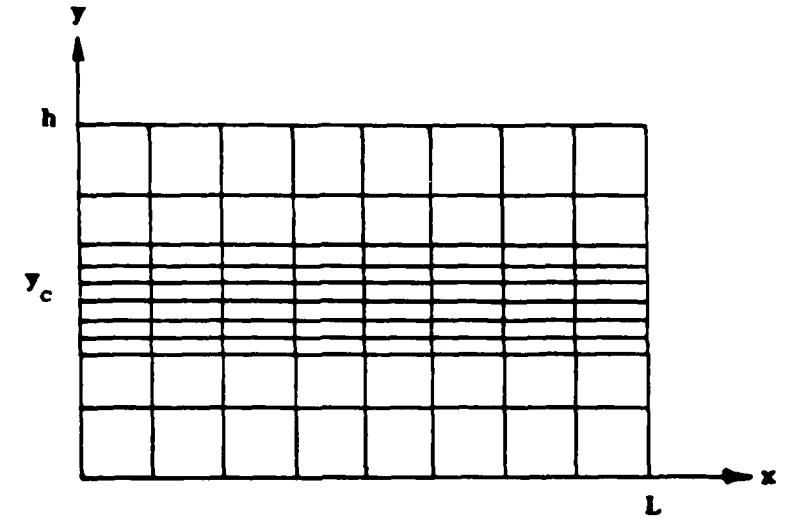

(a) physical plane

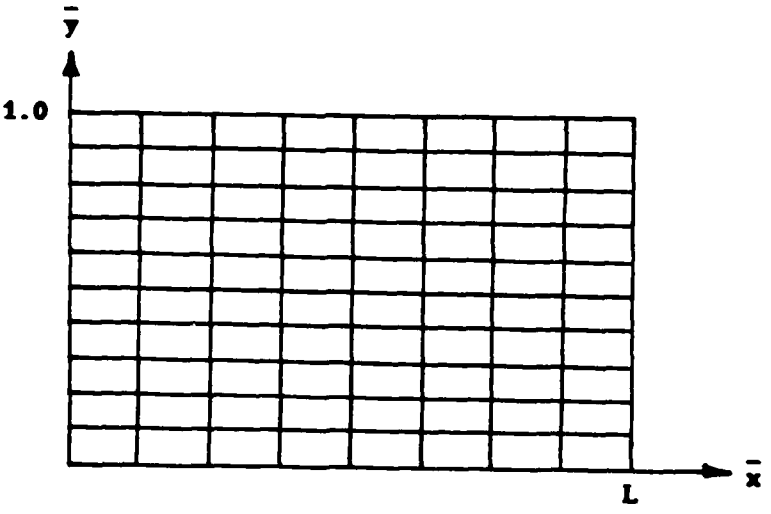

(b) computational plane

Figure II.5 Grid clustering near an interior point.

used to transform a nonrectangular region in the physical plane into a rectangular region in the computational plane, as seen in Figure II.6, will be examined. The required transformation is

Transformation 4: (Figure II.6)

$$\bar{x} = x \ , \tag{II.30}$$

$$\bar{y} = \frac{y}{h(x)} \ . \tag{II.31}$$

The known distance between the lower boundary and the upper boundary (measured along a x=constant line) is designated by h(x). The required partial derivatives are

$$\frac{\partial}{\partial x} = \frac{\partial}{\partial \bar{x}} - \bar{y} \frac{h'(x)}{h(x)} \frac{\partial}{\partial \bar{y}} \ , \tag{II.32}$$

$$\frac{\partial}{\partial y} = \frac{1}{h(x)} \frac{\partial}{\partial \bar{y}} \ , \tag{II.33}$$

where h'(x)=dh(x)/dx. Hence, equation (II.15) is transformed to

$$\frac{\partial u}{\partial \bar{x}} - \bar{y} \frac{h'(\bar{x})}{h(\bar{x})} \frac{\partial u}{\partial \bar{y}} + \frac{1}{h(\bar{x})} \frac{\partial u}{\partial \bar{y}} = 0 \ . \tag{II.34}$$

II.2.2 Generalized Transformation

In the preceding section, the simple independent variable transformations which make it possible to solve the governing equations on a uniformly spaced computational grid were examined. Let us now consider a completely general transformation of the form

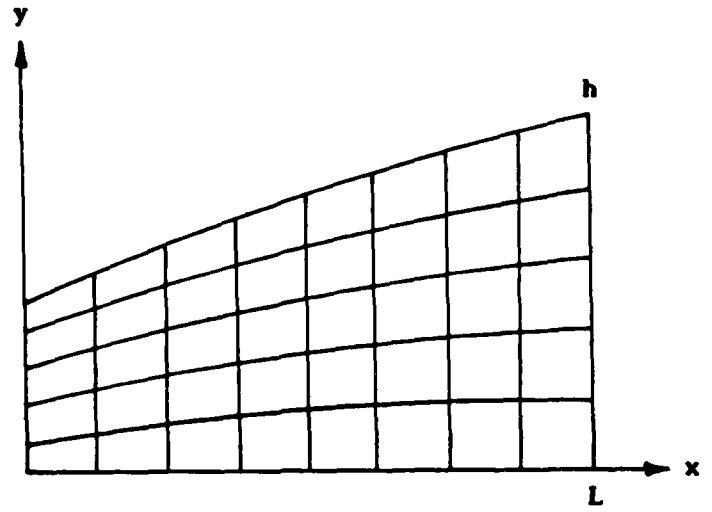

(a) physical plane

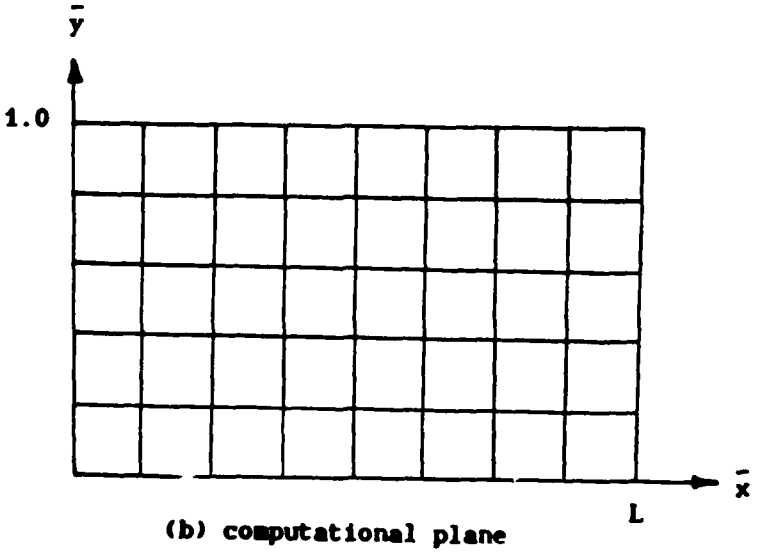

(b) computational plane

Figure II.6 Rectangularization of computational grid.

$$\xi = \xi(x,y,z), \tag{II.35}$$

$$\eta = \eta(x,y,z), \tag{II.36}$$

$$\zeta = \zeta(x,y,z), \tag{II.37}$$

which can be used to transform the governing equations from the physical domain (x,y,z) to the computational domain (ξ,η,ζ). Using the chain rule of partial differentiation, the partial derivatives become

$$\frac{\partial}{\partial x} = \xi_x \frac{\partial}{\partial \xi} + \eta_x \frac{\partial}{\partial \eta} + \zeta_x \frac{\partial}{\partial \zeta} \ , \tag{II.38}$$

$$\frac{\partial}{\partial y} = \xi_y \frac{\partial}{\partial \xi} + \eta_y \frac{\partial}{\partial \eta} + \zeta_y \frac{\partial}{\partial \zeta} \ , \tag{II.39}$$

$$\frac{\partial}{\partial z} = \xi_z \frac{\partial}{\partial \xi} + \eta_z \frac{\partial}{\partial \eta} + \zeta_z \frac{\partial}{\partial \zeta} \ . \tag{II.40}$$

The derivatives $(\xi_x, \eta_x, \zeta_x, \xi_y, \eta_y, \zeta_y, \xi_z, \eta_z, \zeta_z)$ appearing in these equations can be determined in the following manner. We first write the differential expressions

$$d\xi = \xi_x dx + \xi_y dy + \xi_z dz \ , \tag{II.41}$$

$$d\eta = \eta_x dx + \eta_y dy + \eta_z dz \ , \tag{II.42}$$

$$d\zeta = \zeta_x dx + \zeta_y dy + \zeta_z dz \ . \tag{II.43}$$

which in matrix form become

$$\begin{pmatrix} d\xi \\ d\eta \\ d\zeta \end{pmatrix} = \begin{pmatrix} \xi_x & \xi_y & \xi_z \\ \eta_x & \eta_y & \eta_z \\ \zeta_x & \zeta_y & \zeta_z \end{pmatrix} \begin{pmatrix} dx \\ dy \\ dz \end{pmatrix} , \tag{II.44}$$

In a like manner we can write

$$\begin{pmatrix} dx \\ dy \\ dz \end{pmatrix} = \begin{pmatrix} x_\xi & x_\eta & x_\zeta \\ y_\xi & y_\eta & y_\zeta \\ z_\xi & z_\eta & z_\zeta \end{pmatrix} \begin{pmatrix} d\xi \\ d\eta \\ d\zeta \end{pmatrix} , \tag{II.45}$$

Therefore,

$$\begin{pmatrix} \xi_x & \xi_y & \xi_z \\ \eta_x & \eta_y & \eta_z \\ \zeta_x & \zeta_y & \zeta_z \end{pmatrix} = \begin{pmatrix} x_\xi & x_\eta & x_\zeta \\ y_\xi & y_\eta & y_\zeta \\ z_\xi & z_\eta & z_\zeta \end{pmatrix}^{-1} =$$

$$= J \begin{pmatrix} y_\eta z_\zeta - y_\zeta z_\eta & -(x_\eta z_\zeta - x_\zeta z_\eta) & x_\eta y_\zeta - x_\zeta y_\eta \\ -(y_\xi z_\zeta - y_\zeta z_\xi) & x_\xi z_\zeta - x_\zeta z_\xi & -(x_\xi y_\zeta - x_\zeta y_\xi) \\ y_\xi z_\eta - y_\eta z_\xi & -(x_\xi z_\eta - x_\eta z_\xi) & x_\xi y_\eta - x_\eta y_\xi \end{pmatrix} . \tag{II.46}$$

Thus, the derivatives are:

$$\xi_x = J(y_\eta z_\zeta - y_\zeta z_\eta), \tag{II.47}$$

$$\xi_y = -J(x_\eta z_\zeta - x_\zeta z_\eta), \tag{II.48}$$

$$\xi_z = J(x_\eta y_\zeta - x_\zeta y_\eta), \tag{II.49}$$

$$\eta_x = -J(y_\xi z_\zeta - y_\zeta z_\xi), \tag{II.50}$$

$$\eta_y = J(x_\xi z_\zeta - x_\zeta z_\xi), \tag{II.51}$$

$$\eta_z = -J(x_\xi y_\zeta - x_\zeta y_\xi), \tag{II.52}$$

$$\zeta_x = J(y_\xi z_\eta - y_\eta z_\xi), \tag{II.53}$$

$$\zeta_y = -J(x_\xi z_\eta - x_\eta z_\xi), \tag{II.54}$$

$$\zeta_z = J(x_\xi y_\eta - x_\eta y_\xi). \tag{II.55}$$

where J is the Jacobian of the transformation

$$J = \frac{\partial(\xi,\eta,\zeta)}{\partial(x,y,z)} = \begin{pmatrix} \xi_x & \xi_y & \xi_z \\ \eta_x & \eta_y & \eta_z \\ \zeta_x & \zeta_y & \zeta_z \end{pmatrix}, \tag{II.56}$$

which can be evaluated in the following manner

$$J = 1/J^{-1} = 1/\left(\frac{\partial(x,y,z)}{\partial(\xi,\eta,\zeta)} \right) = \begin{pmatrix} x_\xi & x_\eta & x_\zeta \\ y_\xi & y_\eta & y_\zeta \\ z_\xi & z_\eta & z_\zeta \end{pmatrix}^{-1} = \tag{II.57}$$

$$= 1/[x_\xi(y_\eta z_\zeta - y_\zeta z_\eta) - x_\eta(y_\xi z_\zeta - y_\zeta z_\xi) + x_\zeta(y_\xi z_\eta - y_\eta z_\xi)]. \qquad \text{(II.58)}$$

The coordinate derivatives can be readily determined if analytical expressions are available for the inverse of the transformation:

$$x = x(\xi,\eta,\zeta), \qquad \text{(II.59)}$$

$$y = y(\xi,\eta,\zeta), \qquad \text{(II.60)}$$

$$z = z(\xi,\eta,\zeta), \qquad \text{(II.61)}$$

For a two-dimensional problem, the derivatives of a function $f(x,y)$ in the transformed plane (ξ,η) are:

$$f_x = (y_\eta f_\xi - y_\xi f_\eta)/J \ , \qquad \text{(II.62)}$$

$$f_y = (x_\xi f_\eta - x_\eta f_\xi)/J \ , \qquad \text{(II.63)}$$

$$f_{xx} = (y_\eta^2 f_{\xi\xi} - 2y_\xi y_\eta f_{\xi\eta} + y_\xi^2 f_{\eta\eta})/J^2 +$$

$$+ [(y_\eta^2 y_{\xi\xi} - 2y_\xi y_\eta y_{\xi\eta} + y_\xi^2 y_{\eta\eta})(x_\eta f_\xi - x_\xi f_\eta) +$$

$$+ (y_\eta^2 x_{\xi\xi} - 2y_\xi y_\eta x_{\xi\eta} + y_\xi^2 x_{\eta\eta})(y_\xi f_\eta - y_\eta f_\xi)]/J^3, \qquad \text{(II.64)}$$

$$f_{xy} = [(x_\xi y_\eta + x_\eta y_\xi) f_{\xi\eta} - x_\xi y_\xi f_{\eta\eta} - x_\eta y_\eta f_{\xi\xi}]/J^2 +$$

$$+ [x_\eta y_\eta x_{\xi\xi} - (x_\xi y_\eta + x_\eta y_\xi) x_{\xi\eta} + x_\xi y_\xi x_{\eta\eta}](y_\eta f_\xi - y_\xi f_\eta)/J^3 +$$

$$+ [x_\eta y_\eta y_{\xi\xi} - (x_\xi y_\eta + x_\eta y_\xi) y_{\xi\eta} + x_\xi y_\xi y_{\eta\eta}](x_\xi f_\eta - x_\eta f_\xi)/J^3, \quad \text{(II.65)}$$

$$f_{yy} = (x_\eta^2 f_{\xi\xi} - 2x_\xi x_\eta f_{\xi\eta} + x_\xi^2 f_{\eta\eta})/J^2 +$$

$$+ [(x_\eta^2 y_{\xi\xi} - 2x_\xi x_\eta y_{\xi\eta} + x_\xi^2 y_{\eta\eta})(x_\eta f_\xi - x_\xi f_\eta) +$$

$$+ (x_\eta^2 x_{\xi\xi} - 2x_\xi x_\eta x_{\xi\eta} + x_\xi^2 x_{\eta\eta})(y_\xi f_\eta - y_\eta f_\xi)]/J^3. \quad \text{(II.66)}$$

The Laplacian is given by

$$\nabla^2 f = (A_1 f_{\xi\xi} - 2A_2 f_{\xi\eta} + A_3 f_{\eta\eta})/J^2 + [(A_1 x_{\xi\xi} - 2A_2 x_{\xi\eta} + A_3 x_{\eta\eta}) \cdot$$

$$\cdot (y_\xi f_\eta - y_\eta f_\xi) + (A_1 y_{\xi\xi} - 2A_2 y_{\xi\eta} + A_3 y_{\eta\eta})(x_\eta f_\xi - x_\xi f_\eta)]/J^3, \quad \text{(II.67)}$$

or

$$\nabla^2 f = (A_1 f_{\xi\xi} - 2A_2 f_{\xi\eta} + A_3 f_{\eta\eta} + A_4 f_\eta + A_5 f_\xi)/J^2. \quad \text{(II.68)}$$

where

$$A_1 = x_\eta^2 + y_\eta^2 , \quad \text{(II.69)}$$

$$A_2 = x_\xi x_\eta + y_\xi y_\eta , \quad \text{(II.70)}$$

$$A_3 = x_\xi^2 + y_\xi^2 , \quad \text{(II.71)}$$

$$A_4 = (Y_\xi A_6 - x_\xi A_7)/J , \quad \text{(II.72)}$$

$$A_5 = (x_\eta A_7 - y_\eta A_6)/J \ , \tag{II.73}$$

$$A_6 = A_1 x_{\xi\xi} - 2A_2 x_{\xi\eta} + A_3 x_{\eta\eta} \ , \tag{II.74}$$

$$A_7 = A_1 y_{\xi\xi} - 2A_2 y_{\xi\eta} + A_3 y_{\eta\eta} \ . \tag{II.75}$$

Likewise, the Gradient is given by

$$\nabla f = [(y_\eta f_\xi - y_\xi f_\eta)\mathbf{e}_1 + (x_\xi f_\eta - x_\eta f_\xi)\mathbf{e}_2]/J \ . \tag{II.76}$$

and the Divergence is expressed by

$$\nabla.\mathbf{F} = [y_\eta (F_1)_\xi - y_\xi (F_1)_\eta + x_\xi (F_2)_\eta - x_\eta (F_2)_\xi]/J \ . \tag{II.77}$$

where $\mathbf{F} = F_1\mathbf{e}_1 + F_2\mathbf{e}_2$. (II.78)

Finally, the Curl may be written as

$$\text{Curl } \mathbf{F} = \mathbf{e}_3[y_\eta (F_2)_\xi - y_\xi (F_2)_\eta - x_\xi (F_1)_\eta + x_\eta (F_1)_\xi]/J \ , \tag{II.79}$$

where $J = x_\xi y_\eta - x_\eta y_\xi$ is the Jacobian of the transformation, and the subscripts (x,y,ξ,η) denotes partial derivatives in those coordinates, respectively.

For cases where the transformation is the direct result of a grid generation scheme, the metrics can be computed numerically using central difference in the computational plane.

The general coordinate transformation can be employed to transform very complicated curvilinear coordinates to simple

rectangular coordinates. Some examples which transform the problem in physical domain to computational domain are given in Figures II.7,8,9. The detail and more complicated transformations are found in [49,50].

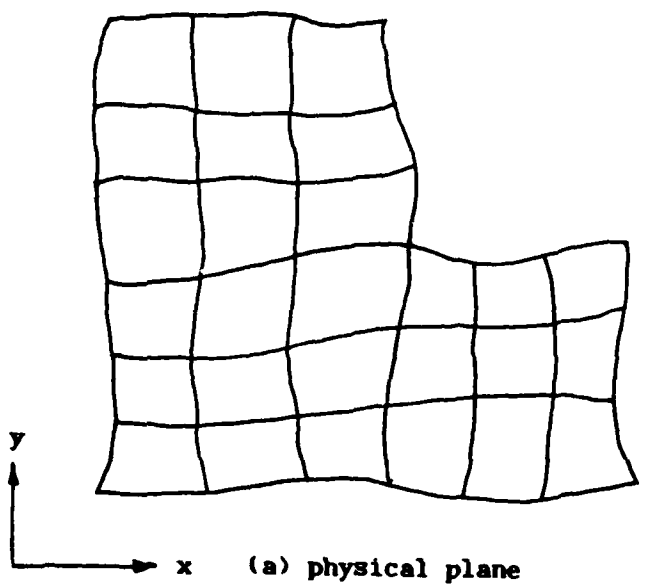

(a) physical plane

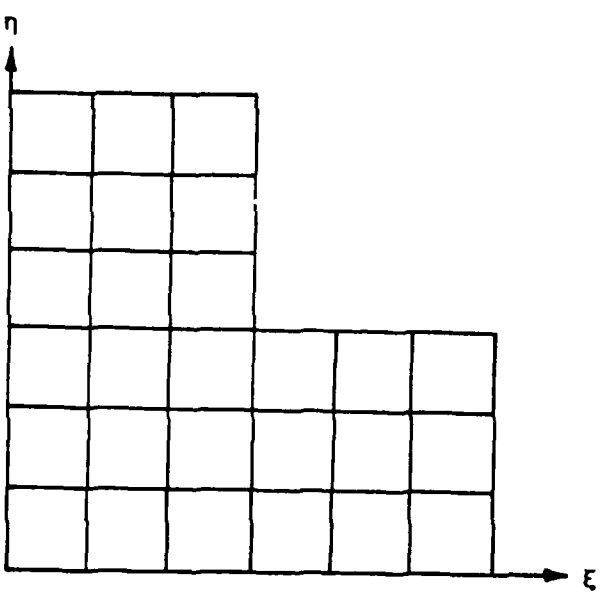

(b) computational plane

Figure II.7 Rectangularization of computational grid.

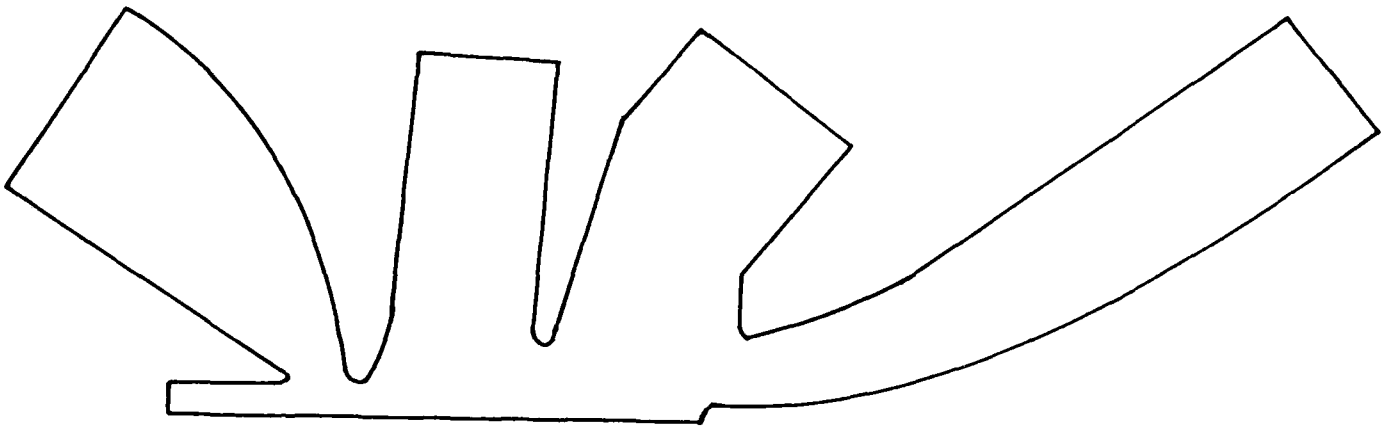

(a) physical plane

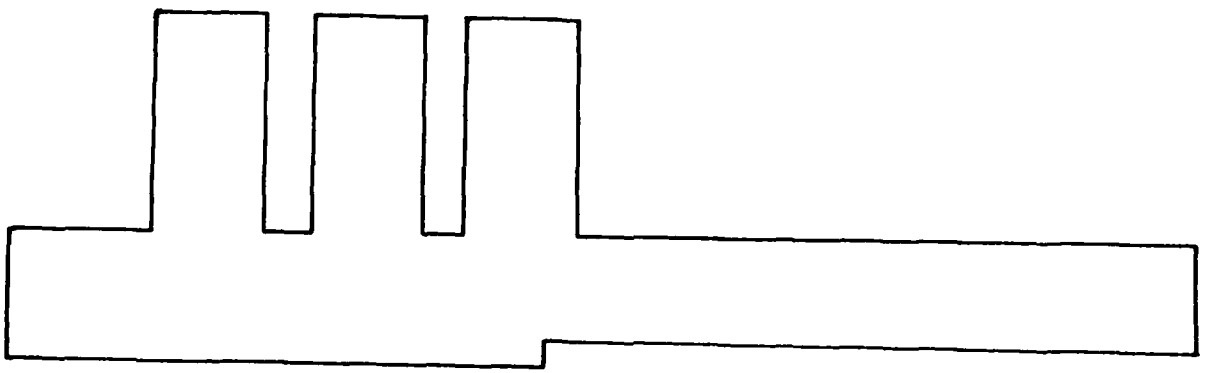

(b) computational plane

Figure II.8 Rectangularization of computational grid.

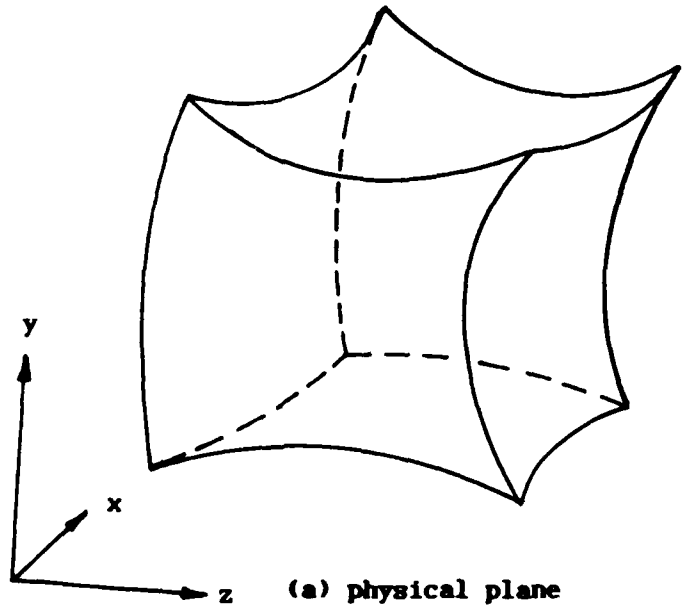

(a) physical plane

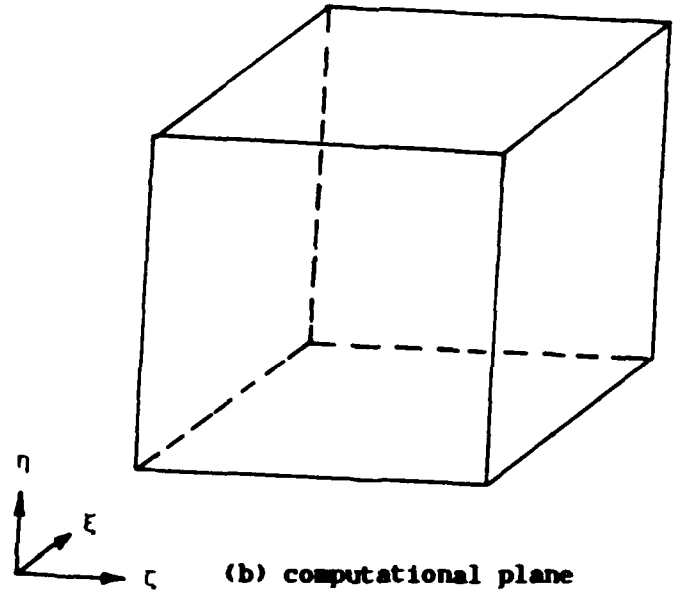

(b) computational plane

Figure II.9 Three-dimensional coordinates transformation.

APPENDIX III

ENERGY BALANCE METHOD

The subjects of thermodynamics and heat transfer are highly complementary. For example, heat transfer is an extension of thermodynamics in that it considers the rate at which energy is transported. Moreover, in many heat transfer analyses the first law of thermodynamics (the law of conservation of energy) plays an important role. In our application of the conservation laws, we first need to identify the control volume, a fixed region of space bounded by a control surface through which energy and matter may pass. With respect to a control volume, a form of the energy conservation requirement that is most useful for heat transfer analyses may be stated as follows.

"The rate at which thermal and mechanical energy enters a control volume minus the rate at which this energy leaves the control volume must equal the rate at which this energy is stored in the control volume."

If the inflow of energy exceeds the outflow, there will be an increase in the amount of energy stored (or accumulated) in the control volume; if the converse is true, there will be a decrease in energy storage. If the inflow of energy equals the outflow, then a steady state condition must prevail in which there will be no change in the amount of energy stored in the control volume. For the heat conduction problem, the inflow and outflow energy of the control volume is the heat flux $Q=-k\nabla T$. The law of conservation of energy is the key concept of the energy balance method.

III.1 Energy Balance on the Cavity Boundaries (Figure 3.3)

On face AB (Figure III.1). Let us examine an arbitrary node P(i,j), on the face AB, surrounded by nodes R, S, and W. When heat conduction from the boundary nodes R or W to P is examined, we observe that the area available for heat flow is only $[(\Delta y/2)\cdot 1]$, although the distance across which heat is conducted is still Δx. Thus we have

$$Q_{S\to P} = k_I(\Delta x)\,\frac{T^I(i,j-1) - T^I(i,j)}{\Delta y}\,, \qquad \text{(III.1)}$$

$$Q_{W\to P} = k_I(\Delta y/2)\,\frac{T^I(i-1,j) - T^I(i,j)}{\Delta x}\,, \qquad \text{(III.2)}$$

$$Q_{R\to P} = k_I(\Delta y/2)\,\frac{T^I(i+1,j) - T^I(i,j)}{\Delta x}\,. \qquad \text{(III.3)}$$

The rate of change of internal energy $\dot{U}_P$ in the time interval Δt at P(i,j) is

$$\dot{U}_P = \rho_I c_I(\Delta x\cdot\Delta y/2)\,\frac{T^I(i,j,n) - T^I(i,j,n-1)}{\Delta t}\,, \qquad n=1 \quad \text{(III.4a)}$$

$$\dot{U}_P = \rho_I c_I(\Delta x\Delta y/2)\,\frac{3T^I(i,j,n)-4T^I(i,j,n-1)+T^I(i,j,n-2)}{2\Delta t}\,. \qquad n>1 \quad \text{(III.4b)}$$

From conservation of energy, $\dot{U}_P = Q_{sum}$, we obtain

$$T^I(i,j,n) = T^I(i,j,n-1) + AB_1\,, \qquad n=1 \quad \text{(III.5a)}$$

$$T^I(i,j,n) = \frac{1}{3}\,[-T^I(i,j,n-2) + 4T^I(i,j,n-1) + 2AB_1]\,, \qquad n>1 \quad \text{(III.5b)}$$

where

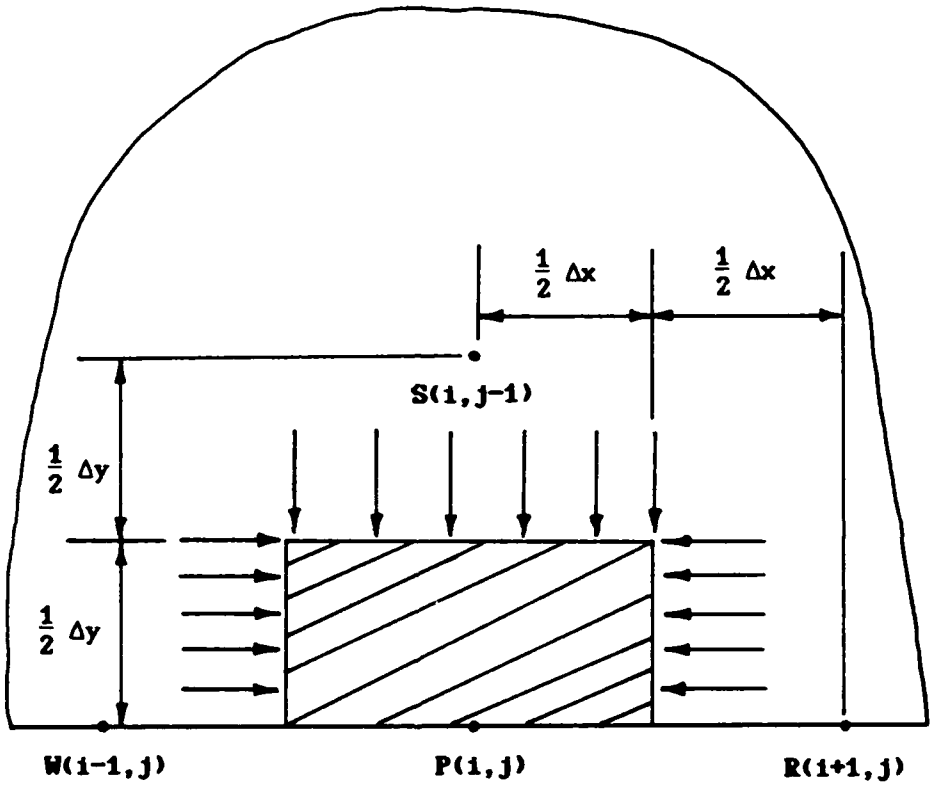

Figure III.1 Energy balance on face AB.

$$AB_1 = \frac{\Delta t k_I}{\rho_I c_I} \{2[T^I(i,j-1,n-1) - T^I(i,j,n-1)]/\Delta y^2$$

$$+ [T^I(i+1,j,n-1) - 2T^I(i,j,n-1) + T^I(i-1,j,n-1)/\Delta x^2\}. \quad \text{(III.6)}$$

The dimensionless forms were given in Equations (3.40a,b).

On face AC (Figure III.2)

$$Q_{W\to P} = k_{II}\left(\frac{\Delta y_1+\Delta y_2}{2}\right) \frac{T^{II}(i-1,j) - T^{II}(i,j)}{\Delta x}, \quad \text{(III.7)}$$

$$Q_{S\to P} = k_{II}(\Delta x/2) \frac{T^{II}(i,j-1) - T^{II}(i,j)}{\Delta y_1}, \quad \text{(III.8)}$$

$$Q_{N\to P} = k_{II}(\Delta x/2) \frac{T^{II}(i,j+1) - T^{II}(i,j)}{\Delta y_2}, \quad \text{(III.9)}$$

and

$$\dot{U}_P = \rho_{II} c_{II}[\Delta x\cdot(\Delta y_1+\Delta y_2)/4] \frac{T^{II}(i,j,n)-T^{II}(i,j,n-1)}{\Delta t}, \quad n=1 \text{ (III.10a)}$$

$$\dot{U}_P = \rho_{II} c_{II}[\Delta x\cdot(\Delta y_1+\Delta y_2)/4] \frac{3T^{II}(i,j,n)-4T^{II}(i,j,n-1)+T^{II}(i,j,n-2)}{2\Delta t}.$$

$$n>1 \text{ (III.10b)}$$

$\dot{U}_P = Q_{sum}$ gives

$$T^{II}(i,j,n) = T^{II}(i,j,n-1) + AB_2, \quad n=1 \text{ (III.11a)}$$

$$T^{II}(i,j,n) = \frac{1}{3}[-T^{II}(i,j,n-2)+4T^{II}(i,j,n-1)+2AB_2], \quad n>1 \text{ (III.11b)}$$

where

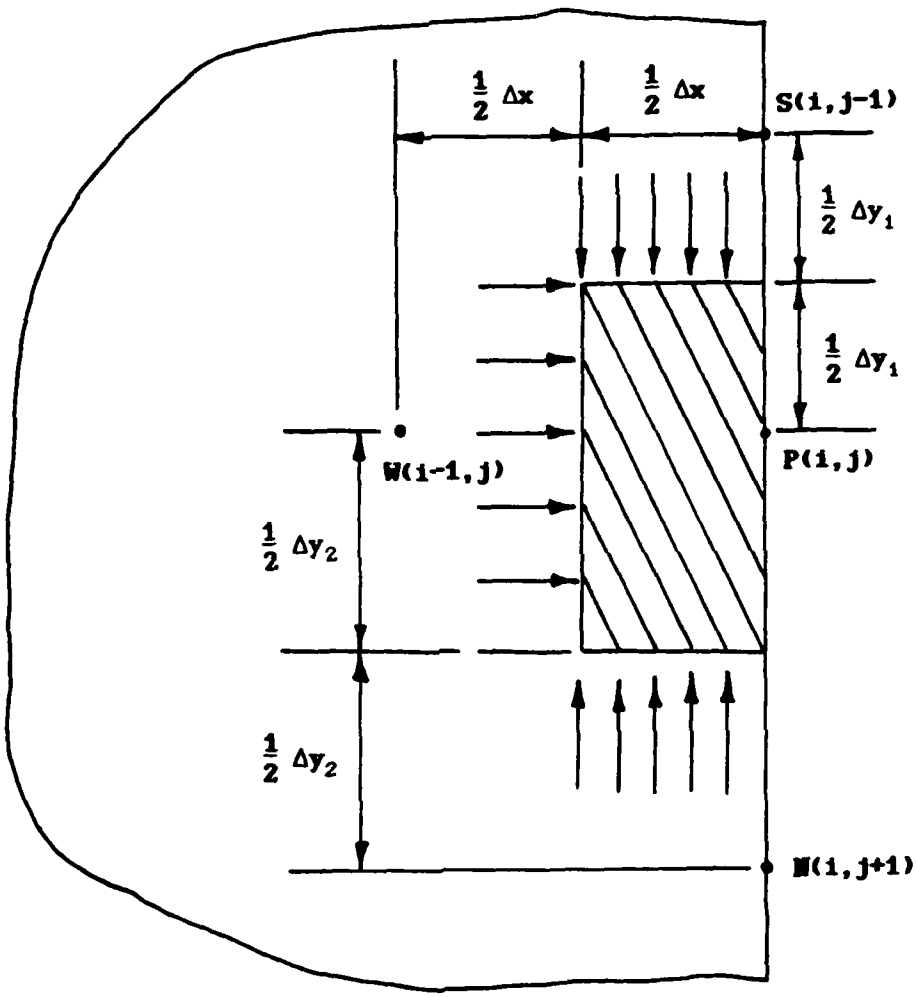

Figure III.2 Energy balance on face AC.

$$AB_2 = \frac{2\Delta t k_{II}}{\rho_{II} c_{II}} \{[T^{II}(i-1,j,n-1) - T^{II}(i,j,n-1)]/\Delta x^2$$

$$+ [T^{II}(i,j-1,n-1) - T^{II}(i,j,n-1)]/(\Delta y_1^2 + \Delta y_1 \Delta y_2)$$

$$+ [T^{II}(i,j+1,n-1) - T^{II}(i,j,n-1)]/(\Delta y_1 \Delta y_2 + \Delta y_2^2)\} \quad . \quad (III.12)$$

The dimensionless forms were given in Equations (3.42a,b).

On face BD (Figure III.3)

$$Q_{R\to P} = k_{II}\left(\frac{\Delta y_1+\Delta y_2}{2}\right) \frac{T^{II}(i+1,j) - T^{II}(i,j)}{\Delta x}, \quad (III.13)$$

$$Q_{S\to P} = k_{II}(\Delta x/2) \frac{T^{II}(i,j-1) - T^{II}(i,j)}{\Delta y_1}, \quad (III.14)$$

$$Q_{N\to P} = k_{II}(\Delta x/2) \frac{T^{II}(i,j+1) - T^{II}(i,j)}{\Delta y_2}, \quad (III.15)$$

and

$$\dot{U}_P = \rho_{II} c_{II}[\Delta x\cdot(\Delta y_1+\Delta y_2)/4] \frac{T^{II}(i,j,n)-T^{II}(i,j,n-1)}{\Delta t}, \quad n=1 \quad (III.16a)$$

$$\dot{U}_P = \rho_{II} c_{II}[\Delta x\cdot(\Delta y_1+\Delta y_2)/4] \frac{3T^{II}(i,j,n)-4T^{II}(i,j,n-1)+T^{II}(i,j,n-2)}{2\Delta t}, \quad n>1 \quad (III.16b)$$

$\dot{U}_P = Q_{sum}$ gives

$$T^{II}(i,j,n) = T^{II}(i,j,n-1) + AB_3, \quad n=1 \quad (III.17a)$$

$$T^{II}(i,j,n) = \frac{1}{3}[-T^{II}(i,j,n-2)+4T^{II}(i,j,n-1)+2AB_3], \quad n>1 \quad (III.17b)$$

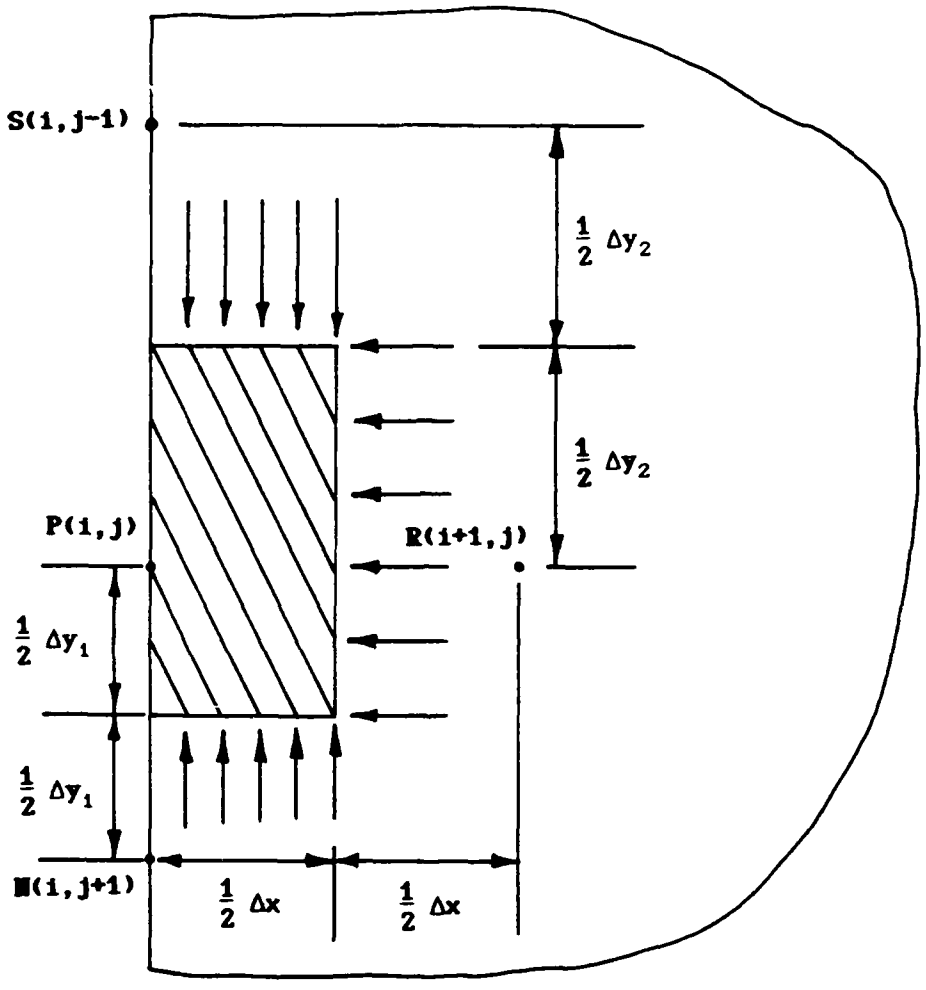

Figure III.3 Energy balance on face BD.

where

$$AB_3 = \frac{2\Delta t k_{II}}{\rho_{II} c_{II}} \{[T^{II}(i+1,j,n-1) - T^{II}(i,j,n-1)]/\Delta x^2$$

$$+ [T^{II}(i,j-1,n-1) - T^{II}(i,j,n-1)]/(\Delta y_1^2 + \Delta y_1 \Delta y_2)$$

$$+ [T^{II}(i,j+1,n-1) - T^{II}(i,j,n-1)]/(\Delta y_1 \Delta y_2 + \Delta y_2^2)\} \quad . \quad (III.18)$$

The dimensionless forms were given in Equations (3.44a,b).

On face CD (Figure III.4)

$$Q_{N\to P} = k_{II}(\Delta x) \frac{T^{II}(i,j+1) - T^{II}(i,j)}{\Delta y} \quad , \quad (III.19)$$

$$Q_{W\to P} = k_{II}(\Delta y/2) \frac{T^{II}(i-1,j) - T^{II}(i,j)}{\Delta x} \quad , \quad (III.20)$$

$$Q_{R\to P} = k_{II}(\Delta y/2) \frac{T^{II}(i+1,j) - T^{II}(i,j)}{\Delta x} \quad , \quad (III.21)$$

and

$$\dot{U}_P = \rho_{II} c_{II}(\Delta x.\Delta y/2) \frac{T^{II}(i,j,n) - T^{II}(i,j,n-1)}{\Delta t} \quad , \quad n=1 \quad (III.22a)$$

$$\dot{U}_P = \rho_{II} c_{II}(\Delta x.\Delta y/2) \frac{3T^{II}(i,j,n) - 4T^{II}(i,j,n-1) + T^{II}(i,j,n-2)}{2\Delta t} \quad .$$

$$n>1 \quad (III.22b)$$

$\dot{U}_P = Q_{sum}$ gives

$$T^{II}(i,j,n) = T^{II}(i,j,n-1) + AB_4 \quad , \quad n=1 \quad (III.23a)$$

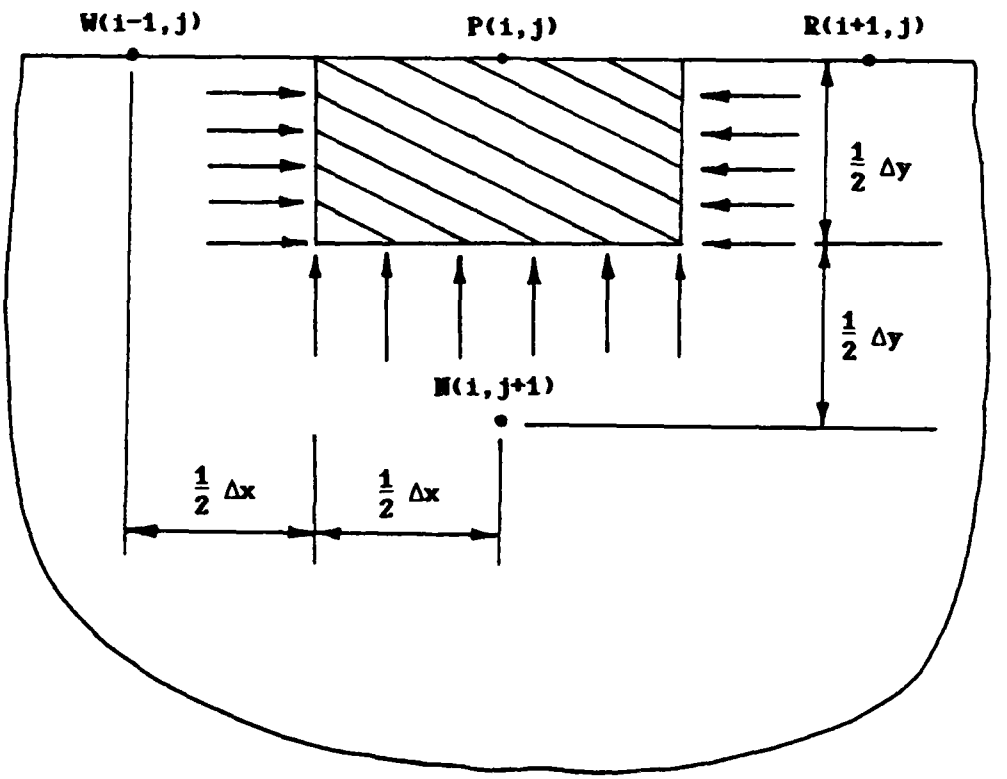

Figure III.4 Energy balance on face CD.

$$T^{II}(i,j,n) = \frac{1}{3}\,[-T^{II}(i,j,n-2)+4T^{II}(i,j,n-1)+2AB_4] \quad , \quad n>1 \qquad \text{(III.23b)}$$

where

$$AB_4 = \frac{\Delta t k_{II}}{\rho_{II} c_{II}} \{[T^{II}(i-1,j,n-1) - 2T^{II}(i,j,n-1) + T^{II}(i+1,j,n-1)]/\Delta x^2$$

$$+ 2[T^{II}(i,j+1,n-1) - T^{II}(i,j,n-1)]\} \; . \qquad \text{(III.24)}$$

The dimensionless forms were given in Equations (3.46a,b).

III.2 Energy Balance at the Corner of the Cavity (Figure 3.3)

If one has a two-dimensional configuration that looks like the cross section of two walls meeting at a corner, the nodal point at the corner so formed is called a reentrant corner.

Corner A. *The node P in Figure III.5 is located at a reentrant* corner. The nodes N, R, S, and W are called exterior corner nodes. Observing that the areas available for the flow of heat from N to P and from R to P are $\frac{\Delta x}{2}\cdot 1$ and $\frac{\Delta y}{2}\cdot 1$, respectively. The heat fluxes toward the corner point P(i,j) are:

$$Q_{W\to P} = \left(\frac{k_I+k_{II}}{2}\right)(\Delta y)\,\frac{T(i-1,j) - T(i,j)}{\Delta x} \; , \qquad \text{(III.25)}$$

$$Q_{N\to P} = k_{II}(\Delta x/2)\,\frac{T(i,j+1) - T(i,j)}{\Delta y} \; , \qquad \text{(III.26)}$$

$$Q_{R\to P} = k_I(\Delta y/2)\,\frac{T(i+1,j) - T(i,j)}{\Delta x} \; , \qquad \text{(III.27)}$$

$$Q_{S\to P} = k_I(\Delta x)\,\frac{T(i,j-1) - T(i,j)}{\Delta y} \; , \qquad \text{(III.28)}$$

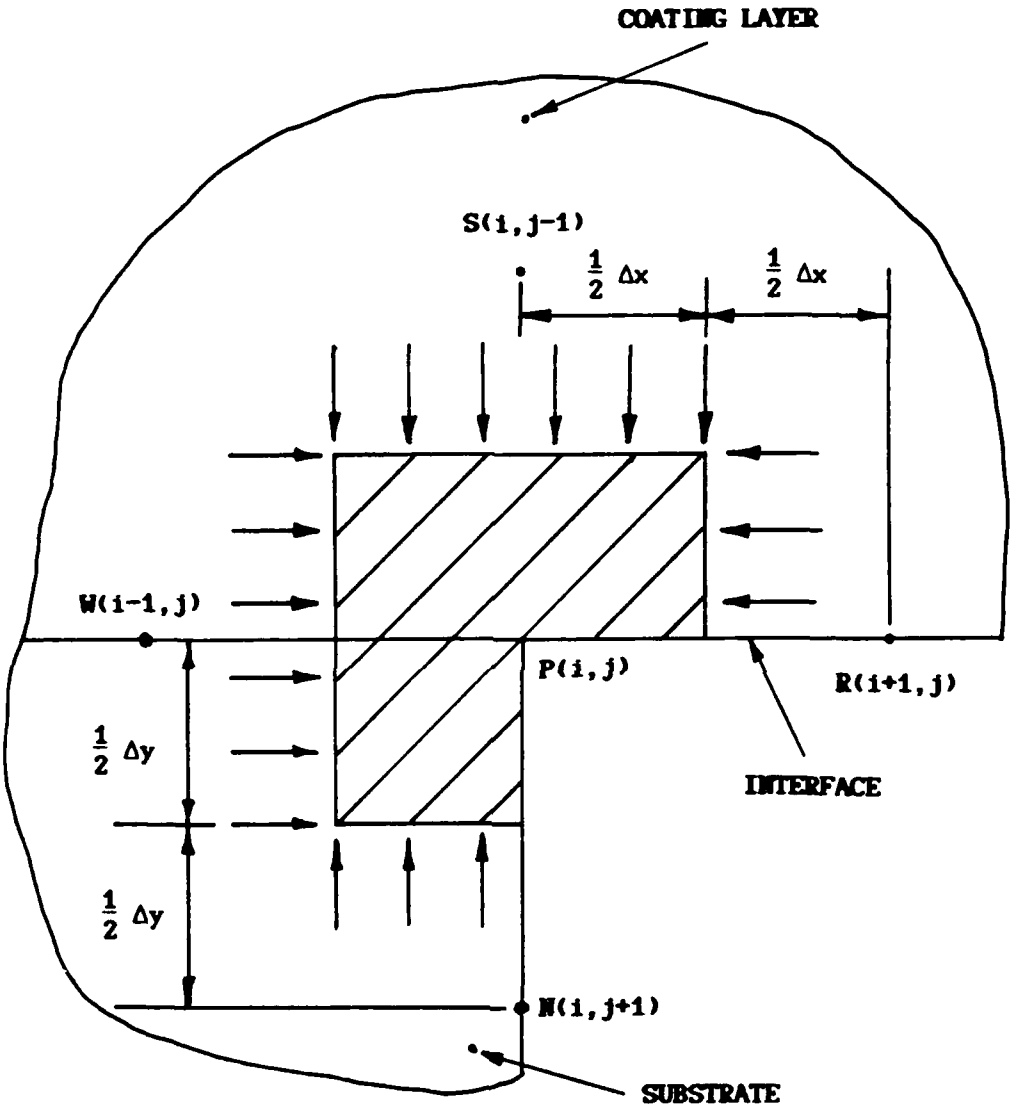

Figure III.5 Energy balance at corner A.

and the rate of change of internal energy is

$$\dot{U}_P = (\rho_I c_I/2 + \rho_{II} c_{II}/4)\ (\Delta x \cdot \Delta y)\ \frac{T(i,j,n)-T(i,j,n-1)}{\Delta t}\ ,\quad n=1 \quad \text{(III.29a)}$$

$$\dot{U}_P = (\rho_I c_I/2 + \rho_{II} c_{II}/4)\ (\Delta x \cdot \Delta y)\ \frac{3T(i,j,n)-4T(i,j,n-1)+T(i,j,n-2)}{2\Delta t}\ ,$$

$$n>1 \quad \text{(III.29b)}$$

From conservation of energy, $\dot{U}_P = Q_{sum}$, one obtains

$$T(i,j,n) = T(i,j,n-1) + AB_S\ , \qquad n=1 \quad \text{(III.30a)}$$

$$T(i,j,n) = \frac{1}{3}\ [-T(i,j,n-2) + 4T(i,j,n-1) + 2AB_S]\ , \qquad n>1 \quad \text{(III.30b)}$$

where

$$AB_S = \frac{\Delta t/2}{(\rho_I c_I/2+\rho_{II} c_{II}/4)}\ \{(k_I+k_{II})[T(i-1,j,n-1)-T(i,j,n-1)]/\Delta x^2$$

$$+ k_{II}[T(i,j+1,n-1)-T(i,j,n-1)]/\Delta y^2 + k_I[T(i+1,j,n-1)$$

$$- T(i,j,n-1)]/\Delta x^2+2k_I[T(i,j-1,n-1)-T(i,j,n-1)]/\Delta y^2\}. \quad \text{(III.31)}$$

Corner B (Figure III.6)

$$Q_{W\to P} = k_I(\Delta y/2)\ \frac{T(i-1,j) - T(i,j)}{\Delta x}\ , \qquad \text{(III.32)}$$

$$Q_{N\to P} = k_{II}(\Delta x/2)\ \frac{T(i,j+1) - T(i,j)}{\Delta y}\ , \qquad \text{(III.33)}$$

$$Q_{R\to P} = \left(\frac{k_I+k_{II}}{2}\right)\ (\Delta y)\ \frac{T(i+1,j) - T(i,j)}{\Delta x}\ , \qquad \text{(III.34)}$$

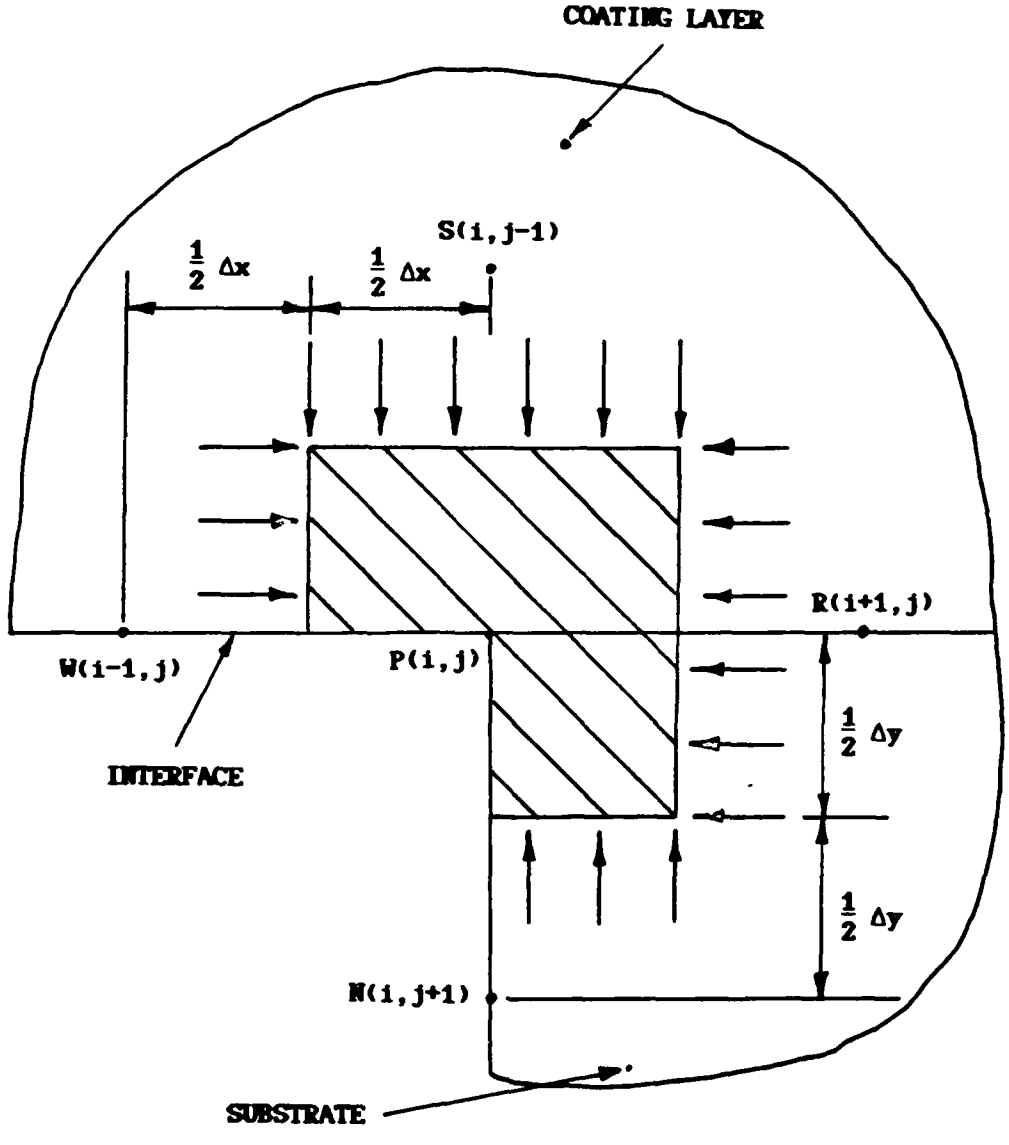

Figure III.6 Energy balance at corner B.

$$Q_{S\to P} = k_I(\Delta x)\,\frac{T(i,j-1) - T(i,j)}{\Delta y}\,, \qquad \text{(III.35)}$$

and

$$\dot{U}_P = (\rho_I c_I/2 + \rho_{II} c_{II}/4)(\Delta x\cdot\Delta y)\,\frac{T(i,j,n)-T(i,j,n-1)}{\Delta t}\,, \quad n=1 \qquad \text{(III.36a)}$$

$$\dot{U}_P = (\rho_I c_I/2 + \rho_{II} c_{II}/4)(\Delta x\cdot\Delta y)\,\frac{3T(i,j,n)-4T(i,j,n-1)+T(i,j,n-2)}{2\Delta t}\,. \quad n>1 \qquad \text{(III.36b)}$$

$\dot{U}_P = Q_{sum}$ gives

$$T(i,j,n) = T(i,j,n-1) + AB_6\,, \qquad n=1 \qquad \text{(III.37a)}$$

$$T(i,j,n) = \frac{1}{3}\,[-T(i,j,n-2) + 4T(i,j,n-1) + 2AB_6]\,, \qquad n>1 \qquad \text{(III.37b)}$$

where

$$AB_6 = \frac{\Delta t/2}{(\rho_I c_I/2+\rho_{II} c_{II}/4)}\,\{k_I[T(i-1,j,n-1) - T(i,j,n-1)]/\Delta x^2$$

$$+ k_{II}[T(i,j+1,n-1) - T(i,j,n-1)]/\Delta y^2 + (k_I+k_{II})[T(i+1,j,n-1)$$

$$- T(i,j,n-1)]/\Delta x^2+2k_I[T(i,j-1,n-1)-T(i,j,n-1)]/\Delta y^2\}\,. \qquad \text{(III.38)}$$

Corner C (Figure III.7)

$$Q_{W\to P} = k_{II}(\Delta y)\,\frac{T^{II}(i-1,j) - T^{II}(i,j)}{\Delta x}\,, \qquad \text{(III.39)}$$

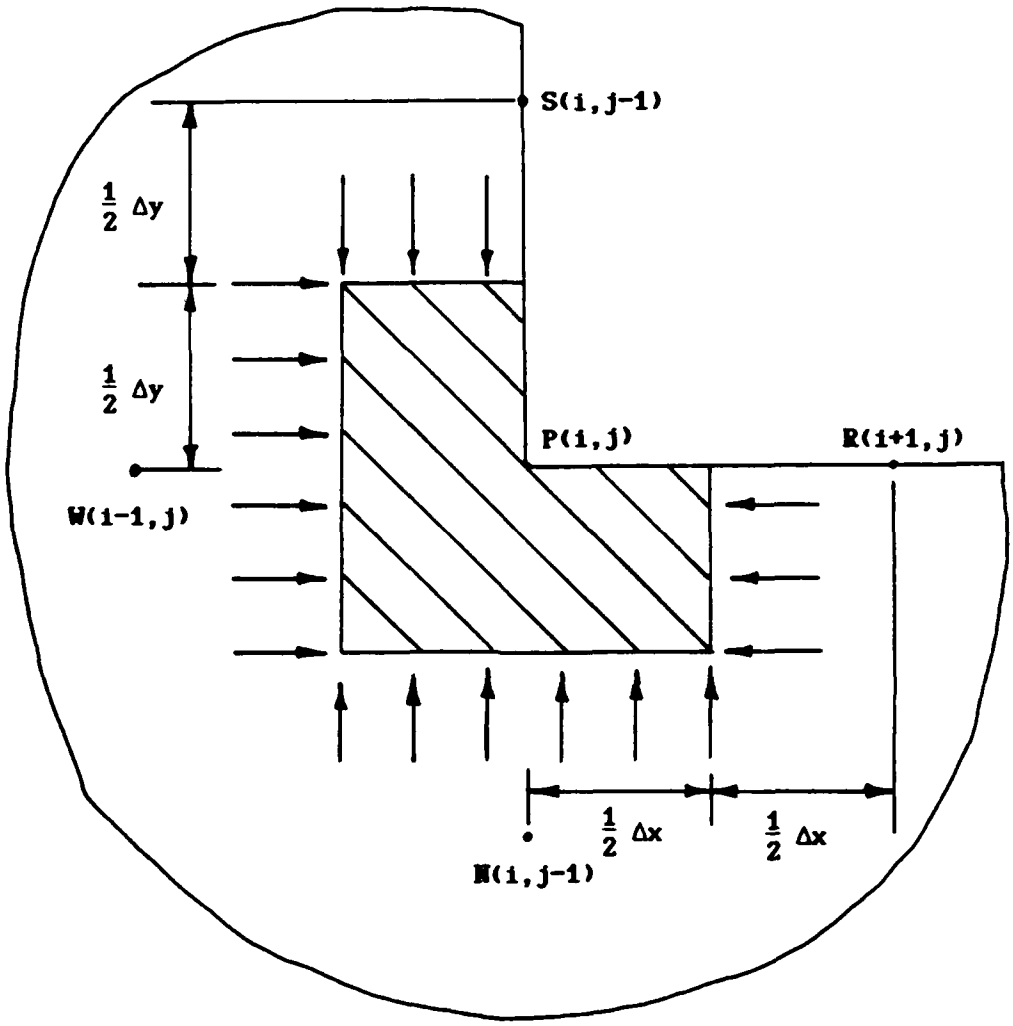

Figure III.7 F

$$Q_{N\to P} = k_{II}(\Delta x)\,\frac{T^{II}(i,j+1) - T^{II}(i,j)}{\Delta y}\,, \qquad \text{(III.40)}$$

$$Q_{R\to P} = k_{II}(\Delta y/2)\,\frac{T^{II}(i+1,j) - T^{II}(i,j)}{\Delta x}\,, \qquad \text{(III.41)}$$

$$Q_{S\to P} = k_{II}(\Delta x/2)\,\frac{T^{II}(i,j-1) - T^{II}(i,j)}{\Delta y}\,, \qquad \text{(III.42)}$$

and

$$\dot{U}_P = \rho_{II}c_{II}\left(\frac{3}{4}\,\Delta x.\Delta y\right)\frac{T^{II}(i,j,n) - T^{II}(i,j,n-1)}{\Delta t}\,, \qquad n=1 \text{ (III.43a)}$$

$$\dot{U}_P = \rho_{II}c_{II}\left(\frac{3}{4}\,\Delta x.\Delta y\right)\frac{3T^{II}(i,j,n)-4T^{II}(i,j,n-1)+T^{II}(i,j,n-2)}{2\Delta t}\,,$$

$$n>1 \text{ (III.43b)}$$

$\dot{U}_P = Q_{sum}$ gives

$$T^{II}(i,j,n) = T^{II}(i,j,n-1) + AB_7\,, \qquad n=1 \text{ (III.44a)}$$

$$T^{II}(i,j,n) = \frac{1}{3}\left[-T^{II}(i,j,n-2)+4T^{II}(i,j,n-1)+2AB_7\right]\,, \qquad n>1 \text{ (III.44b)}$$

where

$$AB_7 = \frac{2\Delta t k_{II}}{3\rho_{II}c_{II}}\left\{\left[2T^{II}(i-1,j,n-1)-3T^{II}(i,j,n-1)+T^{II}(i+1,j,n-1)\right]/\Delta x^2\right.$$

$$\left. + \left[T^{II}(i,j-1,n-1) - 3T^{II}(i,j,n-1) + 2T^{II}(i,j+1,n-1)\right]/\Delta y^2\right\}\,. \qquad \text{(III.45)}$$

Corner D (Figure III.8)

$$Q_{W\to P} = k_{II}(\Delta y/2)\,\frac{T^{II}(i-1,j) - T^{II}(i,j)}{\Delta x}\,, \qquad \text{(III.46)}$$

$$Q_{N\to P} = k_{II}(\Delta x)\,\frac{T^{II}(i,j+1) - T^{II}(i,j)}{\Delta y}\,, \qquad \text{(III.47)}$$

$$Q_{R\to P} = k_{II}(\Delta y)\,\frac{T^{II}(i+1,j) - T^{II}(i,j)}{\Delta x}\,, \qquad \text{(III.48)}$$

$$Q_{S\to P} = k_{II}(\Delta x/2)\,\frac{T^{II}(i,j-1) - T^{II}(i,j)}{\Delta y}\,, \qquad \text{(III.49)}$$

and

$$\dot{U}_P = \rho_{II}c_{II}\left(\frac{3}{4}\,\Delta x.\Delta y\right)\frac{T^{II}(i,j,n) - T^{II}(i,j,n-1)}{\Delta t}\,, \qquad n=1 \text{ (III.50a)}$$

$$\dot{U}_P = \rho_{II}c_{II}\left(\frac{3}{4}\,\Delta x.\Delta y\right)\frac{3T^{II}(i,j,n)-4T^{II}(i,j,n-1)+T^{II}(i,j,n-2)}{2\Delta t}\,. \qquad n>1 \text{ (III.50b)}$$

$\dot{U}_P = Q_{sum}$ gives

$$T^{II}(i,j,n) = T^{II}(i,j,n-1) + AB_8\,, \qquad n=1 \text{ (III.51a)}$$

$$T^{II}(i,j,n) = \frac{1}{3}\,[-T^{II}(i,j,n-2)+4T^{II}(i,j,n-1)+2AB_8]\,, \qquad n>1 \text{ (III.51b)}$$

where

$$AB_8 = \frac{2\Delta t k_{II}}{3\rho_{II}c_{II}}\,\{[T^{II}(i-1,j,n-1)-3T^{II}(i,j,n-1)+2T^{II}(i+1,j,n-1)]/\Delta x^2$$

$$+\,[T^{II}(i,j-1,n-1) - 3T^{II}(i,j,n-1) + 2T^{II}(i,j+1,n-1)]/\Delta y^2\}. \qquad \text{(III.52)}$$

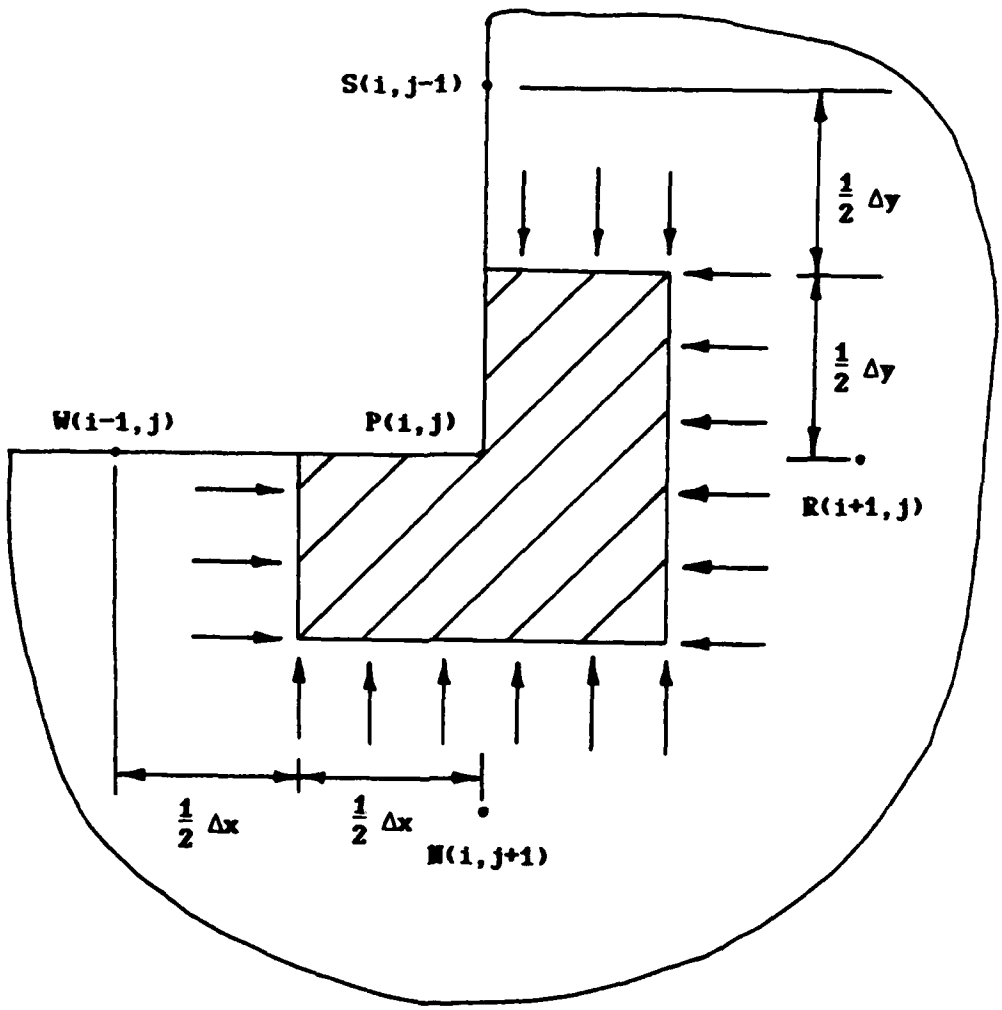

Figure III.8 Energy bal--

The dimensionless forms for the corner points A, B, C, and D were given in Equations (3.48a,b, 3.50a,b, 3.52a,b, 3.54a,b), respectively.

III.3 Energy Balance on the Surface Boundary (Figure III.9)

For the explicit scheme, the time step is limited by the stability criterion. As a result, the moving asperity at some time may not be right above the grid points. To alleviate this situation, one can also use the energy balance method to describe the surface boundary condition.

The heat fluxes toward P(i,j) from material points N, R, and W are

$$Q_{W\to P} = k_I(\Delta y/2)\,\frac{T^I(i-1,1) - T^I(i,1)}{\Delta x}\,, \qquad \text{(III.53)}$$

$$Q_{N\to P} = k_I(\Delta x)\,\frac{T^I(i,2) - T^I(i,1)}{\Delta y}\,, \qquad \text{(III.54)}$$

$$Q_{R\to P} = k_I(\Delta y/2)\,\frac{T^I(i+1,1) - T^I(i,1)}{\Delta x}\,. \qquad \text{(III.55)}$$

The exterior heat which is conducted into the neighborhood surface of the boundary point P(i,j), which is under the asperity, is

$$Q_{ext.} = q(0.5\Delta x + h)/\text{unit thickness}\,, \qquad \text{(III.56)}$$

where h is less than $\Delta x/2$. The formulation thus takes care of all cases when the asperity end points do not fall on the grid point. The rate of change of the internal energy $\dot{U}_P$ in the interval Δt at P(i,j) is

$$\dot{U}_P = \rho_I c_I(\Delta x\cdot\Delta y/2)\,\frac{T^I(i,j,n) - T^I(i,j,n-1)}{\Delta t}\,, \qquad n=1 \quad \text{(III.57a)}$$

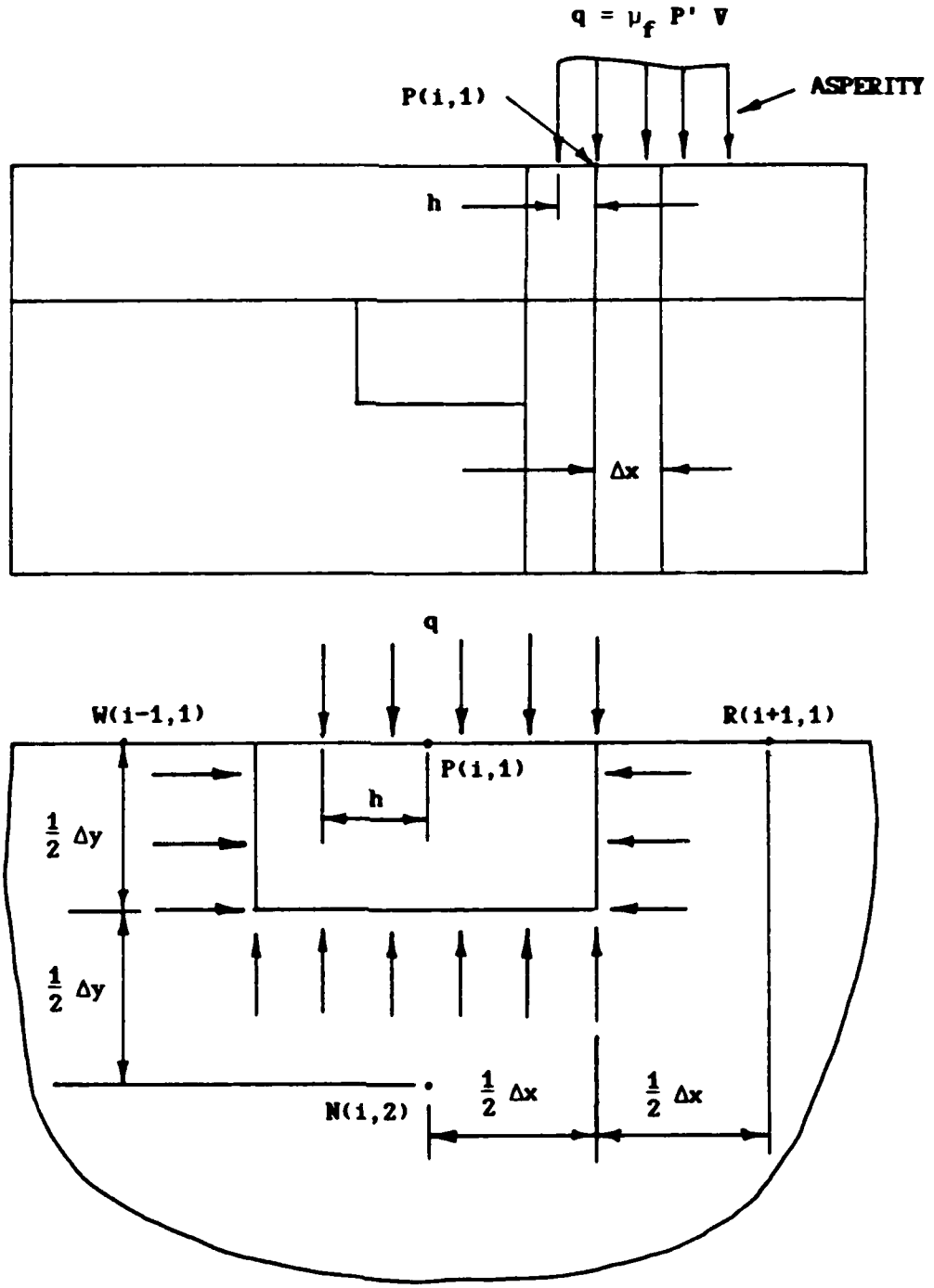

Figure III.9 Energy balance o

$$\dot{U}_P = \rho_I c_I (\Delta x \cdot \Delta y/2) \frac{3T^I(i,j,n) - 4T^I(i,j,n-1) + T^I(i,j,n-2)}{2\Delta t} .$$

$n>1$ (III.57b)

From conservation of energy, $\dot{U}_P = Q_{sum}$, one obtains

$$T^I(i,1,n) = T^I(i,1,n-1) + \frac{2q(\Delta x/2+h)\Delta t}{\rho_I c_I \Delta x \Delta y} + AB_9 , \qquad n=1 \text{ (III.58a)}$$

$$T^I(i,1,n) = \frac{1}{3}\left[-T^I(i,j,n-2) + 4T^I(i,j,n-1) + \frac{2q(\Delta x/2+h)\Delta t}{\rho_I c_I \Delta x \Delta y} + 2AB_9\right],$$

$n>1$ (III.58b)

where

$$AB_9 = \frac{\Delta t k_I}{\rho_I c_I} \{[T^I(i-1,1,n-1) - 2T^I(i,1,n-1) + T^I(i+1,1,n-1)]/\Delta x^2$$

$$+ 2[T^I(i,2,n-1) - T^I(i,1,n-1)]/\Delta y^2\} . \qquad \text{(III.59)}$$

The dimensionless forms for the surface boundary were given in Equations (3.56a,b).

APPENDIX IV

THE PROGRAMS TO COMPUTE THE TEMPERATURE AND THE STRESS FIELDS SOLUTIONS

```
C     MAIN PROGRAM
C     TEMPERATURE FIELD OF A LAYERED MEDIUM WITH A CAVITY, THE TOP
C     EDGE OF THE CAVITY IS AT THE INTERFACE
C
      IMPLICIT REAL*8 (A-H,O-Z)
C
C     T,TT,TTT = TEMPERATURE IN THE CURRENT, PREVIOUS ONE, AND
C     PREVIOUS TWO TIME STEPS
C     FX & FY = HEAT FLUX IN X & Y DIRECTION, RESPECTIVELY
C     Q = SURFACE HEAT INPUT
C     X & Y = COORDINATES IN PHYSICAL PLANE
C     XS,YE,XSS,YEE,... = THE DERIVATIVES OF THE COORDINATES IN
C     PHYSICAL PLANE WITH RESPECT TO THE COORDINATES IN COMPUTATIONAL
C     PLANE
C
      DIMENSION T(145,33),TT(145,33),TTT(145,33),FX(145,33),FY(145,33),
     AQ(145),X(145,33),Y(145,33),XS(145,33),YE(145,33)
C
C     DA,DG,SIG,TAU = THE COEFFICIENTS DEFINED IN TEMPERATURE EQUATION
C
      DIMENSION XSS(145,33),YEE(145,33),DA(145,33),DG(145,33),
     ASIG(145,33),TAU(145,33)
C
C     TS,FXS,FYS = TEMPERATURE AND ITS GRADIENTS IN THE CORRESPONDING
C     POINTS IN STRESS FIELD
C
      DIMENSION TS(67,35),FXS(67,35),FYS(67,35)
      COMMON /A54/ RL1,RL2,RLI,RLC,RMU1,RMU2,RMUI,RMUC,EX1,EX2,
     AEXI,EXC,HAK,RHC
      COMMON /A55/ DV,DL,DIFF1,DIFF2,COND1,COND2,BETA,R1,R2,
     AALPHS,DX,DY1,DY2,DT,R11,R12,R21,R22,A1,A2,A3,A4,A5,A,AA,A6,A7,A8
      COMMON /A56/ DTR1,DTR2,M1,M2,N1,N2,MM1,MM2,NN1,NN2,NA1,NA2,
     AMA1,MA2,K1,K2,K3,NTE,M122,M222,M112,M212,N121
      COMMON /A57/ ID2,ID21,ID3,ID31,I2,J2,I3,J3,I4,J4
C
C     I1 & J1 = TOTAL GRID POINTS OF THE TEMPERATURE FIELD IN X & Y
C     DIRECTION, RESPECTIVELY
C
      I1=145
      J1=33
C
C     LI1 & KJ1 = TOTAL GRID POINTS OF THE STRESS FIELD IN X & Y
C     DIRECTION, RESPECTIVELY
C
      LI1=67
      KJ1=35
      I2=I1-1
      I3=I1-2
      J2=J1-1
      J3=J1-2
      I4=I1-3
      J4=J1-3
C
C     M1 & M2 = X COORDINATES OF THE CAVITY CORNERS
```

```
C
      M1=33
      M2=64
C
C     N1 & N2 = Y COORDINATES OF THE CAVITY CORNERS
C
      N1=14
      N2=24
      MM1=M1-1
      MM2=M2+1
      NN1=N1-1
      NN2=N2+1
      NA1=N1+1
      NA2=N2-1
      MA1=M1+1
      MA2=M2-1
      M122=M1+2
      M222=M2+2
      M112=M1-2
      M212=M2-2
      N121=N1+1
C
C     K1 = LAYERED THICKNESS
C
      K1=N1
      K2=K1-1
      K3=K1+1
      ID2=8
      ID21=ID2+1
      ID3=140
      ID31=ID3-1
C
C     NTE = FINAL TIME STEP
C
      NTE=121
C
C     DV = TRAVERSE SPEED OF ASPERITY
C
      DV=6.D2
C
C     DL = ASPERITY WIDTH
C
      DL=1.D-2
C
C     COND = THERMAL CONDUCTIVITY
C
      COND1=1.213D0
      COND2=1.213D0
      CONDI=(COND1+COND2)/2.D0
      CONDC=(2.D0*COND1+COND2)/3.D0
C
C     DIFF = THERMAL DIFFUSIVITY
C
      DIFF1=4.29D-3
```

```
      DIFF2=4.29D-3
      DIFFI=(DIFF1+DIFF2)/2.D0
      DIFFC=(2.D0*DIFF1+DIFF2)/3.D0
C
C     RNU = POISSON'S RATIO
C
      RNU1=0.285D0
      RNU2=0.285D0
      RNUI=(RNU1+RNU2)/2.D0
      RNUC=(2.D0*RNU1+RNU2)/3.D0
C
C     E = YOUNG'S MODULUS
C
      E1=3.6D7
      E2=3.6D7
      EI=(E1+E2)/2.D0
      EC=(2.D0*E1+E2)/3.D0
C
C     RHO = MASS DENSITY
C
      RHO1=9.31D-3
      RHO2=9.31D-3
      RHOI=(RHO1+RHO2)/2.D0
      RHOC=(2.D0*RHO1+RHO2)/3.D0
C
C     EX = THE COEFFICIENT OF THERMAL EXPANSION
C
      EX1=6.29D-6
      EX2=6.29D-6
      EXI=(EX1+EX2)/2.D0
      EXC=(2.D0*EX1+EX2)/3.D0
C
C     RMUF = COULOMB COEFFICIENT OF FRICTION
C
      RMUF=0.5D0
C
C     RMU & RL = LAME CONSTANTS
C
      RMU1=E1/(2.D0*(1.D0+RNU1))
      RMU2=E2/(2.D0*(1.D0+RNU2))
      RMUI=EI/(2.D0*(1.D0+RNUI))
      RMUC=EC/(2.D0*(1.D0+RNUC))
      RL1=2.D0*RMU1*RNU1/(1.D0-2.D0*RNU1)
      RL2=2.D0*RMU2*RNU2/(1.D0-2.D0*RNU2)
      RLI=2.D0*RMUI*RNUI/(1.D0-2.D0*RNUI)
      RLC=2.D0*RMUC*RNUC/(1.D0-2.D0*RNUC)
      C2=DSQRT(RMU2*1.2D1/RHO2)
      HAK=RMUF*DV*DL/COND1
      RHC=RHO2*C2**2
      BETA=COND2/COND1
      R1=DV*DL/DIFF1
      R2=DV*DL/DIFF2
      ALPHS=DIFF2/DIFF1
      DX=0.2D-1
```

```
      DY1=0.6D-2
      DY2=0.2D-1
C
C     DT = TIME STEP
C
      DT=0.1D-1
      R11=DT/(R1*DX*DX)
      R12=DT/(R1*DY1*DY1)
      R21=DT/(R2*DX*DX)
      R22=DT/(R2*DY2*DY2)
      A1=1.D0+BETA/ALPHS
      A2=1.D0+BETA
      A3=A2/A1
      A4=1.D0-2.D0*A3*R11-2.D0*A3*R12
      A5=0.5D0+0.25D0*BETA/ALPHS
      A=1.D0-2.D0*R21-2.D0*R22
      AA=1.D0-2.D0*R11-2.D0*R12
      A6=0.5D0*A2*R11+0.5D0*BETA*R12+0.5D0*R11+R12
      A7=R1+BETA*R2
      A8=A2/A7
      DTR1=DT/R1
      DTR2=DT/R2
C
      CALL XYLCT(X,Y,XS,YE,XSS,YEE,DA,DG,SIG,TAU,I1,J1)
C
      NC=1
      NT=1
  100 NT=NT+1
      TIME=(NT-1)*DT
C
      CALL QIN(DX,DT,NT,I1,Q,II,JJ)
C
      CALL TEMP(T,TT,TTT,Q,FX,FY,X,Y,XS,YE,XSS,YEE,DA,DG,SIG,TAU,
     AII,JJ,NT,I1,J1)
C
      NC=NC+1
      IF(NT .NE. NTE) GO TO 5
C
      CALL MAP(TS,FXS,FYS,T,FX,FY,I1,J1,LI1,KJ1)
C
      DO 31 J=NN1,NA1
      WRITE(6,*) J
      WRITE(6,*) (T(I,J),I=MM1,MA1)
      WRITE(6,*) (FX(I,J),I=MM1,MA1)
   31 WRITE(6,*) (FY(I,J),I=MM1,MA1)
      DO 32 J=NN1,NA1
      WRITE(6,*) J
      WRITE(6,*) (T(I,J),I=MA2,MM2)
      WRITE(6,*) (FX(I,J),I=MA2,MM2)
   32 WRITE(6,*) (FY(I,J),I=MA2,MM2)
      DO 33 J=NA2,NN2
      WRITE(6,*) J
      WRITE(6,*) (T(I,J),I=MM1,MA1)
      WRITE(6,*) (FX(I,J),I=MM1,MA1)
```

```
 33  WRITE(6,*) (FY(I,J),I=MM1,MA1)
     DO 34 J=NA2,NN2
     WRITE(6,*) J
     WRITE(6,*) (T(I,J),I=MA2,MM2)
     WRITE(6,*) (FX(I,J),I=MA2,MM2)
 34  WRITE(6,*) (FY(I,J),I=MA2,MM2)
     WRITE(6,101)
101  FORMAT(/,5X,'TS',/)
     DO 20 J=1,KJ1
 20  WRITE(6,90) (TS(I,J),I=1,LI1)
     WRITE(6,102)
102  FORMAT(/,5X,'FXS',/)
     DO 21 J=1,KJ1
 21  WRITE(6,90) (FXS(I,J),I=1,LI1)
     WRITE(6,103)
103  FORMAT(/,5X,'FYS',/)
     DO 22 J=1,KJ1
 22  WRITE(6,90) (FYS(I,J),I=1,LI1)
 90  FORMAT(S(1X,D14.7))
 5   IF(NT .LT. NTE) GO TO 100
     STOP
     END
```

```
C     THIS SUBROUTINE INPUTS COORDINATES X & Y AND CALCULATES THE
C     DERIVATIVES OF THE COORDINATES
C
      SUBROUTINE XYLCT(X,Y,XS,YE,XSS,YEE,DA,DG,SIG,TAU,I1,J1)
      IMPLICIT REAL*8 (A-H,O-Z)
C
C     X & Y = COORDINATES IN PHYSICAL PLANE
C     XS,YE,XSS,YEE = THE DERIVATIVES OF THE COORDINATES IN
C     PHYSICAL PLANE WITH RESPECT TO THE COORDINATES IN
C     COMPUTATIONAL PLANE
C     DA,DG,SIG,TAU = COEFFICIENTS DEFINED IN TEMPERATURE EQUATION
C
      DIMENSION X(I1,J1),Y(I1,J1),XS(I1,J1),YE(I1,J1),XSS(I1,J1)
      DIMENSION YEE(I1,J1),DA(I1,J1),DG(I1,J1),SIG(I1,J1),TAU(I1,J1)
      I2=I1-1
      J2=J1-1
      I3=I1-2
      J3=J1-2
C
      DO 90 J=1,J1
      DO 91 I=1,I1
      X(I,J)=0.D0
      Y(I,J)=0.D0
      XS(I,J)=0.D0
      YE(I,J)=0.D0
      XSS(I,J)=0.D0
      YEE(I,J)=0.D0
      DA(I,J)=0.D0
      DG(I,J)=0.D0
      SIG(I,J)=0.D0
      TAU(I,J)=0.D0
 91   CONTINUE
 90   CONTINUE
C
      DO 1 J=1,J1
C
      DO 5 I=1,4
  5   X(I,J)=(I-1)*0.5D0
C
      DO 6 I=5,9
  6   X(I,J)=1.5D0+(I-4)*0.1D0
C
      DO 7 I=10,134
  7   X(I,J)=2.D0+(I-9)*0.02D0
C
      DO 8 I=135,138
  8   X(I,J)=4.5D0+(I-134)*0.05D0
C
      DO 9 I=139,145
  9   X(I,J)=4.7D0+(I-138)*0.1D0
C
  1   CONTINUE
C
      DO 3 I=1,I1
```

```
      Y(I,1)=0.D0
      Y(I,2)=0.005D0
      Y(I,3)=0.01D0
      Y(I,4)=0.016D0
      Y(I,5)=0.023D0
      Y(I,6)=0.031D0
      Y(I,7)=0.04D0
      Y(I,8)=0.05D0
      Y(I,9)=0.059D0
      Y(I,10)=0.067D0
      Y(I,11)=0.075D0
      Y(I,12)=0.082D0
      Y(I,13)=0.088D0
      Y(I,14)=0.094D0
      Y(I,15)=0.1D0
      Y(I,16)=0.107D0
      Y(I,17)=0.115D0
      Y(I,18)=0.125D0
      Y(I,19)=0.137D0
      Y(I,20)=0.151D0
      Y(I,21)=0.167D0
      Y(I,22)=0.185D0
      Y(I,23)=0.205D0
      Y(I,24)=0.225D0
      Y(I,25)=0.245D0
      Y(I,26)=0.27D0
      Y(I,27)=0.3D0
      Y(I,28)=0.34D0
      Y(I,29)=0.4D0
      Y(I,30)=0.48D0
      Y(I,31)=0.58D0
      Y(I,32)=0.78D0
      Y(I,33)=1.08D0
    3 CONTINUE
C
      DO 17 J=2,J2
      DO 18 I=2,I2
      XS(I,J)=(X(I+1,J)-X(I-1,J))/2.D0
      YE(I,J)=(Y(I,J+1)-Y(I,J-1))/2.D0
      XSS(I,J)=X(I-1,J)-2.D0*X(I,J)+X(I+1,J)
      YEE(I,J)=Y(I,J-1)-2.D0*Y(I,J)+Y(I,J+1)
   18 CONTINUE
   17 CONTINUE
C
      I=1
      DO 19 J=2,J2
      XS(I,J)=(-3.D0*X(I,J)+4.D0*X(I+1,J)-X(I+2,J))/2.D0
      YE(I,J)=(Y(I,J+1)-Y(I,J-1))/2.D0
   19 CONTINUE
C
      J=1
      DO 20 I=2,I2
      XS(I,J)=(X(I+1,J)-X(I-1,J))/2.D0
      YE(I,J)=(-3.D0*Y(I,J)+4.D0*Y(I,J+1)-Y(I,J+2))/2.D0
```

```
 20   CONTINUE
C
      I=I1
      DO 21 J=2,J2
      XS(I,J)=(X(I-2,J)-4.D0*X(I-1,J)+3.D0*X(I,J))/2.D0
      YE(I,J)=(Y(I,J+1)-Y(I,J-1))/2.D0
 21   CONTINUE
C
      J=J1
      DO 22 I=2,I2
      XS(I,J)=(X(I+1,J)-X(I-1,J))/2.D0
      YE(I,J)=(Y(I,J-2)-4.D0*Y(I,J-1)+3.D0*Y(I,J))/2.D0
 22   CONTINUE
C
      XS(1,1)=XS(1,2)
      XS(1,J1)=XS(1,2)
      XS(I1,1)=XS(I1,2)
      XS(I1,J1)=XS(I1,2)
      YE(1,1)=YE(2,1)
      YE(1,J1)=YE(2,J1)
      YE(I1,1)=YE(2,1)
      YE(I1,J1)=YE(2,J1)
C
      DO 25 J=1,J1
      DO 26 I=1,I1
      DA(I,J)=1.D0/XS(I,J)**2
      DG(I,J)=1.D0/YE(I,J)**2
      SIG(I,J)=-YEE(I,J)/YE(I,J)**3
      TAU(I,J)=-XSS(I,J)/XS(I,J)**3
      IF(DABS(SIG(I,J)) .LT. 1.D-10) SIG(I,J)=0.D0
      IF(DABS(TAU(I,J)) .LT. 1.D-10) TAU(I,J)=0.D0
 26   CONTINUE
 25   CONTINUE
C
      RETURN
      END
```

```
C     THIS SUBROUTINE INPUTS THE SURFACE B.C.
C
      SUBROUTINE QIN(DX,DT,NT,I1,Q,II,JJ)
      IMPLICIT REAL*8 (A-H,O-Z)
C
C     Q = SURFACE HEAT INPUT
C
      DIMENSION Q(I1)
C
C     NR2=DX/DT,NR1=NR2/2
C
      NR1=1
      NR2=2
C
      DO 24 I=1,I1
      Q(I)=0.D0
   24 CONTINUE
C
      IF(NT .GT. 2) GO TO 21
      NC1=0
      NC2=0
      NC3=0
      NTT=1
      ND1=NR1
      ND2=NR2
      ND3=0
      NNT=1
   21 NC1=NC1+1
      NC2=NC2+1
      IF(NC1 .EQ. NR1) GO TO 1
      GO TO 4
    1 NC3=NC3+1
      IF(NC3 .EQ. 1) GO TO 6
      NC3=0
      GO TO 7
    6 NTT=NTT+1
    7 NC1=0
    4 II=74-NTT+1
      IF(NC2 .GE. NR1) GO TO 2
      PB=0.5D0
      GO TO 5
    2 IF(NC2 .LT. NR2) GO TO 3
      PB=0.5D0
      NC2=0
      GO TO 5
    3 PB=0.D0
    5 Q(II)=PB+DT*NC1/DX
      ND1=ND1-1
      ND2=ND2-1
      IF(ND1 .EQ. 0) GO TO 11
      GO TO 12
   11 ND3=ND3+1
      IF(ND3 .EQ. 1) GO TO 13
      ND3=0
```

```
      GO TO 14
   13 NNT=NNT+1
   14 ND1=NR1
   12 JJ=124-NNT+1
      IF(ND2 .LE. NR1) GO TO 15
      PF=0.D0
      GO TO 16
   15 IF(ND2 .GT. 0) GO TO 17
      ND2=NR2
      PF=0.D0
      GO TO 16
   17 PF=0.5D0
   16 Q(JJ)=PF+DT*ND1/DX
      II1=II+1
      JJ1=JJ-1
C
      DO 23 I=II1,JJ1
      Q(I)=1.D0
   23 CONTINUE
C
      RETURN
      END
```

```
C     THIS SUBROUTINE SOLVED A LAYERED MEDIUM WITH A CAVITY, THE TOP
C     EDGE OF THE CAVITY IS AT THE INTERFACE
C
      SUBROUTINE TEMP(T,TT,TTT,Q,FX,FY,X,Y,XS,YE,XSS,YEE,DA,DG,
     ASIG,TAU,II,JJ,NT,I1,J1)
      IMPLICIT REAL*8 (A-H,O-Z)
      DIMENSION T(I1,J1),TT(I1,J1),TTT(I1,J1),FX(I1,J1),
     AFY(I1,J1),Q(I1),X(I1,J1),Y(I1,J1),XS(I1,J1),YE(I1,J1)
      DIMENSION XSS(I1,J1),YEE(I1,J1),DA(I1,J1),DG(I1,J1),
     ASIG(I1,J1),TAU(I1,J1)
      COMMON /AS4/ RL1,RL2,RLI,RLC,RMU1,RMU2,RMUI,RMUC,EX1,EX2,
     AEXI,EXC,HAK,RHC
      COMMON /AS5/ DV,DL,DIFF1,DIFF2,COND1,COND2,BETA,R1,R2,
     AALPHS,DX,DY1,DY2,DT,R11,R12,R21,R22,A1,A2,A3,A4,A5,A,AA,A6,A7,A8
      COMMON /AS6/ DTR1,DTR2,M1,M2,N1,N2,MM1,MM2,NN1,NN2,NA1,NA2,
     AMA1,MA2,K1,K2,K3,NTE,M122,M222,M112,M212,N121
      COMMON /AS7/ ID2,ID21,ID3,ID31,I2,J2,I3,J3,I4,J4
      IF(NT .NE. 2) GO TO 100
      DO 1 J=1,J1
      DO 2 I=1,I1
      T(I,J)=0.D0
      TT(I,J)=0.D0
      TTT(I,J)=0.D0
    2 CONTINUE
    1 CONTINUE
C
C     COMPUTE TEMPERATURE OF THE COATING LAYER
C     DA,DG,SIG,TAU = THE COEFFICIENTS DEFINED IN THE TEMPERATURE
C     EQUATION
C
  100 DO 3 I=2,I2
      DO 4 J=2,K2
      AA1=DA(I,J)*(TT(I-1,J)-2.D0*TT(I,J)+TT(I+1,J))
      AA2=DG(I,J)*(TT(I,J-1)-2.D0*TT(I,J)+TT(I,J+1))
      AA3=SIG(I,J)*(TT(I,J+1)-TT(I,J-1))/2.D0
      AA4=TAU(I,J)*(TT(I+1,J)-TT(I-1,J))/2.D0
      AAA=AA1+AA2+AA3+AA4
      IF(NT .GT. 2) GO TO 5
C
C     2 POINTS BACKWARD DIFFERENCE IN TIME DERIVATIVE
C
      T(I,J)=TT(I,J)+AAA*DT/R1
      GO TO 4
C
C     3 POINTS BACKWARD DIFFERENCE IN TIME DERIVATIVE
C
    5 T(I,J)=(2.D0*AAA*DT/R1+4.D0*TT(I,J)-TTT(I,J))/3.D0
    4 CONTINUE
    3 CONTINUE
C
C     COMPUTE TEMPERATURE OF THE SUBSTRATE
C
      DO 6 I=2,I2
      DO 7 J=K3,J2
```

```
      AA1=DA(I,J)*(TT(I-1,J)-2.D0*TT(I,J)+TT(I+1,J))
      AA2=DG(I,J)*(TT(I,J-1)-2.D0*TT(I,J)+TT(I,J+1))
      AA3=SIG(I,J)*(TT(I,J+1)-TT(I,J-1))/2.D0
      AA4=TAU(I,J)*(TT(I+1,J)-TT(I-1,J))/2.D0
      AAA=AA1+AA2+AA3+AA4
      IF(NT .GT. 2) GO TO 8
C
C     2 POINTS BACKWARD DIFFERENCE IN TIME DERIVATIVE
C
      T(I,J)=TT(I,J)+AAA*DT/R2
C
      GO TO 7
C
C     3 POINTS BACKWARD DIFFERENCE IN TIME DERIVATIVE
C
   8  T(I,J)=(2.D0*AAA*DT/R2+4.D0*TT(I,J)-TTT(I,J))/3.D0
   7  CONTINUE
   6  CONTINUE
C
      DO 9 J=N1,N2
      DO 10 I=M1,M2
      T(I,J)=0.D0
  10  CONTINUE
   9  CONTINUE
C
C     COMPUTE TEMPERATURE OF THE CORNER POINTS
C
      IF(NT .GT. 2) GO TO 12
C
C     2 POINTS BACKWARD DIFFERENCE IN TIME DERIVATIVE
C
C     CORNER A
C
      T(M1,N1)=TT(M1,N1)+(0.5D0*A2*R11*TT(M1-1,N1)-
     AA6*TT(M1,N1)+0.5D0*BETA*R12*TT(M1,N1+1)+0.5D0*R11*TT(M1+1,N1)+
     AR12*TT(M1,N1-1))/A5
C
C     CORNER B
C
      T(M2,N1)=TT(M2,N1)+(0.5D0*R11*TT(M2-1,N1)-A6
     A*TT(M2,N1)+0.5D0*BETA*R12*TT(M2,N1+1)+0.5D0*A2*R11*TT(M2+1,N1)
     A+R12*TT(M2,N1-1))/A5
C
C     CORNER C
C
      T(M1,N2)=A*TT(M1,N2)+4.D0*(R21*(TT(M1-1,N2)+
     A0.5D0*TT(M1+1,N2))+R22*(0.5D0*TT(M1,N2-1)+TT(M1,N2+1)))/3.D0
C
C     CORNER D
C
      T(M2,N2)=A*TT(M2,N2)+4.D0*(R21*(0.5D0*TT(M2-1,N2)
     A+TT(M2+1,N2))+R22*(0.5D0*TT(M2,N2-1)+TT(M2,N2+1)))/3.D0
C
      GO TO 14
```

```
C     3 POINTS BACKWARD DIFFERENCE IN TIME DERIVATIVE
C
C     CORNER A
C
  12  T(M1,N1)=(-TTT(M1,N1)+4.D0*TT(M1,N1)+2.D0*
     A(0.5D0*A2*R11*TT(M1-1,N1)-A6*TT(M1,N1)+0.5D0*BETA*R12*TT(M1,
     AN1+1)+0.5D0*R11*TT(M1+1,N1)+R12*TT(M1,N1-1))/A5)/3.D0
C
C     CORNER B
C
      T(M2,N1)=(-TTT(M2,N1)+4.D0*TT(M2,N1)+2.D0*
     A(0.5D0*R11*TT(M2-1,N1)-A6*TT(M2,N1)+0.5D0*BETA*R12*TT(M2,N1+1)+
     A0.5D0*A2*R11*TT(M2+1,N1)+R12*TT(M2,N1-1))/A5)/3.D0
C
C     CORNER C
C
      T(M1,N2)=(-TTT(M1,N2)+4.D0*TT(M1,N2)+8.D0*
     A(R21*(TT(M1-1,N2)-1.5D0*TT(M1,N2)+0.5D0*TT(M1+1,N2))+R22*(0.5D0
     A*TT(M1,N2-1)-1.5D0*TT(M1,N2)+TT(M1,N2+1)))/3.D0)/3.D0
C
C     CORNER D
C
      T(M2,N2)=(-TTT(M2,N2)+4.D0*TT(M2,N2)+8.D0*
     A(R21*(0.5D0*TT(M2-1,N2)-1.5D0*TT(M2,N2)+TT(M2+1,N2))+R22*(0.5D0*
     ATT(M2,N2-1)-1.5D0*TT(M2,N2)+TT(M2,N2+1)))/3.D0)/3.D0
C
C     COMPUTE TEMPERATURE ON THE LEFT & RIGHT HAND EDGE OF THE CAVITY
C
  14  DO 15 J=NA1,NA2
      I=M1
      DDY1=Y(I,J)-Y(I,J-1)
      DDY2=Y(I,J+1)-Y(I,J)
      YY1=DDY1**2+DDY1*DDY2
      YY2=DDY1*DDY2+DDY2**2
      EE1=DT*((TT(I-1,J)-TT(I,J))/DX**2+(TT(I,J-1)-TT(I,J))/YY1+
     A(TT(I,J+1)-TT(I,J))/YY2)/R2
      IF(DABS(EE1) .LT. 1.D-65) EE1=0.D0
      I=M2
      EE2=DT*((TT(I+1,J)-TT(I,J))/DX**2+(TT(I,J-1)-TT(I,J))/YY1+
     A(TT(I,J+1)-TT(I,J))/YY2)/R2
      IF(DABS(EE2) .LT. 1.D-65) EE2=0.D0
      IF(NT .GT. 2) GO TO 16
C
C     2 POINTS BACKWARD DIFFERENCE IN TIME DERIVATIVE
C
      I=M1
      T(I,J)=TT(I,J)+2.D0*EE1
      I=M2
      T(I,J)=TT(I,J)+2.D0*EE2
C
      GO TO 15
C
C     3 POINTS BACKWARD DIFFERENCE IN TIME DERIVATIVE
C
```

```
   16  I=M1
       T(I,J)=(-TTT(I,J)+4.D0*TT(I,J)+4.D0*EE1)/3.D0
       I=M2
       T(I,J)=(-TTT(I,J)+4.D0*TT(I,J)+4.D0*EE2)/3.D0
   15  CONTINUE
C
C      COMPUTE THE TEMPERATURE ON THE TOP & BOTTOM EDGE OF THE CAVITY
C
       DO 17 I=MA1,MA2
       IF(NT .GT. 2) GO TO 18
C
C      2 POINTS BACKWARD DIFFERENCE IN TIME DERIVATIVE
C
       J=N1
       T(I,J)=AA*TT(I,J)+R11*(TT(I+1,J)+TT(I-1,J))+2.D0*R12*TT(I,J-1)
       J=N2
       T(I,J)=A*TT(I,J)+R21*(TT(I-1,J)+TT(I+1,J))+2.D0*R22*TT(I,J+1)
C
       GO TO 17
C
C      3 POINTS BACKWARD DIFFERENCE IN TIME DERIVATIVE
C
   18  J=N1
       T(I,J)=(-TTT(I,J)+4.D0*TT(I,J)+4.D0*(R11*(0.5D0*TT(I+1,J)-
      ATT(I,J)+0.5D0*TT(I-1,J))+R12*(TT(I,J-1)-TT(I,J))))/3.D0
       J=N2
       T(I,J)=(-TTT(I,J)+4.D0*TT(I,J)+4.D0*(R21*(0.5D0*TT(I-1,J)
      A-TT(I,J)+0.5D0*TT(I+1,J))+R22*(TT(I,J+1)-TT(I,J))))/3.D0
   17  CONTINUE
C
C      COMPUTE THE TEMPERATURE AT THE INTERFACE
C
       DO 19 IJ=1,2
       IF(IJ .EQ. 1) GO TO 20
       MN1=MM2
       MN2=I2
       GO TO 21
   20  MN1=2
       MN2=MM1
   21  DO 22 I=MN1,MN2
       J=K1
       DDX1=X(I,J)-X(I-1,J)
       DDX2=X(I+1,J)-X(I,J)
       XX1=DDX1**2+DDX1*DDX2
       XX2=DDX1*DDX2+DDX2**2
       EE3=2.D0*A8*DT*(TT(I-1,J)-TT(I
      ATT(I,J))/XX2+2.D0*DT*(TT(I
      ABETA*DT*(TT(I,J+1)-TT(I
       IF(NT .GT. 2) GO TO 23
C
C      2 POINTS BACKWARD DIFFERENCE
C
       T(I,J)=TT(I,J)+EE3
C
```

AD-A193 311 THERMO-MECHANICAL CRACKING IN COATED MEDIA WITH A CAVITY BY A MOVING ASPE (U) NEW MEXICO UNIV ALBUQUERQUE DEPT OF MECHANICAL ENGINEERING F D JU ET AL MAR 88 ME-144(88)ONR-233-3 F/G 20/11 NL

3/3

UNCLASSIFIED

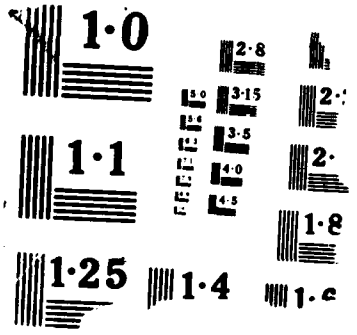
1·0
1·1
1·25
1·4
2·8
3·15
3·5
4·0
4·5
2·
1·8

```
      GO TO 61
   57 EF121=(3.D0*RLC+2.D0*RMUC)*1.2D1*EXC*HAK/RHC
   61 IF(I .LT. MA1 .OR. I .GT. MM2) GO TO 62
      IF(I .GT. MA1 .AND. I .LT. MM2) GO TO 63
      IF(I .EQ. MA1 .OR. I .EQ. MM2) GO TO 64
   62 EF111=(3.D0*RLI+2.D0*RMUI)*1.2D1*EXI*HAK/RHC
      GO TO 65
   63 EF111=(3.D0*RL1+2.D0*RMU1)*1.2D1*EX1*HAK/RHC
      GO TO 65
   64 EF111=(3.D0*RLC+2.D0*RMUC)*1.2D1*EXC*HAK/RHC
   65 IF(I .LT. M1 .OR. I .GT. M2) GO TO 66
      IF(I .GT. M1 .AND. I .LT. M2) GO TO 67
      IF(I .EQ. M1 .OR. I .EQ. M2) GO TO 68
   66 EFIJ=(3.D0*RLI+2.D0*RMUI)*1.2D1*EXI*HAK/RHC
      GO TO 70
   67 EFIJ=(3.D0*RL1+2.D0*RMU1)*1.2D1*EX1*HAK/RHC
      GO TO 70
   68 EFIJ=(3.D0*RLC+2.D0*RMUC)*1.2D1*EXC*HAK/RHC
   70 IF(I .LT. MM1 .OR. I .GT. MA2) GO TO 71
      IF(I .GT. MM1 .AND. I .LT. MA2) GO TO 72
      IF(I .EQ. MM1 .OR. I .EQ. MA2) GO TO 73
   71 EF211=(3.D0*RLI+2.D0*RMUI)*1.2D1*EXI*HAK/RHC
      GO TO 74
   72 EF211=(3.D0*RL1+2.D0*RMU1)*1.2D1*EX1*HAK/RHC
      GO TO 74
   73 EF211=(3.D0*RLC+2.D0*RMUC)*1.2D1*EXC*HAK/RHC
   74 IF(I .LT. M112 .OR. I .GT. M212) GO TO 75
      IF(I .GT. M112 .AND. I .LT. M212) GO TO 76
      IF(I .EQ. M112 .OR. I .EQ. M212) GO TO 77
   75 EF221=(3.D0*RLI+2.D0*RMUI)*1.2D1*EXI*HAK/RHC
      GO TO 54
   76 EF221=(3.D0*RL1+2.D0*RMU1)*1.2D1*EX1*HAK/RHC
      GO TO 54
   77 EF221=(3.D0*RLC+2.D0*RMUC)*1.2D1*EXC*HAK/RHC
      GO TO 54
   53 EF121=(3.D0*RL2+2.D0*RMU2)*1.2D1*EX2*HAK/RHC
      EF111=(3.D0*RL2+2.D0*RMU2)*1.2D1*EX2*HAK/RHC
      EFIJ=(3.D0*RL2+2.D0*RMU2)*1.2D1*EX2*HAK/RHC
      EF211=(3.D0*RL2+2.D0*RMU2)*1.2D1*EX2*HAK/RHC
      EF221=(3.D0*RL2+2.D0*RMU2)*1.2D1*EX2*HAK/RHC
   54 IX=II+J-1
      IF(I .LT. IX) GO TO 30
      IF(I .GT. JJ) GO TO 31
      FX(I,J)=(EF211*T(I+1,J)-EF111*T(I-1,J))/(2.D0*XS(I,J))
      GO TO 29
   30 FX(I,J)=(EF121*T(I-2,J)-4.D0*EF111*T(I-1,J)+3.D0*EFIJ*T(I,J))
     A/(2.D0*XS(I,J))
      GO TO 29
   31 FX(I,J)=(-3.D0*EFIJ*T(I,J)+4.D0*EF211*T(I+1,J)-EF221*T(I+2,J))
     A/(2.D0*XS(I,J))
   29 CONTINUE
   28 CONTINUE
C
      DO 32 J=2,J3
```

```
      DO 33 I=1,I1
      IF(J .LT. NN1) GO TO 83
      IF(J .EQ. NN1) GO TO 84
      IF(J .GE. N1) GO TO 85
   83 ES121=(3.D0*RL1+2.D0*RMU1)*1.2D1*EX1*HAK/RHC
      GO TO 86
   84 IF(I .EQ. M1 .OR. I .EQ. M2) GO TO 87
      IF(I .GT. M1 .AND. I .LT. M2) GO TO 88
      ES121=(3.D0*RLI+2.D0*RMUI)*1.2D1*EXI*HAK/RHC
      GO TO 86
   87 ES121=(3.D0*RLC+2.D0*RMUC)*1.2D1*EXC*HAK/RHC
      GO TO 86
   88 ES121=(3.D0*RL1+2.D0*RMU1)*1.2D1*EX1*HAK/RHC
      GO TO 86
   85 ES121=(3.D0*RL2+2.D0*RMU2)*1.2D1*EX2*HAK/RHC
   86 IF(I .LE. N1) GO TO 91
      IF(J .EQ. N121) GO TO 92
      IF(J .GT. N121) GO TO 93
   91 ES111=(3.D0*RL1+2.D0*RMU1)*1.2D1*EX1*HAK/RHC
      GO TO 94
   92 ES111=(3.D0*RLI+2.D0*RMUI)*1.2D1*EXI*HAK/RHC
      GO TO 94
   93 ES111=(3.D0*RL2+2.D0*RMU2)*1.2D1*EX2*HAK/RHC
   94 FY(I,J)=(ES121*T(I,J+1)-ES111*T(I,J-1))/(2.D0*YE(I,J))
   33 CONTINUE
   32 CONTINUE
C
      J=1
      DO 34 I=1,I1
      FY(I,J)=-Q(I)
   34 CONTINUE
C
      DO 37 J=NA1,NA2
      DO 38 I=M1,M2
      FX(I,J)=0.D0
      FX(I,J)=0.D0
   38 CONTINUE
   37 CONTINUE
C
      DO 39 J=N1,N2
      DO 40 I=MA1,MA2
      FY(I,J)=0.D0
      FY(I,J)=0.D0
   40 CONTINUE
   39 CONTINUE
C
   99 DO 41 I=2,I2
      DO 42 J=1,J2
      TTT(I,J)=TT(I,J)
      TT(I,J)=T(I,J)
   42 CONTINUE
   41 CONTINUE
      RETURN
      END
```

```
C     THIS SUBROUTINE MAPS TEMPERATURE AND ITS GRADIENTS IN
C     THE TEMPERATURE FIELD TO THE CORRESPONDING POINTS IN THE
C     STRESS FIELD
C
      SUBROUTINE MAP(TS,FXS,FYS,T,FX,FY,I1,J1,LI1,KJ1)
      IMPLICIT REAL*8 (A-H,O-Z)
C
C     T,FX,FY = TEMPERATURE AND ITS GRADIENTS IN TEMPERATURE FIELD
C     TS,FXS,FYS = TEMPERATURE AND ITS GRADIENTS IN STRESS FIELD
C
      DIMENSION T(I1,J1),FX(I1,J1),FY(I1,J1),TS(LI1,KJ1),
     AFXS(LI1,KJ1),FYS(LI1,KJ1)
C
      DO 1 J=1,KJ1
      DO 2 I=1,LI1
      TS(I,J)=0.D0
      FXS(I,J)=0.D0
      FYS(I,J)=0.D0
    2 CONTINUE
    1 CONTINUE
C
      DO 3 J=1,J1
      IT1=1
C
      DO 4 I=7,10
      TS(I,J)=T(IT1,J)
      FXS(I,J)=FX(IT1,J)
      FYS(I,J)=FY(IT1,J)
    4 IT1=IT1+1
C
      IT2=9
      DO 5 I=13,15
      TS(I,J)=T(IT2,J)
      FXS(I,J)=FX(IT2,J)
      FYS(I,J)=FY(IT2,J)
    5 IT2=IT2+5
C
      IT3=22
      DO 6 I=16,19
      TS(I,J)=T(IT3,J)
      FXS(I,J)=FX(IT3,J)
      FYS(I,J)=FY(IT3,J)
    6 IT3=IT3+3
C
      IT4=38
      DO 7 I=22,30
      TS(I,J)=T(IT4,J)
      FXS(I,J)=FX(IT4,J)
      FYS(I,J)=FY(IT4,J)
    7 IT4=IT4+3
C
      ITS=69
      DO 8 I=33,39
      TS(I,J)=T(ITS,J)
```

```
      FXS(I,J)=FX(IT5,J)
      FYS(I,J)=FY(IT5,J)
    8 IT5=IT5+3
C
      IT6=91
      DO 9 I=40,42
      TS(I,J)=T(IT6,J)
      FXS(I,J)=FX(IT6,J)
      FYS(I,J)=FY(IT6,J)
    9 IT6=IT6+4
C
      IT7=104
      DO 10 I=43,49
      TS(I,J)=T(IT7,J)
      FXS(I,J)=FX(IT7,J)
      FYS(I,J)=FY(IT7,J)
   10 IT7=IT7+5
C
      IT8=136
      DO 11 I=50,54
      TS(I,J)=T(IT8,J)
      FXS(I,J)=FX(IT8,J)
      FYS(I,J)=FY(IT8,J)
   11 IT8=IT8+2
C
      TS(11,J)=T(6,J)
      FXS(11,J)=FX(6,J)
      FYS(11,J)=FY(6,J)
      TS(12,J)=T(8,J)
      FXS(12,J)=FX(8,J)
      FYS(12,J)=FY(8,J)
      TS(20,J)=T(33,J)
      FXS(20,J)=FX(33,J)
      FYS(20,J)=FY(33,J)
      TS(21,J)=T(35,J)
      FXS(21,J)=FX(35,J)
      FYS(21,J)=FY(35,J)
      TS(31,J)=T(64,J)
      FXS(31,J)=FX(64,J)
      FYS(31,J)=FY(64,J)
      TS(32,J)=T(66,J)
      FXS(32,J)=FX(66,J)
      FYS(32,J)=FY(66,J)
    3 CONTINUE
C
      RETURN
      END
```

```
C     MAIN PROGRAM
C     STRESS FIELD OF A LAYERED MEDIUM WITH A CAVITY, THE TOP
C     EDGE OF THE CAVITY IS AT THE INTERFACE
C
      IMPLICIT REAL*8 (A-H,O-Z)
C
C     X & Y = COORDINATES IN THE PHYSICAL PLANE
C     A = MATRIX TO BE SOLVED
C     B = RIGHT HAND SIDE OF THE ALGEBRAIC EQUATIONS
C     U & V = DISPLACEMENTS IN X AND Y DIRECTION, RESPECTIVELY
C     S11,S12,S22 = STRESSES
C     TS,FXS,FYS = TEMPERATURE AND ITS GRADIENTS FROM TEMPERATURE FIELD
C
      DIMENSION X(67,35),Y(67,35),A(649740),B(4420),TS(67,35),
     AFXS(67,35),FYS(67,35),U(67,35),V(67,35),S11(67,35),
     AS12(67,35),S22(67,35)
      COMMON /Z1/ RMU1,RMU2,RMUI,RMUC,RMUIC,RMUI1,RMUI2,RMUC1,RMUC2
      COMMON /Z2/ RL1,RL2,RLI,RLC,RLIC,RLI1,RLI2,RLC1,RLC2
      COMMON /Z3/ DN1,DN2,DN3,DI,DJ,RHC
C
C     LI1 & KJ1 = THE TOTAL NUMBER OF GRID POINTS IN X AND Y DIRECTION

      LI1=67
      KJ1=35
      L1=LI1-2
      L2=LI1-1
      K1=KJ1-1
C
C     MBAND = HALF BANDWIDTH
C
      MBAND=K1*2+6-1
C
C     NEQ = TOTAL NUMBER OF EQUATIONS TO BE SOLVED
C
      NEQ=L1*K1*2
C
C     NTOT = TOTAL DIMENSION OF "A" VECTOR
C
      NTOT=(2*MBAND+1)*NEQ
      JJ=K1*2
C
C     M1 & M2 = X COORDINATES OF THE CAVITY CORNERS
C
      M1=19
      M2=31
      MR1=M1+1
      MR2=M2+1
C
C     N1 & N2 = Y COORDINATES OF THE CAVITY CORNERS
C
      N1=14
      N2=24
      M111=M1-1
      M121=M1+1
```

END

DATE

FILMED

7-88

DTIC